DISSERTATION

submitted to the

COMBINED FACULTY OF MATHEMATICS,
ENGINEERING, AND NATURAL SCIENCES

of

RUPRECHT KARL UNIVERSITY OF
HEIDELBERG

Germany

for the degree of

DOCTOR OF NATURAL SCIENCES

Put forward by

Klaus Paschek

born in: Villingen-Schwenningen

ORAL EXAMINATION:
10. June 2025

FROM SPACE TO THE HADEAN EARTH: PREBIOTIC SYNTHESIS AND THE ORIGINS OF LIFE

Klaus Paschek

REFEREES:
Prof. Dr. Dr. h.c. Thomas K. HENNING
Prof. Dr. Hans-Christian SCHULTZ-COULON

Abstract:
From Space to the Hadean Earth:
Prebiotic Synthesis and the Origins of Life

For life to emerge, a variety of different molecular building blocks must be available in sufficiently high concentrations to increase the chances of their assembly into the highly complex macromolecular machinery required without the aid of elaborate biological enzymes and compartments. In this thesis, we explore different environments in which prebiotic synthesis of these building blocks is feasible. This ranges from the interplanetary space of the early solar system in the interior of meteorite parent bodies to the surface of the early Hadean Earth in small bodies of water, so-called warm little ponds (WLPs), on the first landmasses emerging from the primordial ocean. The idea is to combine the exogenous and endogenous processes into a consistent and realistic scenario of the early solar system and the Hadean Earth within it. This includes bombardment by meteorites from space, which release excessive amounts of energy during impact, leading to the generation of reducing gases that are injected into the Earth's atmosphere. Meteorites can also deliver prebiotic molecules formed in space, seeding the early Earth with the building blocks of life. In addition, geologic activity within the Earth's mantle is included, leading to serpentinization of upwelling mantle material by chemical reaction with water that penetrates the Earth's crust from the surface, releasing further reducing gases into the atmosphere. The goal is to assess the potential contributions and interactions of these different processes in setting the stage for the origins of life. We find that aqueous chemistry inside meteorite parent bodies can accurately describe and explain the prebiotic synthesis of the various biomolecules found in the meteoritic subclass of carbonaceous chondrites, with simulated and measured abundances of nucleobases, the sugar ribose, and vitamin B_3 in good agreement, shown here for the first time. The key to achieving this was the introduction of a proper understanding of volatile depletion in the source material of meteorite parent bodies. If delivered by meteorites to the Hadean Earth surface, our simulations show that extraterrestrial biomolecules formed in space could have significantly elevated the concentrations of prebiotic molecules in WLPs. In addition, a carbonaceous bombardment in a reducing atmosphere is capable of releasing sufficient amounts of the reducing gas HCN (hydrogen cynanide) to rain-out into WLPs and drive the prebiotic synthesis of sufficient amounts of the building blocks of RNA, one of the most commonly favored starting points for the origins of life. The most important finding of this thesis is that serpentinization alone can reduce an initially oxidizing atmosphere with initial 90 % CO_2 when modeled in a manner appropriate for the Hadean Earth. This might provide a solution to one of the oldest problems in the origins of life sciences, allowing effective prebiotic synthesis despite an initially oxidizing atmosphere that would otherwise be considered highly unfavorable. Not only that, but we were able to show that an initially oxidized atmosphere is actually a desirable state for prebiotic molecules, provided that high enough fluxes of reducing gases are emitted by serpentinization, as we indeed anticipate in the Hadean. The oxidizing atmosphere is reduced and exploited as a carbon source. The modeling of these various contributing mechanisms in this comprehensive scenario for the Hadean Earth and its host planetary system as a whole paints an optimistic picture for the preparation of a potent prebiotic soup on the Hadean Earth and beyond.

Zusammenfassung:
Vom Weltraum bis zur Erde im Hadaikum: Die Präbiotische Synthese und der Ursprung des Lebens

Damit Leben entstehen kann, muss eine Vielzahl verschiedener molekularer Bausteine in ausreichend hoher Konzentration zur Verfügung stehen, um die Wahrscheinlichkeit zu erhöhen, dass sie sich zu der hochkomplexen makromolekularen Maschinerie zusammenfügen, die erforderlich ist, ohne dass aufwendige biologische Enzyme und Kompartimente zum Einsatz kommen. In dieser Arbeit untersuchen wir verschiedene Umgebungen, in denen die präbiotische Synthese dieser Bausteine möglich ist. Dies reicht vom interplanetaren Raum des frühen Sonnensystems im Inneren von Meteoriten-Mutterkörpern bis hin zur Oberfläche der frühen Erde in kleinen stehenden Gewässern, dem so genannten Teich Darwins, auf den ersten Landmassen, die aus dem ursprünglichen Ozean entstanden. Die Idee ist, die exogenen und endogenen Prozesse zu einem konsistenten und realistischen Szenario des frühen Sonnensystems und der Erde im Hadaikum darin zusammenzufügen. Dazu gehört die Bombardierung durch Meteoriten aus dem Weltraum, die beim Aufprall enorme Mengen an Energie freisetzen, was zur Bildung von reduzierenden Gasen führt, die in die Erdatmosphäre gelangen. Meteoriten können auch präbiotische Moleküle aus dem All liefern, die die frühe Erde mit den Bausteinen des Lebens versorgten. Darüber hinaus werden geologische Aktivitäten im Erdmantel mit einbezogen, die zu einer Serpentinisierung von aufsteigendem Mantelmaterial durch chemische Reaktion mit Wasser führen, das von der Oberfläche aus in die Erdkruste eindringt und weitere reduzierende Gase in die Atmosphäre freisetzt. Ziel ist es, die möglichen Beiträge und Wechselwirkungen dieser verschiedenen Prozesse bei der Entstehung des Lebens zu bewerten. Wir stellen fest, dass die wässrige Chemie im Inneren von Meteoriten-Mutterkörpern die präbiotische Synthese der verschiedenen Biomoleküle, die in der Meteoriten-Unterklasse der kohligen Chondrite zu finden sind, genau beschreiben und erklären kann, wobei simulierte und gemessene Häufigkeiten von Nukleobasen, des Zuckers Ribose und des Vitamins B_3 gut übereinstimmen, was wir hier zum ersten Mal demonstrieren. Der entscheidende Faktor hierfür war die Einführung eines angemessenen Verständnisses der Abreicherung von flüchtigen Bestandteilen im Ausgangsmaterial der Meteoritenmutterkörper. Unsere Simulationen zeigen, dass extraterrestrische Biomoleküle, die im Weltraum gebildet wurden, die Konzentrationen präbiotischer Moleküle in Darwins Teich deutlich erhöht haben könnten, falls sie von Meteoriten auf die Erdoberfläche des Hadaikum gebracht wurden. Darüber hinaus ist eine kohlenstoffreich Bombardierung in einer reduzierenden Atmosphäre in der Lage, ausreichende Mengen des reduzierenden Gases HCN (Cyanwasserstoff/Blausäure) freizusetzen, um in Darwins Teich auszuregnen und die präbiotische Synthese ausreichender Mengen der Bausteine der RNA voranzutreiben, einer der am häufigsten favorisierten Ausgangspunkte für den Ursprung des Lebens. Die wichtigste Erkenntnis dieser Arbeit ist, dass die Serpentinisierung allein eine anfänglich oxidierende Atmosphäre mit anfänglich 90 % CO_2 reduzieren kann, wenn sie in einer für die Erde im Hadaikum typischen Umgebung stattfindet. Dies könnte eine Lösung für eines der ältesten Probleme der Erforschung der Ursprünge des Lebens bieten, indem es eine effektive präbiotische Synthese trotz einer anfänglich oxidierenden Atmosphäre ermöglicht, die ansonsten als äußerst ungünstig angesehen würde. Darüber hinaus konnten wir zeigen, dass eine anfänglich oxidierte Atmosphäre für präbiotische Moleküle sogar ein wünschenswerter Zustand ist, vorausgesetzt, dass durch die Serpentinisierung ausreichend hohe Mengen an reduzierenden Gasen freigesetzt werden, wie wir es im Hadaikum tatsächlich erwarten. Die oxidierende Atmosphäre wird reduziert und als Kohlenstoffquelle ausgenutzt. Die Modellierung dieser verschiedenen beitragenden Mechanismen in diesem umfassenden Szenario für die Erde im Hadaikum und ihr Planetensystem als Ganzes zeichnet ein optimistisches Bild für die Vorbereitung einer reichhaltigen präbiotischen Suppe auf der Erde im Hadaikum und anderswo.

Acknowledgments

First of all, I would like to thank my PI Prof. Dr. Thomas Henning for accepting me as a Ph.D. student and offering me to work on this amazing research project. I feel incredibly lucky to be able to work in the sciences of the origins of life. Providing me with the possibility to work both on theory and experiment is truly a privilege. Thank you for giving me the freedom to develop and pursue my own ideas, and guiding me on the way.

Next, many thanks to my supervisor Dr. Dmitry Semenov for always helping me with problems, answering all my questions, and brainstorming together about the next great addition to our models, which was always a lot of fun. Dima, I found in you not only a good mentor, but also a true friend.

Special thanks to Prof. Dr. Ralph Pudritz and Prof. Dr. Ben Pearce for allowing me to stand on their giant shoulders and allowing me to extend their comprehensive frameworks for simulating prebiotic chemistry in so many different and so exciting environments. I truly owe you for the papers we were able to publish together. Thank you for always helping me out and giving me great tips and advice.

Thanks to all my collaborators Karan Molaverdikhani, Yoshinori Miyazaki, Kai Kohler, Kevin Lange, and Oliver Trapp for working together with me for so long and providing me with crucial expertise and data without I would not have published a single paper. Thank you so much for always being available on short notice to help fix all the small problems.

I want to say a big thank you to all the people in the Origins of Life Laboratory, Vanessa, Frederick, Cornelia Jäger, Serge Krasnokutski, and in particular to Tushar Suhasaria, for always caring for me and for all the fun we had in the gym lifting weights together.

I want to thank my student Mijin Lee for the fun projects we worked on and made work together. It was always fun hanging out with you and talking about tasty Asian food.

Thank you to Jan, Dominik, and David for all the laughs we had together and the emotional support through these years.

Last but not least, I want to thank you, Helen, the love of my life for always caring and supporting me in the toughest times. I would have never finished this thesis without you and you are the best thing that ever happened to me.

Publications

First Author Publications as Part of this Thesis

The following first-authored publications are part of this thesis. The last paper in the list is currently in press and available as a preprint on arXiv. The respective Parts of this thesis are given in parentheses after the citations.

1. K. Paschek, K. Kohler, B. K. D. Pearce, K. Lange, T. K. Henning, O. Trapp, R. E. Pudritz, and D. A. Semenov (**2022**). 'Possible Ribose Synthesis in Carbonaceous Planetesimals'. *Life* 12.3. Number: 3 Publisher: Multidisciplinary Digital Publishing Institute, p. 404. DOI: `10.3390/life12030404`
(⇒ Part III)

2. K. Paschek, D. A. Semenov, B. K. D. Pearce, K. Lange, T. K. Henning, and R. E. Pudritz (**2023**). 'Meteorites and the RNA World: Synthesis of Nucleobases in Carbonaceous Planetesimals and the Role of Initial Volatile Content'. *The Astrophysical Journal* 942.1. Publisher: The American Astronomical Society, p. 50. DOI: `10.3847/1538-4357/aca27e`
(⇒ Part II)

3. K. Paschek, M. Lee, D. A. Semenov, and T. K. Henning (**2024b**). 'Prebiotic Vitamin B3 Synthesis in Carbonaceous Planetesimals'. *ChemPlusChem* 89.4, e202300508. DOI: `10.1002/cplu.202300508`
(⇒ Part IV)

4. K. Paschek, T. K. Henning, K. Molaverdikhani, Y. Miyazaki, B. K. D. Pearce, R. E. Pudritz, and D. A. Semenov (**2025**). 'Deep Mantle-Atmosphere Coupling and Carbonaceous Bombardment: Options for Biomolecule Formation on an Oxidized Early Earth'. *The Astrophysical Journal [**in press**]*. DOI: `10.3847/1538-4357/adc39b`. arXiv: `2503.15479 [astro-ph.EP]`
(⇒ Part V)

First Author Publication *not* Part of this Thesis

The following first-authored publication is **not** part of this thesis, but is relevant to the topic of the origins of life.

1. K. Paschek, A. Roßmann, M. Hausmann, and G. Hildenbrand (**2021**). 'Analysis of Tidal Accelerations in the Solar System and in Extrasolar Planetary Systems'. *Applied Sciences* 11.18, p. 8624. DOI: `10.3390/app11188624`

Contributing Author Publications *not* Part of this Thesis

The following co-authored publications are **not** part of this thesis, but are relevant to the topic of the origins of life. The last manuscript in the list is currently under revision in the journal *Cell Reports Physical Science* and is available as a preprint on arXiv.

1. G. Hildenbrand, K. Paschek, M. Schäfer, M. Hausmann, G. Hildenbrand, K. Paschek, M. Schäfer, and M. Hausmann (**2022**). 'Cryovolcanism in the Solar System and beyond: Considerations on Energy Sources, Geological Aspects, and Astrobiological Perspectives'. *Astronomy and Planetary Science - From Cryovolcanism to Black Holes and Galactic Evolution*. IntechOpen. ISBN: 978-1-80356-120-2. DOI: `10.5772/intechopen.105067`
2. Z. Peng, K. Paschek, and J. C. Xavier (**2022**). 'What Wilhelm Ostwald Meant by "Autokatalyse" and Its Significance to Origins-of-Life Research'. *BioEssays* 44.9, p. 2200098. DOI: `10.1002/bies.202200098`
3. OoLEN, S. Asche, C. Bautista, D. Boulesteix, A. Champagne-Ruel, C. Mathis, O. Markovitch, Z. Peng, A. Adams, A. V. Dass, A. Buch, E. Camprubi, E. S. Colizzi, S. Colón-Santos, H. Dromiack, V. Estrova, A. Garcia, G. Grimaud, A. Halpern, S. A. Harrison, S. F. Jordan, T. Z. Jia, A. Kahana, A. Kolchinsky, O. Moron-Garcia, R. Mizuuchi, J. Nan, Y. Orlova, B. K. D. Pearce, K. Paschek, M. Preiner, S. Pinna, E. Rodríguez-Román, L. Schwander, S. Sharma, H. B. Smith, A. Vieira, and J. C. Xavier (**2023**). 'What It Takes to Solve the Origin(s) of Life: An Integrated Review of Techniques'. DOI: `10.48550/arXiv.2308.11665`. arXiv: `2308.11665 [q-bio]`

Manuscripts in Preparation *not* Part of this Thesis

The following manuscripts in preparation are **not** part of this thesis, but extend the work presented here. For details, see Chapter 35.

1. M. Lee, K. Paschek, D. A. Semenov, and T. K. Henning (**2025**). 'Prebiotic Carboxylic Acid Synthesis in Carbonaceous Planetesimals [working title]'. ***in preparation***
2. K. Paschek, U. Malamud, D. A. Semenov, and T. K. Henning (**2025**). 'Volatile Differentiation in Comets and Implications for Prebiotic Synthesis in Carbonaceous Planetesimals [working title]'. ***in preparation***

Contents

Part I

INTRODUCTION

1

Motivation

> *For me, it is far better to grasp the Universe as it really is than to persist in delusion, however satisfying and reassuring.*
>
> **Carl Sagan**, 1995
> *The Demon-Haunted World*

Where do we come from?—is one of the oldest and most fundamental questions that any self-conscious mind, and humanity as a whole, is capable of asking itself. While it remains difficult to answer the question of—Why?—while remaining within the realm of science, we are capable of actively working toward finding the answer of—How?—we and life came to be.

While around 350 BC Aristotle suggested in *History of Animals* that lower forms of life arise spontaneously, such as fish from mud, maggots from wood, or insects from dead flesh (Bondeson 2014), modern science has made great leaps in understanding the fundamentals of living systems. This extends to how life works at the molecular level, e.g., with the discovery of the double helix structure of DNA by Maurice Wilkins, Rosalind Franklin, Raymond Gosling, James Watson, and Francis Crick (J. D. Watson and Crick 1953; Wilkins et al. 1953; Franklin and Gosling 1953; M. Cobb and Comfort 2023).

Contemporary science is bringing us closer to understanding the phenomenon of living matter in the context of the universe, e.g., with the recent development of the streaming instability (Johansen, Oishi, Mac Low, et al. 2007; Johansen, J. Blum, et al. 2014a; Ormel and Klahr 2010; Klahr and Schreiber 2020a), which is advancing planet formation theory toward a better understanding of how planets can rapidly form around stars, just like our oasis of life floating through the otherwise cold, empty, and dead universe. We can now asses what conditions make a planet habitable (Kasting et al. 1993; Lineweaver and Chopra 2012; Lorenz 2020). Recent analyses of meteoritic material and samples returned from asteroids by spacecraft have revealed virtually complete sets of the building blocks of life being present throughout our solar system (see, e.g., Burton et al. 2012; Oba, Takano, Furukawa, et al. 2022; Naraoka et al. 2023; Oba, Koga, et al. 2023; Parker et al. 2023; Glavin, Dworkin, et al. 2025), potentially seeding the early Earth with the necessary ingredients for the prebiotic soup (Pearce, Pudritz, et al. 2017).

There are various theories as to how and where the building blocks form and assemble, e.g., in space in interstellar clouds and protoplanetary disks (see, e.g., Sandford et al. 2020), inside the first rocky bodies formed in the solar system as explored in this thesis based on the previous work by Pearce and Pudritz (2016), or on Earth in the primordial atmosphere (Miller 1953; Catling and Kasting 2017), inside of deep-sea volcanoes (see, e.g., W. Martin, Baross, et al. 2008), or small bodies of water on land (see, e.g., Damer and Deamer 2020a). As the biomolecules assemble into more and more complex structures, new functions emerge as certain complexity thresholds are reached (Pascal et al. 2013), and abiotic matter undergoes several leaps of emergence (Deamer 2007), bringing it closer and closer to aliveness (Sutherland 2017).

There have been many recent advances in exploring the other celestial bodies in our solar system with spacecraft and their potential to host life, e.g., with the Cassini mission detecting organic molecules in the plumes ejected by Saturn's moon Enceladus (Postberg et al. 2018), or the currently ongoing Europa Clipper mission, which will soon investigate the subsurface ocean of Jupiter's moon Europa (Pappalardo et al. 2024) and prepare for a possible future landing mission (Hand et al. 2022).

With the discovery of the first exoplanets (Wolszczan and Frail 1992; Mayor and Queloz 1995; Anglada-Escudé et al. 2016), now numbering over 7000 confirmed exoplanets,[1] the search began for water on exoplanets (Tinetti et al. 2007; Taylor et al. 2023), in planet-forming disks (Perotti et al. 2023), and biosignatures in their atmospheres (Kaltenegger 2017), with recent breakthroughs thanks to the JWST space telescope. This makes it seem more and more realistic that we might actually have a chance of finding inhabited worlds beyond our solar system one day. And while playing with Drake (1965)'s equation, we can ask ourselves another fundamental question—Are we alone? And we can begin to dare to have a realistic hope, based on all these scientific advances, of finding an answer to these fundamental questions.

Perhaps it is the fact that these questions shake people to their core, with the big questions of how and ultimately why we came to be, often adding a kind of "spirituality" to them. While this creates a fascination in many people for the study

---

[1] A total of 7441 exoplanets have been confirmed at the time of this writing (28. March 2025, exoplanet.eu).

of the origins of life, it also, unfortunately, leads some scientists to “believe” too much in their favorite theory of the origins of life, fueling their confirmation bias. This unfortunately leads to what I personally like to call, and this is of course a deliberate exaggeration, something like a “religion war” between the different camps.

This can be easily experienced by attending scientific conferences on the origins of life and related fields such as astrobiology, where scientists regularly argue about which theory is the “right” one. It can be particularly shocking as a young student new to the field to find that many scientists are lost in the same delusions about their theories, as can be described by the quote from Carl Sagan above. By being married to their theories, some scientists lose the original objective of seeking to understand how the origins of life actually occur. Sometimes I am perplexed and saddened by the fact that some researchers completely reject new stimuli from other theories and fields of research, while it is precisely this interdisciplinarity that fascinates and motivates me to do this kind of science.

The solution to the highly complex problem of the origins of life requires an open-minded, interdisciplinary approach that constantly allows the introduction of new concepts from different theories and research fields, and seeks to unify them. The origins of life research community should rather welcome scientists from other fields who try to introduce new concepts into their research efforts, and everyone should have mercy if this is not immediately perfectly implemented by researchers who dare to look outside their own field, instead of judging how allegedly “wrong” someone approaches a concept that is new to them.

In this thesis, I will try to approach the various concepts involved in the origins of life in the most unbiased way possible. If I focus on one particular concept or scenario more than the others, it is so that I can limit myself to a scientific question that is feasible to complete and publish. I am aware that this thesis is heavily biased toward astrophysics, the concepts of the RNA world, and wet-dry cycles in warm little ponds, all of which will be introduced in more detail below. However, I try to integrate concepts that are more commonly used in other fields of research.

One example is the use of concepts commonly studied in the geosciences in the context of the origins of life, with a detailed and realistic treatment of serpentinization, as appropriate for the early Earth, and how it affects prebiotic synthesis. Another example is a study of the prebiotic synthesis of vitamin B_3, a molecule widely studied in biology, where it is known to be a key link between the storage of genetic information and the metabolic capabilities of modern life. Here, we will bring it into the context of planetary science, where it is not yet well recognized, by studying its possible formation in meteorite parent bodies. My motivation, hope, and main goal for this thesis is to help build bridges between all the fascinating scientific fields involved in the origins of life.

2

Origins of Life

2.1 RNA World

In 1994, NASA adopted the working definition of life as a “self-sustaining chemical system capable of Darwinian evolution” at the suggestion of Carl Sagan (Foreword by G. F. Joyce in Deamer and Fleischaker 1994; Benner 2010). This definition emphasizes that a living entity must consist of an assembly of molecules that can replicate in a self-sustaining way, the primary requirement for Darwinian evolution.[1] In short, it must be able to replicate itself without relying on any other system to help it in this process.[2]

Figure 2.1 provide an overview of the four different types of complex macromolecules used by living organisms today, namely DNA, RNA, proteins, and lipids. This in its entirety is also referred to as the “central dogma of life” (Morange 2008). DNA encodes the blueprint for proteins and enzymes in the sequence of the genetic letter molecules, the purines adenine and guanine, and the pyrimidines thymine and cytosine. These are transcribed into RNA using uracil instead of thymine. This requires several RNA polymerase enzymes, which are complexes of proteins (see Figure 2.1(B)). Both DNA and RNA consist of a sequence of nucleotide monomers. A nucleotide is composed of these genetic letter molecules, called nucleobases, bound to a sugar molecule, in the case of RNA D-ribose (D denotes the “right-handed” chirality of sugars in life), and in the case of DNA D-deoxyribose, and a phosphate (see Figure 2.1(A)). The nucleotide monomers are polymerized by an alternating linkage of the sugar and phosphate molecules, forming the so-called sugar-phosphate backbone in DNA and RNA.

RNA is translated into proteins, which are linked chains of L-α-amino acids

---

[1] Replication → Mutation → Selection

[2] This way of defining life would make it possible to exclude viruses, a kind of intermediate state between inanimate and animate matter, from the realm of living organisms, since viruses cannot reproduce without the help of a host cell.

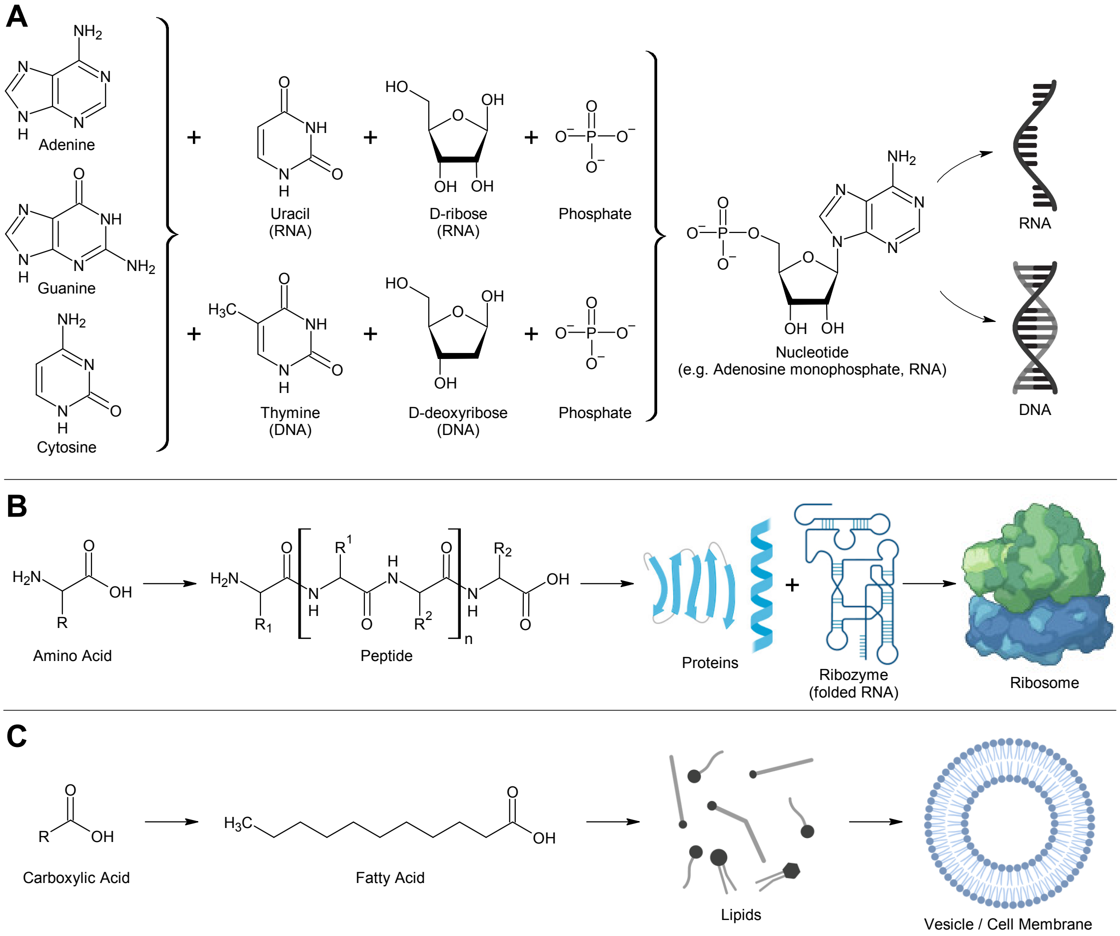

Figure 2.1: Overview of the molecules that make up the basic machinery of life. Panel **A** shows the building blocks of RNA and DNA, the nucleobases, the sugar (deoxy-)ribose, and phosphate. In the center, the top row shows the molecules specific to RNA, and the bottom row shows those specific to DNA. The nucleotide monomers are polymerized to the single-stranded RNA and double-stranded DNA sequences. Panel **B** shows how amino acids form peptides in their polymerized form. The side chains specific to each amino acid are located at the position marked R. These form the secondary structures of proteins (β-sheet and α-helix shown as examples), and can form complex tertiary and quaternary structures, e.g., in combination with ribozymes (folded strands of RNA) the ribosome, the key macromolecule for the translation of RNA into proteins. Panel **C** shows how carboxylic acids with long aliphatic side chains, called fatty acids, might have been the simplest lipids used by life to spontaneously form the first compartments in aqueous solution. Vesicles and the first protocellular membranes made it possible to encapsulate the molecules shown in panels **A** and **B** and to separate them from the open environment. Parts of panels **B** and **C** were created in BioRender.com.

called peptides. The set of 20 amino acids used by life are the so-called proteinogenic amino acids, all of which have “left-handed” L-chirality. This requires the ribosome molecule shown in Figure 2.1(B), which is itself a macromolecule made up of complexes of proteins and RNAs. The sequence for building ribosomes is encoded in the DNA (for more details in the context of the RNA world, see, e.g., Orgel 2004).

Both translation and transcription processes require complex enzymes, which in turn require themselves for their own synthesis. It seems impossible that such a complex machinery, involving three different types of highly complex and mutually compatible macromolecules, could have emerged spontaneously on Earth.

A solution to this “chicken or the egg” problem could be the discovery of ribozymes, RNA capable of enzymatic activity, and gives rise to the so-called RNA world hypothesis (see, e.g., A. Rich 1962; Gilbert 1986; Kruger et al. 1982; Guerrier-Takada, Gardiner, et al. 1983; Guerrier-Takada and Altman 1984; Zaug and Cech 1986; Cech 1986; Johnston et al. 2001; Vaidya et al. 2012; Attwater et al. 2018; Cojocaru and Unrau 2021; Kristoffersen et al. 2022). Ribozymes are strands of RNA that fold into themselves into a “double strand-like” structure (see Figure 2.1(B)), and are able to store genetic information in their sequence as well as replicate themselves (see, e.g., Paul and Joyce 2002). The active site inside the ribosome itself is formed by a ribozyme (Nissen et al. 2000), and might be a kind of “structural fossil” directly indicating its descent from the primordial RNA world (see, e.g., Noller 2012; Kawabata et al. 2022; Dance 2023, and refs. therein). Similar examples are transfer RNAs, small molecules that help decode messenger RNA into proteins, which are folded strands of RNA, and the intron/exon structure of DNA and RNA as a remnant of the first self-altering processes in RNA, all of which might be distant descendants of these first ribozymes.

During abiogenesis, RNA could have been the first step toward chemical evolution and ultimately the origin of life, without requiring the problematic simultaneous formation of compatible proteins. Ribozymes replace proteins in their function as enzymes, allowing a self-sustaining, self-replicating, and much simpler chemical system. By making imperfect copies of themselves, ribozymes also allow for the first appearance of Darwinian evolution, as stated above in NASA’s working definition of life.

DNA might have only appeared later, allowing for less error-prone storage of genetic information in its double-stranded structure, and ribozymes were either improved by incorporating proteins into their structures, as in the case of the ribosome, or were even completely replaced by proteins, forming enzymes with optimized function and the ability to be regulated in the fine-tuned metabolisms of modern living organisms.

2.1.1 Eigen's Paradox

A challenge to the RNA world hypothesis is Eigen's paradox, proposed by Eigen (1971) in his theory of the hypercycle, which links several self-replicating molecules into a closed system, leading to its autocatalytic self-replication as a whole. As visualized in Figure 2.2, the idea is to see a ribozyme as a replicator p that makes copies of itself with a reaction rate of α, but there is a certain probability of error in each such copying process, called the mutation rate μ. This generates a parasite p, in this example also a ribozyme, which can also make copies of itself with a rate of γ.

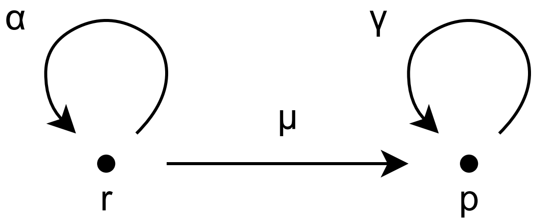

Figure 2.2: Replicator p (ribozyme), which creates copies of itself at rate α, and mutates at rate μ into parasite p (also ribozyme), which also creates copies of itself at rate γ.

The chemical reactions can be summarized by the following simple set of ordinary differential equations (t is time):

$$\begin{cases} dr/dt = \dot{r} = \alpha r - \mu r \\ \dot{p} = \mu r + \gamma p \end{cases} \tag{2.1}$$

This system can be summarized by introducing the vector $\vec{x}$ and a matrix M as

$$\vec{x} = \begin{pmatrix} r \\ p \end{pmatrix} \tag{2.2}$$

$$M = \begin{pmatrix} \alpha - \mu & 0 \\ \mu & \gamma \end{pmatrix} \tag{2.3}$$

$$\dot{\vec{x}} = M\vec{x}. \tag{2.4}$$

A typical solution of such a system of equations is

$$\vec{x}(t) = \exp(Mt)\vec{x}_0 \tag{2.5}$$

with the initial conditions, here the initial concentrations of r and p, summarized in the vector $\vec{x}_0$.

This can be expressed by diagonalizing the matrix with the eigenvectors $\vec{v}_1$ and $\vec{v}_2$ and the eigenvalues λ_1 and λ_2 as

$$M = \begin{pmatrix} \vec{v}_1 & \vec{v}_2 \end{pmatrix} \begin{pmatrix} \lambda_1 & 0 \\ 0 & \lambda_2 \end{pmatrix} \begin{pmatrix} \vec{v}_1 & \vec{v}_2 \end{pmatrix}^{-1}, \tag{2.6}$$

$$\vec{y} \coloneqq \begin{pmatrix} \vec{v}_1 & \vec{v}_2 \end{pmatrix}^{-1} \vec{x}_0, \tag{2.7}$$

$$\vec{x}(t) = \begin{pmatrix} \vec{v}_1 & \vec{v}_2 \end{pmatrix} \begin{pmatrix} \exp(\lambda_1 t) & 0 \\ 0 & \exp(\lambda_2 t) \end{pmatrix} \vec{y} \tag{2.8}$$

$$= \left(\sum_i \vec{v}_i \exp(\lambda_i t) \right) \vec{y}. \tag{2.9}$$

According to the Perron-Frobenius theorem, the term with the largest eigenvalue will dominate for $t \to \infty$, since its exponential term grows the fastest. Defining the largest eigenvalue as λ_1 therefore yields

$$\vec{x}(t) \propto \vec{v}_1 \exp(\lambda_1 t) \vec{y} \quad \text{for} \quad t \to \infty \tag{2.10}$$

Since M is a lower triangular matrix, its eigenvalues are simply the entries on its diagonal, so $\lambda_1 = \alpha - \mu$ and $\lambda_2 = \gamma$ (see Equation (2.3)).

Assuming that we want the replicator r to survive in some kind of Darwinian evolution, this means that the eigenvalue including the replication rate of r must be the largest to guarantee its survival in this dynamical system, which results in

$$r \text{ survives} \iff \alpha - \mu > \gamma. \tag{2.11}$$

Returning to the fact that the replicators r and p are ribozymes, we can define the length of their chain of nucleotide monomers as L, and the error rate ϵ for attaching the wrong next nucleotide during the self-copying process. This allows us to rewrite the term $\alpha - \mu$, which describes the rate difference between correctly replicating r and incorrectly mutating it to p for L consecutive attachments of nucleotides, by introducing the fidelity ϕ as

$$\phi = (1 - \epsilon)^L \tag{2.12}$$

$$\lambda_1 = \alpha - \mu = \alpha\phi = \alpha(1 - \epsilon)^L. \tag{2.13}$$

Putting this back into Equation (2.11) gives

$$\alpha(1 - \epsilon)^L > \gamma \tag{2.14}$$

$$L \ln(1 - \epsilon) > \ln\left(\frac{\gamma}{\alpha}\right) \tag{2.15}$$

Assuming that the error rate is very small, i.e. $\epsilon \ll 1$, we can Taylor expand the term $\ln(1-\epsilon) \approx -\epsilon$, which leads to Eigen's paradox

$$L < \frac{\ln\left(\frac{\alpha}{\gamma}\right)}{\epsilon}. \tag{2.16}$$

The replicator r competes with the parasite p for resources, following Darwin's idea of "survival of the fittest", directly expressed in the selectivity $\frac{\alpha}{\gamma}$, which captures which replicator is better at reproduction.

The problem in the context of the origins of life is now that the length L and the error rate ϵ of a ribozyme are mutually correlated. A ribozyme must be of a certain length L in order to have a sufficiently low error rate ϵ to be able to replicate itself properly, making it a true replicate. However, according to Eigen's paradox in Equation (2.16), the length L of a nascent ribozyme, which is still a short and thus error-prone replicase, is fundamentally capped by its still poor error rate ϵ.

This makes it impossible to evolve this ribozyme from scratch by gradually increasing its length to improve its error rate. Rather, a spontaneous jump to an already long, reliably self-copying and therefore complex ribozyme would be necessary, similar to the initial problem with the origins of life, which required all the complex machinery shown in Figure 2.1. This potentially undermines the whole idea of the RNA world.

2.2 Compartments and Metabolism

To the rescue might come compartmentalization, such as cell membranes, which are the fourth critical component of life today. Figure 2.1(C) gives an overview of the building blocks of cell membranes in life, allowing the inside, containing the molecules in Figure 2.1(A) and (B), to be separated from the outside, allowing the molecules to concentrate and evolve safely without being disturbed or diluted. The earliest life probably formed the first small vesicles and protocell membranes from simple fatty acids, which are carboxylic acids with long aliphatic chains (Deamer, Dworkin, et al. 2002; Lai et al. 2019). Due to their amphiphilic nature with a hydrophilic carboxylic group on one side and their hydrophobic tail on the other side, these molecules can spontaneously assemble in aqueous solution into small compartments (Markvoort et al. 2010) and encapsulate other prebiotic molecules (Deamer, Dworkin, et al. 2002). In the context of life, these molecules are generalized to the class of lipids, with modern life using the more complex phospholipids.

In a mathematical formalism equivalent to Section 2.1.1, Blokhuis et al. (2018) showed that incorporating replicators into compartments and introducing selection before re-pooling them and introducing the next so-called transient compartmentalization can prevent parasites from completely taking over and killing the system. This effectively leads to a relaxation of the constraint in Equation (2.11) to $\alpha - \mu < \gamma$, thus circumventing Eigen's paradox in Equation (2.16).

Prior to the formation of the first vesicles from lipids, these compartments could also have been formed by simpler means more realistic for the origins of life on the early Earth. The use of oil droplets and the introduction of this selection protocol made it possible to successfully demonstrate this coexistence of ribozymes and parasitic ribozymes in laboratory experiments (Matsumura et al. 2016). This opens up the possibility of opportunistic functionality, where parasites not only coexist, but introduce the necessary mutation for Darwinian evolution, and parasites gain "useful" new functions, evolving into the next generation of replicators.

Furthermore, by theoretically studying real ribozymes, Kun et al. (2005) showed that these ribozymes undergo many mutations that are neutral to the fitness of the ribozyme. A slight improvement in their error rate allows them to grow to more than 7000 nucleotides, which coincides with the genome size estimated for the minimal cell, when sequences involved in translation, such as the genes encoding the structure of the ribosome on the right in Figure 2.1(B), are removed.

This allows us to move closer to a unification of the RNA world with the so-called metabolism first dogma, which itself proposes that life did not originate from RNA, but from complex sets of metabolites. Kauffman (1986) suggested that autocatalytic sets of proteins might have formed the basis of chemical evolution and the origins of life, with RNA appearing later. However, the recent developments in both the RNA world and metabolism first theories, including the proposed solutions to Eigen's paradox above, lead to a unification of these previously competing theories of the origins of life in a combined RNA-peptide world (see, e.g., Di Giulio 1997; Müller et al. 2022). Gánti (2003, first published in 1971 in Hungarian) developed the model of the chemoton (chemical automaton), which represents an independently developed extension of Eigen (1971)'s hypercycle model, including intertwined autocatalytic self-replicating systems of information-storing molecules (e.g., RNA), metabolites, and an enclosing compartment.

Another interesting molecule that helps unify metabolism with the RNA world is vitamin B_3 (see top left in Figure 3.1 below). It can replace a nucleobase in a modified nucleotide, forming a nucleotide dimer together with adenosine monophosphate (see Figure 2.1(A)), resulting in the coenzyme NAD(P)($^+$/H) (see Part IV and Figure 17.1 for details). This modified RNA dimer is directly linked to the metabolism in life, enabling cellular redox reactions and energy production (see, e.g., Friedkin and Lehninger 1949; P. Rich 2003). Moreover, in studies of autocatalytic reaction networks within the framework of Kauffman (1986)'s formalism, NAD($^+$/H) has been identified as a key catalyst, greatly expanding the complexity of autocatalytic sets as they might have appeared in the origins of life (Xavier et al. 2020).

2.3 Reaction Pathways

2.3.1 Miller-Urey Experiment

One of the first and most famous experiments demonstrating the prebiotic synthesis of key biomolecules[3] were the Miller-Urey experiments. Using a cyclic configuration of reaction vessels, Miller (1953) and Urey attempted to replicate the conditions on the early Earth. Early Earth conditions are simulated by heating water (representing an ancient ocean) and passing the vapor through a reducing gas mixture of H_2 (molecular hydrogen), CH_4 (methane), and NH_3 (ammonia), which was proposed by Oparin (1924) and Haldane (1929) to represent the composition of the early Earth's atmosphere. The energy needed to produce basic organic matter is provided by electrical discharges that mimic lightning in the early Earth's atmosphere.

In the residue left after the experiments were run for a long time, amino acids were found as biologically significant compounds. This made these experiments a great success that was widely recognized in the scientific community, as it was the first time this was shown in an experiment trying to emulate realistic conditions on the early Earth (Miller 1953). As a key intermediate molecule, the formation of HCN (hydrogen cyanide) was found to be a key driver for the amino acid synthesis (Miller and Urey 1959). UV light was also shown to lead to prebiotic synthesis (Miller and Urey 1959, and refs. therin), and in more modern versions of the experiments the formation of nucleobases was also demonstrated (Ferus, Pietrucci, Saitta, Knížek, et al. 2017; Miyakawa et al. 2002). Sagan and Khare (1979) demonstrated the formation of tholins, complex mixtures of organic molecules including nitriles (e.g., HCN is a nitrile) and hydrocarbons, similar to the organics found in the hazy atmosphere of Saturn's moon Titan.

The important requirement for this prebiotic synthesis was that the atmospheric composition used was rich in reducing gases. This was later questioned and it was assumed that the primordial atmosphere of Earth was more neutral or even oxidizing (see, e.g., Chyba and Sagan 1992; Johansen, Camprubi, et al. 2024). Some experiments showed that the synthesis of prebiotic molecules was still possible under less reducing conditions (see, e.g., Miyakawa et al. 2002; Cleaves, Chalmers, et al. 2008), but with lower yields. This has since become a much debated point in the

---

[3] The terms prebiotic precursor, prebiotic molecule, and biomolecule are used somewhat interchangeably in this thesis. Roughly speaking, a prebiotic precursor is less complex than a prebiotic molecule and could be widely available from the environment, and biomolecules refer to molecules as used by life today. However, the transition between these terms is fuzzy and fluid.

scientific community, and is often used as an argument against the origin of life in surface environments, as will be introduced in Section 4.3.

2.3.2 Strecker Synthesis

The underlying chemical pathway to amino acids formation is the Strecker (1850) and Strecker (1854) synthesis, which starts with an aldehyde (R−CH=O), and by reaction with NH_3 (ammonia) and HCN forms an α-amino acid (see Figure 2.1(B)). The reaction

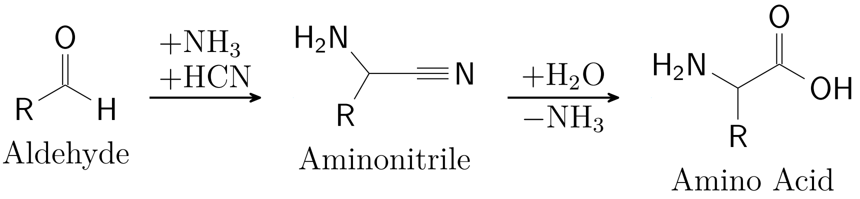

(2.17)

produced an aminonitrile as an intermediate. For example, starting with H_2CO (formaldehyde) leads to the formation of glycine ($C_2H_5NO_2$), the simplest amino acid used by life. The reaction can be summarized as

$$H_2CO + HCN + H_2O + NH_3 \longrightarrow C_2H_5NO_2 + NH_3. \tag{2.18}$$

2.3.3 Fischer-Tropsch Reaction

Another key reaction is the Fisher-Tropsch reaction, which allows the formation of hydrocarbons from H_2 and CO (carbon monoxide) according to the general equation (Dry 2002)

$$(2\,\mathrm{n} + 1)\, H_2 + n\, CO \longrightarrow C_nH_{2n+2} + n\, H_2O. \tag{2.19}$$

In its simplest form for $n = 1$ this leads to the formation of CH_4, a key reducing gas enabling prebiotic synthesis, e.g., in the Miller-Urey experiments discussed above. By adding NH_3 and using metal catalysts, it has been shown experimentally that the Fischer-Tropsch type reaction leads to the formation of nucleobases (Hayatsu, Studier, Oda, et al. 1968; Hayatsu, Studier, Matsuoka, et al. 1972; Yang and Oró 1971).

2.3.4 Formose Reaction

The abiotic way to make sugars from scratch is the formose reaction, which was discovered by Butlerow (1861). The first chemical mechanism was proposed by Breslow (1959). The reaction is a catalyzed reaction of formaldehyde to sugar molecules ($C_nH_{2n}O_n$) and starts with the initial presence of glycolaldehyde ($C_2H_4O_2$), which is sufficient even if present in minute amounts (Socha et al. 1980).

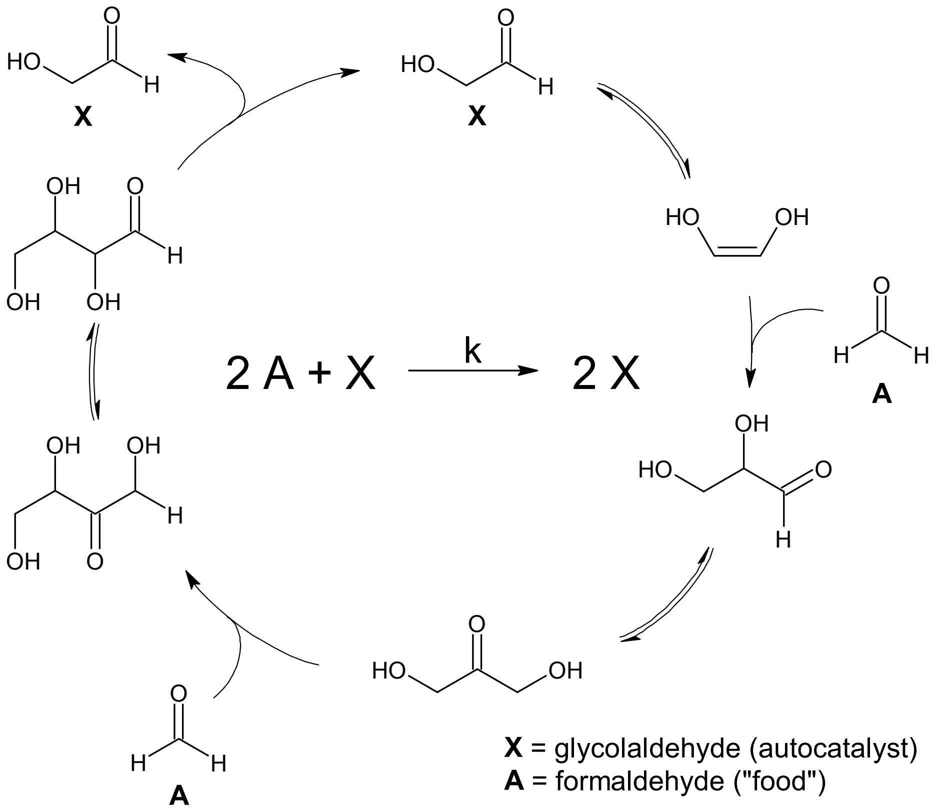

Figure 2.3: The core autocatalytic cycle of the formose reaction.

Figure 2.3 shows the key mechanism of the formose reaction, its autocatalytic cycle. The formose reaction is the only simple chemical reaction known to be involved in the synthesis of prebiotic molecules, making it particularly interesting because replicating molecules, such as the much more complex ribozymes, are a key feature of living organisms. Glycolaldehyde is the autocatalyst, a simple chemical form of a replicator that uses formaldehyde as a supply molecule, also called the "food" of the replicator. With an exponentially increasing reaction rate, glycolaldehyde generates more and more copies of itself until it eventually runs out of formaldehyde, with the reaction rate slowing asymptotically and entering a saturation state. This typical "S" curve of the reaction rate allows a clear identification of an autocatalytic reaction. It was originally thought that formaldehyde alone was sufficient to initiate the formose reaction, in which two formaldehyde molecules form a dimer, creating the first glycolaldehyde and starting the cycle. But when a formose reaction was observed to occur in a formaldehyde solution, it was only due to impurities (Socha et al. 1980).

Typical catalysts are hydroxides and carbonates that form alkaline solutions, but the list of possible catalysts of the formose reaction is vast (Iqbal and Novalin 2012). Figure 2.3 shows how glycolaldehyde can be converted to dihydroxyethene by reversible tautomerization, which in turn forms glyceraldehyde by addition of formaldehyde in an aldol reaction. Another tautomerization leads to dihydroxyacetone, and another addition of formaldehyde in an aldol reaction leads to erythrulose. A final tautomerization leads to an aldotetrose, which splits into two glycolaldehyde molecules in a retro-aldol reaction, completing the autocatalytic cycle. The autocatalytic reaction of this core cycle can be summarized as

$$2\,\mathrm{H_2CO} + \mathrm{C_2H_4O_2} \longrightarrow 2\,\mathrm{C_2H_4O_2}. \tag{2.20}$$

Branching off from glyceraldehyde and dihydroxyacetone, more complex sugars such as pentoses (including ribose, see Figure 2.1(A)) and hexoses can be formed. This happens via a very complex network of reactions, not shown in the vastly simplified Figure 2.3. In addition, there are several decomposition reactions, such as the Cannizzaro (1853) reaction that decomposes formaldehyde to methanol and formate, β-elimination to dicarbonyls, the benzilic acid rearrangement, oxidation, and more (see, e.g., De Bruijn et al. 1986).

The complexity of the reaction network, which produces up to 40 products, its high sensitivity to small changes in the reaction conditions, and its autocatalytic nature make it notoriously difficult to quantify and model in detail, so that parts of its chemical mechanism are still not understood (see, e.g., Weiss et al. 1970; Niitsu et al. 1992; Rauchfuß 2005).

3

Prebiotic Molecules in Space

3.1 Interstellar Medium and Protoplanetary Disks

At first glance, space seems empty and, from the perspective of life, dead. But this is far from the truth. Space is actually full of complex molecules, some of which are organic, some of which are the same molecules we find in our bodies, and some of which are precursors to these biologically relevant molecules. To date, about 330 molecules have been detected in the interstellar medium (see the Cologne Database[1], Endres et al. 2016). For example, nitrogen sources such as NH_3 and HCN, which are crucial for the formation of nucleobases, are widely observed around young stars (Salinas et al. 2016; Pascucci et al. 2009).

Most of the prebiotic synthesis in space occurs in the interstellar medium (ISM) in dense interstellar clouds (Sandford et al. 2020), and in protostellar and protoplanetary disks (Henning and Semenov 2013; Öberg, Facchini, et al. 2023), the birthplaces of new stars and planets. In the context of the solar system, its protoplanetary nebula and disk are also called the solar nebula.

A crucial component for the reaction of molecules are dust grains. On their surface, ices of various volatiles can form, enabling the reaction of the adsorbed molecules due to multiple processes (Potapov and McCoustra 2021; Cuppen, Linnartz, et al. 2024). Examples are the migration of molecules and radicals formed by irradiation on their surface, allowing them to meet and react, potential catalytic capabilities of the surface depending on the composition of the grain (e.g., silicates or carbon), and the grain can act as a substrate absorbing excess energy generated in the reaction between the molecules, preventing their immediate destruction by absorbing this energy by acting as a third body (see, e.g., Pantaleone et al. 2021). In the context of the solar nebula, these ice-covered dust grains are also called icy

---

[1] `https://cdms.astro.uni-koeln.de/classic/molecules`, accessed on 12. March 2025.

pebbles as they begin to grow.

It is important to understand how the volatile ices on the surface of the dust grains behave as they begin to drift inward in protoplanetary disks (Birnstiel 2024), as this determines how much of these volatiles are available for organic and prebiotic synthesis in different regions of the disk. For this purpose, temperature programmed desorption (TPD) experiments are performed in the laboratory (Cuppen, Linnartz, et al. 2024). Ice of the desired composition is grown at a temperature of about 10 K and slowly heated, simulating the radial drift of dust grains in the solar nebula inward toward the proto-Sun. The desorption of the volatiles is measured, defining so-called snowlines.

Snowlines in protoplanetary disks (Pontoppidan et al. 2014) are not only important for chemical reactions, but also play a critical role as the site of the formation of the first planetesimals (Johansen, Oishi, Mac Low, et al. 2007; Johansen, J. Blum, et al. 2014a; Ormel and Klahr 2010; Klahr and Schreiber 2020a), precursors of asteroids and planets. In addition to the classical snowline for water, Öberg, Murray-Clay, et al. (2011) has popularized the CO snowline as a key feature of planet formation theories and its influence on the resulting composition of giant planet atmospheres. In contrast, TPD experiments of CO-H_2O ices have shown that the major desorption of CO occurs at much higher temperatures due to trapping effects within the water ice matrix, which desorbs at much higher temperatures (Ayotte et al. 2001; Collings et al. 2004). This challenges the notion of singular snowlines and implies that there are in fact multiple snowlines. Thus, this has significant implications for planet formation and the amount of volatiles present in planetesimals formed in the early solar system.

3.2 Planetesimals

Recently, there has been a boom in spacecraft missions visiting some of the many small bodies floating through our solar system. Probably the best known is ESA's Rosetta mission, which visited and orbited comet 67P/Churyumov–Gerasimenko and landed on its surface with the Philae module (Glassmeier et al. 2007). As the most complex biologically relevant molecule, the amino acid glycine was found in particles collected from the coma ejected by the comet (Altwegg, Balsiger, Bar-Nun, et al. 2016).

However, an even richer inventory of prebiotic molecules floating through our solar system has been revealed by the recent sample return missions to asteroids. Figure 3.1 shows on the lower left the carbonaceous asteroid (162173) Ryugu, which was visited by the JAXA Hayabusa2 sample return mission (S.-i. Watanabe et al. 2017). After sampling directly from the asteroid's surface, the samples were returned

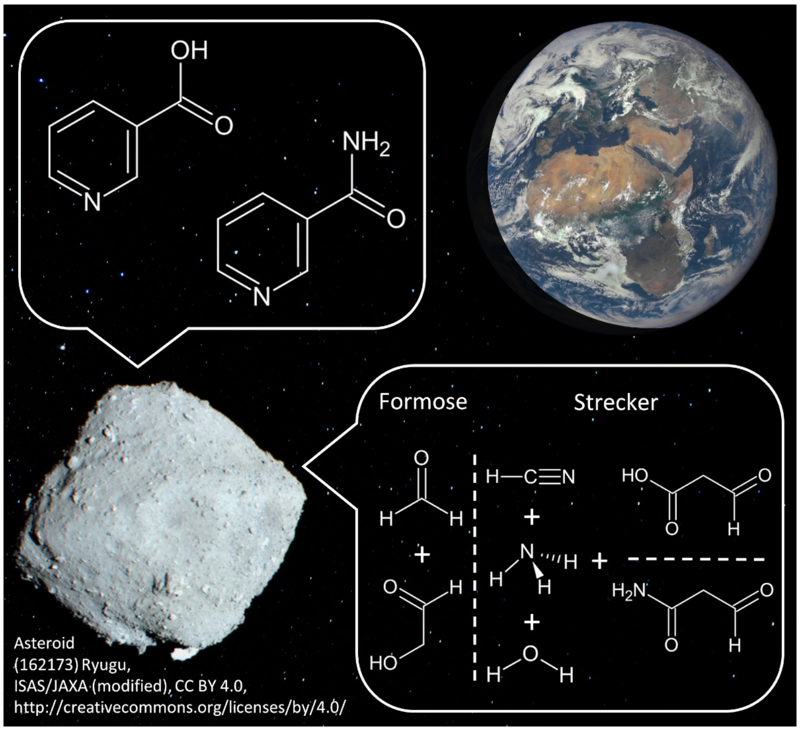

Asteroid
(162173) Ryugu,
ISAS/JAXA (modified), CC BY 4.0,
http://creativecommons.org/licenses/by/4.0/

Figure 3.1: Present-day asteroids such as (162173) Ryugu (lower left) contain many prebiotic molecules and might be remnants of planetesimals that formed in our early solar system. These planetesimals might contain liquid water in their interiors due to radiogenic heating, allowing complex organic chemistry to form these prebiotic molecules. Image from Paschek, M. Lee, et al. (2024b), own creation.

to Earth, and analyzed in laboratories. Several proteinogenic amino acids, carboxylic acids (Naraoka et al. 2023; Parker et al. 2023), the RNA building block uracil, and vitamin B_3 (see top left in Figure 3.1) were found in the recovered material (Oba, Koga, et al. 2023).

The most recent sample return mission was NASA's OSIRIS-REx mission, which visited the carbonaceous asteroid (101955) Bennu (Lauretta et al. 2017), sampled the surface, and returned the collected material to Earth in September 2023. Laboratory analysis revealed the presence of a comprehensive collection of prebiotic molecules, including 33 amino acids, 14 of which are proteinogenic, carboxylic acids, all five nucleobases found in RNA and DNA, formaldehyde, the key supply molecule in the formose sugar synthesis, and many more (Glavin, Dworkin, et al. 2025).

This raises the question of where these prebiotic molecules could come from. There are two scenarios for their origin. The first possibility is that the molecules were formed in the interstellar and interplanetary environment as described in Section 3.1, and inherited from the solar nebula during the formation process of the original planetesimal body, incorporating the molecules during the accretion process. The asteroid as we find it today in the solar system might be a fragment left over from the original parent body after collisions with other planetesimals.

The analysis of the ratio of the hydrogen isotopes helps to understand whether the prebiotic molecules were inherited from the ISM and the interplanetary medium. When the molecules formed at the low temperatures of 10–30 K in the ISM, molecules including deuterium (D) may be enriched compared to molecules formed at higher temperatures. Due to the higher mass of deuterium, molecules containing deuterium have a higher dissociation energy and therefore a higher thermodynamic favorability to be formed compared to their non-deuterated counterparts (Ceccarelli et al. 2014). The isotopic fractionation depends on the dissociation energy difference between the different isotopomers ΔE and temperature T proportional to $\exp(-\Delta E/T)$ (Pizzarello and Shock 2010), leading to a deuterium enrichment especially at the low temperatures prevailing in the ISM. The analysis of the D/H ratios of the organic matter found in meteorites, which could also derive as fragments from the same parent bodies (Burbine, Mccoy, et al. 2002; Yada et al. 2022; Nakamura et al. 2022; Pilorget et al. 2022; Yokoyama et al. 2022; Oba, Koga, et al. 2023), indicates a D enrichment. The values are not as high as those found in the ISM, indicating that some organic molecules were inherited from the ISM, including prebiotic molecules and their precursors, but also chemical reactions at higher temperatures have contributed to their formation (see, e.g., Pizzarello and Shock 2010).

These reactions at higher temperatures lead us to the other possibility for the origin of the plethora of prebiotic molecules found inside planetesimals, in situ formation inside the asteroid's parent body. Radiogenic heating inside the planetesimal, particularly by the short-lived isotope ^{26}Al in the early solar system (see, e.g., Cameron and Truran 1977; Fujiya et al. 2012; Gaches et al. 2020), warms the interior of the planetesimal. Inside the porous body, water ice accreted from the solar nebula might become liquid, as illustrated in Figure 3.2. The presence of salts in the samples returned from Bennu (McCoy et al. 2025) is direct evidence for the former presence of brine, highly concentrated salt water, and thus for the former presence of liquid water in its interior. These salt deposits were likely formed as the water in its interior was evaporated, either due to the internal heating or as Bennu migrated from the outer regions of the solar system closer to the Sun. This likely presence of liquid water in the interior of the parent body might have allowed for aqueous chemistry to be possible, allowing for the effective synthesis of prebiotic molecules, as described in Section 2.3.

Finally, as mentioned above, these planetesimals might also be the parent bodies of meteorites. The aqueous chemistry might allow the synthesis of prebiotic molecules to be pushed to much higher complexities. This might explain the much richer organic molecular inventory of asteroids and meteorites (see next Section) compared to comets, which remain in the frozen phase, as becomes clear when comparing the prebiotic molecules found in carbonaceous asteroids and comets in the

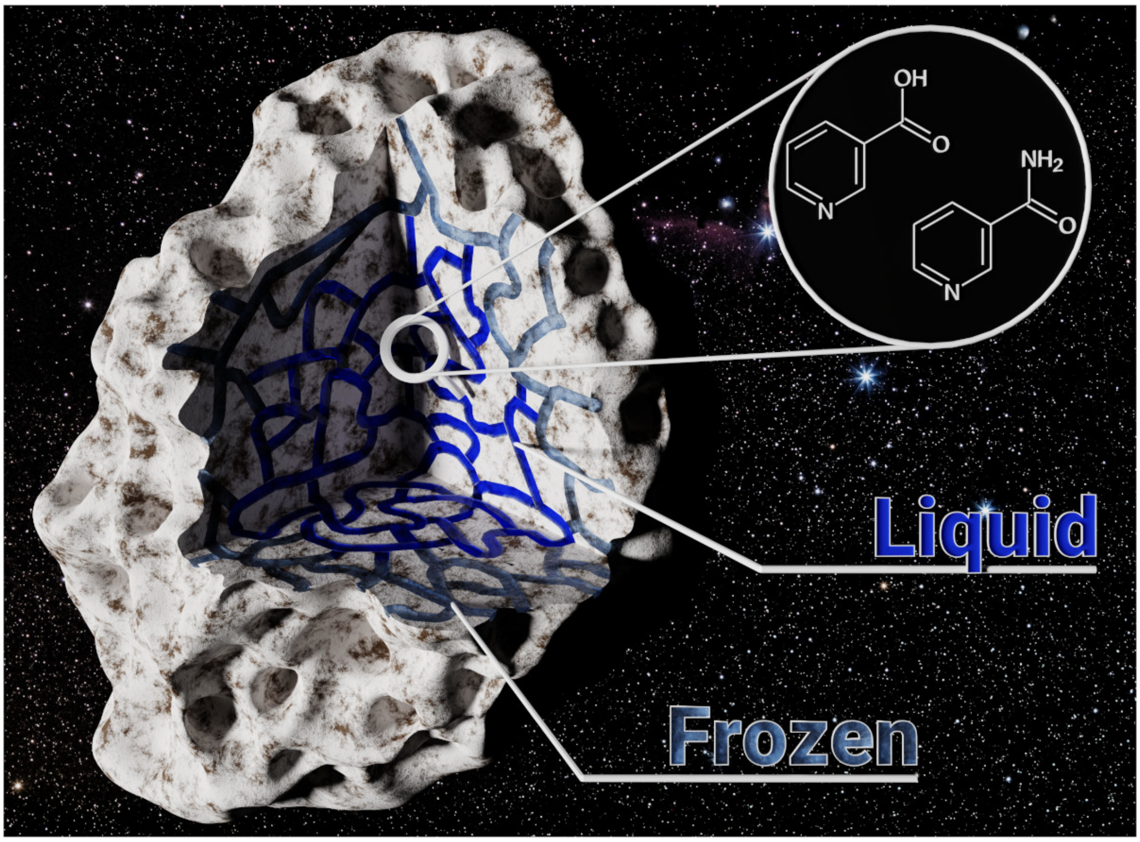

Figure 3.2: The interior of a planetesimal formed in the early solar system might contain liquid water due to radiogenic heating. Inside the porous body, liquid water might be trapped by an outer shell of frozen pores, allowing the aqueous synthesis of key prebiotic molecules. Image modified from Paschek, M. Lee, et al. (2024a), artist's impression, own creation.

sample return missions described above.

3.3 Meteorites

Meteorites are mainly divided into three categories, chondrites, achondrites (both stony meteorites), and iron meteorites, although the actual classification is more complex (Krot et al. 2007). Achondrites and iron meteorites probably originated from parent bodies that melted completely due to the radiogenic heating in the early solar system. This led to a separation of heavy iron, which sank to the core, the origin of the iron meteorites, and lighter stony material, e.g., silicates, which remained closer to the surface from which achondrites were derived.

Chondrites, on the other hand, might originate from unmelted and undifferentiated parent bodies and show small chondrules, directly representing the small pebbles accreted by the planetesimal during its formation. Due to the lack of differentiation of the parent body, metals are also present, especially NiFe alloys. Chondrites are further divided into ordinary chondrites, enstatite chondrites, and carbonaceous

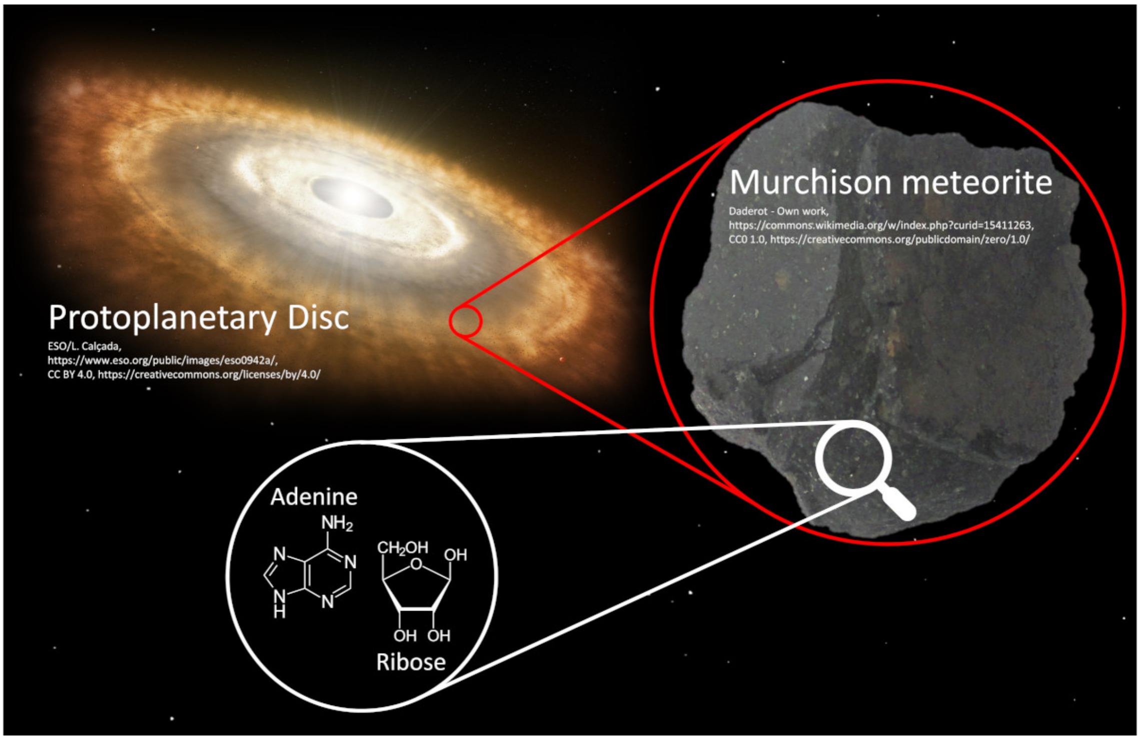

ESO/L. Calçada, https://www.eso.org/public/images/eso0942a/, CC BY 4.0, https://creativecommons.org/licenses/by/4.0/

Daderot - Own work, https://commons.wikimedia.org/w/index.php?curid=15411263, CC0 1.0, https://creativecommons.org/publicdomain/zero/1.0/

Figure 3.3: Carbonaceous chondrites, a class of carbon-rich meteorites, contain an abundance of prebiotic molecules that might have been formed in the protoplanetary disk stage of our solar nebula. Image from Paschek, Kohler, et al. (2022), own creation.

chondrites. Ordinary chondrites are divided into the LL, L, and H types, with low metal plus low iron, low metal, and high metal content, respectively. The peculiarity of enstatite meteorites is their high proportion of reduced iron (Krot et al. 2007), which makes them an interesting material to provide a reducing potential for the prebiotic pathways described in Section 2.3, and as explored in Part V.

Finally, carbonaceous chondrites are particularly rich in carbon and water and contain a plethora of organics (Krot et al. 2007), which makes them particularly interesting in the context of the origin of life. The right side of Figure 3.3 shows a fragment of the famous Murchison meteorite fall, which has revealed a wide variety of biomolecules in laboratory studies. These include many biomolecules relevant for life, such as nucleobases (Callahan et al. 2011; Shimoyama et al. 1990; Stoks and Schwartz 1981; Stoks and Schwartz 1979; Velden and Schwartz 1977; Pearce and Pudritz 2015; Oba, Takano, Furukawa, et al. 2022), the sugar ribose (Furukawa et al. 2019), amino acids (A. K. Cobb and Pudritz 2014b, see refs. therein), carboxylic acids (Lai et al. 2019, see refs. therein), and vitamin B_3 (Smith et al. 2014; Oba, Takano, Furukawa, et al. 2022).

Carbonaceous chondrites are classified into groups that reflect similar bulk mineralogical compositions. The names of these groups are derived from representative meteorite falls, typically the first to be recorded. The names follow the two-letter

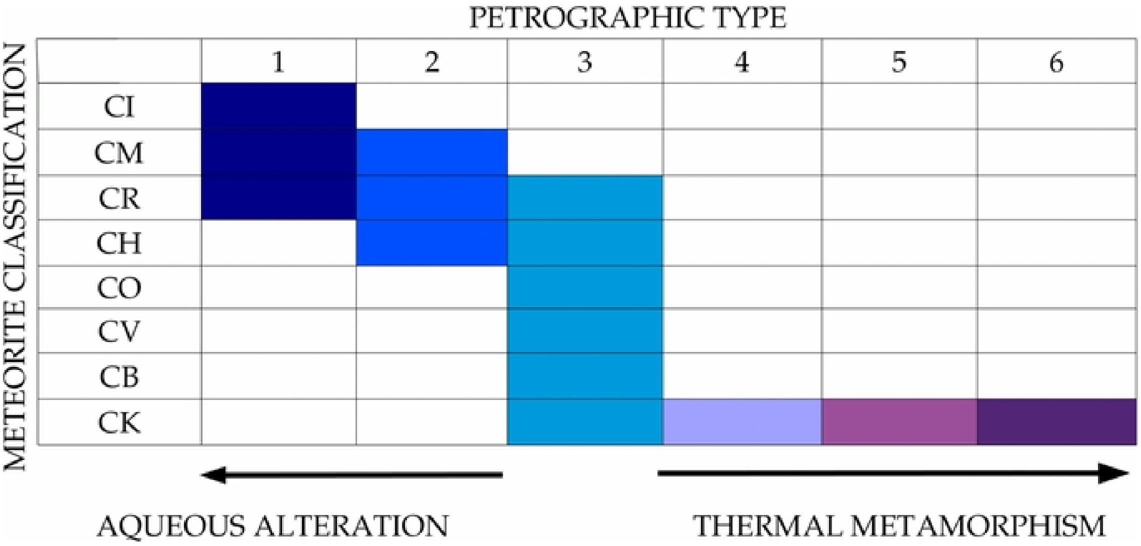

	1	2	3	4	5	6
CI	🟦					
CM	🟦	🟦				
CR	🟦	🟦	🟦			
CH		🟦	🟦			
CO			🟦			
CV			🟦			
CB			🟦			
CK			🟦	🟪	🟪	🟪

Figure 3.4: Classification of carbonaceous chondrite groups into petrographic types. Plot from A. K. Cobb and Pudritz (2014b).

'CX' naming system, where 'C' stands for "carbonaceous" and 'X' for the first letter of the representative fall. The petrographic type is indicated by the number following these two letters. Figure 3.4 gives an overview of these groups and indicates which group has a member that has been sorted into the respective type. From '3' to '2' to '1' the alteration by liquid water, the so-called aqueous alteration of the meteorite material, increases. '3' and above indicates thermal metamorphic alteration of the rock material, which increases with increasing number, while '3.0' indicates the most pristine state, completely unaltered by any metamorphic or aqueous influences. The higher the aqueous or metamorphic alteration, the less distinct the chondrules can be recognized, and with increasing thermal metamorphism, the temperature the material experienced in the parent body increases, but the exact temperature ranges are debated (A. K. Cobb and Pudritz 2014b).

Some groups might possibly be derived from a shared parent body and sometimes have been directly linked to present-day asteroids, e.g., the CI chondrites might share a parent body with Ryugu (Yada et al. 2022; Nakamura et al. 2022; Pilorget et al. 2022; Yokoyama et al. 2022; Oba, Koga, et al. 2023) and CM chondrites might share a parent body with (19) Fortuna and (13) Egeria (Burbine 1998; Burbine, Mccoy, et al. 2002). This demonstrates the direct link between planetesimals formed in the early solar system and meteorites impacting the Earth, possibly seeding it with the building blocks of life (Pearce, Pudritz, et al. 2017).

In the predominant literature, there is a widespread notion that the influence of liquid water in the parent bodies is merely a destructive mechanism that degrades prebiotic molecules inherited from space, hence the term aqueous *alteration* (see, e.g., Smith et al. 2014; Oba, Takano, Furukawa, et al. 2022). In this thesis, in Parts II to IV, we want to challenge this dogma in the research community and propose that aqueous alteration might in fact allow the synthesis of original prebiotic molecules in the interior of meteorite parent bodies, planetesimals formed in the early solar system, by aqueous chemistry, building on and extending the previous work by A. K. Cobb, Pudritz, and Pearce (2015), Pearce and Pudritz (2016), and Pearce, Pudritz, et al. (2017).

Prebiotic Molecules on the Hadean Earth 4

The Hadean is the first geologic eon on the geologic time scale, beginning with the formation of the Earth and the solar system at 4.567 Gyr, dated by calcium-aluminum-rich inclusions in meteorites (Dalrymple 2001), and ending at 4 Gyr. At about 4.52–4.42 Gyr, a collision between the proto-Earth (named Gaia) and another planetary embryo (named Theia) created the Moon (Pearce, Tupper, et al. 2018), referred to as the Moon-forming impact. The Hadean Earth was probably dominated by a global ocean, and the first land masses emerged, volcanic islands created by hotspot volcanism. These get pushed together by the onset of plate tectonics to form the first continental crust, which may have reached above sea level (Korenaga 2021). The only surviving minerals from this time are zircons ($ZrSiO_4$, Harrison 2009), the oldest dating back to 4.4 Gyr (Wilde et al. 2001), while the rock record only reaches back to the Archean, the next geologic eon. The earliest signs of life date back to 3.7 Gyr (Ohtomo et al. 2014; Pearce, Tupper, et al. 2018), possibly even 4.1 Gyr (Bell et al. 2015), derived from biologically fractionated $^{12}C/^{13}C$ isotopic studies (life prefers to fix ^{12}C over ^{13}C in its organic matter) in Archean sediments and Hadean zircons, respectively.

4.1 Hydrothermal Vents

The early Earth was dominated by a global ocean (Korenaga 2021; Russell 2021). Whether or not plate tectonics was active in the Hadean is still debated in the geoscience research community (Chowdhury et al. 2023; Tarduno et al. 2023; Hastie et al. 2023). Assuming that it was active in the Hadean, computational modeling suggests that at mid-ocean ridges, the places where new oceanic crust is formed, underwater volcanoes, called hydrothermal vents, were globally distributed over the entire ocean floor (Miyazaki and Korenaga 2022). Their gas emissions might have had a global influence on the Hadean atmosphere and prebiotic synthesis on land, and are also one of the potential places for prebiotic synthesis and the origins of

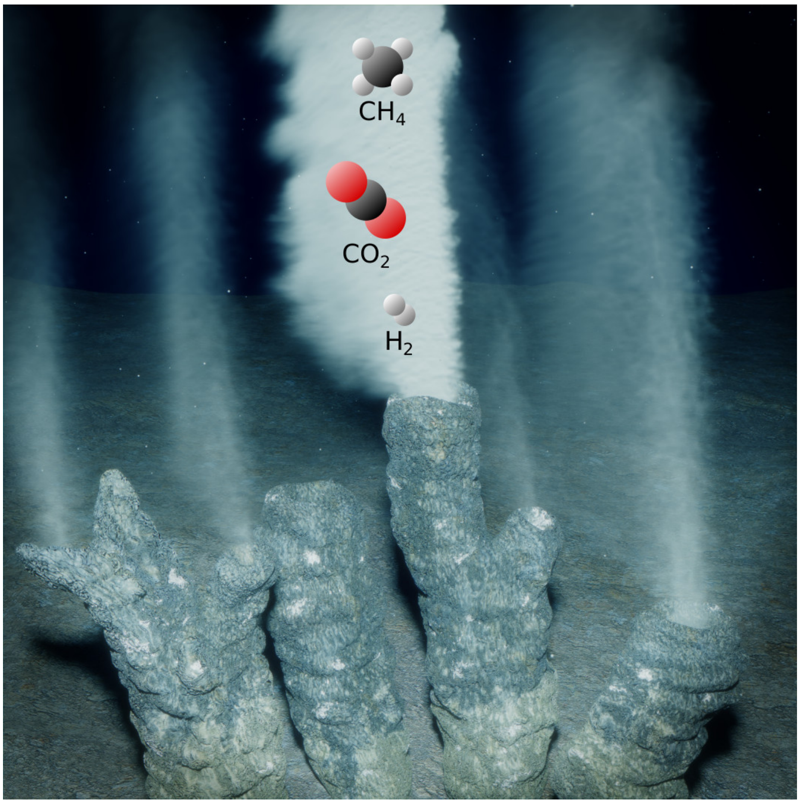

Figure 4.1: Hydrothermal vents at the bottom of the Earth's ocean (artist's impression, own creation). This white smoker is powered by the serpentinization reaction, which results in the emission of H_2, CO_2, and CH_4 gases. Image modified from Paschek, Henning, et al. (2025).

life in the porous structures of their chimneys (see, e.g., W. Martin, Baross, et al. 2008), as shown in Figure 4.1.

The white smoke in Figure 4.1 identifies the depicted hydrothermal vent as a so-called white smoker. This subtype of hydrothermal vents can be found off-center at some distance from mid-ocean ridges. Unlike black smokers (not shown here), white smokers are not powered directly by erupting magma, but the erupting gases are the products of the serpentinization reaction.

4.1.1 Serpentinization

Convection within the Earth's mantle, as shown in Figure 4.2, leads to the upwelling of ferrous iron-rich material (Fe^{2+}), which comes close to the thin crust of the Hadean at mid-ocean ridges (Miyazaki and Korenaga 2022). Through cracks in the crust, ocean water can seep down and come into contact with the mineral group olivine, which is formed from the ferrous iron-rich magma. This triggers the serpentinization reaction, oxidizing the ferrous iron to ferric iron (Fe^{3+}) and transforming the olivine to serpentine, as shown in the lower half of Figure 4.2. The full reaction, which is

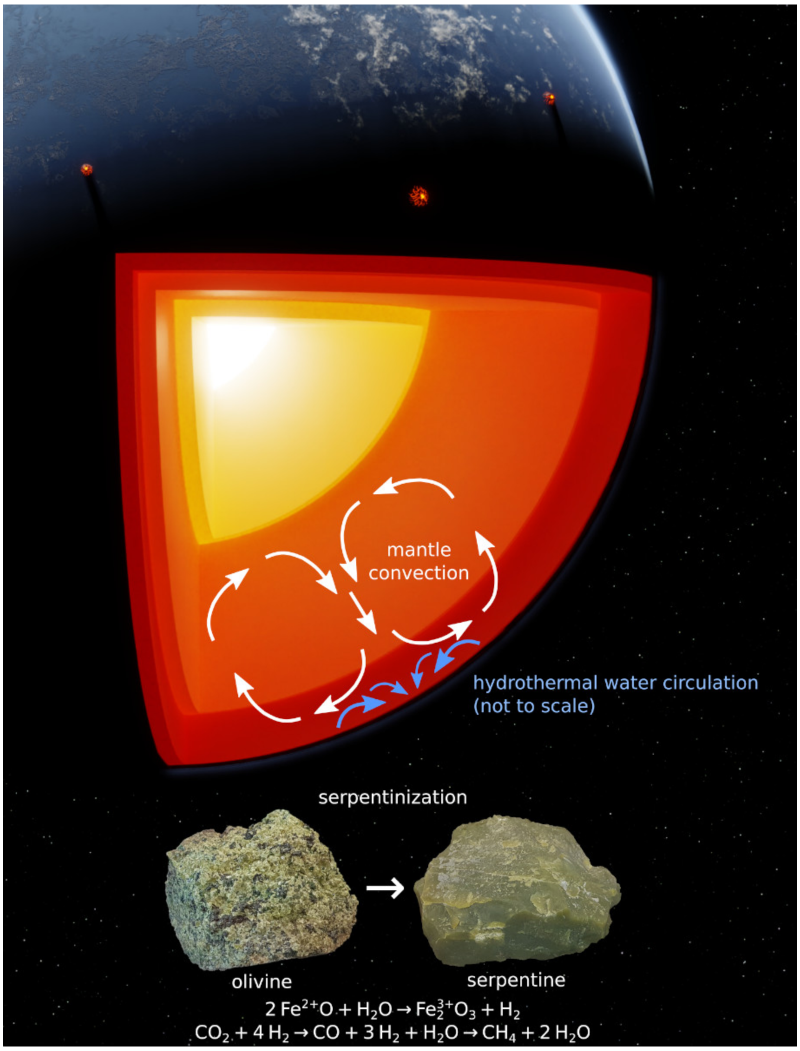

Figure 4.2: Upwelling material in the Earth's mantle brings iron-rich olivine rocks close to the surface. There it comes into contact with water at mid-ocean ridges and forms serpentine in the serpentinization reaction. This process releases H_2 gas, which can combine with CO_2 to form CH_4. Image modified from Paschek, Henning, et al. (2025), own creation.

given in full detail in Equation (27.1), can be simplified into

$$2\,\mathrm{Fe}^{2+}\mathrm{O} + \mathrm{H_2O} \longrightarrow \mathrm{Fe}_2^{3+}\mathrm{O}_3 + \mathrm{H}_{2(\mathrm{aq})}. \tag{4.1}$$

As a by-product, H_2 gas is released (Klein et al. 2013). In combination with the reverse water-gas shift reaction, which converts the in magma abundant CO_2 to CO at the high pressures and temperatures found in hydrothermal vents. The Fischer-Tropsch reaction (see Equation (2.19)) can further convert this CO to CH_4 (McCollom and Seewald 2007, for full details, see Equations (27.4) to (27.6)). These gases are emitted from the hydrothermal vents found around the globe in the Hadean.

Serpentinization also has the potential to drive prebiotic synthesis and enable the origins of life within hydrothermal vent systems (see, e.g., Russell et al. 2010).

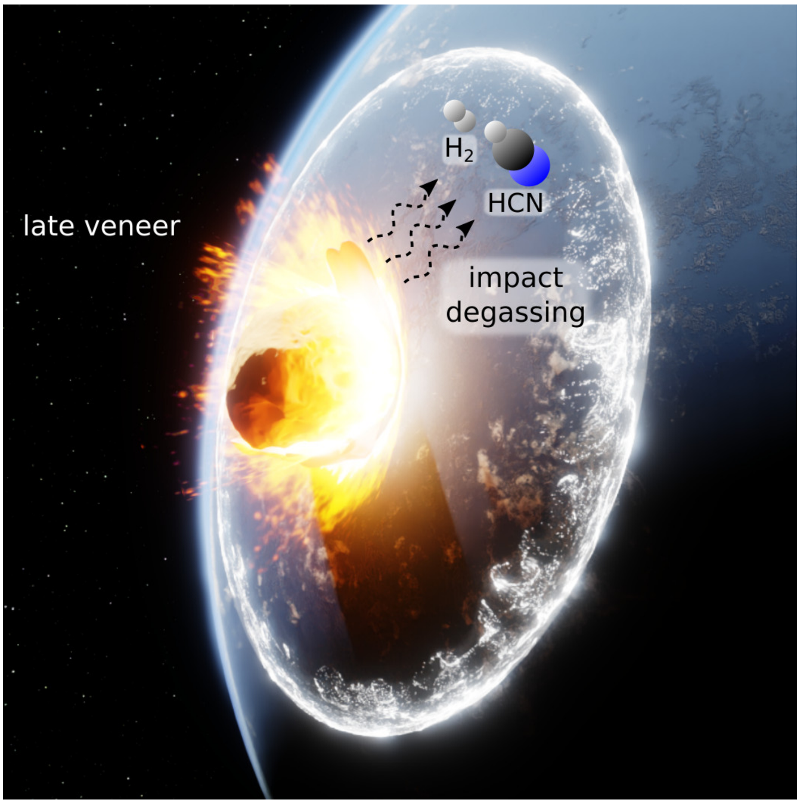

Figure 4.3: The energy released by impacts on the early Earth might have allowed for the synthesis of reducing gases such as H_2 and HCN. The late veneer, an isotopic signature in the Earth's crust, indicates that the early Earth was subjected to an intense bombardment after its formation was already complete. Image modified from Paschek, Henning, et al. (2025), own creation.

However, in this thesis I will focus on the influence of the emitted reducing gases on the atmosphere and land surface of the Hadean Earth, as this enables the link to impacts and the delivery of molecules formed in space by meteorites. This is because dilution in the vast global ocean makes it highly unlikely that molecules delivered from space or synthesized in the atmosphere are able to reach hydrothermal vents in concentrations significant for prebiotic synthesis.

4.2 Atmosphere

The Earth's crust and mantle show an excess of siderophile (iron-loving) elements, which is unexpected given the differentiation process during the formation of our planet. As the interior melted completely, these siderophile elements should have sunk to the core, leaving a depleted mantle and crust closer to the surface (similar to the meteorite parent bodies described in Section 3.3). However, an excess of these siderophile elements was found in the bulk silicates of the Earth's crust and mantle. This gave rise to the idea of a late veneer, a prolonged phase of intense bombardment

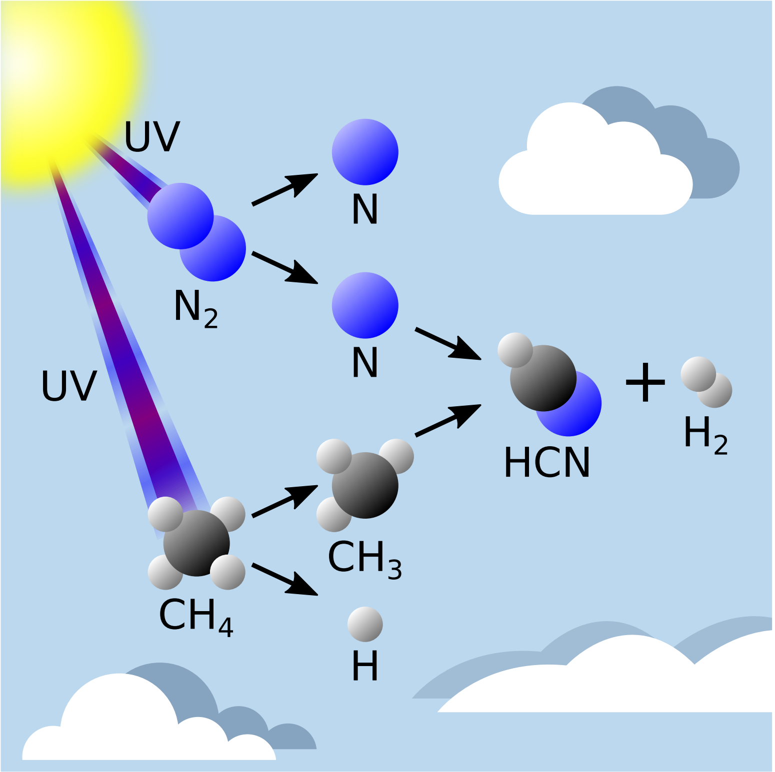

Figure 4.4: Examples of photochemical reactions that occur in the upper layers of the Earth's atmosphere. Here, UV irradiation splits molecules into radicals that can recombine to form new molecules. Image modified from Paschek, Henning, et al. (2025), own creation.

of the Earth after its formation process was complete (see, e.g., Morbidelli and B. J. Wood 2015; Li 2022). The impacting meteorites of undifferentiated chondritic composition delivered these siderophile elements to Earth, explaining the otherwise unexpected excess found.

If the bombardment contained enstatite chondrites, it was proposed that their rich content of reduced iron could react during the impact with water in the atmosphere and oceans, the reaction being driven by the energy released during impact, and similar to Equation (4.1) releasing H_2 in the process (see, e.g., Catling and Kasting 2017; Zahnle, Lupu, et al. 2020; Wogan, Catling, et al. 2023), as depicted in Figure 4.3.

On the other hand, if the late veneer had a carbonaceous chondrite component, this could generate a reaction of the impacting carbon with an N_2 and water atmosphere, while tolerating some levels of CO_2 being present, as shown in an experimental study by Kurosawa et al. (2013).

Figure 4.4 gives an idea of how the reducing gases emitted by serpentinization and impact degassing are processed in the atmosphere and contribute to the formation of prebiotic molecule precursors. UV radiation in the upper layers of the atmosphere can split gas molecules, here, e.g., N_2 and CH_4, into radicals. These can recombine to form new molecules, here HCN as a key prebiotic precursor of interest for many prebiotic reaction mechanisms (see Section 2.3). The reactions likely pass through H_2CN as an intermediate (Pearce, Ayers, et al. 2019, not shown here). Another important prebiotic precursor of interest formed by photochemistry is H_2CO.

Pearce, Molaverdikhani, Pudritz, Henning, and Cerrillo (2022) found in simulations of photochemical reactions in the Hadean atmosphere that ordinary lightning caused by storms accounts for only negligible amounts of prebiotic precursors produced, as proposed in the original version of the Miller-Urey experiments (see Section 2.3.1). Recently, however, lightning generated in the vicinity of volcanic eruptions, with the erupting clouds of volcanic ash particles capable of producing significantly higher lightning intensities, has been proposed as a potent driver of prebiotic synthesis on Hadean Earth and is being studied in laboratory experiments (Springsklee et al. 2023).

4.3 Warm Little Ponds and Wet-Dry Cycling

The earliest land-based water reservoirs on the Hadean Earth, such as lakes and ponds on the first continental crust, could have formed as early as 4.2 Gyr ago (McCulloch and Bennett 1993; Pearce, Pudritz, et al. 2017; Chowdhury et al. 2023), and are an intriguing habitat for prebiotic syntheses. Already Charles Darwin suggested a warm little pond (WLP) as a possible location for the origins of life (Deamer 2017; Damer and Deamer 2020b).

Figure 4.5 gives an overview of the different processes active in WLPs as described by Pearce, Pudritz, et al. (2017) and Pearce, Molaverdikhani, Pudritz, Henning, and Cerrillo (2022). During the wet phase, key prebiotic precursor molecules formed in the atmosphere accumulate in WLPs as a result of rain-out from the atmosphere, e.g., the HCN molecules shown on the right side of Figure 4.5. This source term of prebiotic precursor material and eventually formed biomolecules is counteracted by hydrolysis (reaction with water), leading to the destruction of the molecules. Some of the molecules can be lost by seepage through pores at the bottom of the WLP. As a result, the concentration inside the WLP will stabilize at a steady state.

Due to seasonal changes in the weather or day-night fluctuations in temperature and humidity around the WLP, enhanced desiccation may occur in cyclically repeating periods, partially or completely drying the WLP and increasing the concentrations of the dissolved molecules manifold. The left side of Figure 4.5 illustrates that in this dry state, new biomolecules can form due to the increased concentrations of precursor molecules. Additionally, the removal of water allows chemical reactions

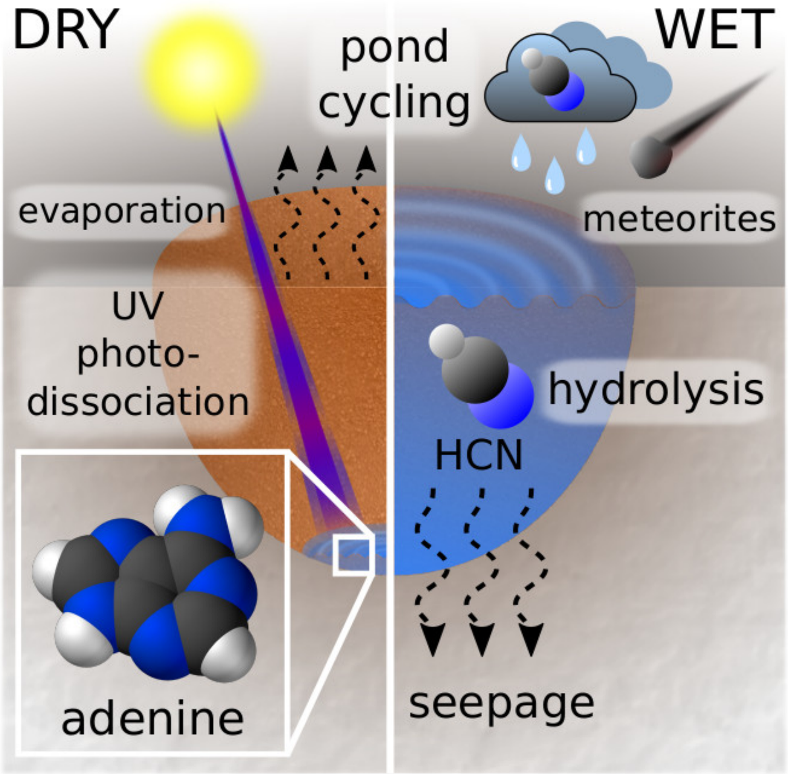

Figure 4.5: A warm little pond (WLP) that undergoes seasonal or daily cycles of desiccation and rewetting. Rain can deposit molecules such as HCN formed in the atmosphere in the WLP, and dry periods can promote otherwise inhibited reactions, possibly leading to the synthesis of biomolecules such as the genetic letter adenine. Image modified from Paschek, Henning, et al. (2025), own creation.

to be favorable, in which water molecules are split off in the process, as the immediate re-hydrolysis of the synthesized molecules is suppressed. On the other hand, in the dry state, destruction by UV photons acts on the formed molecules, potentially limiting their yield.

This wet-dry cycling is the key effect that promotes the synthesis of the first biomolecules in WLPs. It has been shown experimentally that wet-dry cycling in WLPs enables the synthesis of the key prebiotic molecules shown in Figure 2.1, including amino acids and the building blocks of RNA, the nucleobases and the sugar ribose (Oró and Kimball 1961; Johnson et al. 2008; Larowe and Regnier 2008; Bada 2013; Ferus, Pietrucci, Saitta, Ivanek, et al. 2019; Yi et al. 2020). Moreover, it can further promote their condensation into nucleotides (Powner et al. 2009; S. Becker, Thoma, et al. 2016; Sutherland 2016; S. Becker, Schneider, et al. 2018; Yadav et al. 2020), and finally their polymerization into the first proto-strands of RNA of lengths up to 300 monomers (Da Silva et al. 2015; Benner, Bell, et al. 2019).

In addition, meteorite fragments can fall into the WLP and supply it with the many different biomolecules found in its matrix. Pearce, Pudritz, et al. (2017) have studied and quantified in detail whether is likely that fragments of meteorites hit a WLP, including a model of the growth of the land masses, which are still very scarce on the Hadean Earth. They found that this is very likely, and calculated the maximum concentrations reached during the dry phase of a modeled WLP. In Part V, we revisit this model to see how this meteoritic delivery of molecules compares to the influence of rain-out of molecules formed in the atmosphere, either from the release of prebiotic precursor molecules by impact chemistry, as described in Section 4.2, or from geological sources such as serpentinization, as described in Section 4.1.1. This allows the connection from the Earth's surface environment of the WLPs to the biomolecules formed in space, as described in Chapter 3 and explored in the following Parts II to IV.

5

Overview

This thesis aims to link the biomolecules necessary for life with their origin in an (inter)planetary context. If we succeed in explaining the origins of life as a natural consequence of the processes active in space, during planet formation, and during the early developments on Earth, this would mean that life is not a special random coincidence that happened on our home planet. It might be that other planets in our solar system or exoplanetary systems also harbor the potential for life. Furthermore, it would allow us to see the origins of life in the broader context of the universe, as a phenomenon that occurs naturally within it. This would bring us closer to understanding the emergence of life as a natural consequence of the processes and natural laws that govern our universe, and as a final consequence, the emergence of sentient creatures like us humans who are capable of reflecting on their own origins, just as this thesis does.

To make this connection between the interplanetary space of our solar system (and possibly even exosystems) and the surface of the one planet we know of that harbors life, our Earth, Parts II to IV explore how prebiotic molecules could have formed in the first planetesimals embedded in the context of our solar system. The formed molecules could have been delivered to the surface of the early Earth by meteorites that were collision fragments derived from these planetesimal parent bodies.

Part II is based on the published paper Paschek, Semenov, et al. (2023) and presents simulations of the synthesis of the nucleobases adenine, guanine, uracil, cytosine, and thymine inside meteorite parent bodies. In particular, the idea of volatile depletion in planetesimals is introduced for the first time. As the small icy pebbles that form the planetesimal drift closer to the proto-Sun in the protoplanetary disk, they begin to warm up and lose some of their volatile ices from their interior to space. Some of these volatiles are basic reactants for the modeled prebiotic chemical reactions. It is therefore crucial to accurately estimate the initial abundances of these volatiles, as they are expected to be present in the planetesimal before the chemistry starts, and directly influence the resulting abundances of biomolecules found in asteroids and meteorites. To do this, experimental data from TPD experiments (see Section 3.1) are used to understand how ice mixtures of volatiles and water realistically behave as they warm up.

The results will be compared with abundances found in meteorites. This allows us to test whether our thermochemical simulations accurately model the formation of these molecules and whether they can quantitatively reproduce the abundances as found in real-world meteorites.

Similarly, Part III, based on the published paper Paschek, Kohler, et al. (2022), presents simulations of the synthesis of the sugar ribose, and Part IV, based on the published paper Paschek, M. Lee, et al. (2024b), presents simulations of the synthesis of vitamin B_3 inside meteorite parent bodies.

Part V is devoted to combining this in the context of the early Earth's surface and atmosphere. It is based on the paper Paschek, Henning, et al. (2025, in press) accepted for publication in *The Astrophysical Journal*. The goal is to evaluate the interplay between geological processes such as serpentinization driven by the Earth's interior and bombardment from outer space. Reducing gases released during meteorite impacts influence the atmospheric chemistry, possibly leading to the rain-out of key precursors, in particular HCN, and eventually to the synthesis of prebiotic molecules on the early Earth's surface. Furthermore, meteorites can also deliver prebiotic molecules formed in space directly to the Earth's surface, as investigated in Parts II to IV. On the first land masses to emerge from the Hadean ocean, the wet-dry cycling in WLPs allowed the formation of the building blocks of ribonucleotides, the monomer building blocks of RNA, potentially initiating the emergence of the RNA world. Consequently, all these endogenous geological and exogenous meteoritic processes together can prepare the ingredients for the origins of life on Earth.

To evaluate how well the different scenarios are suited to contribute to the emergence of the RNA world, the calculated concentrations of biomolecules and RNA building blocks are compared with the minimum concentrations required to form nucleotides, as shown in experimental studies. If the required concentration thresholds are exceeded, this means that the respective scenario under consideration might be a promising candidate to trigger the origins of life.

Finally, Part VI summarizes the main conclusions of this thesis and provides an outlook for future work.

Part II

Meteorites and the RNA World: Synthesis of Nucleobases in Carbonaceous Planetesimals and the Role of Initial Volatile Content[1]

Klaus Paschek, Dmitry A. Semenov, Ben K. D. Pearce, Kevin Lange,
Thomas K. Henning, Ralph E. Pudritz

This following Part is based on the work *"Meteorites and the RNA World: Synthesis of Nucleobases in Carbonaceous Planetesimals and the Role of Initial Volatile Content"*, published in the first issue of January 2023, part of Volume 942, of *The Astrophysical Journal* (Paschek, Semenov, et al. 2023) as part of the Ph.D. thesis.

The published paper has been reformatted to fit the format of this thesis. The work on the paper was divided as follows: I wrote the main simulation code, building on the pre-existing code published by Pearce and Pudritz (2016), and heavily editing and extending it. This included porting of the core thermochemical computations, originally written in FORTRAN, to C++, and binding then in a Python3 wrapper together with support for accessing the thermodynamic database CHNOSZ available in R. Kevin Lange contributed the thermodynamic planetesimal model developed during his bachelor and master thesis under the supervision of Prof. Dr. Cornelis P. Dullemond.

I drafted the first version of the manuscript, except that Dmitry A. Semenov helped to restructure and refine the explanations of Section 7.4 on the determination of the initial concentrations of the reactants and edited parts of this Section. The other co-authors contributed by commenting on at least one version of the draft.

---

[1] Supporting figure sets are available: figshare, doi: 10.6084/m9.figshare.21545148

Abstract

Prebiotic molecules, fundamental building blocks for the origin of life, have been found in carbonaceous chondrites. The exogenous delivery of these organic molecules onto the Hadean Earth could have sparked the polymerization of the first RNA molecules in Darwinian ponds during wet-dry cycles. Here, we investigate the formation of the RNA and DNA nucleobases adenine, uracil, cytosine, guanine, and thymine inside parent body planetesimals of carbonaceous chondrites. An up-to-date thermochemical equilibrium model coupled with a 1D thermodynamic planetesimal model is used to calculate the nucleobase concentrations. Different from the previous study (Pearce and Pudritz 2016), we assume initial volatile concentrations more appropriate for the formation zone of carbonaceous chondrite parent bodies. This represents more accurately cosmochemical findings that these bodies have formed inside the inner, $\sim$ 2–5 au, warm region of the solar system. Due to these improvements, our model represents the concentrations of adenine and guanine measured in carbonaceous chondrites. Our model did not reproduce *per se* the measurements of uracil, cytosine, and thymine in these meteorites. This can be explained by transformation reactions between nucleobases and potential decomposition of thymine. The synthesis of prebiotic organic matter in carbonaceous asteroids could be well explained by a combination of i) radiogenic heating, ii) aqueous chemistry involving a few key processes at a specific range of radii inside planetesimals where water can exist in the liquid phase, and iii) a reduced initial volatile content (H_2, CO, HCN, CH_2O) of the protoplanetary disk material in the parent body region compared to the outer region of comets.

6

Introduction

The origin of biomolecules on the early Earth is still a major question to those researching the emergence of life. RNA molecules are favored for being the crucial intermediate step toward the emergence of living systems (A. Rich 1962; Gilbert 1986). RNA is able to store genetic information encoded in the order of its monomers, the ribonucleotides, as well as to catalyze its own polymerization, and to self-replicate (see, e.g., Kruger et al. 1982; Guerrier-Takada, Gardiner, et al. 1983; Guerrier-Takada and Altman 1984; Zaug and Cech 1986; Cech 1986; Johnston et al. 2001; Vaidya et al. 2012; Attwater et al. 2018; Cojocaru and Unrau 2021; Kristoffersen et al. 2022).

There are generally two sites considered for the emergence of RNA: freshwater ponds and hydrothermal vents. How the abiotic polymerization of the first long and complex biomolecules could have occurred in the pristine oceans in the vicinity of hydrothermal vents is an open question, as necessary concentrations are unlikely to be reached (Pearce, Pudritz, et al. 2017). Concentrated nitrogen (N_2) necessary for the nucleobase synthesis is probably missing, as most of it might be reduced to ammonium (${NH_4}^+$) due to the presence of hydrogen sulfide (H_2S) in this setting (Schoonen and Xu 2001). As only little N_2 is present, it is questioned if nucleobases could be formed *in situ* in hydrothermal vents. Therefore, for the emergence of the first RNA world in hydrothermal vents, a delivery by an exogenous source would be necessary. Furthermore, cells today have different ion concentrations than the ocean water (cells contain more K^+, Zn^{2+}, phosphate, and transition metals (e.g., Mn^{2+}), and less Na^+; Mulkidjanian et al. 2012). As the first proto-cells likely did not possess ion-tight membranes nor membrane pumps, it is proposed that modern cells might reflect the ion concentration of proto-cells, and hence, of present-day or reconstructed primeval oceans. This is used as an argument to cast doubt upon whether hydrothermal vents at the bottom of the oceans were a likely place for the origin of life (see, e.g., Deamer, Damer, et al. 2019).

It might be possible that RNA was not the first biomolecule that played the role of genetic material. Several other candidates have been proposed and studied, e.g., glycol nucleic acids (Seita et al. 1972; Zhang et al. 2005), polyamide nucleic acids (Nielsen et al. 1991), threose nucleic acids (Schöning et al. 2000; Yu et al. 2012), or different nucleobases (Crick 1968; Cafferty and Hud 2015; Cafferty, Fialho, et al. 2016). It is possible that chemical evolution started with the emergence of other types of information-coding molecules, which then eventually transitions into (proto-)RNA via an evolutionary process in the so-called pre-RNA world (see, e.g., Hud 2018).

The idea to locate the origin of life in small freshwater basins or ponds on the first continental crust units or volcanic islands attracts more and more attention nowadays. Charles Darwin originally posited in 1871 that life might have emerged in a warm little pond (WLP) filled with simple prebiotic ingredients (Deamer 2017; Damer and Deamer 2020b). Pearce, Pudritz, et al. (2017) extended this concept by simulating the outcome of the exogenous organic delivery to a WLP. One of the main advantages of WLPs compared to the subsea hydrothermal vent environment for abiogenesis is that the WLPs allow for wet-dry cycles, which promote polymerization and formation of oligonucleotide chains with lengths up to 300 nucleotides (Da Silva et al. 2015). To drive this polymerization, all four essential RNA nucleotides or other monomers of the alternative RNA-predecessors listed above have to be present in sufficient concentrations to form the first oligomers. S. Becker, Schneider, et al. (2018) and S. Becker, Feldmann, et al. (2019) showed in laboratory experiments that the formation of RNA nucleosides and nucleotides is plausible in WLPs during wet-dry cycles. Moreover, the polymerization of ribonucleotides was demonstrated in the presence of clays or salts (Ferris, A. R. Hill, et al. 1996; Ferris, Joshi, K. J. Wang, et al. 2004; Da Silva et al. 2015), metal ion catalysts (Orgel 2004), and in lipid bilayers (Chakrabarti et al. 1994; Toppozini et al. 2013) in WLP settings (including geothermal fields and hot springs).

The building blocks of the nucleotides and other vital prebiotic molecules have been exogenously delivered onto the Hadean and Eoarchean Earth during the late heavy bombardment, either by comets or asteroids (see, e.g., Gomes et al. 2005). Even nowadays, meteorites seed our planet with these organics. Theoretical models suggest that inward-drifting pebbles delivered water and carbon to the forming Earth from the outer nebular regions located beyond the orbit of the proto-Jupiter (Johansen, Ronnet, Bizzarro, et al. 2021). Kooten et al. (2021) developed a model based on the experimental studies of the CV (Vigarano-type) chondrite Leoville. They concluded that the forming Earth could have accreted a substantial fraction of the inward-drifting dust from the outer solar system, with a composition similar to CI (Ivuna-type) chondrites. Analysis of the ruthenium isotope ^{100}Ru in Eoarchean rocks and meteorites showed that the Earth's mantle is partly composed of the same material as carbonaceous chondrites (Fischer-Gödde and Kleine 2017; Fischer-Gödde, Elfers, et al. 2020).

Based on these recent findings, primitive carbonaceous chondrites could be promising candidates for seeding WLPs on the early Earth with necessary life building blocks, as compared to the carbon-rich interplanetary dust particles and comets (Pearce, Pudritz, et al. 2017; Dauphas and Marty 2002). Carbonaceous chondrites contain up to 20 % water, and 1–5 % carbon by weight (Mason 1963). The organic matter in the carbonaceous chondrites consists of an insoluble and a soluble part, with a ratio of roughly 70:30 (Bitz and Nagy 1966). The insoluble organic matter (IOM) consists of kerogen-like compounds made of many aromatic rings or chains. Most of the IOM is formed in the interstellar medium and protoplanetary disks (Derenne and Robert 2010; Alexander, Cody, et al. 2017). Still, laboratory experiments showed that IOM might also be formed in hydrothermically active carbonaceous chondrites alongside amino acid precursors (Kebukawa et al. 2017). It is even proposed that IOM could have played a role in the (pre-)biotic synthesis and abiogenesis, as it shows various similarities to melanin polymers in microorganism and could act as catalysts (d'Ischia et al. 2021). The soluble organic matter (SOM) consists of much smaller organic molecules important for the origin of life, such as purines and pyrimidines, carboxylic acids, amines, amides, alcohols, aldehydes, ketones, amino acids, etc. (see, e.g., Gilmour 2003; Pizzarello, Cooper, et al. 2006). Carbonaceous chondrites also contain P-rich minerals such as schreibersite, which can phosphorylate nucleosides, creating nucleotides (Gull et al. 2015).

The SOM also contains the nucleobases guanine, adenine, and uracil with measured concentrations of 0.25–515 ppb (parts per billion; Velden and Schwartz 1977; Stoks and Schwartz 1979; Stoks and Schwartz 1981; Shimoyama et al. 1990; Callahan et al. 2011; Pearce and Pudritz 2015). Recently, cytosine and thymine were also found with concentrations of 1–5 ppb (Oba, Takano, Furukawa, et al. 2022). Furthermore, the sugar ribose, a fundamental building block of RNA, was recently identified, with concentrations of 4.5–25 ppb (Furukawa et al. 2019). These molecules could have been precursors of RNA-like polymers needed for abiogenesis.

In this study, we model abiotic reaction pathways and calculate the evolution and abundances of the nucleobases adenine (**A**), uracil (**U**, not to be confused with uranium), cytosine (**C**, not to be confused with carbon), guanine (**G**), and thymine (**T**) inside carbonaceous chondrite's parent bodies, following the previous study by Pearce and Pudritz (2016). We adopted the thermodynamic conditions inside various hypothetical parent bodies as computed in the study by K. Lange et al. (2022, in preparation), using a simplified version of their model here. This allowed us for the first time to determine from which parts of the parent bodies nucleobase-rich meteorites might have originated. The resulting nucleobase abundances were compared to the values measured in carbonaceous chondrites found on Earth.

In the next Section 7, we outline all reaction pathways considered in our model for the nucleobase synthesis in carbonaceous planetesimals. We outline how the Gibbs free energies of formation are used to perform the thermochemical equilibrium calculations for these nucleobases. Also, we present our new, more feasible approach to set up the initial concentrations of reactants, which better suits the formation history of these parent bodies. Further, we introduce the adopted planetesimal model by K. Lange et al. (2022, in preparation) and give a short summary of the nucleobase abundances found in carbonaceous chondrites. Next, in Section 8, we describe our computational methods. In Section 9, we present and analyze the computed abundances and compare them to the previous results by Pearce and Pudritz (2016) and measured values. In Section 10, we evaluate the necessity of our new approach to apply the appropriate initial concentrations of volatiles. We discuss how the overproduction of **U** in our model could be related to the low **C** and **T** abundances found in carbonaceous chondrites. Finally, conclusions about the relevance of our findings for the origin of carbonaceous chondrites with high nucleobase content and the origin of life follow in Section 11.

7

Model Setup

To set up our model we first define the set of reaction pathways used to simulate the synthesis of the canonical nucleobases. This set was previously compiled by Pearce and Pudritz (2015) and Pearce and Pudritz (2016) based on experimental studies and considerations of the environment in parent body planetesimals.

Second, we shortly review why chemical equilibrium is a suitable assumption in this planetesimal environment (see Section 7.2). We introduce the Gibbs free energies of formation, which allow us to run the thermodynamic calculations.

As we finally want to obtain predictions of the nucleobase abundances from the simulated reaction pathways, we need to understand the composition of the relevant reactants in the source material of carbonaceous planetesimals. We start from the measured composition of comets (Mumma and Charnley 2011, and references therein) as the most pristine and best-preserved reservoir of material in the outskirts of the solar system (Rauer 2008). Guided by solar nebula models (Semenov and Wiebe 2011; Drozdovskaya, C. Walsh, et al. 2016; Bergner and Ciesla 2021; Lichtenberg and Krijt 2021) and experimental insights from temperature-programmed desorption experiments (Ayotte et al. 2001; Collings et al. 2004; Bergner, Rajappan, et al. 2022, J. He (private communication)), we derive initial conditions appropriate for the parent bodies of carbonaceous chondrites. This improvement upon the initial cometary abundances gives us a better representation of the amounts of reactants available to the chemical pathways in the carbonaceous planetesimals.

To run our calculations in a realistic environment, we introduce a full thermodynamic planetesimal model (K. Lange et al. 2022, in preparation).

Finally, we summarize the measured nucleobase abundances in actual carbonaceous chondrites (Stoks and Schwartz 1979; Stoks and Schwartz 1981; Shimoyama et al. 1990; Callahan et al. 2011; Pearce and Pudritz 2015; Oba, Takano, Furukawa, et al. 2022), which will serve as the benchmark to verify our simulated results.

7.1 Reaction Pathways

In the context of abiogenesis, all essential biomolecules have to form via abiotic reaction pathways, using only primordially occurring simple molecules as reactants. The reaction pathways for the formation of the nucleobases **A** ($C_5H_5N_5$), **G** ($C_5H_5N_5O$), **C** ($C_4H_5N_3O$), **U** ($C_4H_4N_2O_2$), and **T** ($C_5H_6N_2O_2$) used in this study were taken from Pearce and Pudritz (2016, Table 1). In our model, we excluded reactions with formamide as a reactant since these reactions did not significantly contribute to the aqueous synthesis of the nucleobases (nos. 24, 61, 49, and 63 in Pearce and Pudritz 2016).

All reactions in our model are summarized in Table 7.1. There are two types of processes, namely, Fischer-Tropsch (FT) and non-catalytic (NC) synthesis. FT reactions involve gaseous ammonia, carbon monoxide, and hydrogen and require a catalyst such as alumina or silica. NC reactions proceed in both gaseous and aqueous phases and do not require a catalyst.

This list of reactions was compiled in a previous study by Pearce and Pudritz (2015) (and extended by three pathways by Pearce and Pudritz 2016) mostly based on laboratory experiments, in which it was shown that each of these pathways forms the respective nucleobase in the presence of the corresponding reactants and catalysts (see references in last column of Table 7.1). The exceptions are the five pathways nos. 3, 29, 44, 54, and 58 from Larowe and Regnier (2008), which were found to be thermodynamically favorable in hydrothermal environments in theoretical calculations.

If the cited study proposed a chemical equation, we adopted the same equation in Table 7.1. On the other hand, if no balanced chemical equation was suggested, we follow the simple scheme

$$\text{reactants} \xrightarrow{\text{catalysts}} \text{nucleobase} + \text{further products}. \tag{7.1}$$

This explains why some of the reactions are not balanced, as the respective study did not follow a particular chemical equation, but only found the reactants to produce the nucleobase in their experiments. Later, this will become interesting when comparing the results from the different **A** pathways, as reaction no. 6 could be a balanced and NC version of no. 1, and no. 3 could be a balanced version of no. 4. We will also investigate the significance of NH_3 in reaction nos. 4 and 8 compared to nos. 3 and 7, respectively. Pearce and Pudritz (2016) already analyzed this aspect in their simulations, but we will re-examine their findings, as we changed the initial concentrations of reactants (see Section 7.4) and will analyze if this affected the balance of the chemical equilibrium in the results.

No.	Type[a]	Reaction[b]	Source(s)
Adenine			
1	FT	$CO + H_2 + NH_3 \xrightarrow{NiFe+\|\|Al_2O_3+\|\|SiO_2} \mathbf{A} + H_2O$	Yang and Oró (1971); Hayatsu, Studier, Oda, et al. (1968)
3	NC	$5\,HCN_{(aq)} \longrightarrow \mathbf{A}_{(aq)}$	Larowe and Regnier (2008)
4	NC	$HCN + NH_3 \longrightarrow \mathbf{A}$	Yamada et al. (1969); Wakamatsu et al. (1966)
6	NC	$5\,CO + 5\,NH_3 \longrightarrow \mathbf{A} + 5\,H_2O$	Hayatsu, Studier, Oda, et al. (1968)
7	NC	$HCN + H_2O \longrightarrow \mathbf{A}$	Ferris, Joshi, Edelson, et al. (1978)
8	NC	$HCN + NH_3 + H_2O \longrightarrow \mathbf{A}$	Oró and Kimball (1961)
Uracil			
29	NC	$2\,HCN_{(aq)} + 2\,CH_2O_{(aq)} \longrightarrow \mathbf{U}_{(aq)} + H_{2(aq)}$	Larowe and Regnier (2008)
32	NC	$\mathbf{C} + H_2O \longrightarrow \mathbf{U} + NH_3$	Robertson and Miller (1995); Garrett and Tsau (1972); Ferris, Sanchez, et al. (1968)
Cytosine			
43	FT	$CO + H_2 + NH_3 \xrightarrow{NiFe+\|\|Al_2O_3+\|\|SiO_2} \mathbf{C} + H_2O$	Yang and Oró (1971); Hayatsu, Studier, Oda, et al. (1968)
44	NC	$3\,HCN_{(aq)} + CH_2O_{(aq)} \longrightarrow \mathbf{C}_{(aq)}$	Larowe and Regnier (2008)
Guanine			
51	FT	$CO + H_2 + NH_3 \xrightarrow{NiFe+\|\|Al_2O_3+\|\|SiO_2} \mathbf{G} + H_2O$	Yang and Oró (1971); Hayatsu, Studier, Oda, et al. (1968)
54	NC	$5\,HCN_{(aq)} + H_2O \longrightarrow \mathbf{G}_{(aq)} + H_{2(aq)}$	Larowe and Regnier (2008)
Thymine			
58	NC	$2\,HCN_{(aq)} + 3\,CH_2O_{(aq)} \longrightarrow \mathbf{T}_{(aq)} + H_2O$	Larowe and Regnier (2008)
62	NC	$\mathbf{U} + CH_2O + HCOOH + H_2O \longrightarrow \mathbf{T}$	Choughuley et al. (1977)

Notes. The pathways are taken from Pearce and Pudritz (2016, Table 1), excluding reactions with formamide as reactant, since these reactions turned out to be negligible (nos. 24, 61, 49, and 63 there). All pathways were shown to produce the respective nucleobases in laboratory experiments under conditions present in parent body planetesimals, except nos. 3, 29, 44, 54, and 58, which are theoretical and thermodynamically favorable (Larowe and Regnier 2008). Sometimes real meteorite powder was used as a catalyst, e.g., NiFe alloy powder (90.2 % Fe, 7.1 % Ni, 0.46 % Co, 0.26 % P, 1 % C, 1 % S, 80 ppm Ga, 320 ppm Ge, 1.9 ppm Ir; Buchwald 1975) from the Canyon Diablo meteorite (Hayatsu, Studier, Oda, et al. 1968; Yang and Oró 1971).

[a] FT: Fischer-Tropsch, NC: Non-catalytic.

[b] +||: One, or the other, or all catalysts used in laboratory experiments.

Table 7.1: Potential Reaction Pathways within Meteorite Parent Bodies.

Water forms alongside nucleobases in FT reactions (Hayatsu and Anders 1981), and therefore, was added as a product to all FT reaction pathways.

Pearce and Pudritz (2015) and Pearce and Pudritz (2016) reviewed a total of 63 reaction pathways as those applicable to the environment in planetesimals. Criteria for disregarding one of the pathways were the lack of necessary reactants, catalysts, or too high temperatures necessary for the pathways to proceed in the experiments. As meteorite parent body planetesimals might have incorporated the same material as present in comets (Schulte and Shock 2004; Alexander 2011), all pathways were ruled out if they required reactants or catalysts not found in comets. For example, pathway no. 43 (in Pearce and Pudritz 2015) starting from cyanoacetaldehyde and urea (e.g., Shapiro 1999; Nelson et al. 2001) forming **C** was ruled out as cyanoacetaldehyde was not found in comets (Mumma and Charnley 2011, and references therein) or the interstellar medium (Ballotta et al. 2021, and references therein). All five canonical nucleobases decompose in seconds at temperatures $\gg 400\,\mathrm{K}$ in aqueous conditions (Levy and Miller 1998). Hence, pathways requiring these temperatures in the lab were ruled out. Thus, in this study, we use only experimentally verified pathways and disregarded other potential processes that have no laboratory data. In addition, we would like to keep our new model comparable to the Pearce and Pudritz (2016) study with an emphasis on a more realistic asteroid model and more appropriate initial chemical composition of ices.

When running the chemical model, *weak coupling* was assumed. This implies that different reactions do not compete for reactants and hence could be simulated independently. This is a safe assumption when reactants are simple molecules with much higher concentrations in the simulated environment than the synthesized complex reaction products (A. K. Cobb, Pudritz, and Pearce 2015). In the previous studies by A. K. Cobb, Pudritz, and Pearce (2015) and Pearce and Pudritz (2016), they found that the computed concentrations did not match the abundances measured in carbonaceous chondrites when multiple reactions were modeled simultaneously. Another reason why specific pathways may not have competed with each other for reactants is the porous structure of the carbonaceous chondrites, where different reaction processes could have been separated from each other by the thermochemical conditions (temperature, pressure, phase, presence of catalysts, etc.).

Pearce and Pudritz (2016) attempted to simulate the synthesis of multiple nucleobases together by running several reaction pathways simultaneously. For example, when simulating the three FT reactions nos. 1, 43, and 51 (Hayatsu, Studier, Oda, et al. 1968) together they found that only **C** was produced while the other nucleobases **A** or **G** stayed absent at any temperature in a 0–500 °C range. Their explanation for this was that the set of reactions in Table 7.1 is the only experimentally verified one available, but might be incomplete and further molecules would be required, which were also detected as products in the laboratory experiments, e.g., urea, melamine, or guanidine (Hayatsu, Studier, Oda, et al. 1968). This might lower the thermodynamic favorability of **C** and would allow for the other nucleobases to be produced. For further discussion regarding modeling competition between reactions, we refer to Pearce and Pudritz (2016, Section 4.4, Figure 8, and Appendix B).

To explore the possible transformation of nucleobases into each other, as a test case, reaction nos. 32 and 62 were also considered. As the resulting abundances of other pathways were used as initial concentrations for these two transformation reactions, this leads to a coupling of pathways. As this was not simulated simultaneously but individually, the resulting **U** and **T** abundances of nos. 32 and 62 represent only upper bounds, and the resulting **C** and **U** abundances resulting from other pathways might be lowered as they were consumed in these transformation reactions. This is discussed in Section 10.2.

7.2 Chemical Equilibrium in Planetesimals

Our model assumes that all reactions in Table 7.1 reach chemical equilibrium (see also Section 2.3 in Pearce and Pudritz (2016) for an extensive discussion). This is also a prerequisite for the utilized chemical modeling software *ChemApp* (see Section 8.1.1). To achieve chemical equilibrium, the environment has to be in stable conditions over a duration that is longer than the time it needs to complete the reactions. The reactants involved in each reaction must be retained in the phase in which they react.

The planetesimal models (see Section 7.5) show that the interiors of typical parent bodies sustain temperatures allowing for liquid water and stay aqueous for several hundred thousand years in the smallest and earliest formed planetesimals, and up to several billion years in the biggest and latest formed ones. This was also confirmed by other studies. For example, planetesimals simulated in the study by Travis and Schubert (2005) with radii of 50–80 km and different initial content of ^{26}Al resulted in an aqueous phase longer than 1 Myr. Lichtenberg, Golabek, et al. (2016) found for planetesimals with solid silicates and radii of around 100 km similar timescales of several ten million years with a temperature range allowing for liquid water.

Compared to these aqueous timescales inside the planetesimals, the half-lives of the reactants involved and the duration of the reactions until their completion are orders of magnitude shorter. The half-life of HCN in aqueous solution is less than ten thousand years (Peltzer et al. 1984). The HCN measured in the Murchison meteorite was suggested not to be a free reactant, but was probably bound to $-$CN salts formed in reactions with Fe^{2+}, Mg^{2+}, and Ca^{2+} in the aqueuos phase of the planetesimal. Acidification of the meteorite samples was shown to lead to the release of this bound HCN (Pizzarello 2012). Consequently, all NC reactions involving HCN in Table 7.1 (nos. 3, 4, 7, 8, 29, 44, 54, and 58) used up all the freely available reactant and should have finished long before the planetesimals froze again.

The deamination of **C** to **U** in reaction no. 32 occurs on a timescale of $\sim 17\,000$ yr at 0 °C and drops down in duration to 3.5 h at 165 °C (Levy and Miller 1998). As these temperatures are easily reached in the planetesimal models and persist over longer timescales, this reaction should reach equilibrium. The recent detection of **C** in carbonaceous chondrites (Oba, Takano, Furukawa, et al. 2022) suggests that **C** is produced more rapidly via reactions nos. 43 and 44 than it is destroyed by deamination.

The reactions involving CO and NH_3 (nos. 1, 6, 43, and 51) formed the respective nucleobases in 2–288 h (Hayatsu, Studier, Oda, et al. 1968), which is a negligible duration compared to the aqueous phase of the planetesimals. In the previous study (Pearce and Pudritz 2016, Section 5.6) CO was identified as a limiting reactant in these FT reactions and the lack of it in carbonaceous chondrites could verify that these reactions reached equilibrium.

Ultimately, reaction no. 62 transforming **U** into **T** with formaldehyde and formic acid finishes on the timescale of hours to days (Choughuley et al. 1977). Formaldehyde as the limiting reactant was found in carbonaceous chondrites (Pizzarello and Holmes 2009; Monroe and Pizzarello 2011), but it was suggested that this formaldehyde was not freely available, but tied up in other organic compounds or chemically adsorbed onto clays (Pizzarello and Holmes 2009), similar to HCN as mentioned above.

At low concentrations, sufficient mixing of the dissolved reactants is required to achieve chemical equilibrium. The simulations of Travis and Schubert (2005) showed for planetesimals of 50–80 km strong hydrothermal convection inside these porous bodies. Up- and downwelling plumes took $\sim 50\,000$ yr to complete a full circulation, which would allow for many full cycles in the aqueous phase of our considered planetesimal models. Therefore, a well mixed and equilibrated distribution of the reactants can be assumed, even at the low concentrations of compounds in our model. When specific reactants necessary for a particular reaction pathway get available at a specific location inside the planetesimal due to convection, the short reaction times allow to restore chemical equilibrium quickly compared to the timescales of hydrothermal convection and period of aqueous conditions.

We conclude that chemical equilibrium is a well-constrained assumption in this context.

7.3 Gibbs Free Energy of Formation

Every molecule has a Gibbs free energy of formation ΔG_f that varies with temperature and pressure. The lower the value of ΔG_f, the higher the molecule's formation probability. For negative values of ΔG_f, the molecule should form spontaneously (given all the necessary reactants are available).

ΔG_f as a function of temperature T and pressure p can be described by fitting the corresponding thermodynamical data (see Section 8.1.2) with the function:

$$\Delta G_f(T,p) = a + bT + cT\ln(T) + dT^2 + eT^3 + fT^{-1} + gp, \tag{7.2}$$

where a–g are the Gibbs coefficients (see Pearce and Pudritz 2016, Section 2.2).

As the pressure dependence of ΔG_f is very marginal (A. K. Cobb, Pudritz, and Pearce 2015; Pearce and Pudritz 2016), the Gibbs coefficient g can be neglected. For example, the relative percent difference of ΔG_f for $\mathrm{HCN_{(aq)}}$ between 1 bar and 100 bar at 300 K is 0.4 % and similar for all the other molecules and temperatures considered. This makes the ΔG_f values pressure independent. The only pressure-dependent parameter of the model that one has to consider is the boiling point of water because the reactions are partly modeled in an aqueous phase. When water evaporates, we assume that the aqueous synthesis stops and the newly formed organic molecules are preserved at their current abundances. As the pressure does not influence the dynamics of the reactions, we did not calculate the lithostatic pressure as a function of radius inside the planetesimal. Instead, constant pressure of 100 bar was assumed in the thermochemical calculations for the entire planetesimal. Only in the smallest considered planetesimals (see Section 7.5) with radii of only several kilometers is this pressure likely an overestimate. It could be that some reactions actually shut off as water starts to evaporate in the hottest central region (lower boiling point of water at lower pressures). This was not explicitly considered, and therefore, the calculated nucleobase abundances in the core regions of the smallest planetesimals are only valid if water stays in the liquid phase. However, when assuming that water stays liquid, the calculated abundances are correct as the Gibbs energies are nearly pressure-independent, as mentioned above. For the biggest considered planetesimals, the boiling point of water at 100 bar was never reached.

The Gibbs coefficients a–f are the input for the equilibrium chemistry software to model the chemical reactions (see Section 8.1.1). To each reaction, one can assign a Gibbs free energy of the reaction ΔG_r, which is defined as

$$\Delta G_r = \sum_{\text{products}} \Delta G_f - \sum_{\text{reactants}} \Delta G_f, \tag{7.3}$$

and which has to be negative to be thermodynamically favorable. Otherwise, with a positive ΔG_r, the reaction would require activation energy to proceed. This increases the system's total Gibbs free energy ΔG, moving it away from the equilibrium (see below). The Gibbs free energy of the system ΔG is calculated by adding up each molecule's Gibbs free energy of formation,

$$\Delta G = \sum_{\text{all}} \Delta G_f . \tag{7.4}$$

The chemical reactions will have essentially ceased when the system has reached equilibrium. At the concentrations of the reactants and products in the reaction at equilibrium, there can no longer occur a series of reactions that leads to a negative Gibbs free energy of the reaction ΔG_r. We assumed chemical equilibrium and performed calculations to minimize the Gibbs free energy of the system ΔG.

7.4 Initial Concentrations of Reactants

In order to determine the initial concentrations of reactants, one faces the challenge that one does not have immediate access to the initial conditions present in carbonaceous chondrite parent bodies. As we always tried to feed as much experimental data and evidence as possible into our model, we started with the only preserved reservoir from the early stages of the solar system accessible to measurements, comets. However, comets formed in the outer solar system, and therefore, are not the representative reservoir at the correct radial location for the parent bodies of carbonaceous chondrites. Parent bodies of carbonaceous chondrites formed closer to the proto-Sun. The disk has a radial gradient in the concentrations of volatiles in ices as these start to desorb. To address this, we used a combination of solar nebula models (Semenov and Wiebe 2011; Drozdovskaya, C. Walsh, et al. 2016; Bergner and Ciesla 2021; Lichtenberg and Krijt 2021) that predicted this volatile desorption, and accordingly, depletion in icy pebbles in the inner protoplanetary disk. We combine these models with insights from temperature-programmed desorption (TPD) experiments showing partial trapping of volatiles above their desorption temperatures.

7.4.1 Comets

Today, the most pristine and unmodified reservoir of material available are comets in our solar system (Rauer 2008; Mumma and Charnley 2011). Meteorite parent body planetesimals might have incorporated some of the same material as present in comets (Schulte and Shock 2004; Alexander 2011). Therefore, comets represent a good starting point to obtain a prediction for the initial concentrations of reactants available in the source material of carbonaceous chondrites.

The remote studies of comets from Earth and *in situ* measurements of 67P/Churyumov-Gerasimenko by the ROSINA mass spectrometer aboard the Rosetta mission showed that comets consist of dust and pristine chemical constituents that formed at very low temperatures ($\lesssim 30\,\mathrm{K}$; Mumma and Charnley 2011; Le Roy et al. 2015; Altwegg, Balsiger, Bar-Nun, et al. 2016; Drozdovskaya, van Dishoeck, et al. 2019; Eistrup et al. 2019). Comets have formed in the outer region of the solar system beyond 5–20 au, including some source material originating from further inner regions (Brownlee et al. 2006; Ciesla and Sandford 2012), and were able to retain volatile species such as CO, CH_4, and O_2. Even though they contain key prebiotic ingredients, including precursors of sugars and the amino acid glycine, it was estimated that comets might not have contributed much to the Earth's surface inventory of carbon, nitrogen, and water (Marty et al. 2016). Instead, it is believed that carbonaceous chondrites have delivered a significant fraction of organics and volatiles to the Earth's upper crust and surface (Dauphas and Marty 2002; Bergin et al. 2015; Fischer-Gödde, Elfers, et al. 2020; Kooten et al. 2021).

7.4.2 Solar Nebula Models

Comets and asteroids represent two distinct pristine and partly processed matter reservoirs. Unlike icy comets, most carbonaceous chondrites probably originate from parent bodies formed in the much warmer region of the solar nebula at $\sim$ 2–3 au (Van Schmus and J. A. Wood 1967; Lodders 2003; R. G. Martin and Livio 2021), as, e.g., the asteroid 19 Fortuna was postulated to be the parent body source of CM (Mighei-type) meteorites (Burbine, Mccoy, et al. 2002). The formation and composition of the carbonaceous asteroids have been shaped by a complex history of the growth and fragmentation of solids starting from dust grains, the inward radial drift of pebbles, and the gravitational interactions with (proto-)Jupiter and Saturn at a later stage (Gomes et al. 2005; Minton and Malhotra 2010; K. J. Walsh et al. 2011; Johansen, J. Blum, et al. 2014a; Elbakyan et al. 2020). According to current models, these 100 km-sized planetesimals could have been formed via streaming instability by the gravitational collapse of pebble-sized solids within several orbital timescales (Johansen, Oishi, Mac Low, et al. 2007; Johansen, J. Blum, et al. 2014a; Ormel and Klahr 2010; Klahr and Schreiber 2020a). Recently, this theoretical idea has been supported by the analysis of the measured chondral sizes in several CO (Ornans-type) chondrites (G. A. Pinto et al. 2021).

The inner 2–3 au region in the solar nebula has been located right outside the water snowline at $T \lesssim 150\,\mathrm{K}$, and well inside the evaporation zones of more volatile ices such as N_2, CO, formaldehyde, and CH_4 (Wai and Wasson 1977; Alexander, Boss, et al. 2001; Cassen 2001; Lodders 2003; Bland et al. 2005; Braukmüller, Wombacher, Hezel, et al. 2018; Vollstaedt et al. 2020; Lichtenberg and Krijt 2021; Öberg and Bergin 2021). The inward-migrating icy pebbles, out of which carbonaceous asteroids could have been formed via spontaneous gravitational collapse, should have experienced a substantial loss of moderate to very volatile species, even prior to later thermal metamorphism inside the parent bodies (see, e.g., Piso et al. 2015). Carbonaceous chondrite matrices were found to be significantly depleted in volatile species (Bland et al. 2005). Therefore, the idea to use a pristine cometary volatile composition as the composition of volatiles in the icy pebbles may lead to a substantial overestimate of the concentrations of the initial material for organic syntheses inside the carbonaceous chondrite parent bodies. This may explain why in the study by Pearce and Pudritz (2016) some nucleobases were severely overproduced compared to the concentrations measured in carbonaceous chondrites unless the total volatile content per unit solid mass would be lowered artificially to substantially lower values.

The building blocks of carbonaceous chondrites, mm-sized icy pebbles, were slowly radially migrating and gradually losing their most volatile content due to thermal evaporation and diffusion through porous water ice layers. For example, CO, formaldehyde, and HCN should be depleted in the water ice of the pebbles, because their desorption temperatures (~ 20–$70\,\mathrm{K}$) are much lower than that of water ice (~ 140–$160\,\mathrm{K}$, depending on gas pressure). Accordingly, a severe depletion of the volatiles in the water ice mantles of dust grains in the warm inner solar nebula was predicted by various physico-chemical nebula models (see, e.g., Visser et al. 2009; Semenov and Wiebe 2011; Drozdovskaya, C. Walsh, et al. 2016; Bergner and Ciesla 2021; Lichtenberg and Krijt 2021).

For example, in the extended model of Semenov and Wiebe (2011) both the laminar and turbulent mixing chemical models of the solar nebula show that at a final moment in time of 5 Myr the abundances of CO, HCN, and formaldehyde ices become depleted by about 5–8 orders of magnitude at the radius of 3 au compared to the pristine-like values at 20 au. One has to keep in mind that in this study and the other solar nebula models, it was assumed that the volatile ices are able to leave the water ice matrix freely.

7.4.3 Trapping of Volatiles

In TPD experiments under ultra-high vacuum conditions, the major fraction of these volatile ices remains trapped in the water ice. Most of the trapped volatiles then desorb during the so-called “molecular volcano” desorption as the water ice matrix changes from the amorphous to the crystalline structure at $T \approx 150\text{–}160\,\mathrm{K}$ (May et al. 2012; May et al. 2013a; May et al. 2013b). The remaining fraction co-desorbs with water at higher temperatures of $T \gtrsim 160\,\mathrm{K}$ (Ayotte et al. 2001; Collings et al. 2004; Cuppen, C. Walsh, et al. 2017; Potapov and McCoustra 2021; Bergner, Rajappan, et al. 2022). As our prediction for the temperature present at 2–3 au in the early solar system is $T \approx 160\,\mathrm{K}$ (see Section 7.5.1), the remaining volatile content in the source material of carbonaceous chondrites should be the amount left after the volcano desorption took place on the icy pebbles. Therefore, the remaining volatile content is everything that only co-desorbs with water at higher temperatures.

However, this trapping could be explained by the short timescales (hours–days) employed in these experiments, while icy pebbles in the solar nebula could have been gradually losing their volatile content over thousands of years, becoming more volatile-poor compared to the TPD results (Cuppen, C. Walsh, et al. 2017; Potapov and McCoustra 2021). As the temperatures when trapping occurs are above the desorption temperatures of the volatiles (see above), molecules should be able to desorb from the walls of the water ice pores and move by diffusion. Indeed, the relatively efficient diffusion rates for the volatile ices such as CO, formaldehyde, and CO_2 at $T \gtrsim 90\,\mathrm{K}$ were measured experimentally or predicted via molecular dynamics calculations (Ghesquière et al. 2015, and references therein). Diffusion parameters of CO, CO_2, H_2, D_2, O_2, N_2, CH_4, and Ar moving along pores inside amorphous water ice were measured (He et al. 2017; He et al. 2018). By desorbing and adsorbing again on the walls of the water ice pore channels, the volatile molecules would slowly diffuse through the porous crystalline water ice in a random walk and finally be lost to space before the pebbles form the first planetesimals by accretion.

This diffusion process might lead to a final volatile content that is somewhere in between the amounts found trapped after the volcano desorption in the TPD experiments and the many orders of magnitude lower amounts predicted by the solar nebula models. Therefore, the results from the TPD experiments and the solar nebula models represent only upper and lower constraints on the actual volatile content present in the accreted source material of carbonaceous chondrites, respectively.

Accurate modeling of this complex diffusion process of volatiles leaving slowly the porous water ice is beyond the scope of the present study. We used these constraints to get a first-order estimate of the volatile content in our planetesimals and used it to model the chemical pathways.

Volatile	Name	Depletion Factor				
		TPD		solar nebula models		mean OOM[a]
CO	carbon monoxide	2.75×10^{-2}	J. He (priv. comm.)[b]	$\sim 10^{-8}$	Semenov and Wiebe (2011)[e]	$10^{-4.8}$
		$\sim 10^{-2}$	Collings et al. (2004)[c]			10^{-5}
		$\lesssim 10^{-2}$	Ayotte et al. (2001)[c]			10^{-5}
				$< 10^{-11}$	Lichtenberg and Krijt (2021)[f]	
				$\ll 10^{-2}$	Bergner and Ciesla (2021)[g]	
H_2 (D_2)	hydrogen	3.17×10^{-4}	J. He (priv. comm.)[b]	No data		No data
HCN	hydrogen cyanide	6.6×10^{-2}	Bergner, Rajappan, et al. (2022)[d]	$\sim 10^{-5}$	Semenov and Wiebe (2011)[e]	$10^{-3.1}$
				~ 0	Bergner and Ciesla (2021)[g]	No data
CH_2O	formaldehyde	No data		$\leq 4.25 \times 10^{-3}$	Drozdovskaya, C. Walsh, et al. (2016)	No data
				~ 0	Bergner and Ciesla (2021)[g]	

Notes.

[a] OOM: Order of magnitude. To calculate the OOM for CO and HCN, the solar nebula model by Semenov and Wiebe (2011) was used.

[b] See also Figures 12.1 and 12.2 in the Appendix. In the experiments, the isotopes deuterium (molecular, D_2) and ^{13}CO were used to avoid contamination by residual gases in the ultra-high vacuum chamber.

[c] The integrated amount of the volatiles left above 161.3 K was estimated from the published TPD spectra.

[d] This value from the the published plot was verified by the corresponding author.

[e] Extra modeling data from Semenov and Wiebe (2011) that was not published.

[f] As the radial range considered in this solar nebula model did not reach into the inner regions at 2–3 au, the volatile abundance there was approximated by linear extrapolation from the data at 20 au.

[g] This model did not reach into the inner regions at 2–3 au and the values given here correspond to the radial distance of 20 au.

Table 7.2: Depletion of the volatiles CO, H_2, HCN, and formaldehyde measured by TPD experiments at 161.3 K (see Section 7.5.1) or predicted by solar nebula models at 2–3 au in comparison to cometary regions.

Molecule i	Name	Cometary Concentration[a] $[\mathrm{mol}_i \cdot \mathrm{mol}_{H_2O}^{-1}]$	Depletion Factor[b]	Predicted Concentration[c] $[\mathrm{mol}_i \cdot \mathrm{mol}_{H_2O}^{-1}]$
H_2O	water	1	None	1
CO	carbon monoxide	1.75×10^{-1}	10^{-5}	1.75×10^{-6}
H_2	hydrogen	1.75×10^{-1}	10^{-4}	1.75×10^{-5}
NH_3	ammonia	7.0×10^{-3}	None	7.0×10^{-3}
HCN	hydrogen cyanide	2.5×10^{-3}	10^{-3}	2.5×10^{-6}
HCOOH	formic acid	7.5×10^{-4}	None	7.5×10^{-4}
CH_2O	formaldehyde	6.6×10^{-4}	10^{-3}	6.6×10^{-7}

Notes. All concentrations are normalized to water.

[a] Concentrations spectroscopically measured in comets (Mumma and Charnley 2011, and references therein) and used in the previous studies by A. K. Cobb, Pudritz, and Pearce (2015) and Pearce and Pudritz (2016).

[b] The cometary concentrations are adjusted to be more in line with the carbonaceous chondrites' pristine composition. The cometary concentrations are multiplied by a depletion factor to give the predicted concentration values listed in the last column.

[c] Concentrations predicted for the source material forming carbonaceous chondrite parent bodies. The concentrations listed here are the ones used as input parameters in the thermochemical equilibrium calculations.

Table 7.3: Initial concentrations of reactants used for simulating the reaction pathways in Table 7.1.

7.4.4 Predicting the Initial Reactant Concentrations

Table 7.2 gives an overview over the available studies and their results concerning the depletion of the volatiles CO, H_2, HCN, and formaldehyde, as predicted for the region where carbonaceous chondrite parent bodies have been formed. Results from both TPD experiments and solar nebula models are listed.

7.4.4.1 Experimental TPD Results

TPD spectra for ^{13}CO and D_2 were provided by J. He (private communication). This allowed us to accurately determine the remaining volatile fraction for the temperature that might have prevailed in the formation region of carbonaceous chondrite parent bodies (see Figures 12.1 and 12.2 in the Appendix). These isotopes were used to avoid contamination by residual gases in the ultra-high vacuum chamber. As H_2 is more volatile than D_2, one would expect less trapping for H_2 in comparison to D_2. We show in Section 10.1 that the initial H_2 concentration has no impact on the resulting nucleobase abundances even for two orders of magnitude lower values. Therefore, it is a safe assumption to use the data for D_2 as a proxy for the trapping of H_2 in our study. ^{13}CO is less volatile than ^{12}CO, and one would expect more efficient trapping for ^{13}CO than for ^{12}CO. However, the mass and size difference between ^{13}CO and ^{12}CO is very small and the difference in trapping is negligible. In the conducted experiments, a mixture of volatile ice and water ice was deposited at 10 K in a ratio of 1:10, which is close to the CO and H_2 composition in comets ($\sim$1:6, see Table 7.3). The other studies, e.g., by Ayotte et al. (2001) and Collings et al. (2004), used a lower volatile component in the deposited ice of $\sim$1:20 and $\sim$1:100, respectively. To prepare the sample, J. He (private communication) directly deposited the CO-H_2O ice mixture onto the substrate before warming up, as has been done in Collings et al. (2004). In contrast, Ayotte et al. (2001) first deposited the porous amorphous water ice and then the CO ice on top of the ice matrix.

Bergner, Rajappan, et al. (2022) performed TPD experiments with HCN. The cometary abundance of HCN in water ice is 1:400 (see Table 7.3). Bergner, Rajappan, et al. (2022) used a higher ratio of 1:20 due to detection constraints in the experiments. We refer in their study to the amount of HCN trapped above 160 K in 55 monolayers of water ice.

7.4.4.2 Results of Solar Nebula Models

The considered solar nebula models predicted significantly lower volatile concentrations in the inner regions of the protoplanetary disk, as they did not consider trapping in water ice. We used the extended model by Semenov and Wiebe (2011) as we had direct access to all chemical data, such as the CO and HCN ice concentrations in the inner ≤ 5 au region of the solar nebula. Additionally, we used the published data of Bergner and Ciesla (2021) and Lichtenberg and Krijt (2021) and extrapolated the values from 20 au to ≤ 5 au. The abundances of formaldehyde ice in the inner region at 1–10 au as well as outer cometary regions > 30 au were adapted from the study by Drozdovskaya, C. Walsh, et al. (2016). This study allowed us to derive an upper limit for the formaldehyde ice depletion factor of $\leq 4.25 \times 10^{-3}$ (compare to Table 4 in their publication).

7.4.4.3 Volatile Depletion Factors

To estimate the depletion of the volatile ices in the inner solar nebula as compared to cometary ices, we take the $\log_{10}$ of the depletion factors obtained in TPD experiments and the solar nebula models, and average them (see Table 7.2). Unlike in both TPD experiments and solar nebula models, these mean order of magnitude (OOM) values roughly account for trapping of the volatile ices and their slow diffusion out of the bulk water ice over long physical timescales associated with the growth and radial drift of the icy pebbles in the solar nebula. We regard the mean OOM as a reasonable first step in obtaining a more realistic composition of the source material of icy planetesimals in the inner solar system. We used the results from the solar nebula model by Semenov and Wiebe (2011) for CO and HCN, since the other considered models have not presented results for the inner 2–3 au.

Table 7.3 provides the cometary abundances (Mumma and Charnley 2011, and references therein) for all the reactants relevant to model the chemical pathways in Table 7.1. To derive the extra depletion factor to be applied to the cometary abundances, we used the mean OOM values obtained from TPD experiments and solar nebula models, whenever possible. In summary, we found that the initial cometary concentrations of HCN, formaldehyde, H_2, and CO from A. K. Cobb, Pudritz, and Pearce (2015) and Pearce and Pudritz (2016) should be reduced by factors of 10^{-3} (HCN), 10^{-3} (CH_2O), 10^{-4} (H_2), and 10^{-5} (CO), respectively (see Table 7.3). These factors were chosen in this approximate manner to account for the large uncertainties and necessary assumptions involved. There are large discrepancies between and within the TPD and solar nebula studies (see Table 7.2). Thus, these factors are rather approximate, but may provide a more realistic representation of the initial volatile content of carbonaceous chondrites than cometary values. We see it as the most realistic attempt justifiable in the context of the broad uncertainties involved.

Another possible depletion process is the radiogenically powered outgassing of volatiles from planetesimals formed from the icy pebbles in the protoplanetary disk. The thermodynamic model of K. Lange et al. (2022, in preparation) that we use here (see Section 7.5) considers sublimation and deposition processes of the volatiles CO,

CH_4, CO_2, NH_3, and water in planetesimals. Except for water, they find significant outgassing of these volatiles. For low-temperature models designed for comets, they see a depletion of the volatiles in the core and a deposition of ice at outer shells. For higher temperatures, as considered here for asteroids, a main portion of the volatile content is outgassing and leaves the planetesimal. Only water stays evenly distributed over the radius of the planetesimals. Lichtenberg and Krijt (2021) saw the same outgassing effect for CO, CO_2, and water, with a radially even distribution and only moderate depletion of water in the evolved planetesimals.

By combining available experimental information, theoretical predictions, and the above arguments, our estimates of the depletion factors for the volatile ices in carbonaceous chondrites (w.r.t. to the cometary values) might be considered reasonable.

7.5 Planetesimal Model

One of the most significant advancements in our study is the direct coupling of equilibrium nucleobase chemistry and a comprehensive 1D thermodynamic planetesimal model. A. K. Cobb, Pudritz, and Pearce (2015) and Pearce and Pudritz (2016) only considered the parameters for a single planetesimal parent body to discuss their results without using a comprehensive model. They did not couple the models directly. Their reaction calculations were carried out for the entire temperature range where water is expected to be liquid. Since the Gibbs energies of the molecules are pressure independent, as mentioned in Section 7.3, their assumption of the pressure of 100 bar for each modeled planetesimal body was kept in our simulations. Consequently, the interesting temperature range where water can become liquid at 100 bar is 273 K (0 °C) to 584 K (311 °C).

In our simulations, we used a more advanced thermal model of a planetesimal developed by K. Lange et al. (2022, in preparation). This model simulated the thermal evolution of planetesimals from their formation in the solar system until today. The thermal history for each considered planetesimal as a function of the radius was used for the thermochemical reaction simulations with *ChemApp* (see Section 8.1.1). This allowed us to track the evolution of the nucleobase abundances with the planetesimal's thermal evolution over time.

It is important to note that the planetesimal models represent a simplified model adapted to parent bodies of carbonaceous chondrites compared to the more complex models of K. Lange et al. (2022, in preparation).

For the planetesimal simulation, the object's radius, its surface temperature corresponding to its distance to the Sun, the time of formation after calcium-aluminium-rich inclusions (CAI), and its porosity ϕ were adjustable parameters. CAI are inclusions found in carbonaceous chondrites (T. Lee et al. 1977, first evidence found in Allende chondrite), defining the age of the solar system as the oldest dated solids. In particular, the aluminium part with the isotope ^{26}Al is the main source of radiogenic heating inside planetesimals. Therefore, the time of formation after CAI defines the formation time of the planetesimal after the start of the formation of the solar system. This is important as this determines the amount of accreted radiogenic isotopes and hence the heat energy available inside the planetesimal.

The radioactive decay of the two short-lived isotopes ^{26}Al as the primary contributor and ^{60}Fe (half-lives $\approx$ Myr), and the four long-lived isotopes ^{40}K, ^{232}Th, ^{235}U, and ^{238}U (half-lives $>$ Gyr) were considered as the heat source inside the simulated planetesimals. We had access to several models of planetesimals with radii of 3–150 km and times of formation after CAI of 0.5–3.5 Myr. For the porosity, $\phi = 0.2$ was used in all the models as this corresponds to the typical value in carbonaceous chondrites (Mason 1963). Recent studies show coinciding ranges and similar average values, e.g., 10–30 % (Flynn et al. 1999) or 17 % (Macke et al. 2011).

The equations of energy, gas, and ice conservation were implicitly discretized on a 1D grid and solved, including sublimation and deposition of volatiles and a source term accounting for radiogenic heating. Sublimation and deposition are several orders of magnitude faster than gas transport. Therefore, we assumed that the local gas pressure is at the local equilibrium vapor pressure at all times. Then, the porous body is in a quasi-steady-state, where the difference between the incoming and outgoing gas flux in a grid cell is immediately compensated by sublimation or deposition as long as the ice is locally present. We neglected the transport of latent heat for the simplicity of the model so that the equations for temperature diffusion and gas diffusion can be decoupled. The decoupled quasi-steady-state temperature diffusion and gas diffusion equations are both tridiagonal, allowing us to solve them separately with the *scipy.linalg.solve_banded()* routine, part of the *scipy Python3* packages (`https://github.com/scipy/scipy`, Virtanen et al. 2020).

7.5.1 Surface Temperature

As mentioned above, an essential parameter of the adopted planetesimal model was its surface temperature. When assuming a black body, the body's distance to the Sun can be used to determine its surface temperature. The typical distance of asteroids today that are believed to be parts of the same parent bodies as carbonaceous chondrites is between 2–3 au. For example, 19 Fortuna was postulated to be the parent body source of CM meteorites (Burbine, Mccoy, et al. 2002). Accordingly, we assumed 2.5 au as the semi-major axis a from the Sun for a parent planetesimal of typical carbonaceous chondrites. The unattenuated incident power P_{in} on the planetesimal at the time when the solar nebula had disappeared can be roughly calculated as:

$$P_{\text{in}} = \frac{(1-A)L'_{\odot}\pi r^2}{4\pi a^2}, \tag{7.5}$$

with the planetesimal's albedo A, the solar luminosity at that time $L'_{\odot}$, and the planetesimal's radius r. Further assumptions were a spherical planetesimal on a circular orbit and an isotropic energy output of the Sun. Using the Stefan-Boltzmann law, the radiated power P_{out} from the surface of the planetesimal is

$$P_{\text{out}} = 4\pi r^2 \epsilon\sigma T^4, \tag{7.6}$$

where σ is the Stefan-Boltzmann constant, T is the surface temperature in Kelvin, and ϵ is the gray body emissivity of the planetesimal. Equating $P_{\text{in}} = P_{\text{out}}$ gives

$$T = \left(\frac{(1-A)L'_{\odot}}{\epsilon\sigma 16\pi a^2}\right)^{\frac{1}{4}}. \tag{7.7}$$

As the early Sun was fainter than today, for the considered times of formation after CAI of 0.5–3.5 Myr, $L'_{\odot}$ was assumed to be approximately 70 % of the present-day solar luminosity $L_{\odot}$ (Bahcall et al. 2001). Assuming a black body ($A = 0$, $\epsilon = 1$) and that there was no large radial migration of the parent bodies in the young solar system (neglecting, e.g., possible effects due to the “Grand Tack” hypothesis at early times, see, e.g., Masset and Snellgrove 2001; K. J. Walsh et al. 2011), we obtained $T = 161.3$ K.

7.5.2 Simulated Conditions Inside Carbonaceous Planetesimals

Figure 7.1 shows the computed temperature evolution over time for a selection of the chondritic parent bodies with different sizes and times of formation after CAI. The supporting figure set (figshare, doi: 10.6084/m9.figshare.21545148) shows all the available planetesimal models. The surface temperature derived above was used in the calculations and can be seen as the common baseline for all the temperature curves.

In Figure 7.1a, most of the temperature curves inside a small, 4 km-sized planetesimal show a single strong temperature peak at $t \sim 0.2$–0.6 Myr after formation, which was caused solely by the decay of the short-lived radionuclides. Due to the fast cooling of this small body, the influence of the long-lived isotopes was not noticeable.

However, in the larger bodies with a radius $\gtrsim 50$ km the internal heat conduction was not efficient enough. Thus, their internal temperatures continued to increase after the half-life decay time of the short-lived isotopes (see Figures 7.1b and c). This

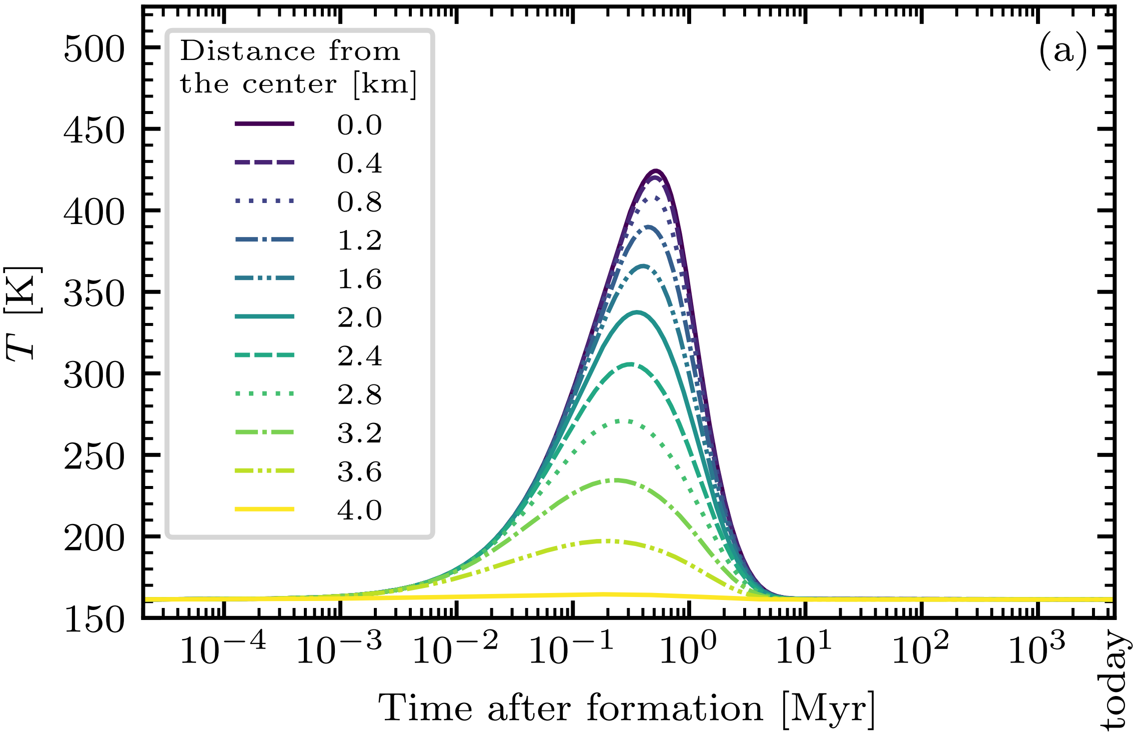

(a) Radius = 4 km, time of formation after CAI = 1 Myr.

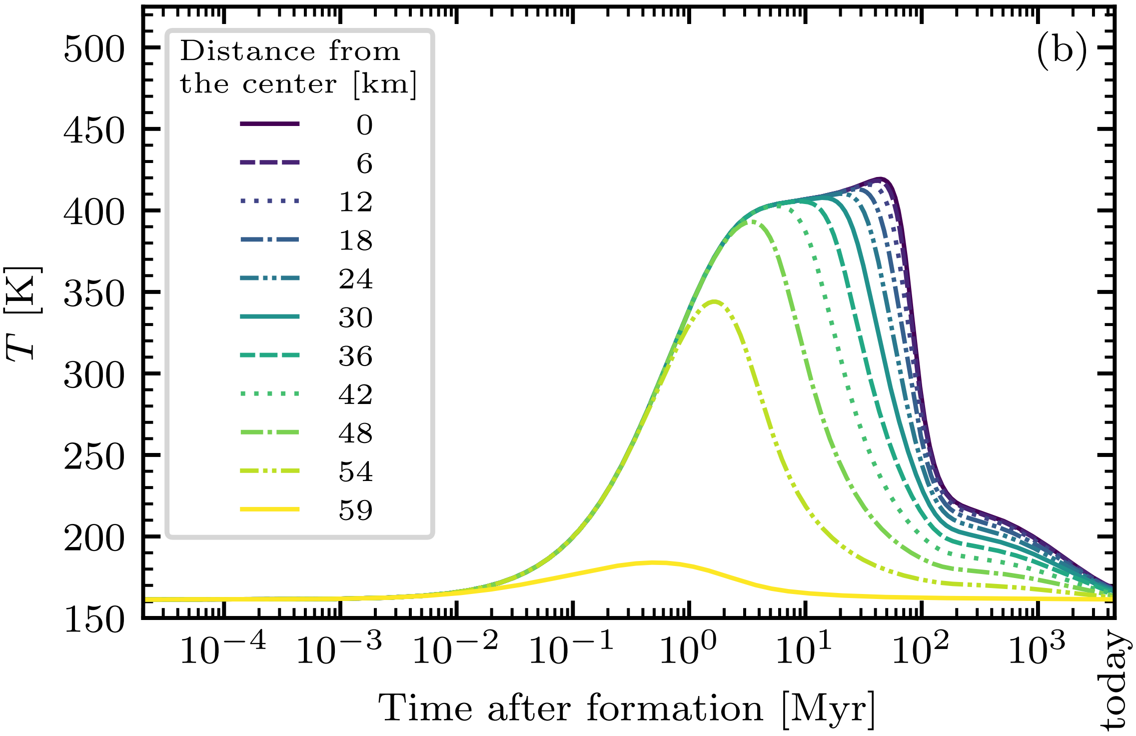

(b) Radius = 60 km, time of formation after CAI = 2.5 Myr.

Figure 7.1: Continued on next page.

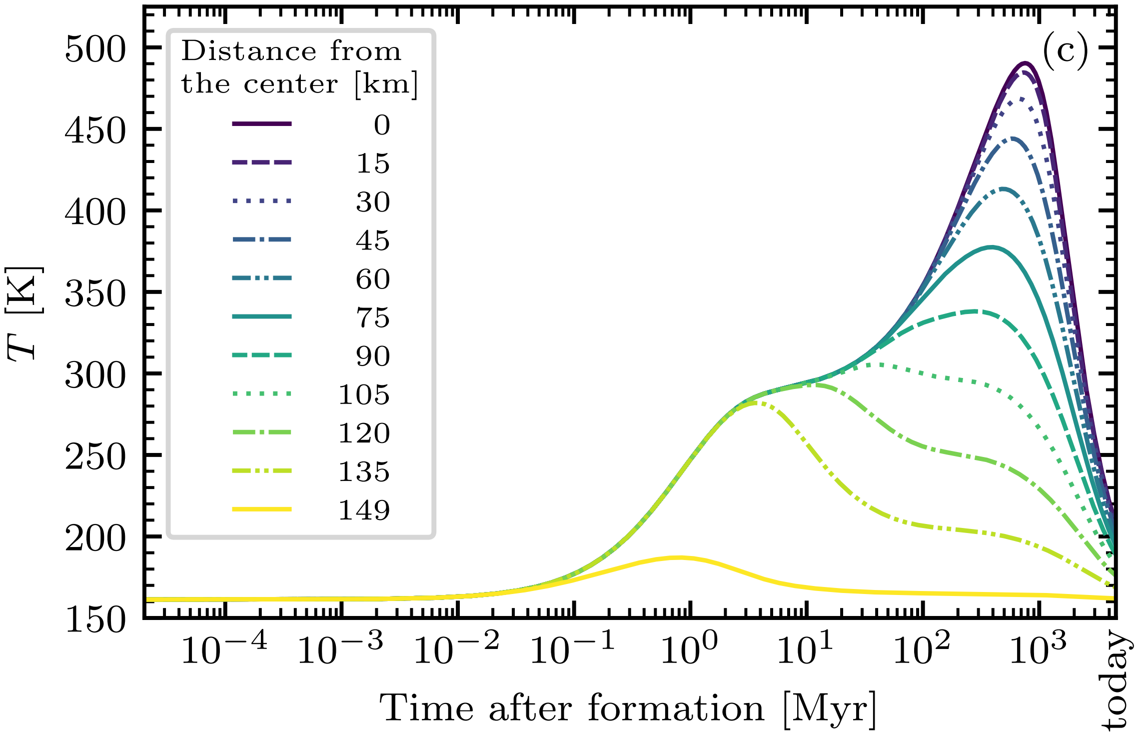

(c) Radius = 150 km, time of formation after CAI = 3.5 Myr.

Figure 7.1: Temperature evolution inside different planetesimals with a porosity ϕ of 0.2 over time. Temperature curves are given for different radii inside the body (relative to the center). Reproduced from a simplified version of the model by K. Lange et al. (2022, in preparation). The complete figure set (10 images) is available (figshare, doi: 10.6084/m9.figshare.21545148). It contains all planetesimal models with different radii and times of formation after CAI.

lead to a second temperature bump at $t \sim 50$ Myr after formation in Figure 7.1b. Shortly thereafter, the temperature dropped due to the slow heat conduction and the declining abundances of the short-lived isotopes. Around 200 Myr after the formation, thermal profiles became flatter since the long-lived isotopes still supplied heat (see Figure 7.1b). For an even larger planetesimal with a radius of 150 km in Figure 7.1c, the trapped heat from the short-lived isotopes started to overlap with the plateau caused by the long-lived ones in the core. This significantly extended the time span during which water could remain liquid, which is a key for the synthesis of the complex prebiotic molecules.

7.5.3 Uncertainties of Planetesimal Model

The utilized planetesimal model has several limitations. The latent heat of water ice was not considered in the planetesimal model. As the latent heat is significantly higher than the heat capacity of the bulk material, the phase transition from solid to liquid requires a considerable amount of energy. As a result, our planetesimal model overestimated the internal temperatures. In addition, crystallization of liquid water to amorphous ice releases heat during the cooling, resulting in less severe temperature decreases than computed by our model.

Furthermore, serpentinization reactions between rocks and water could produce additional heat and affect the calculated temperatures (see, e.g., Góbi and Kereszturi 2017; Farkas-Takacs et al. 2021). Moreover, if serpentinization happens, it could also distort the chemical reactions by binding the water necessary as the solvent for the chemistry or pushing the temperatures too high.

Sintering is another process that may occur. At high temperatures, a compactification of the rocks occurs, which allows even small porous bodies to reach high temperatures in a feedback loop. The increasingly compact body heats more easily, pushing sintering even more, while the material's melting point is still far from being reached. This strong feedback loop is expected to become important above 700 K (Henke, Gail, Trieloff, Schwarz, and Kleine 2012; Henke, Gail, Trieloff, and Schwarz 2013), which is well above the temperatures considered here. This was ensured by assuming the relatively late formation time after CAI (3.5 Myr) for the largest considered planetesimals of 100 km radial size and larger. If these large planetesimals had formed earlier, they would reach temperatures above 700 K and would probably experience strong sintering or even differentiation. No compactification and, therefore, change in porosity by sintering should be expected in the parent bodies considered here (thermal and aqueous metamorphosis could still change the porosity). Accordingly, fragments originating from any part of the bodies should have a chondritic structure and could be carbonaceous chondrites. At least the core region of early formed and large planetesimals is probably not of interest as the origin of fragments harboring prebiotic molecules, as these are only found in slightly aqueously altered meteorites (petrologic type ~ 2) that experienced no sintering. Sintering was only proposed as an explanation for the structure and petrologic type of some H- and L-chondrites (Yomogida and Matsui 1983), which probably descended from the core region of hotter (larger or earlier formed) parent bodies (Henke, Gail, Trieloff, Schwarz, and Kleine 2012) and were classified with high petrologic types > 3.0.

The surface temperature used in the simulations was only roughly estimated, as explained in Section 7.5.1. The remaining dust in the protoplanetary disk could have partly shielded the light of the young Sun significantly. How much fainter the young Sun was is also uncertain. However, as the simulated reaction pathways were temperature-dependent only at high temperatures, a different surface temperature of the parent body only slightly shifts the minimum radius and maximum time of formation after CAI needed to start the synthesis of nucleobases. Hence, the resulting molecular abundances should not be affected much by such uncertainties.

The planetesimal model of Travis and Schubert (2005) showed hydrothermal convection in the interior of carbonaceous chondrite parent bodies. As our model did not consider this, convection could redistribute the water and, therefore, the reactants and products in our reaction pathways. In their study, they gave 50 000 yr as the rough timescale of a full convection cycle. As the aqueous phase of planetesimals lasts for several million years, in a first approximation, a well-mixed, roughly spherically and radially even water distribution could be assumed. Specifically for large 100 km-sized and late formed planetesimals, heating by long-lived isotopes (not considered by Travis and Schubert 2005) extends the aqueous phase significantly. Nonetheless, considering convection could be interesting for a possible follow-up study.

7.6 Meteoritic Abundances of the Canonical Nucleobases

Pearce and Pudritz (2015) reviewed the abundances measured in carbonaceous chondrites and gave ranges of 1–515 ppb for **G**, 0.25–267 ppb for **A**, and 37–73 ppb for **U**. Table 7.4 gives an overview over the nucleobase content found in several CM meteorites (for abundances in carbonaceous chondrites of other types, see Pearce and Pudritz 2015). The meteorite samples were ordered by decreasing **G** abundance.

Meteorite	Sample Number	Type	**G**	**A**	**U**
Murray	Murr.	CM2	515	236	37
Yamato	Yamato 74.	CM2	420	n.d.	n.d.
Lonewolf Nunataks	LON	CM2	244	30	n.d.
Murchison	ASU 1	CM2	234	267	63
Yamato	Yamato 79.	CM2	230	n.d.	n.d.
Lewis Cliff	LEW	CM2	167	10	n.d.
Murchison	Smith.	CM2	56	5	n.d.
Meteorite Hills	MET	CM1	29	5	n.d.
Allan Hills	ALH	CM2	21	1	n.d.
Scott Glacier	SCO	CM1	2	4	n.d.

Notes. n.d.: Not detected. The sample numbers given here are abbreviated and shortened versions of the ones given in the review by Pearce and Pudritz (2015). Please refer to there for the full sample numbers. Sources of measured abundances: Stoks and Schwartz (1979), Stoks and Schwartz (1981), Shimoyama et al. (1990), and Callahan et al. (2011).

Table 7.4: Abundances of **G**, **A**, and **U** in ppb measured in carbonaceous chondrites of type CM.

Very recently, Oba, Takano, Furukawa, et al. (2022) found the pyrimidines **C** and **T** in carbonaceous chondrites, with ranges of 2–5 ppb and 1–5 ppb, respectively. Nevertheless, it is important to note that they used a different technique to extract the SOM in comparison to the previous studies that were reviewed in Pearce and Pudritz (2015). Oba, Takano, Furukawa, et al. (2022) used water for 10 min under ultra-sonication at room temperature, whereas the previous studies, e.g., Callahan et al. (2011), used 95 % formic acid for 24 h at 100 °C. Using this more gentle extraction method, Oba, Takano, Furukawa, et al. (2022) were able to preserve and detect the fragile **C** and **T** molecules for the first time, but measured systematically lower abundances for the other nucleobases **G**, **A**, and **U** in comparison to the previous studies. Therefore, the measured abundances are not comparable between the studies. Nevertheless, we will discuss these new findings in comparison to our simulated predictions.

8

Computational Methods

To perform the thermodynamic calculations we used the chemical equilibrium software *ChemApp* and as input the Gibbs energies from the *CHNOSZ* database. Taking into account the typical properties of carbonaceous chondrite parent bodies, we calculated the resulting nucleobase abundances.

8.1 Program Structure

With our model, we calculated the abundances of nucleobases using the reaction pathways from Table 7.1 and typical conditions found inside the parent bodies of carbonaceous chondrites. A detailed planetesimal heating model was adopted (see Section 7.5). Our model consisted of programs written in the four programming languages *Python3*, *C++*, *FORTRAN*, and *R*, which were combined into a single executable script. The source code, excluding the proprietary *ChemApp* library, and including the data of the planetesimal models, is openly available on Zenodo and as a Git repository (`https://github.com/klauspaschek/prebiotic_synthesis_planetesimal`, Paschek 2021).

8.1.1 Equilibrium Chemistry Software

The thermochemical equilibrium calculations were performed using the software *ChemApp* distributed by GTT Technologies (`https://gtt-technologies.de/software/chemapp/`, Petersen and Hack 2007). The *ChemApp* subroutines, provided as binaries in the *FORTRAN* programming language, were called in a program written in *C++*. The compiled *C++* source code and the *FORTRAN* binary files containing the *ChemApp* library were linked together using the compiler *g++*, which is part of the GNU Compiler Collection (GCC; `https://gcc.gnu.org/`). To use this mixed *C++*/*FORTRAN* code inside a *Python3* script, it was compiled into a *Cython* module usable in *Python3* with the *pybind11* library (`https:`

`//github.com/pybind/pybind11`, Jakob et al. 2017). A *Makefile* handles the necessary compiler flags and file extensions for easy building of the software with *g++*.

ChemApp requires the Gibbs coefficients from Equation 7.2 for each reactant and product, their initial abundances, and the temperature and pressure in the system. To compute the reactant and product abundances, including the targeted molecules for each reaction at equilibrium, *ChemApp* first breaks down the initial molecular abundances of the reactants into their elemental abundances (here carbon, hydrogen, oxygen, and nitrogen). Then it builds the system back up into the combination of reactants and product abundances that provides the minimum value of ΔG (Equation 7.4; Pearce and Pudritz 2016).

8.1.2 Gibbs Energy Data

The Gibbs energy data was obtained from the *CHNOSZ* thermodynamic database (version 1.3.6 (2020-03-16), `https://www.chnosz.net`, Dick 2019), a package for the programming language *R*. From these Gibbs energy data, the Gibbs coefficients used by *ChemApp* were derived by fitting Equation 7.2. By using the *Python3* module *rpy2* (`https://github.com/rpy2/rpy2`), the access of the data was managed from *Python3* as an embedded *R* session. Fitting of Equation 7.2 to the data to obtain the Gibbs coefficients was done with the *scipy.optimize.curve_fit()* function, part of the *scipy Python3* packages (`https://github.com/scipy/scipy`, Virtanen et al. 2020).

For a more detailed explanation about obtaining the Gibbs coefficients, we refer to A. K. Cobb, Pudritz, and Pearce (2015, Section 4.1) and Pearce and Pudritz (2016, Section 3.1).

8.1.3 Calculation of Abundances

The calculated molecular abundances were scaled to represent the absolute concentrations in the planetesimals for easy comparison with the values measured in carbonaceous chondrites. It was assumed that the synthesized molecules have been preserved in the icy form inside the planetesimals after they cooled at the end of the radioactive heating (see Section 7.5). Furthermore, it was assumed that the water ice completely filled the pores within the parent body, to remain consistent with the previous studies by A. K. Cobb, Pudritz, and Pearce (2015) and Pearce and Pudritz (2016) (who referred to Travis and Schubert 2005). By taking the porosity, the densities of ice and the bulk planetesimal material, and the molecular masses into account, the correct concentrations Z_i were calculated as follows:

$$Z_i = Y_i \cdot \phi \frac{\rho_{\text{ice}}}{\rho_{\text{rock}}} = X_i \frac{M_i}{M_{\text{H}_2\text{O}}} \cdot \phi \frac{\rho_{\text{ice}}}{\rho_{\text{rock}}}, \tag{8.1}$$

with X_i being the resulting concentration from *ChemApp* for the molecule i in units $[\text{mol}_i \cdot \text{mol}^{-1}_{\text{H}_2\text{O}}]$, M_i being the molar mass of the molecule i, $M_{\text{H}_2\text{O}}$ being the molar mass of water, Y_i being the absolute concentration, ϕ being the porosity, ρ_{ice} being the density of ice, and ρ_{rock} being the density of the bulk planetesimal material.

9

Results

The abundances of products of the reaction pathways from Table 7.1 were simulated using planetesimal models with different radii and times of formation after CAI. Figures 9.1, 9.2, and 9.3 show the adopted temperature curves (solid and dotted lines) in the largest considered planetesimal and the resulting target molecular abundances (dashed lines with symbols). The complete figure sets (3×10 images) are available (figshare, doi: 10.6084/m9.figshare.21545148). The supporting figure sets show the molecular abundances calculated using the other available planetesimal models. In each panel (a), for every distance from the center inside the planetesimal, the maximum temperature reached over the entire time evolution was used to calculate the molecular abundances. This corresponds to the conditions at which the synthesis of organics should be the fastest and hence the most efficient. The panels (b) show the time evolution in the center of the planetesimal, where the highest temperatures were reached.

As can be clearly seen, nucleobase abundances for some reactions varied with temperature, especially at $T \gtrsim 370$–$450\,\mathrm{K}$ when several reactions shut off, as already found by Pearce and Pudritz (2016). At these high temperatures, the reactions nos. 1, 6, 7, 8, 32, 43, and 51 showed this behavior in their study. The same was observed in our study, except the synthesis in reaction no. 43 shut off already at lower temperatures ($\sim 370\,\mathrm{K}$) compared to Pearce and Pudritz (2016, $\sim 530\,\mathrm{K}$). This was because of the lower initial concentrations of reactants used in our simulation, shifting the chemical equilibrium at these high temperatures compared to their previous study. Additionally, reaction no. 32 did not shut off at high temperatures, as explained below.

The model of Pearce and Pudritz (2016) that used the cometary ice abundances of the reactants led to an overproduction of the nucleobase concentrations by many orders of magnitude in comparison to the measurements in carbonaceous chondrites (10^5–10^6 ppb vs. 0.25–515 ppb, respectively). Only by scaling down the water content of the planetesimal by a factor of 5×10^{-4}, the upper limits of the abundances found in the carbonaceous chondrites were reached in the simulations by Pearce and Pudritz (2016).

Instead, in our model, the initial concentrations of the volatiles inside the parent bodies of carbonaceous chondrites were lowered by significant factors (but not the water abundance, see Table 7.3). With these scaled-down input abundances, an overall satisfactory agreement between the simulated and measured values was achieved for **A** and **G** (see Figures 9.1 and 9.3). For **U**, the simulated abundances are higher, but by less than one order of magnitude (see Figure 9.2), and these values are close to an agreement now. This confirms the findings by Pearce and Pudritz (2016) that the initial concentrations of reactants matter, in particular, those for HCN and formaldehyde. We found that the concentrations of CO and H_2 are a limiting factor as well (see below).

The meteoritic **C** and **T** abundances of 1–5 ppb (Oba, Takano, Furukawa, et al. 2022) are lower than the amounts resulting from the individual pathways (see Figures 9.2 and 9.3). The recent discovery of **C** and **T** suggests that these nucleobases were either easily decomposed or were involved in further chemical reactions. Therefore, this discrepancy is to be expected, as pathways transforming these nucleobases (in combination with **U**) into each other were considered in our model (reactions nos. 32 and 62). Combining these pathways with the possible decomposition of **T** by hydrogen peroxide (Shadyro et al. 2008, not considered here) might explain the **C** and **T** abundances found in carbonaceous chondrites (see Section 10.2 for a detailed discussion).

Pearce and Pudritz (2016) already investigated the importance of NH_3 in reactions nos. 3 and 4 along with nos. 7 and 8. They found that NH_3, and hence, the respective pathways nos. 4 and 8 might not be important, since the resulting **A** abundances were identical. We re-examined these pathways to check if the change in initial concentrations shifted the chemical equilibrium. Figure 9.1 shows that this was not the case and the resulting **A** abundances in the respective pairs of reactions stayed identical in comparison to each other. Therefore, we confirmed the findings of Pearce and Pudritz (2016). We further deduce from this that the proposed reaction pathway no. 3 in the theoretical study by Larowe and Regnier (2008) could explain which reaction is actually happening. It might be the balanced version of the reaction pathways no. 4 analyzed in the experimental work by Yamada et al. (1969) and Wakamatsu et al. (1966), at least in the environment inside planetesimals. This means that NH_3 either does not take part in the formation of **A** from HCN or acts as a catalyst. This is consistent with the experimental findings for reactions nos. 7 and 8, which resulted in similar produced maximum **A** amounts with (0.05 %, no. 8, Oró and Kimball 1961) and without (0.04 %, no. 7, Ferris, Joshi, Edelson, et al. 1978) NH_3 as a reactant.

The FT synthesis reaction no. 1 of **A** and the NC reaction no. 6 start both from CO and NH_3 as reactants, but no. 1 also involves H_2 and catalysts. Figure 9.1 shows very similar **A** abundances for these two reactions, which might rule out the necessity of H_2 in the formation of **A** in planetesimals. Nonetheless, Hayatsu, Studier, Oda, et al. (1968) found that reaction no. 6 synthesizes **A** only at temperatures above 500 °C, but **A** decomposes at these temperatures in less than 1 s (Pearce and Pudritz 2016, Table 2). The catalysts in reaction no. 1 might be necessary to form A at lower temperatures.

In summary, we found that the reaction pathways nos. 3 and 6 might be the balanced chemical equations for the unbalanced experimentally studied pathways nos. 4 and 1, respectively.

One significant new result from our study is the identification of the regions within the parent bodies from where nucleobase-containing meteorites have most likely been originated. Figure 9.1a shows that the reactions nos. 1 and 6 stopped producing **A** completely in the central regions of large planetesimals, and nos. 7 and 8 experienced a substantial decrease in the core region. If higher temperatures were reached inside the planetesimal (smaller time of formation after CAI or a bigger body), nos. 7 and 8 would stop completely. All other **A** reaction pathways would produce the same **A** abundances for the entire temperature range over which water remains liquid. However, when looking at Figure 9.1b, one can see that at later times, when the planetesimal cooled off, the shutdown reactions became again as productive as before the drop. This would suggest that these reaction pathways could have contributed to the production of the nucleobases in the core region. Still, one has to be careful as at such high temperatures, the formation of more refractory IOM could be favored, preventing the formation of **A** by irreversible "trapping" of the necessary reactants and by the improbable thermal destruction of IOM. Reaction nos. 43 and 51 showed the same behavior for **C** and **G** in Figures 9.2 and 9.3.

Further, Pearce and Pudritz (2016) set the resulting abundance of **C** in reaction no. 43 as the input **C** concentration in reaction no. 32. They observed that **C** was converted nearly completely to **U**, which means that nearly all of the **C** in a planetesimal deaminated into **U**. They used the output **C** of reaction no. 43 as the input for reaction no. 32, as reaction no. 43 produced the highest amount of **C** in their study, in particular, higher than the "direct" synthesis of **U** from HCN and formaldehyde in reaction no. 29. This situation has changed here, as we used lower initial concentrations of reactants. Here, reaction no. 44 (not no. 43) produced the highest amount of **C**. This was because the initial concentrations for HCN and formaldehyde were lowered less than for CO and H_2 (see depletion factors in Table 7.3), making a higher amount of reactants available to reaction no. 44 than to reaction no. 43. As mentioned above, the initial concentrations play a significant role and determine which reaction has the more abundant output. Therefore, we used the output **C** of reaction no. 44 as the input for the deamination reaction no. 32 to look for the upper limit of "indirect" formation of **U** via **C**, confirming the findings of Pearce and Pudritz (2016) once again, as all **C** was deaminated to **U** (see nearly identical resulting abundances of **U** in reactions nos. 32 and 44 in Figure 9.2). This is a very important result for understanding the overproduction of **U** and the low amounts of **C** and **T** in carbonaceous chondrites (see Section 10.2). Moreover, this explains why in our simulations, reaction no. 32 did not shut off at high temperatures as it did for Pearce and Pudritz (2016, $\sim 530\,\mathrm{K}$ there), but remained productive up to the boiling point of water. This is the case because reaction no. 32 now directly followed reaction no. 44 since it took its output **C** as input.

Taking a look at the individual meteorite samples in Table 7.4 and comparing them to the simulated nucleobase abundances allows us to determine from where inside the parent bodies a meteorite most likely originated. Further, the most suitable parent body for an individual meteorite can be inferred. To make this easier for the reader, the individual meteorites are marked on the abundance axis in Figures 9.1, 9.2, and 9.3 on the left.

Roughly three regimes can be identified inside the parent bodies when considering the temperatures and distances from the center at which particular types of chemical pathways shut off. The outermost and coolest regime ends when CO-consuming (including FT) reactions (nos. 1, 6, 43, and 51) shut off. This happens at ~350–400 K, corresponding to distances of ~55–100 km from the center in the 150 km-sized model planetesimal. Second, at temperatures above 400 K the water-consuming pathways no. 7, 8, and 54 start to decrease or shut off (at $\lesssim 50\,\mathrm{km}$ distance from the center in the 150 km-sized planetesimal). For **A**, one more regime can be identified. The high temperatures in the innermost core region allow only the remaining HCN- and NH_3-consuming pathways no. 3 and 4 to be fully productive.

For example, the interplay between these regimes can be illustrated by comparing the meteorite fragments *Murchison ASU 1* and *Murray* (*Murr.*). The **A** abundance of these meteorites is similar (267 ppb vs. 236 ppb) and at the high end of abundances found in CM meteorites, but the **G** abundance is much lower in *ASU 1* (234 ppb vs. 515 ppb, see Table 7.4). A possible explanation might be that these two meteorites originated from two different regions inside parent bodies. As *Murray* is at the upper end of both **A** and **G** abundances this meteorite should have originated from the uppermost location where all pathways are active. This would correspond to distances of $\gtrsim 100\,\mathrm{km}$ up to 138 km from the center in the 150 km-sized planetesimal when taking the always frozen and inactive surface shell into account. Smaller planetesimals might also have been the parent body of *Murray*, where it might have originated from the respective regime with temperatures $< 350\,\mathrm{K}$. *ASU 1*, in contrast, might have originated from the core of its parent body, which would explain the lower **G** abundance. In the 150 km-sized planetesimal this corresponds to distances of $\lesssim 50\,\mathrm{km}$ from the center.

Other CM2 meteorite samples with rather low **A** and **G** abundances such as *Lewis Cliff* (*LEW*), *Murchison Smith.*, and *Allan Hills* (*ALH*) might have been part of meteorites that originated from core regions as well. Another possibility might be that these meteorites originated from parent bodies with low initial CO and H_2 concentrations. As these were the most volatile reactants considered, the parent bodies of these meteorites might have formed inside the CO snowline, leaving no CO ice in the pebbles forming the parent body and shutting the respective CO-consuming pathways down. Together with the other pathways, this might explain the lower **A** and **G** abundances found.

In general, an early-formed and small parent body is beneficial to explain these lower abundances in CM2 meteorites. These parent bodies allow for liquid water only over several hundred thousand years but are still able to reach high enough temperatures leading to shut-off pathways in their cores (see supporting figure sets of Figures 9.1, 9.2, and 9.3; figshare, doi: 10.6084/m9.figshare.21545148). This might explain why these meteorites of petrologic type 2 (only medium aqueous alteration of chondrules) might have experienced such high temperatures without accelerating aqueous alteration too much as the high temperatures only persisted for a short duration.

On the other hand, the CM1 meteorites *Meteorite Hills* (*MET*) and *Scott Glacier* (*SCO*) might have originated from core regions of larger and late-formed planetesimals as aqueous alteration might have been possible over long timescales (several million years), accelerated additionally by high temperatures in the core. This would explain why CM2 and CM1 meteorites with similar (low) **A** and **G** abundances were found.

Finally, we could explain the ranges of nucleobases found in CM2 and CM1 meteorites, respectively, with a scenario that all CM2 meteorites originated from the same early-formed and small parent bodies, and all CM1 from the same late-formed and large parent bodies. By being fragments from different distances from the center of the same two types of parent bodies, the whole range of nucleobase abundances can be explained.

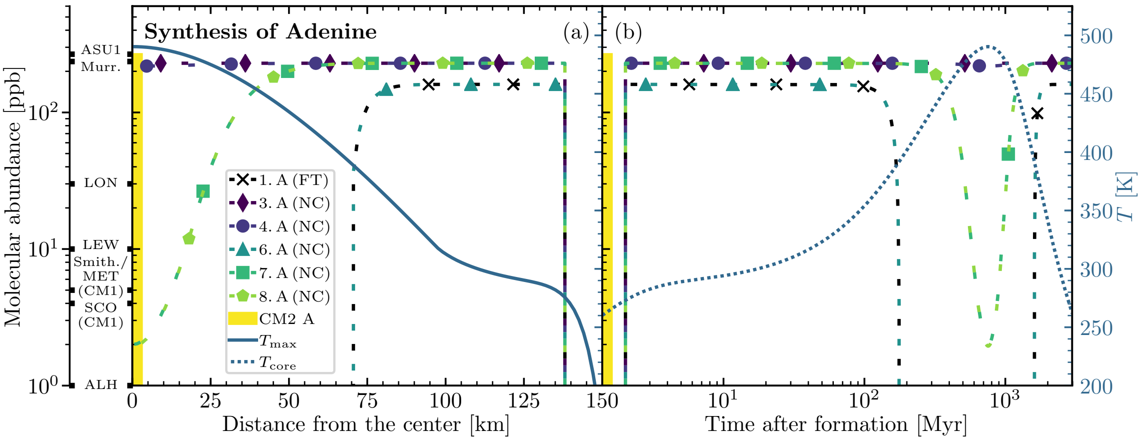

Figure 9.1: Adenine abundances from simulations of the adenine reaction pathways nos. 1, 3, 4, 6, 7, and 8 in Table 7.1. Properties of planetesimal: Radius = 150 km, densities $\rho_{\rm rock} = 3\,{\rm g\,cm^{-3}}$, $\rho_{\rm ice} = 0.917\,{\rm g\,cm^{-3}}$, porosity $\phi = 0.2$, and time of formation after CAI = 3.5 Myr. All simulations were run at 100 bar. In both panels (a) and (b) the left vertical axis corresponds to the abundances (dashed lines with symbols) and the right vertical axis corresponds to the temperatures from the planetesimal model (solid and dotted lines). In the figure legend, each reaction pathway no. is assigned to a symbol, the nucleobase produced is indicated with its initial letter in upper case, and the respective reaction type (FT or NC) in parenthesis. Each pathway is plotted as a dashed line with its assigned symbol. The left panel (a) shows the distribution of abundances for the maximum temperature $T_{\rm max}$ (solid line) reached at a specific distance from the center inside the planetesimal (center at the left and surface at the right). Adenine was synthesized at and below a distance of 138 km from the center. The right panel (b) shows the temporal evolution of abundances at temperatures $T_{\rm core}$ (dotted line) in the center of the planetesimal (the same temperature evolution curve can be found in Figure 7.1c). Adenine synthesis started at 2 Myr after formation. The shaded part of the abundance axis represents the range of adenine abundances measured in CM2 meteorites (Callahan et al. 2011; Stoks and Schwartz 1981), and has no correlation to the radial location inside the object or the point in time (horizontal axes). On the left vertical abundance axis, the adenine abundances measured in individual meteorites are marked (using the abbreviated sample numbers in Table 7.4). All meteorites are of type CM2 unless otherwise noted. Meteorites of type CM1 are indicated as such in parentheses below the abbreviated sample number. The complete figure set (10 images) is available (figshare, doi: 10.6084/m9.figshare.21545148). It contains the calculated abundances for the other available planetesimal models with different radii and times of formation after CAI.

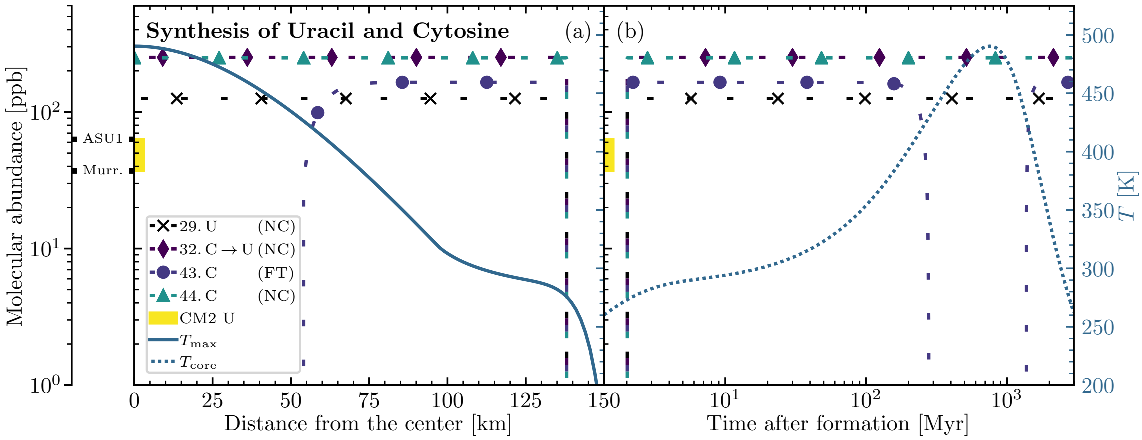

Figure 9.2: Uracil and cytosine abundances from simulations of their reaction pathways nos. 29, 32, 43, and 44 in Table 7.1. Properties of planetesimal: Radius = 150 km, densities $\rho_{\mathrm{rock}} = 3\,\mathrm{g\,cm^{-3}}$, $\rho_{\mathrm{ice}} = 0.917\,\mathrm{g\,cm^{-3}}$, porosity $\phi = 0.2$, and time of formation after CAI = 3.5 Myr. All simulations were run at 100 bar. In both panels (a) and (b) the left vertical axis corresponds to the abundances (dashed lines with symbols) and the right vertical axis corresponds to the temperatures from the planetesimal model (solid and dotted lines). In the figure legend, each reaction pathway no. is assigned to a symbol, the nucleobase produced (or transformation between nucleobases indicated by a reaction arrow) is indicated with its initial letter in upper case, and the respective reaction type (FT or NC) in parenthesis. Each pathway is plotted as a dashed line with its assigned symbol. The left panel (a) shows the distribution of abundances for the maximum temperature T_{max} (solid line) reached at a specific distance from the center inside the planetesimal (center at the left and surface at the right). Uracil and cytosine were synthesized at and below a distance of 138 km from the center. The right panel (b) shows the temporal evolution of abundances at temperatures T_{core} (dotted line) in the center of the planetesimal (the same temperature evolution curve can be found in Figure 7.1c). Uracil and cytosine synthesis started at 2 Myr after formation. The shaded part of the abundance axis represents the range of uracil abundances measured in CM2 meteorites (Stoks and Schwartz 1979), and has no correlation to the radial location inside the object or the point in time (horizontal axes). On the left vertical abundance axis, the uracil abundances measured in individual meteorites of type CM2 are marked (using the abbreviated sample numbers in Table 7.4). The complete figure set (10 images) is available (figshare, doi: 10.6084/m9.figshare.21545148). It contains the calculated abundances for the other available planetesimal models with different radii and times of formation after CAI.

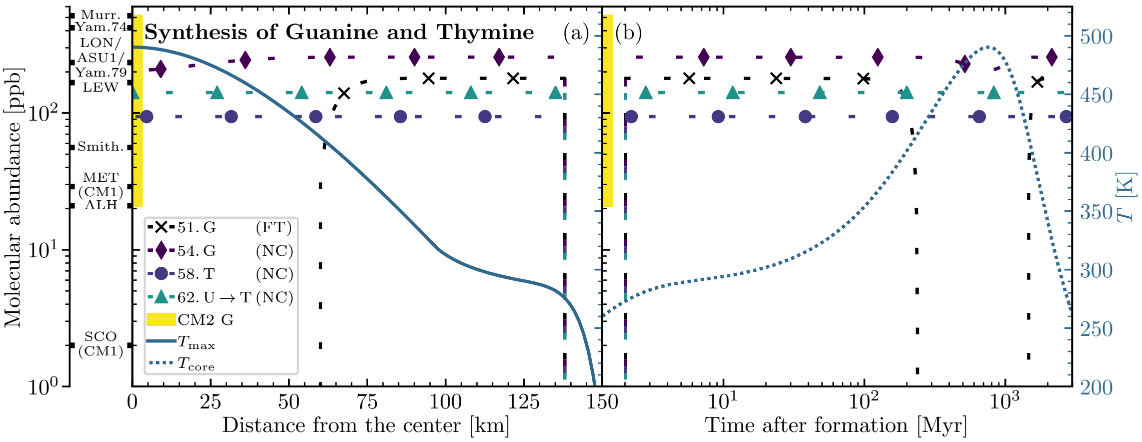

Figure 9.3: Guanine and thymine abundances from simulations of their reaction pathways nos. 51, 54, 58, and 62 in Table 7.1. Properties of planetesimal: Radius = 150 km, densities $\rho_{\text{rock}} = 3\,\text{g}\,\text{cm}^{-3}$, $\rho_{\text{ice}} = 0.917\,\text{g}\,\text{cm}^{-3}$, porosity $\phi = 0.2$, and time of formation after CAI = 3.5 Myr. All simulations were run at 100 bar. In both panels (a) and (b) the left vertical axis corresponds to the abundances (dashed lines with symbols) and the right vertical axis corresponds to the temperatures from the planetesimal model (solid and dotted lines). In the figure legend, each reaction pathway no. is assigned to a symbol, the nucleobase produced (or transformation between nucleobases indicated by a reaction arrow) is indicated with its initial letter in upper case, and the respective reaction type (FT or NC) in parenthesis. Each pathway is plotted as a dashed line with its assigned symbol. The left panel (a) shows the distribution of abundances for the maximum temperature T_{max} (solid line) reached at a specific distance from the center inside the planetesimal (center at the left and surface at the right). Guanine and thymine were synthesized at and below a distance of 138 km from the center. The right panel (b) shows the temporal evolution of abundances at temperatures T_{core} (dotted line) in the center of the planetesimal (the same temperature evolution curve can be found in Figure 7.1c). Guanine and thymine synthesis started at 2 Myr after formation. The shaded part of the abundance axis represents the range of guanine abundances measured in CM2 meteorites (Callahan et al. 2011; Shimoyama et al. 1990; Stoks and Schwartz 1981; Velden and Schwartz 1977), and has no correlation to the radial location inside the object or the point in time (horizontal axes). On the left vertical abundance axis, the guanine abundances measured in individual meteorites are marked (using the abbreviated sample numbers in Table 7.4). All meteorites are of type CM2 unless otherwise noted. Meteorites of type CM1 are indicated as such in parentheses below the abbreviated sample number. The complete figure set (10 images) is available (figshare, doi: 10.6084/m9.figshare.21545148). It contains the calculated abundances for the other available planetesimal models with different radii and times of formation after CAI.

10

Discussion

As the resulting amounts of nucleobases produced by various reaction pathways depend strongly on the initial concentrations of the volatiles, and these can only be estimated roughly, the presented results represent the best-case scenario. Pearce and Pudritz (2016) used the measured abundances of the volatiles in comets, but this pristine matter may not represent the actual source material of the carbonaceous chondrites' parent bodies formed in a much warmer region of the solar nebula (as described in Section 7.4). The application of solar nebula chemistry models and constraints from TPD experiments allowed us to constrain the abundances of volatiles in the regions of the carbonaceous chondrite parent bodies.

10.1 Influence of Initial Volatile Concentrations

The disagreement between experimental findings and theoretical models is visualized in Figure 10.1. To explore the influence of the initial concentrations of the volatile reactants, the concentration of one of the volatiles was varied. The other involved reactants in each pathway were left at their predicted concentrations in Table 7.3. Using standard conditions of 0 °C and 100 bar, the dependence of the resulting nucleobase abundances was calculated.

The amount of CO and HCN initially available in the planetesimals influenced the nucleobase abundances the most, whereas the depletion applied to the cometary abundances of H_2 and formaldehyde had a minor effect. The chemical pathways show a linear dependence on the initial volatile concentration, and the majority of species reaches a saturation plateau for high volatile concentrations. A higher abundance of initial volatile reactants does not lead to more nucleobase production, in short, the nucleobase abundance does not depend on the initial volatile content any longer at high concentrations.

The reduction of the cometary H_2 concentration did not change the results and would not even change them for two orders of magnitude stronger depletion (see

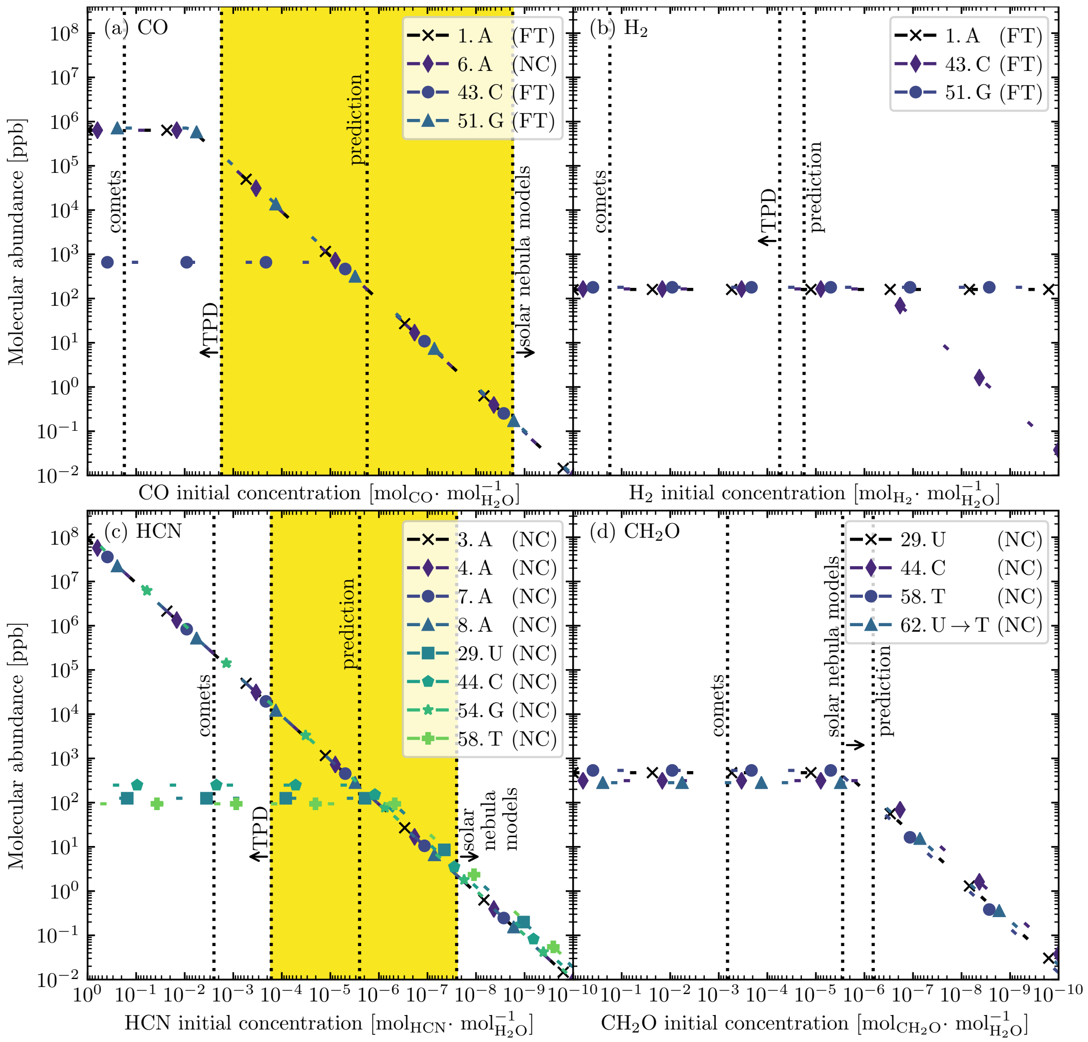

Figure 10.1: Nucleobase abundances from simulations of their reaction pathways in Table 7.1 depending on variable initial concentrations of one of the volatile reactants CO, H_2, HCN, or CH_2O. All simulations were performed at 0 °C and 100 bar. Properties of planetesimal: Densities $\rho_{\text{rock}} = 3\,\text{g}\,\text{cm}^{-3}$, $\rho_{\text{ice}} = 0.917\,\text{g}\,\text{cm}^{-3}$, and porosity $\phi = 0.2$. Panel (a) shows how the resulting abundances (dashed lines with symbols) for the nucleobases in the pathways involving CO depended on its initial concentration while the other involved reactants in each pathway were left at their predicted concentrations in Table 7.3. Panels (b), (c), and (d) show the same for H_2, HCN, and CH_2O, respectively. In the figure legends in each panel, each reaction pathway no. is assigned to a symbol, the nucleobase produced (or transformation between nucleobases indicated by a reaction arrow) is indicated with its initial letter in upper case, and the respective reaction type (FT or NC) in parenthesis. Each pathway is plotted as a dashed line with its assigned symbol. The vertical dotted lines indicate the initial volatile concentrations for the values i) measured in *comets*, ii) reduced by the fraction found to be left at 161.3 K in the measurements of *TPD* experiments (if available), iii) the best *prediction* obtained in the present study, and iv) (if available) obtained from *solar nebula models* (see Tables 7.2 and 7.3). If both TPD and solar nebula models were available for the respective volatile, the yellow shaded area indicates the range in between as the possible span of initial concentrations for the respective volatile in meteorite parent body planetesimals, and therefore also possible resulting nucleobase abundances.

Figure 10.1b). Therefore, it is a safe assumption to use the TPD spectra of D_2 in Figure 12.2 as a proxy for the initial H_2 concentration in carbonaceous chondrite parent bodies (see Section 7.4.4). For formaldehyde, the depletion had the least impact, as the saturation plateau is close to the predicted concentration used (see Figure 10.1d). For these two volatiles either results from TPD experiments or solar nebula models were taken into account (see Table 7.2), but as their influence on the nucleobase abundances is minor this imposes a negligible limitation on the validity of the presented results.

A change in the CO and HCN concentrations resulted in a one-to-one shift in the nucleobase abundances (see Figures 10.1a and c). Clearly, the use of cometary concentrations provides an incorrect impression of the potential for nucleobase synthesis in parent bodies, and thus in carbonaceous chondrites, by several orders of magnitude. Nevertheless, the constraints on the volatile depletion by TPD experiments and chemical solar nebula models still allow for a broad spectrum of theoretically possible nucleobase abundances in carbonaceous chondrites (highlighted as yellow areas in Figure 10.1). It is the task of future solar nebula models to include the experimental findings of volatile trapping and diffusion in a more appropriate way. The fact that the predicted abundances of **A** and **G** are in close agreement with the measured ones shows that considering all these effects is crucial to understanding why we find such abundances in meteorites.

10.2 Overproduction of U and the Low Amounts of C and T in Carbonaceous Chondrites

A possible explanation for the slight overproduction of **U** is a combination of the reactions with nos. 32 and 62 and the fact that low **C** and **T** abundances have been found in carbonaceous chondrites (1–5 ppb; Oba, Takano, Furukawa, et al. 2022). The initial concentration of **C** in reaction no. 32 was set to the resulting one in reaction no. 44. Figure 9.2 shows that the deamination reaction no. 32 was capable of converting **C** ultimately to **U**, as the resulting abundances in both reactions match each other perfectly for all temperatures. This could explain why little **C** has been found in carbonaceous chondrites, as it was probably formed, but was then almost completely transformed to **U** (for another possible explanation for the low amount of **C** see Pearce and Pudritz 2016, Section 5.5). Furthermore, the resulting abundance of **U** in reaction no. 32 was used as the initial concentration in reaction no. 62, and half the amount of **U** was converted to **T**. This could explain why the measured abundances of **U** in carbonaceous chondrites (shaded regions in Figure 9.2) are lower than the simulated values. This explanation may only work if there is an additional destruction pathway for **T** as low abundances were found in the meteorites, as mentioned above. Pearce and Pudritz (2016) have proposed destruction of **T** by hydrogen peroxide (H_2O_2; Shadyro et al. 2008). Thus, when taking this possible explanation into account, our model is able to consistently explain the measured concentrations for all nucleobases.

However, because the reactions were handled separately, the coupling of reactions nos. 32 and 62 was not adequately simulated, and as a consequence, the resulting **U** and **T** abundances in those reactions merely reflect upper bounds. The trends for the **C** and **T** abundances in meteorites (Oba, Takano, Furukawa, et al. 2022) are qualitatively confirmed by these particular results, which only indicate trends with presumably lower actual abundances.

10.3 Alternative Pathways, Isomers, Derivatives

In addition to the canonical nucleobases studied in this paper, other purines and pyrimidines have been found in carbonaceous chondrites. Pearce and Pudritz (2015) discussed the presence of xanthine, hypoxanthine, purine, 2,6-diaminopurine, and 6,8-diaminopurine in these meteorites, but due to the lack of experimentally verified pathways applicable to the environment of planetesimals, they were not considered further. If new experimental data become available it would of course be worth applying our model to these molecules. This could also shift the view on the canonical nucleobases, as these alternative molecules could be competing for reactants or be side products shifting the resulting abundances for the canonical nucleobases as presented here.

For the first time, Oba, Takano, Furukawa, et al. (2022) found **C** and **T** in carbonaceous chondrites. Besides all the canonical nucleobases, they also found isomers of the canonical nucleobases and other derivatives, most prominently imidazole and several alkylated analogs. Most of these nucleobase and imidazole derivatives are missing in the *CHNOSZ* Gibbs energy database and cannot be modeled yet.

The fundamental isomers of **G** and **C**, isoguanine and isocytosine, respectively, are critical as they might be direct side products in the formation process. On the other hand, the isomers have minor to negligible abundances in comparison to their canonical counterparts (Oba, Takano, Furukawa, et al. 2022). The ratio of isoguanine to **G** was found to be $\sim 0.6\,\%$, the ratio of isocytosine and **C** was $\sim$10–25 % (depending on meteorite fragment). We did not consider these isomers in the present study because of their low abundances and the lack of experimental data.

We acknowledge this as a limitation of our study. When new experimentally verified pathways applicable in this context become available in the future, they should be added to the set of reactions. This might allow to determine if they have the potential to compete for the available reactants, and hence, also change the resulting canonical nucleobase abundances.

10.3.1 Non-aqueous Formation Pathways and Inherited Organics

We want to note that asteroids and meteorites might contain material that was formed in radiation-induced chemical reactions in the interstellar medium or the protosolar disk stage of the solar system and then inherited into these bodies. Ciesla and Sandford (2012) showed in their model that icy pebbles might have traveled to different parts of the protosolar disk. On their irregular paths, they were exposed to ultraviolet irradiation and thermal warming that, in laboratory studies, have been demonstrated to produce complex organics (see, e.g., Nuevo et al. 2014; Materese et al. 2018; Oba, Takano, Naraoka, N. Watanabe, et al. 2019). This was also verified by theoretical quantum calculations (see, e.g., Bera, Nuevo, Milam, et al. 2010; Bera, Nuevo, Materese, et al. 2016; Bera, Stein, et al. 2017). Analysis of the particles returned from comet 81P/Wild 2 by the Stardust mission showed that the nonvolatile part of the comet is made of an unequilibrated assortment of materials from both presolar and solar system origins. Some of these cometary particles were formed in the inner solar system (Brownlee et al. 2006). Therefore, the inheritance and mixing of radiation-induced organics into carbonaceous chondrite parent bodies might be imaginable. Still, we want to highlight the distinction between comets and carbonaceous chondrites. The amount of inherited organic material in carbonaceous chondrites is not precisely quantified, as they represent highly processes bodies in comparison to comets. Further, handling the environment for the synthesis of irradiation-induced organics, their incorporation into carbonaceous chondrite parent bodies, and their survival there requires an additional model completely different from the scenario investigated here. Calculating the synthesis and exact amount of possibly inherited organic material in carbonaceous chondrites is far beyond the scope of the present study.

11

Conclusions

By lowering the initially high pristine cometary concentrations of volatile ices to values appropriate for the location of carbonaceous chondrite parent bodies and introducing a comprehensive planetesimal model of the parent bodies of carbonaceous chondrites, we successfully simulated the synthesis of all canonical nucleobases in meteorites in a consistent approach. Meteorites are time capsules from when the solar system formed $\sim 4.56\,\mathrm{Gyr}$ ago. They may reveal how the first building blocks of life could have been formed without the highly complex metabolism of the present life on Earth. The reaction pathways suggested by Pearce and Pudritz (2015) and Pearce and Pudritz (2016) and listed in Table 7.1 seem to explain reasonably well how nucleobases might have been formed abiotically.

The coupling of a thermochemical equilibrium model with a 1D thermodynamic planetesimal model allows to understand the history of the prebiotic synthesis in the carbonaceous chondrites' parent bodies over time. Further, it allows us to predict which regions of the parent bodies might have been the origin of the fragments containing the rich prebiotic molecule content that we find today in carbonaceous chondrites. The intermediate shell of a medium-sized parent body, which is not too close to the hot core and far enough away from the cold surface, should be the primary source of nucleobase-rich organics in carbonaceous chondrites. The fragments descending from this shell upon planetesimal collisions in the nebula might have been the source of the first prebiotic molecules on Earth, delivered to the young planet during the late heavy bombardment phase.

We confirm the finding of Pearce and Pudritz (2016) that the "indirect" formation of **U** via **C** (deamination reaction no. 32) should have contributed more to the **U** abundance in carbonaceous chondrites than the "direct" synthesis from HCN and formaldehyde in reaction no. 29, even for the lower initial concentrations of reactants used here. Reaction no. 44 and not reaction no. 43 (which shuts off at high temperatures) was the most effective one in producing **C** and therefore **U** via reaction no. 32. This implies that the hottest central parts of the parent bodies could have been the origin of **U**-rich carbonaceous chondrites (see Figure 9.2a). The reduction of the initial concentrations of reactants leads to a situation where the planetesimal cores contribute significantly to carbonaceous chondrites containing **U**.

This is in agreement with the **U** abundances measured in the meteorites *ASU 1* and *Murray* (see Table 7.4 and Figure 9.2). *ASU 1* was found to originate from a location closer to the core of its parent body than *Murray*, as inferred from the simulated abundances of **A** and **G** (see Section 9). This is reflected in the **U** abundances measured in these meteorites, as the core fragment *ASU 1* contains a higher **U** concentration than *Murray*. This confirms the above conclusion regarding the enhanced **U** synthesis in planetesimal cores due to reduced initial volatile concentrations. Thus, this validates the need to account for the depletion of volatiles and substantiates that our model can consistently identify the origins of individual meteorites.

Future studies of the solar nebula evolution with detailed gas-ice chemistry, growth, dynamics of the solids, gravitational collapse, and formation of asteroids from pebbles are needed to better constrain the original composition in organics in the carbonaceous chondrite parent bodies.

Pearce and Pudritz (2016) found that the FT synthesis was the dominant mechanism to form nucleobases in planetesimals. This has changed here as the initial concentrations of CO and H_2 involved in FT synthesis were reduced more than for HCN and formaldehyde involved in NC synthesis (see Table 7.3), making now the NC synthesis the dominating mechanism for producing nucleobases in planetesimals. Still, FT and NC synthesis both contribute significantly.

An almost perfect match between the results of our calculations and the nucleobase concentrations measured in carbonaceous chondrites suggests that our new approach to adjusting the initial abundances of volatiles may indeed be correct (see also Dauphas and Marty 2002).

The sugar ribose, making up the backbone of RNA together with phosphates, was just found recently in carbonaceous chondrites (Furukawa et al. 2019). This molecule offers another excellent chance to model its formation in the parent bodies of the carbonaceous chondrites. In a follow-up study, we modeled its synthesis with our model, starting from formaldehyde and glycolaldehyde as reactants (Paschek, Kohler, et al. 2022). Thermodynamic data and initial concentrations for glycolaldehyde are available from the previous study by A. K. Cobb, Pudritz, and Pearce (2015). As another key building block of the RNA world, ribose gives valuable insights into the possible exogenous origin of life on our planet and beyond.

11.1 Acknowledgments

K.P. acknowledges financial support by the Deutsche Forschungsgemeinschaft (DFG, German Research Foundation) under Germany's Excellence Strategy EXC 2181/1 - 390900948 (the Heidelberg STRUCTURES Excellence Cluster). K.P. is a fellow of the International Max Planck Research School for Astronomy and Cosmic Physics at the University of Heidelberg (IMPRS-HD). D.A.S. acknowledges financial support by the Deutsche Forschungsgemeinschaft through SPP 1833: "Building a Habitable Earth" (SE 1962/6-1). T.K.H. acknowledges financial support by the European Research Council under the Horizon 2020 Framework Program via the ERC Advanced Grant Origins 83 24 28. R.E.P. is supported by an NSERC Discovery Grant. The authors thank Cornelis P. Dullemond for his extensive help in understanding the planetesimal model and the background attached to its theory. We thank Jiao He for providing his measured data of TPD spectra to us, which helped to constrain the trapping and depletion of volatiles substantially. The authors would like to thank an anonymous reviewer for valuable comments and suggestions, which helped to improve the quality of the manuscript significantly. We would also like to thank Catharina Fairchild for her stylistic review of the manuscript.

11.2 Software

prebiotic_synthesis_planetesimal (Klaus Paschek 2021, https://github.com/klauspaschek/prebiotic_synthesis_planetesimal, Paschek 2021), ChemApp (GTT Technologies 2020, https://gtt-technologies.de/software/chemapp/, Petersen and Hack 2007), GNU Compiler Collection (GCC, Free Software Foundation, Inc. 2020, https://gcc.gnu.org/), pybind11 (Wenzel Jakob 2016, https://github.com/pybind/pybind11, Jakob et al. 2017), CHNOSZ (Jeffrey M. Dick 2020, version 1.3.6 (2020-03-16), https://www.chnosz.net, Dick 2019), rpy2 (Laurent Gautier 2008 - 2010, https://github.com/rpy2/rpy2), NumPy (NumPy Developers 2005 - 2021, https://numpy.org/, Harris et al. 2020), SciPy (Enthought, Inc. 2001 - 2002, SciPy Developers 2003 - 2019, https://docs.scipy.org/doc/scipy/reference/, Virtanen et al. 2020), Matplotlib (John Hunter, Darren Dale, Eric Firing, Michael Droettboom and the Matplotlib development team 2002 - 2012, The Matplotlib development team 2012 - 2021, https://matplotlib.org/, Hunter 2007)

12

Appendix: TPD Spectra Provided with Permission by J. He (Private Communication)

The Figures 12.1 and 12.2 show measured TPD spectra for the volatiles ^{13}CO and D_2 deposited together with water ice. These spectra were used to constrain the depletion of volatiles in carbonaceous chondrite parent bodies in comparison to comets (see Section 7.4.4 and Table 7.2). The measurements were provided with permission by J. He (private communication).

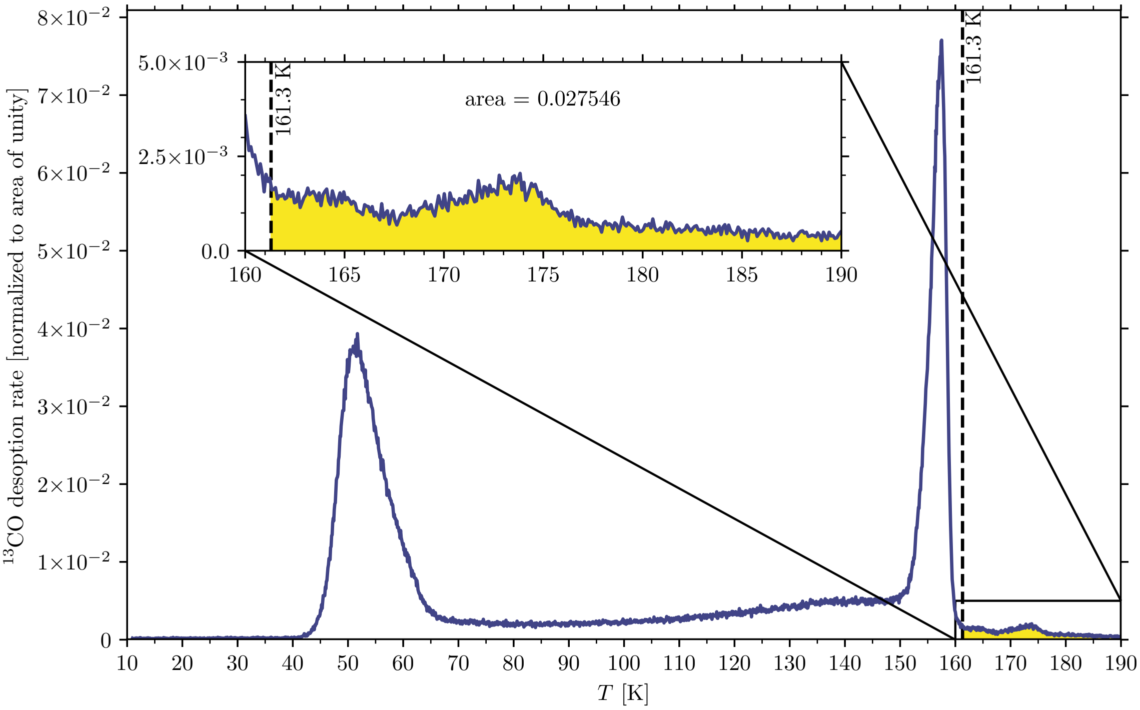

Figure 12.1: Results of TPD experiment for ^{13}CO-H$_2$O ice provided with permission by J. He (private communication). The ratio between the volatile and water was 1:10, and the mixture was deposited at 10 K and then warmed up while measuring the volatile desorption rate. The inset plot shows a zoom of the volatile trapped in the bulk water ice after "molecular volcano" desorption. The yellow shaded area indicates the integrated amount of volatile trapped above 161.3 K, which corresponds to the temperature in the region of carbonaceous chondrite parent bodies at 2.5 au in the solar nebula (see Section 7.5.1).

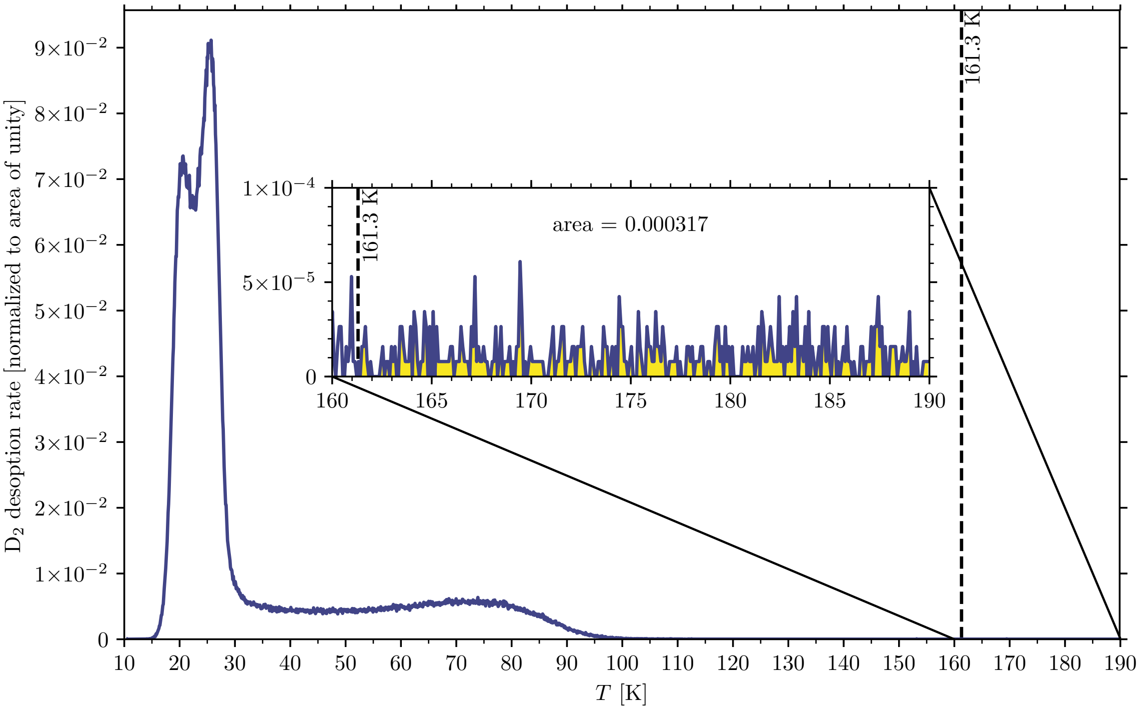

Figure 12.2: Results of TPD experiment for D_2-H_2O ice provided with permission by J. He (private communication). The ratio between the volatile and water was 1:10, and the mixture was deposited at 10 K and then warmed up while measuring the volatile desorption rate. In the zoomed-in inset plot, the yellow shaded area indicates the integrated amount of volatile trapped above 161.3 K, which corresponds to the temperature in the region of carbonaceous chondrite parent bodies at 2.5 au in the solar nebula (see Section 7.5.1).

Part III

POSSIBLE RIBOSE SYNTHESIS IN CARBONACEOUS PLANETESIMALS

Klaus Paschek, Kai Kohler, Ben K. D. Pearce, Kevin Lange, Thomas K. Henning, Oliver Trapp, Ralph E. Pudritz, Dmitry A. Semenov

This following Part is based on the work *"Possible Ribose Synthesis in Carbonaceous Planetesimals"*, published in the March 2022 issue 3, part of Volume 12, of the journal *Life* (Paschek, Kohler, et al. 2022) as part of the Ph.D. thesis.

The published paper has been reformatted to fit the format of this thesis. The work on the paper was divided as follows: I wrote the main simulation code, building on the pre-existing code published by Pearce and Pudritz (2016) and Paschek, Semenov, et al. (2023). Kevin Lange contributed the thermodynamic planetesimal model developed during his bachelor and master thesis under the supervision of Prof. Dr. Cornelis P. Dullemond. Kai Kohler performed the formose reaction in the laboratory of Prof. Dr. Oliver Trapp and provided the yields of ribose as a fraction of all pentoses, see Section 15.1.

I drafted the first version of the whole manuscript. The other co-authors contributed by commenting on at least one version of the draft.

Graphical Abstract

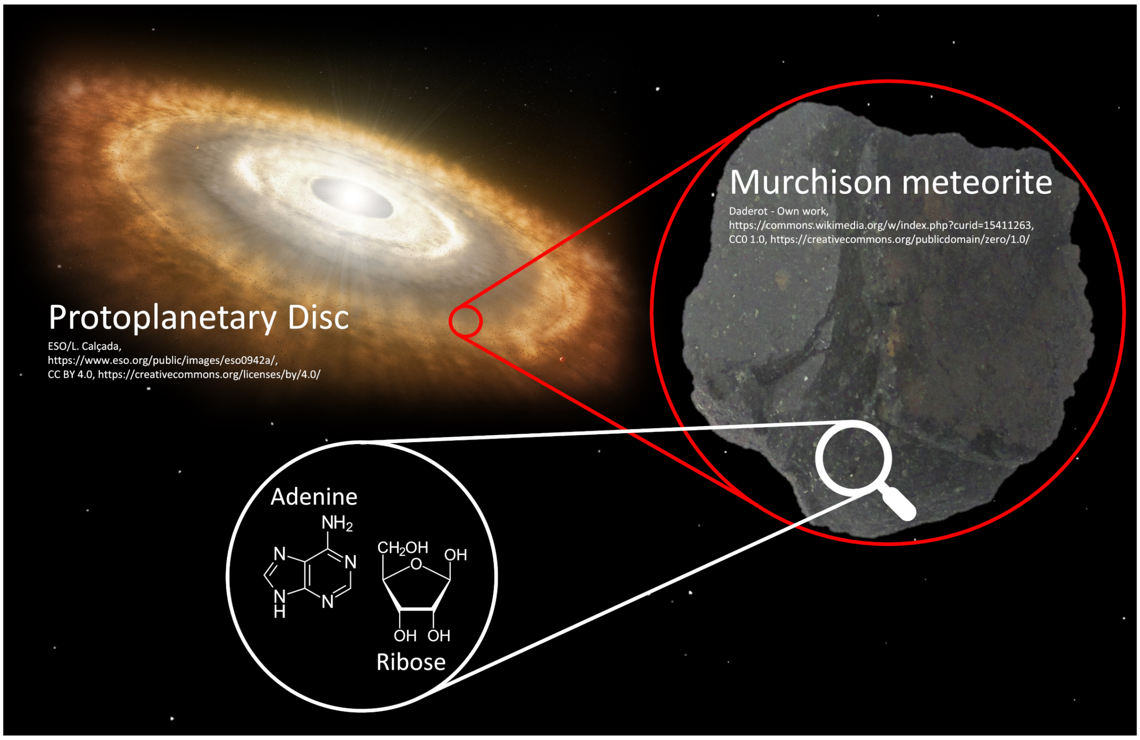

Figure 12.3: Graphical abstract of Paschek, Kohler, et al. (2022).

Abstract

The origin of life might be sparked by the polymerization of the first RNA molecules in Darwinian ponds during wet-dry cycles. The key life-building block ribose was found in carbonaceous chondrites. Its exogenous delivery onto the Hadean Earth could be a crucial step toward the emergence of the RNA world. Here, we investigate the formation of ribose through a simplified version of the formose reaction inside carbonaceous chondrite parent bodies. Following up on our previous studies regarding nucleobases with the same coupled physico-chemical model, we calculate the abundance of ribose within planetesimals of different sizes and heating histories. We perform laboratory experiments using catalysts present in carbonaceous chondrites to infer the yield of ribose among all pentoses (5Cs) forming during the formose reaction. These laboratory yields are used to tune our theoretical model that can only predict the total abundance of 5Cs. We found that the calculated abundances of ribose were similar to the ones measured in carbonaceous chondrites. We discuss the possibilities of chemical decomposition and preservation of ribose and derived constraints on time and location in planetesimals. In conclusion, the aqueous formose reaction might produce most of the ribose in carbonaceous chondrites. Together with our previous studies on nucleobases, we found that life-building blocks of the RNA world could be synthesized inside parent bodies and later delivered onto the early Earth.

13

Introduction

Ribose was recently identified in the soluble organic matter of carbonaceous chondrites (Furukawa et al. 2019), with measured concentrations of 4.5–25 ppb (parts per billion). Along with comets, the parent bodies of carbonaceous chondrites or their fragments are considered as one of the major sources of pristine organic matter that have been exogenously delivered onto the Hadean and Eoarchean Earth during the late heavy bombardment, see, e.g., (Chyba, Thomas, et al. 1990; Chyba and Sagan 1992; Gomes et al. 2005; Kooten et al. 2021; Fischer-Gödde, Elfers, et al. 2020; Pizzarello and Shock 2017), and are still falling to Earth nowadays.

One of the favored theories of the origin of life relies on the finding that RNA molecules can act as both catalysts of self-replication and genetic information storage, see, e.g., (A. Rich 1962; Gilbert 1986; Kruger et al. 1982; Guerrier-Takada, Gardiner, et al. 1983; Guerrier-Takada and Altman 1984; Zaug and Cech 1986; Cech 1986; Johnston et al. 2001; Vaidya et al. 2012). So-called ribozymes allow solving the fundamental "chicken-or-the-egg" problem in the process of abiogenesis and the emergence of life: What came first, the genetic information macromolecules like RNA and DNA coding for protein sequences or the enzymatic proteins catalyzing the formation of information storage molecules and other biomolecular reactions? One mutually compatible molecule is needed for the synthesis and *survival* of the other one, and vice versa.

RNA polymers could solve this dilemma by providing both these functionalities, serving as the universal "Swiss Army knife" to the organocatalysis of the first complex biomolecules. The polymerization of oligonucleotides and RNA-like molecules was shown to be possible in the hydrothermal field settings, in the presence of clays or salts (Ferris, A. R. Hill, et al. 1996; Ferris, Joshi, K. J. Wang, et al. 2004; Da Silva et al. 2015), metal ion catalysts (Orgel 2004), and in lipid bilayers (Toppozini et al. 2013). In particular, wet-dry cycles, which were meant to simulate the natural cycling in warm little ponds (WLPs) on freshly formed volcanic islands on the Hadean Earth, were shown to promote the formation of RNA-like chains made up of up to 300 linked residues (Da Silva et al. 2015; Damer and Deamer 2020a). S. Becker, Schneider, et al. (2018) and S. Becker, Feldmann, et al. (2019) showed in lab experiments that the formation of RNA nucleosides and nucleotides was plausible in *one pot* in WLPs during wet-dry cycles (requiring specific and changing conditions with respect to temperature and pH). They added ribose without forming it in the same pot, which makes the possibility of an exogenous delivery by meteorites an intriguing hypothesis. The different pathways to nucleosides and nucleotides shown in experiments by Orgel and colleagues (Fuller et al. 1972c; Fuller et al. 1972a), Kim and Benner (2017) and Kim and Benner (2018), and Nam et al. (2018) also all required the prior presence of ribose. Pearce, Pudritz, et al. (2017) considered the delivery of nucleobases by carbonaceous chondrites to WLPs as a source for the formation and polymerization of oligonucleotides during wet-dry cycles. Similarly, ribose-rich meteorites might provide another crucial ingredient for this process that lead to the emergence of the first RNA-like molecules on the early Earth.

The crucial components that make up the backbone of these linked oligonucleotides are the pentose (5C), ribose, and phosphate groups. Our study sought to model the formose reaction pathway leading to the synthesis of ribose inside carbonaceous planetesimals. We used the same model as developed in our previous study by Paschek, Semenov, et al. (2022), where we studied the formation of nucleobases inside the parent bodies of carbonaceous chondrites. Our model comprised an up-to-date thermochemical equilibrium model coupled with a 1D thermodynamic planetesimal model to calculate the abundances of prebiotic molecules via abiotic synthesis pathways under realistic conditions inside parent body planetesimals. By applying the same model to ribose, we elucidated a more comprehensive understanding of the formation of crucial building blocks of the RNA world in outer space, very early in the history of our solar system.

The theoretical background is provided in Section 14.1. First, we introduce our approach to model the formose reaction pathway, focusing on the synthesis of ribose. Further, we briefly recall our new concept to estimate the initial concentrations of the volatiles in carbonaceous planetesimals, which was explained in more detail in Paschek, Semenov, et al. (2022). Next, in Section 14.2, we outline our computational methods. We also explain how the Gibbs free energy of formation of glycolaldehyde needed for our theoretical model was estimated, as it is missing in the database that we used. In Section 15, we first present our experimental results regarding the efficiency of ribose formation among other 5Cs in the presence of various mineral catalysts representative of carbonaceous chondrites. Second, we present our theoretical results, incorporating the ribose yields obtained in our experiments. We analyze our results and compare them to the measured values in carbonaceous chondrites. The discussion and conclusions follow in Section 16. We discuss the possible decomposition processes of ribose and gave a suggestion for the region within the planetesimals with the likely highest ribose abundance.

14

Materials and Methods

14.1 Theory

14.1.1 Formose Reaction Pathway

The formose reaction, first described by Butlerow (1861), is a reaction network forming a variety of sugars. It starts with formaldehyde in an aqueous solution. In a self-condensation, a dimerization of formaldehyde leads to the formation of glycolaldehyde, starting an autocatalytic cycle (Breslow 1959). The formation of glycolaldehyde itself is not yet fully understood, since a freshly distilled formaldehyde solution leads only to the nonproductive reaction to methanol and formate (Cannizzaro 1853). Small amounts of sugars or impurities are needed to start the formose reaction, e.g., 3 ppm (parts per million) of glycolaldehyde are sufficient (Socha et al. 1980). Recent experimental and numerical studies suggested that glycolaldehyde could be formed in interstellar clouds, either by surface hydrogenation of CO molecules on icy dust grains (Fedoseev et al. 2015), or by formaldehyde reacting with its isomer hydroxymethylene (Eckhardt et al. 2018). Glycolaldehyde drives the formose reaction toward more complex sugars. For this reason, we started our laboratory experiments with a solution of formaldehyde and glycolaldehyde and modeled the reaction accordingly in our theoretical studies.

A multitude of different catalysts is effective in the formose reaction. Very effective catalysts are hydroxides, carbonates, and oxides of alkali/alkaline earth metals, as well as aluminosilicates, tertiary amines, lanthanide hydroxides, thallium hydroxide, and lead oxide, see, e.g., (Iqbal and Novalin 2012). In particular, hydroxides and carbonates are of great interest, as these are commonly found in carbonaceous chondrites, see, e.g., (Barber 1981). In the context of prebiotic chemistry, a presumed reaction pathway for the synthesis of molecules involved in the emergence of life has to start from abiotic and naturally abundant molecules. Our considered reaction pathway for the formation of ribose ($C_5H_{10}O_5$) from formaldehyde (CH_2O)

and glycolaldehyde ($C_2H_4O_2$) can be summarized as

$$CH_2O_{(aq)} + 2\,C_2H_4O_{2(aq)} \xrightarrow{\text{catalyst}} C_5H_{10}O_{5(aq)}. \tag{14.1}$$

Here, “catalyst” stands for either one or the other of the following hydroxides or carbonates: $Ca(OH)_2$, $CaCO_3$, KOH, or K_2CO_3. We used one of these catalysts in each run of our laboratory experiments. The formose reaction in Equation (14.1) is an oversimplification of the far more complex reaction network toward sugars. Hence, we performed the laboratory work to correct our theoretical results by using realistic ribose yields measured in our experiments.

In the framework of the previous studies of Pearce and Pudritz (2015) and Pearce and Pudritz (2016) and Paschek, Semenov, et al. (2022), an ID-number was assigned (maximum two digits) to each considered reaction pathway (there reaction pathways for the formation of nucleobases). We extended this numbering scheme to the formose reaction and assigned the no. 101 to the reaction pathway considered here in Equation (14.1) (we reserved no. 100 for the potential formation of ribose from formaldehyde only, without initially present glycolaldehyde, which was not considered here).

Theoretical and experimental studies proposed other possible reactants and reaction pathways for the formation of ribose and RNA precursors in combination with nucleobases. Weber and Pizzarello (2006) demonstrated a stereospecific formation of tetroses from glycolaldehyde catalyzed by peptides. This could be one of the possible solutions to the unsolved question of how the homochirality of life emerged. Jeilani and Nguyen (2020) used quantum chemistry calculations to verify the possibility of abiotic ribose and RNA nucleoside synthesis by free radical reactions. They started from formaldehyde and used Ca^{2+} and $CaOH^+$ cations as catalysts. The hydroxymethyl radical $^\bullet CH_2OH$ was identified as a potential intermediate in the dimerization of formaldehyde and the autocatalytic cycle. Teichert et al. (2019) and Kruse et al. (2020) presented a new direct formation pathway to DNA nucleosides. They started with nucleobases and specifically formed deoxyribose by condensation with acetaldehyde and sugar-forming precursors. Saladino, Carota, et al. (2015) and Šponer et al. (2016) showed the formation of nucleosides starting from formamide catalyzed by powdered meteorites. Additionally, Eschenmoser (2007a) and Eschenmoser (2007b) proposed a hypothetical reaction pathway starting from HCN. Amino acids and carbohydrates might be formed with glyoxylate (glyoxylic acid in neutral solution) and its dimer dihydroxyfumarate as intermediates in the so-called “glyoxylate scenario”. Banfalvi (2021) reviewed this scenario in comparison to the formose reaction. Further reviewed aspects are an alternative mechanism for the formation of RNA starting with the ribose-phosphate backbone, which then binds nucleobases, skipping ribonucleotides as intermediate molecules. Moreover, this study described why ribose is the best fitting aldopentose for the build-up of RNA, as ribose allows for the maximum flexibility of RNA.

14.1.2 Initial Concentrations of Reactants

In order to model the formose reaction in Equation (14.1) with our theoretical chemical model, we used the initial concentrations of the reactants as inputs to determine the resulting abundance of ribose. Comets are believed to have the most pristine composition, and to most closely reflect the conditions that prevailed before or during the early stages in the formation of our solar system. Therefore, comets are the only reservoir of such pristine objects in the solar system that still exists and is accessible to measurements. We took the abundances measured spectroscopically in comets (Mumma and Charnley 2011) (and references therein) as the first reference values. With this, we followed the same approach as described in the previous studies by A. K. Cobb, Pudritz, and Pearce (2015) and Pearce and Pudritz (2016).

Nevertheless, the icy pebbles making up the source material of the parent bodies of carbonaceous chondrites are believed to originate from more inner and warmer regions further inside the solar nebula than those of comets. The main-belt asteroid 19 Fortuna, orbiting the Sun at ∼2.5 au, was identified as the potential parent body source of CM (Mighei-type) meteorites (Burbine, Mccoy, et al. 2002). Therefore, we assumed the inner region of 2–3 au to be the forming location of carbonaceous chondrite parent bodies in the solar nebula (in a first approximation neglecting possible radial migration processes). This region was more distant to the proto-Sun than the water snowline at $T \lesssim 150\,\mathrm{K}$ (Wai and Wasson 1977; Alexander, Boss, et al. 2001; Cassen 2001; Lodders 2003; Bland et al. 2005; Braukmüller, Wombacher, Hezel, et al. 2018; Vollstaedt et al. 2020; Öberg and Bergin 2021; Lichtenberg and Krijt 2021). As a result, water ice was supposed to be preserved in the source material of carbonaceous chondrites. On the other hand, this region is inside the sublimation zone of the reactant formaldehyde (Wai and Wasson 1977; Alexander, Boss, et al. 2001; Cassen 2001; Lodders 2003; Bland et al. 2005; Braukmüller, Wombacher, Hezel, et al. 2018; Vollstaedt et al. 2020; Öberg and Bergin 2021; Lichtenberg and Krijt 2021), which has a sublimation temperature of ∼40–45 K (Cuppen, C. Walsh, et al. 2017). Consequently, the icy pebbles in this region are expected to lose a substantial fraction of the most volatile constituents, e.g., formaldehyde, which diffused through the monolayers of water ice and sublimed into space, leading to a more volatile-poor water ice mantle (Ghesquière et al. 2015). Thus, the more volatile formaldehyde should have been depleted in the carbonaceous chondrites' building blocks compared to the pristine ices in the comet-forming zone.

It was predicted that carbonaceous planetesimals were rapidly assembled via streaming instabilities from the source material (Johansen, Oishi, Mac Low, et al. 2007; Ormel and Klahr 2010; Klahr and Schreiber 2020a). However, unlike comets, these pristine pebbles were not preserved. Therefore, we had to refer to models predicting the depletion of formaldehyde (Ghesquière et al. 2015) to simulate the physico-chemical processes in the whole solar nebula (Visser et al. 2009; Semenov and Wiebe 2011; Drozdovskaya, C. Walsh, et al. 2016; Bergner and Ciesla 2021; Lichtenberg and Krijt 2021). We then compared the remaining volatile abundances between the forming regions of comets and carbonaceous chondrite parent bodies in these solar nebular models. Drozdovskaya, C. Walsh, et al. (2016) simulated two different scenarios of the solar nebula collapsing into a protoplanetary disc. They predicted a depletion of formaldehyde ice by about three or more orders of magnitude when comparing between regions at 1–10 au and >30 au. The abundance changed between outer and inner regions by a factor of $\leq 4.25 \times 10^{-3}$ (compare to Table 4 in their publication). In the models of Visser et al. (2009), Semenov and Wiebe (2011), and Bergner and Ciesla (2021) similar or even higher depletion factors were predicted. The large range of possible depletion factors results from different model assumptions, different computed scenarios, considered physico-chemical mechanisms, and large uncertainties within and between the models. Note that the water ice was not substantially depleted at 2–3 au in all the models, which coincides with the considerations about the water snowline mentioned above. This allowed us to normalize all molecular abundances to that of water ice.

In the temperature programmed desorption (TPD) experiments in the laboratory, it was shown that the sublimed volatiles were not able to leave the water ice matrix freely. A fraction of the volatile ices remained trapped in the water ice and co-desorbed at higher temperatures of $T \gtrsim 150\,\mathrm{K}$ when the water ice sublimed. However, icy pebbles in the solar nebula might have gradually lost their volatile content over thousands of years and became more volatile-poor compared to the results of the TPD experiments, which were conducted over short timescales (hours–days) (Cuppen, C. Walsh, et al. 2017; Potapov and McCoustra 2021). Another TPD experiment showed that some of the formaldehyde polymerizes in reaction with water to polyoxymethylene and therefore did not co-desorb with water at high temperatures (Noble, J. A. et al. 2012). Polymerization of formaldehyde could reduce the amount of its monomer form that was available to the synthesis of ribose in the formose reaction. When the formed parent body planetesimal heated up, a fraction of the formaldehyde could be trapped in its polymeric form, preventing it from participating in the synthesis of more complex organics.

In summary, we used a factor of 10^{-3} to reduce the abundance of formaldehyde measured in comets, corresponding to a conservative estimate of an upper bound motivated by the value of $\leq 4.25 \times 10^{-3}$, given in the solar nebula model by Drozdovskaya, C. Walsh, et al. (2016). This value was chosen in this approximate manner since it was based on many assumptions and uncertainties. As the solar nebula models are in general strong simplifications of the different complex desorption, trapping, and chemical mechanisms, which were observed in, and deduced from, the TPD experiments and could have occurred during the formation of the protoplanetary disc of the solar system, they most likely overestimate the depletion of volatiles.

Moreover, different assumed sizes of the icy pebbles forming the carbonaceous planetesimals introduce largely different predictions for the diffusion times of formaldehyde and other volatiles, since the molecules can leave faster through the porous water ice layers in smaller pebbles. The diffusion rate of formaldehyde at $T \gtrsim 90\,\mathrm{K}$ was measured experimentally and predicted via molecular dynamics calculations (Ghesquière et al. 2015) (and references therein). The resulting diffusion and depletion timescales of volatiles then depend on the thickness of the bulk water ice that needs to be passed, and on the sizes of the icy pebbles accordingly. Further, uncertainties are caused by possible migration processes within the solar nebula and the protoplanetary disc (Burkhardt et al. 2021; Johansen, Ronnet, Bizzarro, et al. 2021; Kooten et al. 2021), as reservoirs of pebbles from different regions further outside the solar nebula could contribute to the volatile content in the forming carbonaceous chondrite parent bodies.

The chosen depletion factor of formaldehyde provided us with a conservative estimate of the least depletion predicted in the solar nebula models and thus indicated a possible upper limit for the initial formaldehyde concentrations in the source material of carbonaceous chondrite parent bodies. Other processes, e.g., the outgassing in these porous bodies heated by the decay of short-lived radioactive isotopes, was shown to potentially reduce their most volatile content even further (Lichtenberg and Krijt 2021).

TPD experiments with glycolaldehyde showed that its desorption was dictated by water ice (Burke et al. 2014). As we assumed water ice to stay frozen in the pebbles, we expected the glycolaldehyde abundance to be similar to cometary values and therefore we introduced no additional depletion factor. A more in-depth and detailed analysis of the depletion of volatiles was described in our previous study (Paschek, Semenov, et al. 2022).

It is important to note that our prediction of the concentrations of the volatile reactants was tailored to the view that carbonaceous planetesimals were assembled mostly instantaneously via streaming instabilities in the expected 2–3 au region inside the solar nebula. For this reason, it is strongly dependent on assumptions on the physico-chemical processes dominating the solar nebula and protoplanetary disc of the solar system.

Table 14.1 lists the concentrations of the considered reactants. The cometary concentrations were corrected by the depletion factor of formaldehyde in the correction factor column, giving rise to the solar nebula model-guided estimate for the initial concentrations in carbonaceous chondrite parent bodies in the predicted concentration column. The predicted concentrations were then used as the input parameters in our theoretical chemistry calculations for the abundances of ribose in this study.

Molecule i	**Name**	**Cometary Concentration** $[\mathrm{mol}_i \cdot \mathrm{mol}_{\mathrm{H_2O}}^{-1}]$	**Correction Factor**	**Predicted Concentration** $[\mathrm{mol}_i \cdot \mathrm{mol}_{\mathrm{H_2O}}^{-1}]$
H_2O	water	1	-	1
CH_2O	formaldehyde	6.60×10^{-4}	10^{-3}	6.60×10^{-7}
$C_2H_4O_2$	glycolaldehyde	$(0.05–4.00) \times 10^{-4}$	-	$(0.05–4.00) \times 10^{-4}$

Table 14.1: Initial concentrations of reactants. The concentrations were normalized to water. The predicted concentrations using solar nebula models (except glycolaldehyde) were already used in the previous study (Paschek, Semenov, et al. 2022), which were the adjusted version of the ones found in comets (Mumma and Charnley 2011) (and references therein) used by A. K. Cobb, Pudritz, and Pearce (2015) and Pearce and Pudritz (2016). This correction was applied to be more representative of the concentrations present in pristine carbonaceous chondrite parent bodies. The predicted concentrations (the last column) are the ones used for the theoretical abundance calculations in this study and were derived by multiplying the cometary concentrations (the third column) with the correction factors (the fourth column).

14.2 Computations

We calculated the amounts of ribose using the formose reaction pathway (see Equation (14.1)) under the conditions inside the carbonaceous planetesimals. The thermochemical equilibrium calculations were performed using the software *ChemApp*, distributed by GTT Technologies (Petersen and Hack 2007) (version 740 (6 April 2020), available online: `https://gtt-technologies.de/software/chemapp/`, accessed on 17 November 2021). The central input for these calculations with ChemApp was the Gibbs free energies of formation of the molecules involved in the modeled reaction. This Gibbs energy data were taken from the thermodynamic database *CHNOSZ* (Dick 2019) (version 1.3.6 (16 March 2020), authored by Jeffrey M. Dick, available online: `https://www.chnosz.net`, accessed on 17 November 2021). Further, we used the *GCC* compiler (Free Software Foundation, Inc. 2020) and the following software packages: *pybind11* (Jakob et al. 2017), *rpy2* (Gautier 2010), *NumPy* (Harris et al. 2020), *SciPy* (Virtanen et al. 2020), and *Matplotlib* (Hunter 2007).

14.2.1 Planetesimal Model

The environmental conditions, mainly the temperatures, inside the parent bodies were provided by the thermal planetesimal model developed by Lange et al. (2022). This 1D model considered the radioactive decay of short- and long-lived isotopes as the heat source in the planetesimal interiors. It simulated the thermal evolution of planetesimals from their formation in the solar system until the present time. The available data provided us with the radial, time-dependent temperature profiles inside these bodies. The adjustable parameters for the simulation of these planetesimals were mainly their radius and the time of formation after calcium-aluminium-rich inclusions (CAI). As in our previous study (Paschek, Semenov, et al. 2022), we considered hypothetical planetesimals with radii of 3–150 km and times of formation after CAI of 0.5–3.5 Myr. A porosity of $\phi = 0.2$ was assumed in all models, representing a typical value found in carbonaceous chondrites (Mason 1963).

One important aspect to note is that, compared to the more complex models of Lange et al. (2022), the planetesimal models here are a simplified version adapted to parent bodies of carbonaceous chondrites.

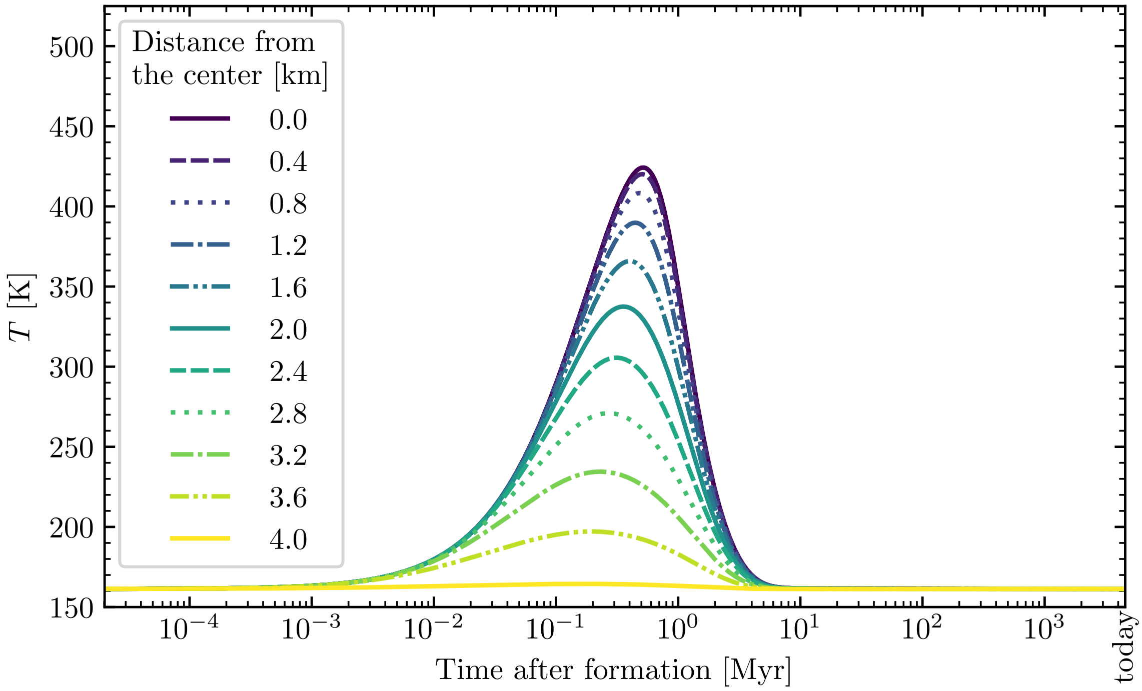

Figure 14.1: Temperature evolution inside a small- and early-formed model planetesimal over time. The temperature curves are given for different distances from the center inside the planetesimal. Properties of the planetesimal: Radius = 4 km, porosity $\phi = 0.2$, and time of formation after calcium-aluminium-rich inclusions (CAI) = 1 Myr. Reproduced from a simplified and adapted version of the model by Lange et al. (2022). The temperature evolution for the other available model planetesimals was described in the previous study (Paschek, Semenov, et al. 2022).

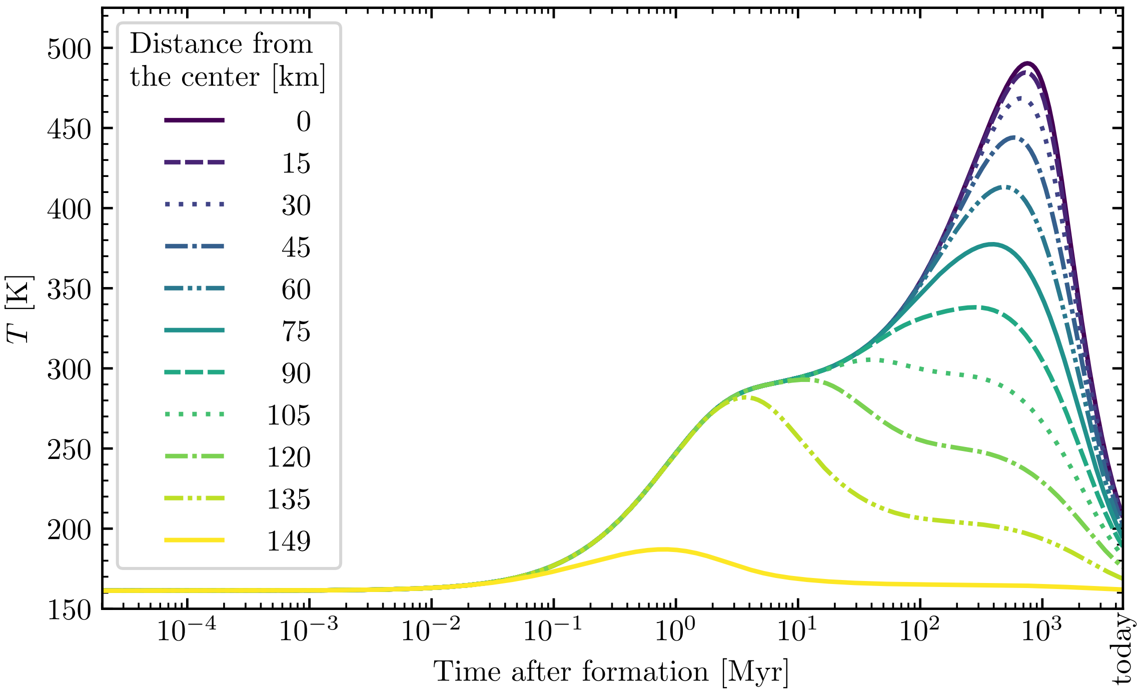

Figure 14.2: Temperature evolution inside a large- and late-formed model planetesimal over time. The temperature curves are given for different distances from the center inside the planetesimal. Properties of the planetesimal: Radius = 150 km, porosity $\phi = 0.2$, and time of formation after CAI = 3.5 Myr. Reproduced from a simplified and adapted version of the model by Lange et al. (2022). The temperature evolution for the other available model planetesimals was described in the previous study (Paschek, Semenov, et al. 2022).

Two examples of this planetesimal model can be seen in Figures 14.1 and 14.2. The first rise of temperature is caused by the decay of short-lived radionuclides (mainly ^{26}Al, with a small contribution of ^{60}Fe). For larger planetesimals, such as the one shown in Figure 14.2 with a radius of 150 km, long-lived radionuclides (^{40}K, ^{232}Th, ^{235}U, and ^{238}U) can also have a significant contribution. This results in a second temperature rise or plateau in the outer shells of the planetesimal over time.

For a more comprehensive overview of the software, the Gibbs free energies of formation, and more details about the planetesimal model, we refer to our previous study (Paschek, Semenov, et al. 2022). The pressure dependence of the Gibbs free energies of formation is very marginal, allowing us to assume 100 bar for all thermochemical calculations inside the entire planetesimal interiors. Further information about the thermochemical equilibrium calculations can be found in Pearce and Pudritz (2016) and A. K. Cobb, Pudritz, and Pearce (2015). The source code, excluding the proprietary ChemApp library, and including the data of the planetesimal models, is openly available on Zenodo at ((Paschek 2021), `https://doi.org/10.5281/zenodo.5774880`, accessed on 1 March 2022) and as a Git repository: `https://github.com/klauspaschek/prebiotic_synthesis_planetesimal`, accessed on

17 November 2021.

14.2.2 Gibbs Free Energies of Formation of Glycolaldehyde

The CHNOSZ database used in our modeling does not contain the Gibbs energies for glycolaldehyde. Therefore, we provide and compare the two ways of estimating these energies, which we used in our calculations. A. K. Cobb, Pudritz, and Pearce (2015) gave an estimate by modeling glycolaldehyde as a mixture of acetaldehyde and acetic acid, for which the CHNOSZ database does have the Gibbs energies. The motivation is that the combination of acetaldehyde and acetic acid roughly resembles glycolaldehyde's functional groups and structure. In the works of Emberson (2010) and Fernandez (2013), the respective enthalpies of formation ΔH_f for acetaldehyde and acetic acid were weighted to fit the one of glycolaldehyde given by Espinosa-García and Dóbé (2005) at standard conditions. The weights were found to be 61.1 % and 38.2 %, respectively. The same weighting coefficients were used to weight the Gibbs free energies of formation ΔG_f of acetaldehyde and acetic acid (taken from CHNOSZ) to estimate the one for glycolaldehyde. These weighted energies can be found in Figure 14.3a.

For the second method of estimation, we performed quantum chemistry calculations using the *Gaussian 09* software package (Frisch et al. 2009) (available online: `https://gaussian.com/`, accessed on 17 November 2021). These quantum chemistry calculations were used to obtain the atomic and molecular energies and entropies necessary to directly calculate the Gibbs free energy of formation for glycolaldehyde. All quantum chemistry calculations were performed using the Becke-3–Lee–Yang–Parr (B3LYP) hybrid density functional (Stephens et al. 1994; Becke 1993; C. Lee et al. 1988) and the polarizable continuum model (PCM) for aqueous solution effects (Miertuš et al. 1981; Cammi and Tomasi 1995). Geometries were optimized using the 6-31G(d,p) basis set, and single-point energies and frequencies were calculated at a higher level basis set, i.e., 6-311++G(2df,2p), using the geometries optimized in the previous step. This particular method was used in the past by Espinosa-García and Dóbé (2005) to calculate the enthalpy of glycolaldehyde (see first estimation method above). All calculations were performed at 100 bar to match the peak pressures inside the meteoritic parent bodies (Pearce and Pudritz 2016), for reasons explained in previous studies (see Section 14.2 above). The Gibbs free energies of formation were calculated using the three-step method outlined by Ochterski (2000), i.e., (1) calculate the enthalpy of formation at 0 K, (2) calculate the enthalpy of formation at 298 K from elements in their standard states, and (3) calculate the entropy of formation ΔS_f from elements in their standard states at 298 K, and insert everything into the standard Gibbs formula $\Delta G_f = \Delta H_f - T\Delta S_f$.

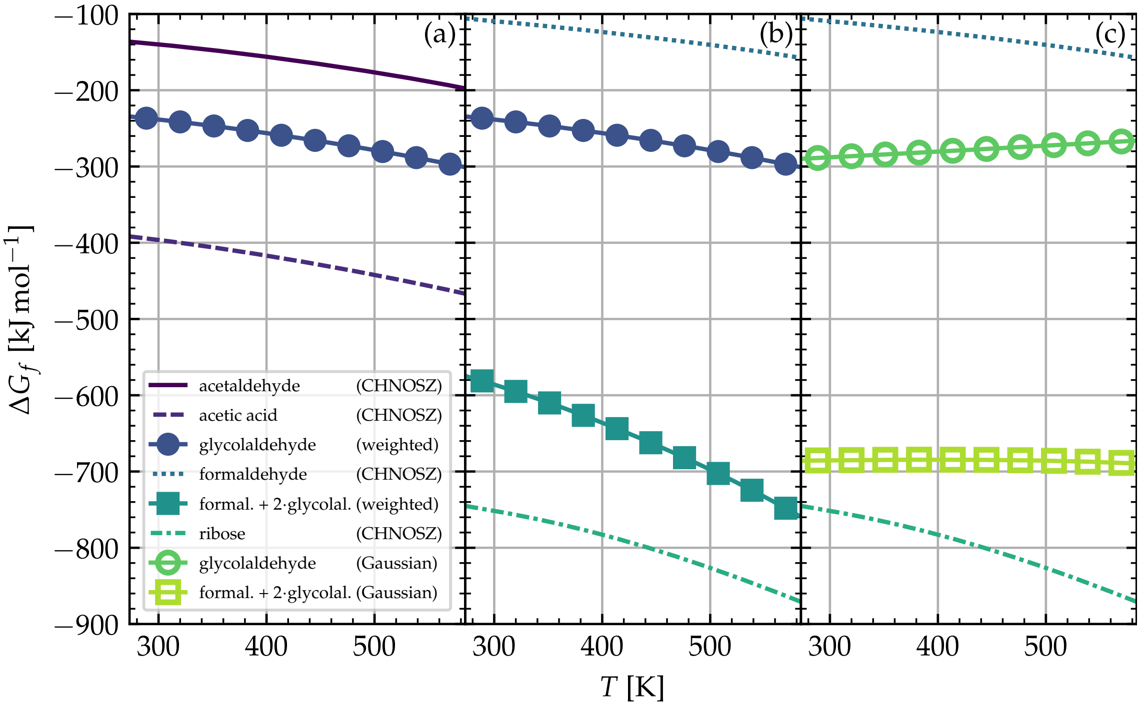

Figure 14.3: Gibbs free energies of formation of different molecules plotted against temperature at 100 bar. The energies for glycolaldehyde were estimated values calculated (**a**,**b**) either by the technique developed by Emberson (2010) and Fernandez (2013), and used in A. K. Cobb, Pudritz, and Pearce (2015) (denoted in figure legend as “weighted”, plotted as solid lines with filled symbols), (**c**) or by using the computational quantum chemistry software Gaussian (Frisch et al. 2009) (denoted in figure legend as “Gaussian”, plotted as solid lines with hollow symbols). Data taken from the CHNOSZ database are plotted as solid and dashed lines without symbols.

The atomic and molecular energies and entropies used for the ΔG_f calculations were obtained from our quantum chemistry calculations. The only exceptions were the heats of formation for the atoms and the entropy for standard state carbon (graphite) at 298 K, which were obtained from experiments (Curtiss et al. 1997) and National Bureau of Standards (current name: National Institute of Standards and Technology) tables of the chemical thermodynamic properties (Wagman et al. 1982), respectively. Due to the lack of experimental entropic data for carbon (graphite) above 298 K, a 1 % increase per 25 K was introduced to the experimental carbon (graphite) entropy. This correction was done to match similar entropy increases from our quantum chemistry calculations of hydrogen and oxygen. Lastly, the atomic enthalpy correction was calculated regarding the gas-state carbon rather than carbon (graphite), which introduced ~3 kJ mol^{-1} error into our calculations.

We validated this method by calculating ΔG_f for acetaldehyde and formaldehyde at 298 K. Our calculated values were within 6 kJ mol^{-1} and 10 kJ mol^{-1} of the values from the CHNOSZ database, respectively. Improvements may be made to this method by calculating enthalpies and entropies for carbon (graphite) to be consistent with the quantum calculations of the other entropies. However, given that the results of the ribose synthesis in this study were not sensitive to our glycolaldehyde calculations for neither the first nor this second estimate (see the explanation below), we did not further improve upon these calculations this time. The resulting second estimate for ΔG_f of glycolaldehyde is plotted in Figure 14.3c.

Although the two estimates for ΔG_f of glycolaldehyde were slightly different, they both showed the same theoretical results for the ribose abundances. This was because the adopted reaction pathway for the synthesis of ribose is limited by the initial abundances of reactants, and hence is less sensitive to the ΔG_f values. This was verified by analyzing the output abundances from ChemApp, which showed that all initially present reactants had zero abundances after ribose was formed.

Consequently, comparing the Gibbs energies of reactants and products allows us to determine whether ribose should be formed. When looking at the modeled reaction pathway for ribose (see Equation (14.1)), one molecule of formaldehyde and two of glycolaldehyde are combined to form one molecule of ribose. Following this stoichiometry, one has to compare the Gibbs energies of ribose with the sum of the energies of formaldehyde and twice the energies of glycolaldehyde ($1\,\text{formaldehyde} + 2\,\text{glycolaldehyde} \longrightarrow 1\,\text{ribose}$, Equation (14.1)). Ribose should only be formed if the energies for ribose are more negative than the stoichiometric sum of those for formaldehyde and glycolaldehyde.

Figure 14.3b shows this sum compared to ribose with the first weighted estimate for glycolaldehyde, and Figure 14.3c shows the comparison with the second estimate with Gaussian. The stoichiometric sum of the Gibbs energies of formaldehyde and glycolaldehyde was less negative than the Gibbs energies of ribose in both cases. Thus, indeed, only the limitation by the initial abundances of reactants mattered for the ribose formation. If the stoichiometric sum of formaldehyde and glycolaldehyde crossed with the energies of ribose, no ribose would be formed at the respective temperatures. Therefore, both estimates of the Gibbs energies of glycolaldehyde allowed us to model this reaction pathway in the same way.

14.3 Laboratory Experiments

There are about 40 different products formed in the formose reaction (Rauchfuß 2005). These include plenty of sugars such as aldoses and ketoses, sugar alcohols, sugar acids, branched sugars, and even decomposition products such as lactic acid, see also, e.g., (Omran et al. 2020). Modeling the complex formose network with its different reactions such as aldol reactions, retro-aldol reactions, arrangements, and decomposition reactions is a big challenge for theoretical and analytical chemistry, see, e.g., (Kim, Ricardo, et al. 2011). Accordingly, following the kinetics of every single molecule is almost impossible, and the thermodynamic data of the molecules and reactions are often missing.

Therefore, the reaction pathway considered here and summarized in Equation (14.1) is a major simplification. To compensate for this, we performed laboratory experiments of the formose reaction in an aqueous solution and measured the amounts of the resulting sugars. This allowed us to find the fraction of ribose in all forming 5Cs.

In our experiments, the reaction was started with a very concentrated solution of formaldehyde ($1.34\,\mathrm{mol\,L^{-1}}$) and glycolaldehyde ($0.269\,\mathrm{mol\,L^{-1}}$, $20\,\mathrm{mol\,\%}$) based on the prebiotic DNA formation pathway demonstrated by Teichert et al. (2019) (for more context, see the review by Kruse et al. (2020)). To this solution, $10\,\mathrm{mol\,\%}$ of one of the catalysts were added, and the temperature was kept stable. At different time intervals, depending on the activity of the catalyst, a sample was taken. The whole solution had a volume of $1\,\mathrm{mL}$ at the start of each run, and samples were taken in volumes of $50\,\mathrm{\mu L}$ each. The formose reaction was stopped by adding citric acid and freezing the sample. After lyophilization, the sample was analyzed via gas chromatography in combination with a mass spectrometer, as described in the preceding studies by Haas, Lamour, and Trapp (2018) and Haas, Lamour, Christ, et al. (2020) (abbreviated there as GC-MS).

There are also other possibilities to analyze products in the formose reaction, e.g., coupling liquid chromatography with UV and electrospray ionization-mass spectrometry (abbreviated as LC-UV and ESI-MS) (Zweckmair et al. 2013). This other method could help overcome problems, e.g., thermal instability of some of the analyzed molecules in GC-MS analysis, and could be interesting for follow-up studies.

The maximum yields of ribose in all 5Cs inferred from our measurements were used as a correction factor for the ribose abundances resulting from our theoretical thermochemical equilibrium model.

15

Results

15.1 Experimentally Found Yields of Ribose in All 5Cs

Figure 15.1 shows our experimental results for the fraction of ribose in all 5Cs plotted against the elapsed time of the reaction. Calcium hydroxide was the catalyst with the highest activity. Compared to the other catalysts, it formed the highest amount of ribose in the shortest amount of time. However, one has to be aware that the decomposition of the formose products is also more rapid (see Discussion in Section 16). Focusing on ribose, it took less than 20 min to reach its maximum yield. Likewise, potassium hydroxide and potassium carbonate produced ribose very quickly in significant amounts, with the maximum values being lower than those obtained with calcium hydroxide. Calcium carbonate took significantly longer to produce higher sugars, which can be explained by its lower solubility. Since we used 10 mol % of the catalyst in each experiment, calcium carbonate reached its maximum aqueous solubility. This was done in order to stay consistent within the framework of our experiments and with the previous study by Teichert et al. (2019). Still, after 180 min the experimental run with calcium carbonate resulted in the second-highest yield for ribose. All catalysts did not seem to differ much in effectiveness. They produced ribose with yields of the same order of magnitude.

The maximum yields of ribose reached in Figure 15.1 are listed in Table 15.1. These values were the correction factors used in the theoretical model to compensate for the oversimplification of the modeled reaction in Equation (14.1).

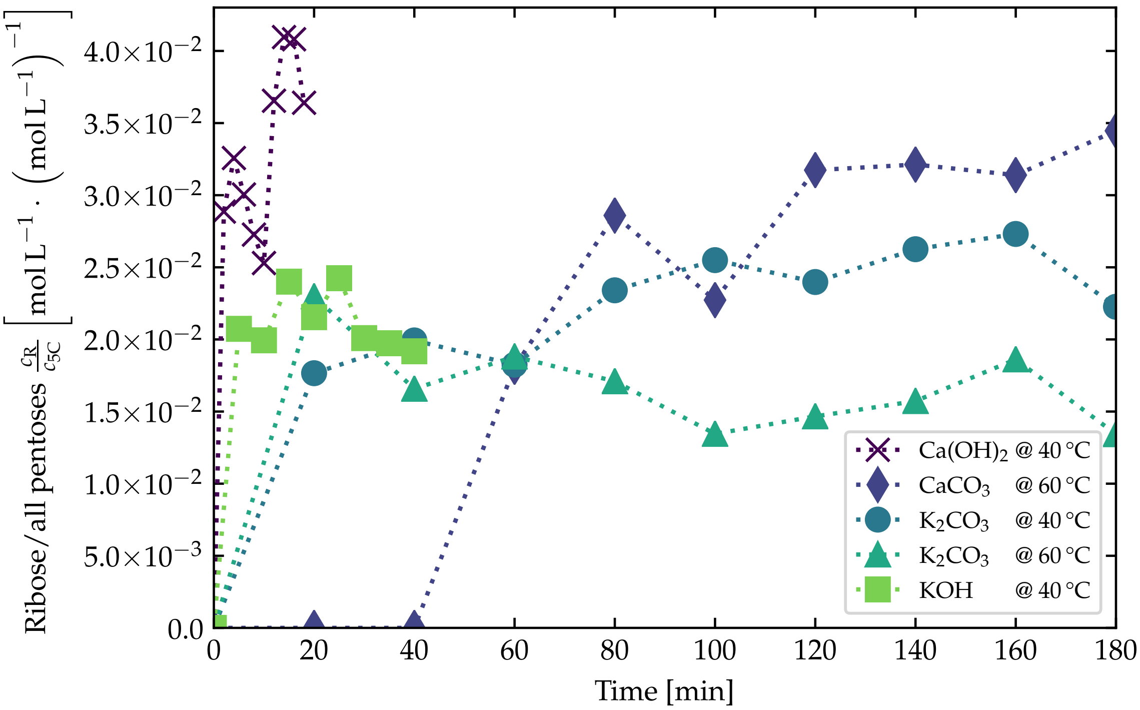

Figure 15.1: Fraction of ribose (R) in all pentoses (5Cs) synthesized over time in lab experiments. The reaction started with concentrations for formaldehyde of 1.34 mol L^{-1}, for glycolaldehyde of 0.269 mol L^{-1} or 20 mol %, and for the respective catalyst of 10 mol %, in a solution volume of 1 mL, with samples taken over time in volumes of 50 µL each. The temperature of the solution was kept constant over time at the values denoted in the figure legend for each catalyst run.

15.2 Theoretically Calculated Ribose Abundances in Planetesimals

The resulting ribose abundances were calculated for the temperatures taken from a simplified version of the planetesimal model by Lange et al. (2022) (see Section 14.2). The temperatures inside the planetesimal are plotted as solid and dashed lines in Figures 15.2 and 15.3 and correspond to the example planetesimal model shown in Figure 14.2. Figures 15.2 and 15.3 show the resulting ribose abundances for several parameters and are a representative selection among all the available thermal profiles. We also calculated the abundances for the other available planetesimal models with our chemical simulations, but the results share the same characteristics and trends as for the shown planetesimal model in Figures 15.2 and 15.3 (for the other available planetesimal models see also the previous study (Paschek, Semenov, et al. 2022)). The resulting ribose abundances for different catalyst correction factors (see Table 15.1) are plotted as dashed lines with symbols (see legends). The shaded part of the abundance axis in both figures represents the range of measured ribose concentrations in carbonaceous chondrites (Furukawa et al. 2019). These measured

Catalyst	**Name**	**Maximum Yield of Ribose** $\left\{\frac{c_R}{c_{5C}}\right\}_{\max}$ $\left[\text{mol L}^{-1} \cdot (\text{mol L}^{-1})^{-1}\right]$
$Ca(OH)_2$	Calcium hydroxide	4.1×10^{-2}
$CaCO_3$	Calcium carbonate	3.5×10^{-2}
K_2CO_3	Potassium carbonate	2.7×10^{-2}
KOH	Potassium hydroxide	2.4×10^{-2}

Table 15.1: Maximum yield of ribose (R) in all 5Cs reached in lab experiments for different present catalysts, respectively (see Figure 15.1). The reaction always started from formaldehyde and glycolaldehyde as reactants in aqueous solution.

abundances represent the to-be-achieved benchmark and real-world reference to our theoretically calculated values.

Figures 15.2a and 15.3a show the radial distribution of the calculated ribose abundances in the planetesimal's interior. The maximum temperature $T_{\max}$ (solid line) reached at a specific distance from the center inside the planetesimal over the entire simulation time (from the planetesimal's formation until today) was taken into account to calculate the ribose abundances. In this case, we inherently assumed that the peak production of the ribose sugar was achieved at the peak temperature at each distance from the center. The left side of these panels (a) defines the center, and the right side the surface of the planetesimal.

In Figures 15.2b and 15.3b, the dashed curve shows the temperature T_{core} in the center of the planetesimal over time. The ribose abundances were calculated by iterating over time and using the abundances of reactants and products resulting from previous steps as the initial abundances in each step. This allowed us to follow the equilibrium of the reaction proceeding through time.

In Figure 15.2, the *lower* bound of the initial concentration of glycolaldehyde of $5 \times 10^{-6}\,\text{mol} \cdot \text{mol}_{H_2O}^{-1}$ from Table 14.1 was used. As a result, the simulated ribose abundances coincided with measurements in carbonaceous chondrites (Furukawa et al. 2019) within a factor of 2–3. On the other hand, in Figure 15.3 we used the *upper* bound of $4 \times 10^{-4}\,\text{mol} \cdot \text{mol}_{H_2O}^{-1}$, and the calculated ribose abundances were higher than the measured values by about two orders of magnitude.

As the reduction of the initial cometary formaldehyde concentration by 10^{-3} (see Table 14.1) was a very broad assumption, a change of this reduction will change the resulting ribose abundances. Keeping this in mind, the theoretically simulated abundances can be considered to be in reasonable agreement with the measured ones. Further, we suspect that decomposition and other complex reactions that we did not take into account could be responsible for the slightly overestimated theoretical ribose abundances.

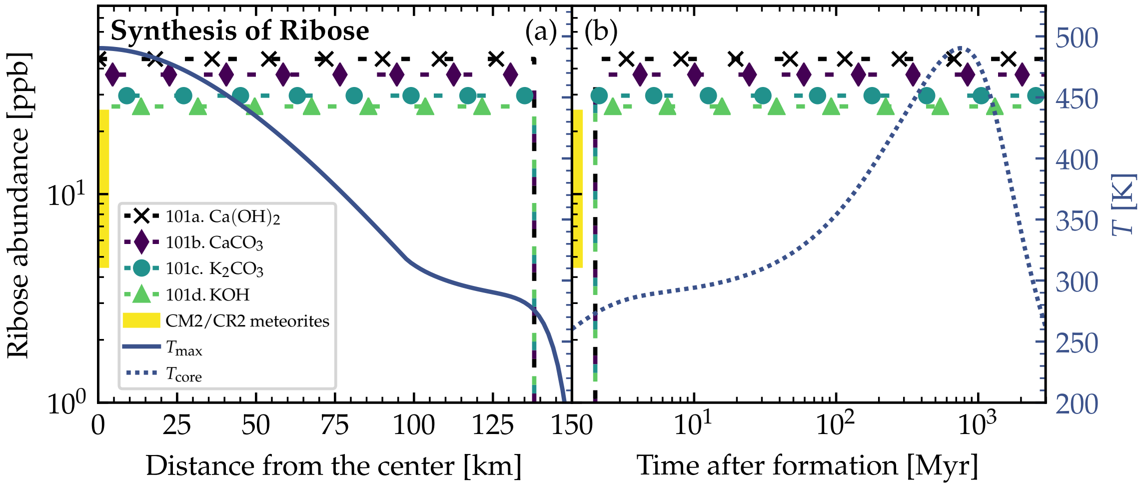

Figure 15.2: Lower bound theoretical ribose abundances from simulations of formose reaction pathway in Equation (14.1). Properties of planetesimal: Radius = 150 km, densities $\rho_{\text{rock}} = 3\,\text{g}\,\text{cm}^{-3}$, $\rho_{\text{ice}} = 0.917\,\text{g}\,\text{cm}^{-3}$, porosity $\phi = 0.2$, and time of formation after CAI = 3.5 Myr. The experimentally found yields of ribose within 5Cs for each catalyst (see Table 15.1) were multiplied with the theoretically calculated 5C abundance to obtain the ribose abundances (dashed lines with symbols). This simulation was run with the *lower* (opposite to Figure 15.3) bound of the initial concentration of glycolaldehyde of $5 \times 10^{-6}\,\text{mol} \cdot \text{mol}_{\text{H}_2\text{O}}^{-1}$ (see Table 14.1). All simulations were run at 100 bar. In both panels (**a**) and (**b**) the left vertical axis corresponds to the abundances (dashed lines with symbols) and the right vertical axis corresponds to the temperatures from the planetesimal model (solid and dotted lines). The shaded part of the abundance axis represents the range of ribose abundances measured in CM2 (Mighei-type, Murchison, upper limit) and CR2 (Renazzo-type, NWA 801, lower limit) meteorites (Furukawa et al. 2019), and has no correlation to the radial location inside the object or the point in time (horizontal axes). (**a**) Distribution of abundances for the maximum temperature T_{max} (solid line) reached at a specific distance from the center inside the planetesimal (center at the left and surface at the right). Ribose was synthesized at and below 138 km distance from the center. (**b**) Evolution of abundances at temperatures T_{core} (dotted line) in the center of the planetesimal over time (the same temperature evolution curve can be found in Figure 14.2). Ribose synthesis started at 2 Myr after formation.

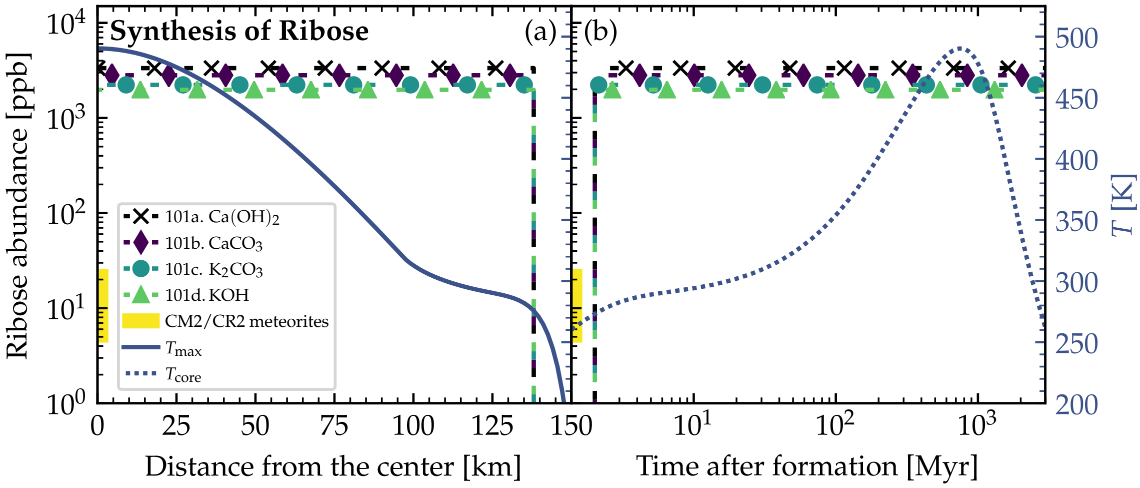

Figure 15.3: Upper bound theoretical ribose abundances from simulations of formose reaction pathway in Equation (14.1). Properties of planetesimal: Radius = 150 km, densities $\rho_{\mathrm{rock}} = 3\,\mathrm{g\,cm^{-3}}$, $\rho_{\mathrm{ice}} = 0.917\,\mathrm{g\,cm^{-3}}$, porosity $\phi = 0.2$, and time of formation after CAI = 3.5 Myr. The experimentally found yields of ribose within 5Cs for each catalyst (see Table 15.1) were multiplied with the theoretically calculated 5C abundance to obtain the ribose abundances (dashed lines with symbols). This simulation was run with the *upper* (opposite to Figure 15.2) bound of the initial concentration of glycolaldehyde of $4 \times 10^{-4}\,\mathrm{mol \cdot mol_{H_2O}^{-1}}$ (see Table 14.1). All simulations were run at 100 bar. In both panels (**a**) and (**b**) the left vertical axis corresponds to the abundances (dashed lines with symbols) and the right vertical axis corresponds to the temperatures from the planetesimal model (solid and dotted lines). The shaded part of the abundance axis represents the range of ribose abundances measured in CM2 (Murchison, upper limit) and CR2 (NWA 801, lower limit) meteorites (Furukawa et al. 2019), and has no correlation to the radial location inside the object or the point in time (horizontal axes). (**a**) Distribution of abundances for the maximum temperature T_{max} (solid line) reached at a specific distance from the center inside the planetesimal (center at the left and surface at the right). Ribose was synthesized at and below 138 km distance from the center. (**b**) Evolution of abundances at temperatures T_{core} (dotted line) in the center of the planetesimal over time (the same temperature evolution curve can be found in Figure 14.2). Ribose synthesis started at 2 Myr after formation.

16

Discussion and Conclusions

In the thermochemical equilibrium calculations, the resulting abundances of the reaction products depend strongly on the initial concentrations of the reactants (see Table 14.1). Therefore, the resulting ribose abundances in Figures 15.2 and 15.3 were strongly dependent on the initial abundance of glycolaldehyde. Furthermore, a different estimate for the initial abundance of formaldehyde and the proper rescaling of the pristine cometary values guided by solar nebula models would also change the resulting ribose concentrations. This rescaling had to be made and is hard to verify via measurements, observations, or modeling, since the icy pebbles out of which the carbonaceous chondrite planetesimals formed in the solar nebula have been gone for too long. Considering all these limitations, uncertainties, and the fact that our correction factor for the initial formaldehyde abundance was an upper limit, the simulated and measured ribose abundances shown in Figures 15.2 and 15.3 still coincide reasonably well.

We see this as the confirmation that the formose reaction could be the pathway to forming sugars such as ribose abiotically. Pristine carbonaceous chondrites are time capsules showing us how the foundations for the emergence of life might have been laid in our early solar system.

Ribose is susceptible to decomposition, see, e.g., (Larralde et al. 1995). Particularly at higher temperatures further away from the freezing point of water, significant portions of ribose and other sugars could be destroyed or converted to even more complex species (e.g., polysaccharides). In this context, typical decomposition processes of sugars are the β-elimination to dicarbonyls, the benzilic acid rearrangement, oxidation, and others, see, e.g., (De Bruijn et al. 1986). In laboratory experiments, the solution containing the freshly formed sugars starts to turn yellow (the so-called "yellowing point") when the maximum abundances of sugars are reached. This corresponds roughly to the point in time when the maximum fraction of ribose was reached in Figure 15.1. After a while, the solution starts to turn brownish (forming so-called "brown tar") as the decomposition proceeds.

Since we used the maximum yields of ribose reached in the experiments (see Table 15.1) as the correction for our theoretical studies, our results represent an estimate of the possible upper limit. This probably led to the slightly too high ribose abundances when compared to the measurements in carbonaceous chondrites (see Figures 15.2 and 15.3). Decomposition plus other reactions could have lowered the ribose abundance in the planetesimals over time, which might explain the lower values measured in carbonaceous chondrites.

Our results seemed to be reasonable when taking these potentially adverse effects into account. Ribose is still found today in meteorites (Furukawa et al. 2019), indicating that it only decomposed to a certain extent. Ricardo et al. (2004) showed in laboratory experiments that boron from borate minerals stabilized ribose and other 5Cs in their cyclic furanose form. The solution did not turn brownish for 2 months as decomposition was prevented. They also postulated that boron could stabilize glyceraldehyde, an intermediate reaction product in the formose reaction, keeping it from decomposing into “brown tar”, and therefore enhancing the formation of complex sugars from glycolaldehyde and glyceraldehyde. Since boron was found in carbonaceous chondrites (Mills 1968), it could stabilize the formed ribose in meteorites and their parent bodies.

Ribose destruction rates by hydrolysis could be dampened by many orders of magnitude at temperatures below 60 °C at pH between 4–8 (Larralde et al. 1995). The outer shells of planetesimals were heated only for short periods of time to temperatures above the melting point of water before they were frozen again. Therefore, in these outer shells, the freshly formed ribose (besides other prebiotic molecules) might be quickly frozen in the water. This potentially reduced the chance of decomposition as the temperatures were lower compared to the core region of the planetesimal, and liquid water only existed over a shorter period of time. The frozen ribose might have been preserved until it was distributed in the solar system as fragments of the parent body, and some of the fragments fell to the Earth as meteorites. Extraterrestrial organic and prebiotic molecules were found in meteorites on the Earth’s surface today, see, e.g., (Furukawa et al. 2019; A. K. Cobb and Pudritz 2014b; Pearce and Pudritz 2015; Lai et al. 2019; Gilmour 2003; Pizzarello, Cooper, et al. 2006; Derenne and Robert 2010), although the possibility of at least partial terrestrial contamination has to be considered. Theoretical studies coupled with experimental data (Chyba, Thomas, et al. 1990; Chyba and Sagan 1992; Basiuk and Navarro-González 1998; Pierazzo and Chyba 1999) suggested that a significant portion of organics might survive the heating due to friction in the atmosphere and the energy of the impact (Brinton and Bada 1996) and arrive intact on the Earth’s surface even in comets and interplanetary dust particles. Destruction during the atmospheric entry and impact could be another reason why the detected abundances of ribose in carbonaceous chondrites were lower than our calculated results.

Figures 16.1 and 16.2 show the ribose synthesis in the outer shells of the example planetesimal models in Figures 14.1 and 14.2. At the distance of 2.76 km from the center of the 4 km-sized planetesimal model (time of formation after CAI = 1 Myr), the synthesis of ribose that started shortly before the peak temperature was reached in this region and allowed for liquid water to exist over $\lesssim$200,000 yr. When the water froze again, the formed ribose was preserved (see Figure 16.1). The similar phenomenon happened in the outer shell at the distance of 138 km from the center of the 150 km-sized planetesimal model (time of formation after CAI = 3.5 Myr), where the water stayed liquid for $\lesssim 2$ Myr (see Figure 16.2).

It is worth noting that the planetesimal model by Lange et al. (2022), which was used in our study, did not take into account the latent heat of water. Therefore, we were not able to accurately model the phase transitions of water and their effects on the temperature evolution. The phase transitions require a considerable amount of energy and cause the temperature evolution to stagnate until the water is completely melted or frozen. Since the periods estimated above were in between the melting and freezing times of water, our estimates were only approximations of the actual duration.

There should be a layer below the consistently frozen crust of planetesimal parent bodies, which could be the most promising part that contained the highest amounts of ribose. This region should be frozen rapidly due to the low and declining internal radioactive heating, preventing decomposition processes. On the other hand, the cores of the parent bodies were more likely to reach critically high temperatures over longer periods of time and probably led to significant sugar decomposition. Therefore, Figures 15.2b and 15.3b could not depict the actual truth, as decomposition was not considered in our calculations.

The surface and outer shells of the parent bodies were more likely to be shattered and blown off by collisions with other asteroids. If impactors were able to penetrate through the surface layers of the parent bodies and reach the potentially ribose-rich intermediate part, the generated fragments would most likely contain the organic complexity that is characteristic for carbonaceous chondrites. This could explain why we were able to find ribose in carbonaceous chondrites on the Earth (Furukawa et al. 2019). The origin of these meteorites was likely biased to the outer shells of the parent bodies in fragmentation events, which could (partly) coincide with the most promising regions identified in Figures 16.1 and 16.2.

Larralde et al. (1995) suspected that ribose was not stable enough to take part in the origin of life, questioning the RNA world hypothesis. However, ribose could be preserved in the icy fragments for a long time. This illustrates a possible explanation for how the concerns about the instability of ribose could be resolved in the scope of

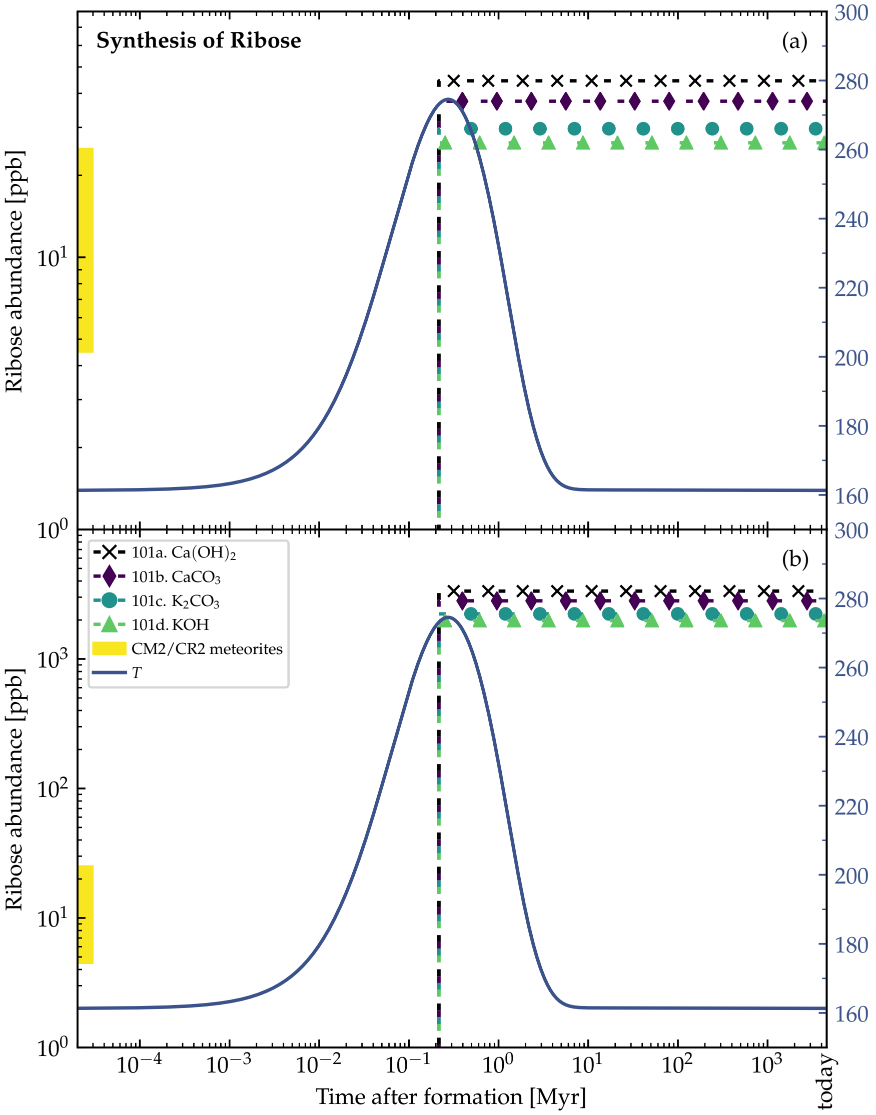

Figure 16.1: Theoretical ribose abundances in an outer shell at 2.76 km distance from the center of the 4 km-sized planetesimal model. The whole planetesimal model is shown in Figure 14.1. Properties of planetesimal: Radius = 4 km, densities $\rho_{\text{rock}} = 3\,\text{g}\,\text{cm}^{-3}$, $\rho_{\text{ice}} = 0.917\,\text{g}\,\text{cm}^{-3}$, porosity $\phi = 0.2$, and time of formation after CAI = 1 Myr. The formose reaction pathway in Equation (14.1) was used in the simulations. The experimentally found yields of ribose within 5Cs for each catalyst (see Table 15.1) were multiplied with the theoretically calculated 5C abundance to obtain the ribose abundances (dashed lines with symbols). Ribose synthesis started at ∼210,000 yr after formation. All simulations were run at 100 bar. In both panels (**a**,**b**), the left vertical axis corresponds to the abundances (dashed lines with symbols) and the right vertical axis corresponds to the temperatures T (solid lines) in the outer shell of the planetesimal model. The shaded part of the abundance axis represents the range of ribose abundances measured in CM2 (Murchison, upper limit) and CR2 (NWA 801, lower limit) meteorites (Furukawa et al. 2019), and has no correlation to the point in time (horizontal axis). (**a**) Time evolution of lower bound abundances simulated using the *lower* (opposite to panel (**b**)) bound of the initial concentration of glycolaldehyde of $5 \times 10^{-6}\,\text{mol} \cdot \text{mol}_{\text{H}_2\text{O}}^{-1}$ (see Table 14.1). (**b**) Time evolution of upper bound abundances simulated using the *upper* (opposite to panel (**a**)) bound of the initial concentration of glycolaldehyde of $4 \times 10^{-4}\,\text{mol} \cdot \text{mol}_{\text{H}_2\text{O}}^{-1}$.

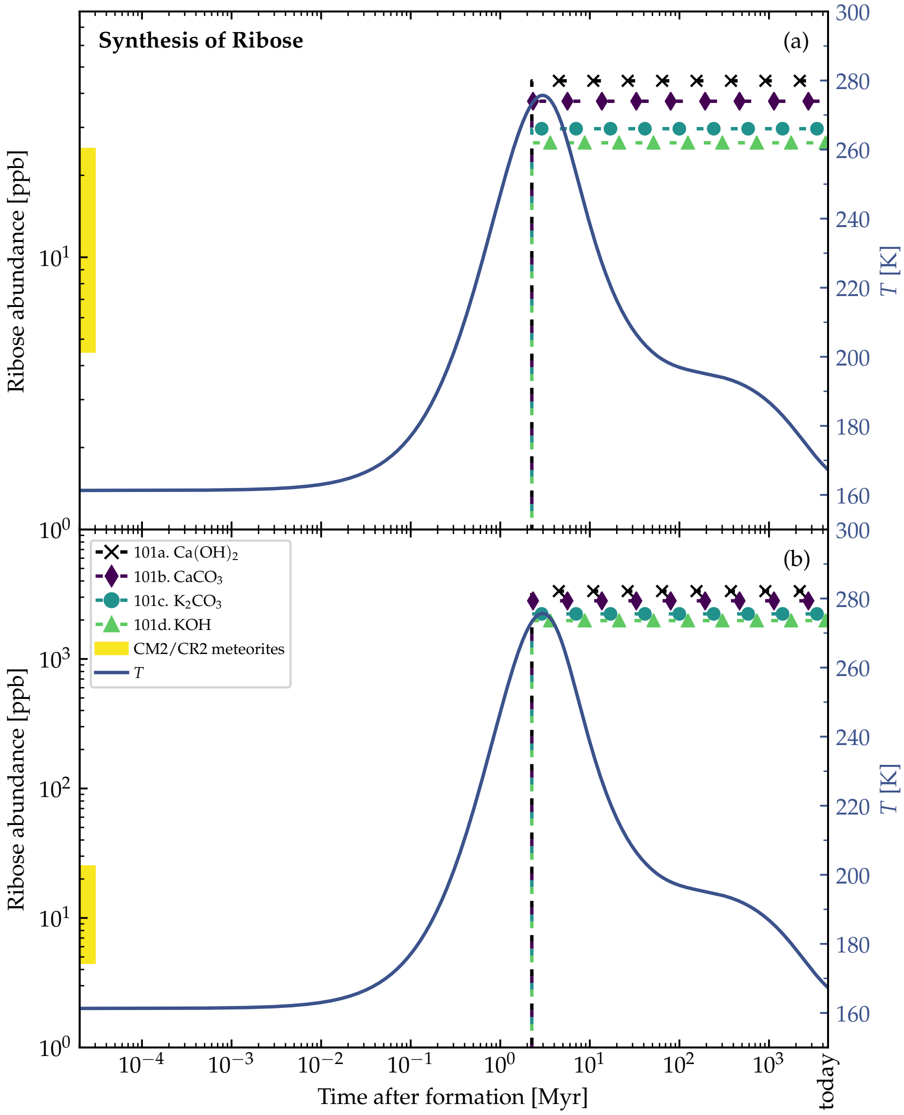

Figure 16.2: Theoretical ribose abundances in an outer shell at 138 km distance from the center of the 150 km-sized planetesimal model. The whole planetesimal model is shown in Figure 14.2. Properties of planetesimal: Radius = 150 km, densities $\rho_{\mathrm{rock}} = 3\,\mathrm{g\,cm^{-3}}$, $\rho_{\mathrm{ice}} = 0.917\,\mathrm{g\,cm^{-3}}$, porosity $\phi = 0.2$, and time of formation after CAI = 3.5 Myr. The formose reaction pathway in Equation (14.1) was used in the simulations. The experimentally found yields of ribose within 5Cs for each catalyst (see Table 15.1) were multiplied with the theoretically calculated 5C abundance to obtain the ribose abundances (dashed lines with symbols). Ribose synthesis started at ~2.1 Myr after formation. All simulations were run at 100 bar. In both panels (**a**,**b**), the left vertical axis corresponds to the abundances (dashed lines with symbols) and the right vertical axis corresponds to the temperatures T (solid lines) in the outer shell of the planetesimal model. The shaded part of the abundance axis represents the range of ribose abundances measured in CM2 (Murchison, upper limit) and CR2 (NWA 801, lower limit) meteorites (Furukawa et al. 2019), and has no correlation to the point in time (horizontal axis). (**a**) Time evolution of lower bound abundances simulated using the *lower* (opposite to panel (**b**)) bound of the initial concentration of glycolaldehyde of $5 \times 10^{-6}\,\mathrm{mol \cdot mol_{H_2O}^{-1}}$ (see Table 14.1). (**b**) Time evolution of upper bound abundances simulated using the *upper* (opposite to panel (**a**)) bound of the initial concentration of glycolaldehyde of $4 \times 10^{-4}\,\mathrm{mol \cdot mol_{H_2O}^{-1}}$.

the chemical synthesis in planetesimals. By eventually falling as meteorites to the Earth into WLPs, the ribose-rich fragments might provide ribose for the origin of life, as described by Pearce, Pudritz, et al. (2017).

Smaller planetesimals, such as the 4 km-sized one in Figures 14.1 and 16.1, had to be formed earlier than larger planetesimals to become aqueous, and allow for the formose reaction to take place in its interior. At 1 Myr after CAI, there was enough ^{26}Al left to even heat the outer shells of the 4 km-sized planetesimal above the melting point of water (see Figure 16.1). The large 150 km-sized planetesimal was formed later at 3.5 Myr after CAI (see Figures 14.2, 15.2, 15.3 and 16.2). If it was formed earlier as the smaller planetesimal, this large body would have reached such high temperatures that strong thermal metamorphism or even siliceous volcanism would have occurred, resulting in hostile conditions for the synthesis of organic molecules. Therefore, when comparing these moderately heated planetesimals, the time intervals of the aqueous phase in the outer shells occurred earlier in the smaller bodies and over a shorter interval than in the larger ones (∼200,000 yr in Figure 16.1 vs. ∼2 Myr in Figure 16.2). This leads to the conclusion that smaller planetesimals with moderate heating might preserve ribose better than larger planetesimals since the aqueous time interval allowing for decomposition of the formed ribose was shorter by around one order of magnitude.

In follow-up studies, when more detailed thermodynamic and kinetic data with a higher temperature resolution for the decomposition rates become available, it could be interesting to consider the decomposition of ribose in more detail and constrain the region with the likely highest ribose abundances with more accuracy compared to our approximate estimates. This could also help to identify the part of parent bodies where carbonaceous chondrites with high ribose content could have most likely originated.

In this study, we used the same model and the same initial concentrations of reactants as in our previous study for nucleobases (Paschek, Semenov, et al. 2022), in which we found abundances matching the measured values in meteorites. It seems that the formation of crucial RNA-building blocks such as nucleobases and ribose could be explained uniformly with our model and the selected reaction pathways. Note that carbonaceous chondrites also contain P-rich minerals, e.g., schreibersite, which could provide the last missing piece for the synthesis of the RNA nucleotides, the phosphates ($[PO_4]^{3-}$, $[HPO_4]^{2-}$, and $[H_2PO_4]^{-}$ depending on pH) (Gull et al. 2015). Moreover, the clay minerals at the bottom of WLPs could also provide the phosphates needed for the phosphorylation of nucleosides (Ferris, A. R. Hill, et al. 1996). In addition, metal-doped-clays were shown to select ribose from a formose mixture (Zhao and X. Wang 2021) and catalyze the formation of ribonucleosides (Q.-Q. Chen et al. 2021).

Thus, ribose and nucleobases (see our previous studies (Pearce and Pudritz 2016; Paschek, Semenov, et al. 2022)) delivered by carbonaceous chondrites could have been an essential ingredient for the build-up of the first RNA molecules in WLPs (including geothermal fields and hot springs), or around subsea hydrothermal vents, or all of them, setting the stage for the emergence of the RNA world and the origin of life on the Earth and elsewhere.

Funding

K.P. acknowledges financial support by the Deutsche Forschungsgemeinschaft (DFG, German Research Foundation) under Germany's Excellence Strategy EXC 2181/1-390900948 (the Heidelberg STRUCTURES Excellence Cluster). K.P. is a fellow of the International Max Planck Research School for Astronomy and Cosmic Physics at the University of Heidelberg (IMPRS-HD). T.K.H. acknowledges financial support by the European Research Council under the Horizon 2020 Framework Program via the ERC Advanced Grant Origins 83 24 28. D.A.S. acknowledges financial support by the Deutsche Forschungsgemeinschaft through SPP 1833: "Building a Habitable Earth" (SE 1962/6-1).

Data Availability

The source code, excluding the proprietary ChemApp library, and including the data of the planetesimal models, is openly available on Zenodo at ((Paschek 2021), `https://doi.org/10.5281/zenodo.5774880`, accessed on 1 March 2022) and as a Git repository: `https://github.com/klauspaschek/prebiotic_synthesis_planetesimal`, accessed on 17 November 2021.

Acknowledgments

The authors thank Cornelis P. Dullemond for his extensive help in understanding the planetesimal model and the background attached to its theory. We would also like to thank Catharina Fairchild and Hao-En Huang for their stylistic review of the manuscript. We wish to thank an anonymous reviewer for corrections, comments, and suggestions.

Abbreviations

The following abbreviations are used in this manuscript:

RNA	Ribonucleic acid
DNA	Deoxyribonucleic acid
5C	Pentose
WLP	Warm little pond/Darwinian pond
ppb	Parts per billion
ppm	Parts per million
CAI	Calcium-aluminium-rich inclusions
yr	Year(s)
GC-MS	gas chromatography coupled with a mass spectrometer
CM2	Mighei-type chondrites (CM), a group of meteorites of petrologic type 2
CR2	Renazzo-type chondrites (CR), a group of meteorites of petrologic type 2

Part IV

PREBIOTIC VITAMIN B_3 SYNTHESIS IN CARBONACEOUS PLANETESIMALS

Klaus Paschek[1], Mijin Lee[1], Dmitry A. Semenov, Thomas K. Henning

This following Part is based on the work *"Prebiotic Vitamin B_3 Synthesis in Carbonaceous Planetesimals"*, published in the April 2024 issue 4, part of Volume 89, of the journal *ChemPlusChem* (Paschek, M. Lee, et al. 2024b) as part of the Ph.D. thesis. This publication was featured as the cover of the journal (Paschek, M. Lee, et al. 2024a).

The published paper has been reformatted to fit the format of this thesis. The work on the paper was divided as follows: Mijin Lee and I shared the first authorship and contributed equally to this manuscript. Mijin Lee and I wrote the main simulation code, building on the pre-existing code published by Pearce and Pudritz (2016), Paschek, Kohler, et al. (2022), and Paschek, Semenov, et al. (2023). Mijin Lee performed the main analysis of the resulting simulations data with my help. Mijin Lee and I both contributed equally to the literature review and derived together the necessary methods to obtain Gibbs free energies of formation for molecules missing in the database CHNOSZ, see Section 20.3. Prof. Dr. Oliver Trapp helped deriving parts of the reaction pathways in Section 18.1 and Figure 18.1 and was mentioned for that in the acknowledgments Section. Ben K. D. Pearce performed quantum computational calculations for us to derive the Gibbs free energies of formation for the molecule glycolaldehyde and was also mentioned in the acknowledgments for that.

I drafted the first version of the whole manuscript, except Mijin Lee contributed major parts of computational methods Section 20. The other co-authors contributed by commenting on at least one version of the draft.

---

[1] These authors contributed equally.

Journal Cover

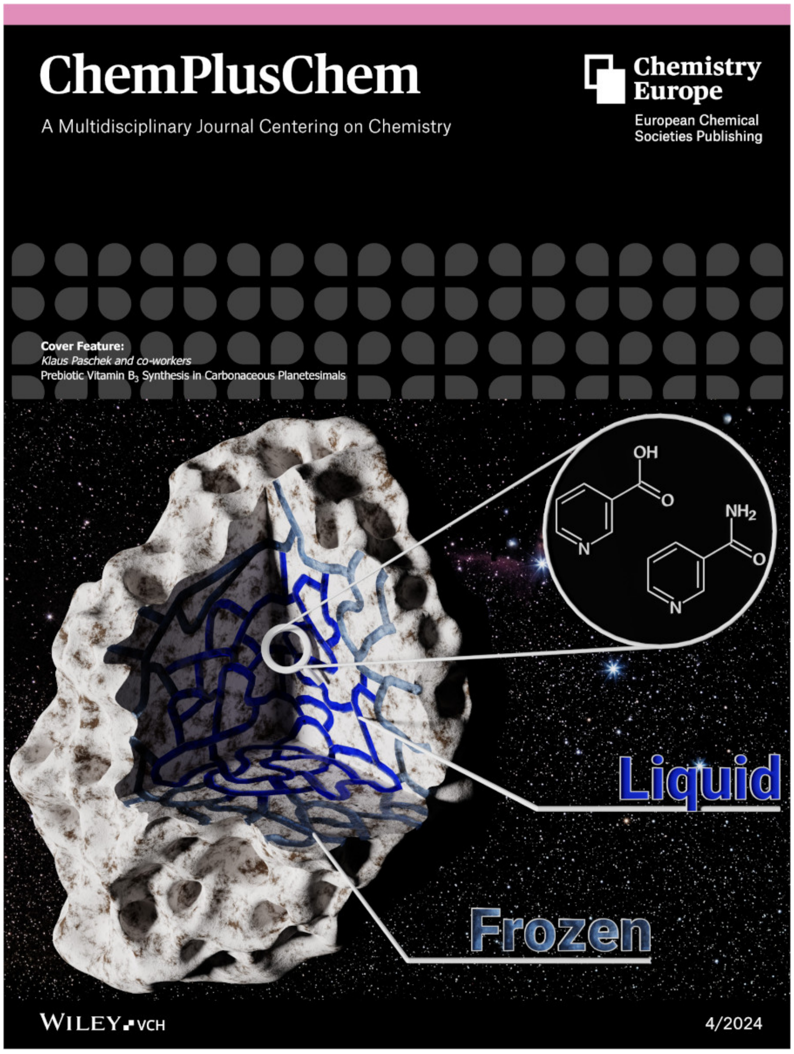

ChemPlusChem

A Multidisciplinary Journal Centering on Chemistry

Chemistry Europe
European Chemical
Societies Publishing

Cover Feature:
Klaus Paschek and co-workers
Prebiotic Vitamin B_3 Synthesis in Carbonaceous Planetesimals

WILEY-VCH

4/2024

Figure 16.3: The cover feature image illustrates that the first asteroids in the solar system might have contained liquid water due to radioactive heating. Effectively, this made them huge chemical reactors floating in space. Aqueous chemistry enabled the prebiotic synthesis of key building blocks of life, such as vitamin B3 found in the samples returned by the Hayabusa2 space probe. Delivered to Earth by meteorites, these prebiotic molecules might have kick-started the origins of life on our planet. More information can be found in the Research Article by Klaus Paschek and co-workers (Paschek, M. Lee, et al. 2024b).

Graphical Abstract

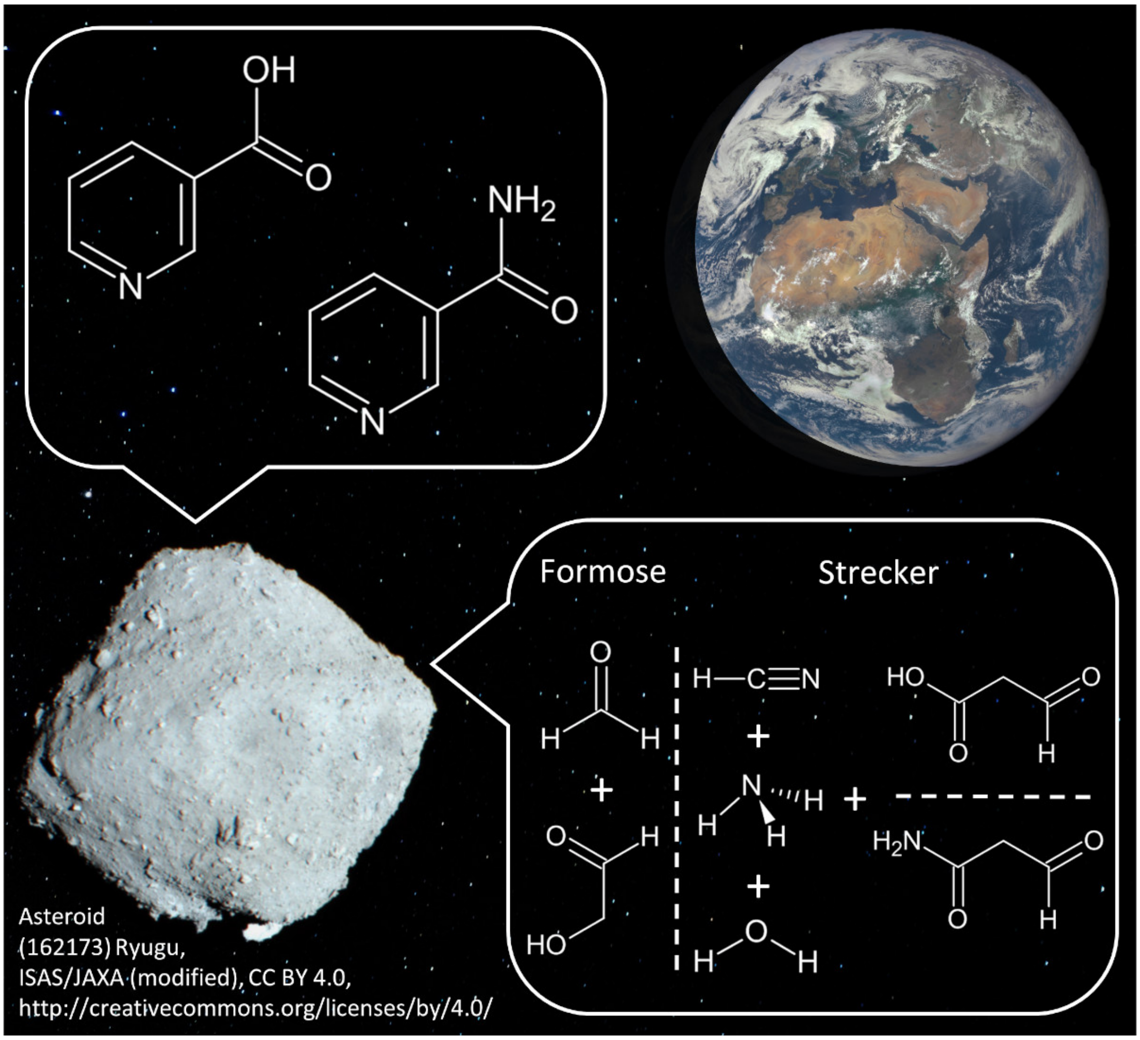

Figure 16.4: Aqueous chemistry inside meteorite parent bodies allows the formation of prebiotic molecules crucial for all life in the early solar system. We present a reaction mechanism suitable for vitamin B3 synthesis in this environment, which is experimentally verified in the literature. Vitamin B3 was transported to the Hadean Earth by meteorite falls and initiated redox chemistry in the form of NAD(P)H, potentially participating in the origins of life.

Abstract

Aqueous chemistry within carbonaceous planetesimals is promising for synthesizing prebiotic organic matter essential to all life. Meteorites derived from these planetesimals delivered these life building blocks to the early Earth, potentially facilitating the origins of life. Here, we studied the formation of vitamin B_3 as it is an important precursor of the coenzyme NAD(P)(H), which is essential for the metabolism of all life as we know it. We propose a new reaction mechanism based on known experiments in the literature that explains the synthesis of vitamin B_3. It combines the sugar precursors glyceraldehyde or dihydroxyacetone with the amino acids aspartic acid or asparagine in aqueous solution without oxygen or other oxidizing agents. We performed thermochemical equilibrium calculations to test the thermodynamic favorability. The predicted vitamin B_3 abundances resulting from this new pathway were compared with measured values in asteroids and meteorites. We conclude that competition for reactants and decomposition by hydrolysis are necessary to explain the prebiotic content of meteorites. In sum, our model fits well into the complex network of chemical pathways active in this environment.

17

Introduction

The origins of life on Earth remain an intriguing and extensively studied topic across many disciplines, and the exact mechanism that sparked life is still unknown. However, recent studies have suggested that meteorites might have played a critical role in delivering an essential portion of prebiotic material to the early Earth (Chyba and Sagan 1992; Morbidelli and B. J. Wood 2015; Pearce, Pudritz, et al. 2017). Carbonaceous chondrites, carbon-rich meteorites, might have contributed a large fraction of the Hadean and Eoarchaean Earth's crust and upper mantle during the Late Veneer (Varas-Reus et al. 2019; Fischer-Gödde, Elfers, et al. 2020, also referred to as the "Late Heavy Bombardment" or "Late Accretion") and delivered organic molecules to the various postulated environments that are thought to have provided the necessary conditions for the origins of life. Two prominent examples of these environments on Earth are the so-called "warm little ponds" located on the early Earth's first continental crust, and the "hydrothermal vents" located at the bottom of the primordial ocean.

The warm little pond hypothesis, proposed by Charles Darwin (Peretó et al. 2009), suggests that life originated in small bodies of water on the surface of the early Earth. These ponds would have provided the necessary conditions for life to emerge, such as a favorable temperature, shielding from the UV radiation by water, and a rich variety of organic molecules, possibly delivered there by meteorites (Pearce, Pudritz, et al. 2017). By going through daily or seasonal wet-dry cycles, warm little ponds could have promoted the polymerization of these simple prebiotic molecules into highly complex organics, initiating molecular chemical evolution and possibly culminating in the origins of life (Da Silva et al. 2015; S. Becker, Schneider, et al. 2018; S. Becker, Feldmann, et al. 2019; Damer and Deamer 2020a).

Another favored site for the origins of life is hydrothermal vents (also called "smokers"), where mineral-rich, superheated water emerges from the ocean floor. These unique environments are thought to have provided many of the necessary conditions for abiogenesis. The high temperature and mineral-rich waters at hydrothermal vents might have created the perfect conditions for organic molecules to form and evolve into more complex structures (W. Martin, Baross, et al. 2008). The question whether the impacts could have made a significant contribution to the reservoir of prebiotic organics in these environments due to the high dilution in the vast ocean remains open. Recent evidence that the mass accreted via the impacts of carbonaceous asteroids during the Late Veneer could have been as high as $\sim 0.3\,\%$ of the Earth's mass (Varas-Reus et al. 2019; Fischer-Gödde, Elfers, et al. 2020) makes it conceivable that the exogenous delivery of organics could have been important also for these deep water environments.

Among numerous key prebiotic organics such as fatty acids, amino acids, and nucleobases, the two forms of vitamin B_3 (rarely called vitamin PP), nicotinic acid and nicotinamide, also known as niacin and niacinamide, have been found in carbonaceous chondrites at concentrations of 5–715 pbb (Smith et al. 2014; Oba, Takano, Furukawa, et al. 2022, see Figure 17.1**A**). Furthermore, in the returned samples from the Hayabusa2 space mission that visited the near-Earth carbonaceous asteroid (162173) Ryugu, nicotinic acid was found in abundances of 49–99 ppb (Oba, Koga, et al. 2023). This reinforces the idea that these organics have been already present in the parent bodies of carbonaceous chondrites in the early history of the solar system. The nicotinic acid and nicotinamide could either have been formed in their interior by aqueous chemistry, or they could have been inherited by the solar nebula from the interstellar medium and incorporated into the source material of the planetesimals.

Vitamin B_3 is essential to all life. It is used in a variety of biological functions and plays a critical role in cellular metabolism (R. Blum 2015). It is the precursor of the coenzymes NAD^+/NADH and $NADP^+$/NADPH (Elvehjem et al. 1938), which are among the most important coenzymes in living systems (see Figure 17.1**B**). In studies of autocatalytic reaction networks associated with the origin of metabolism, NAD has been identified as the key catalyst that might have kick-started redox chemistry at the time of the origins of life (Xavier et al. 2020). NAD stands for "nicotinamide adenine dinucleotide" and is, as the name implies, a dimer of two ribonucleotides. In the context of RNA nucleotides, nicotinamide, like adenine, takes the place otherwise occupied by nucleobases. This might link its first emergence to RNA molecules.

According to the so-called "RNA world" hypothesis, RNA might have been the starting point of chemical evolution, as some RNA molecules were shown to be able to store genetic information while catalyzing other chemical reactions, including their own polymerization, and replicating themselves (Kruger et al. 1982; Guerrier-Takada, Gardiner, et al. 1983; Guerrier-Takada and Altman 1984; Zaug and Cech 1986; Cech 1986; Johnston et al. 2001; Vaidya et al. 2012; Attwater et al. 2018; Co-

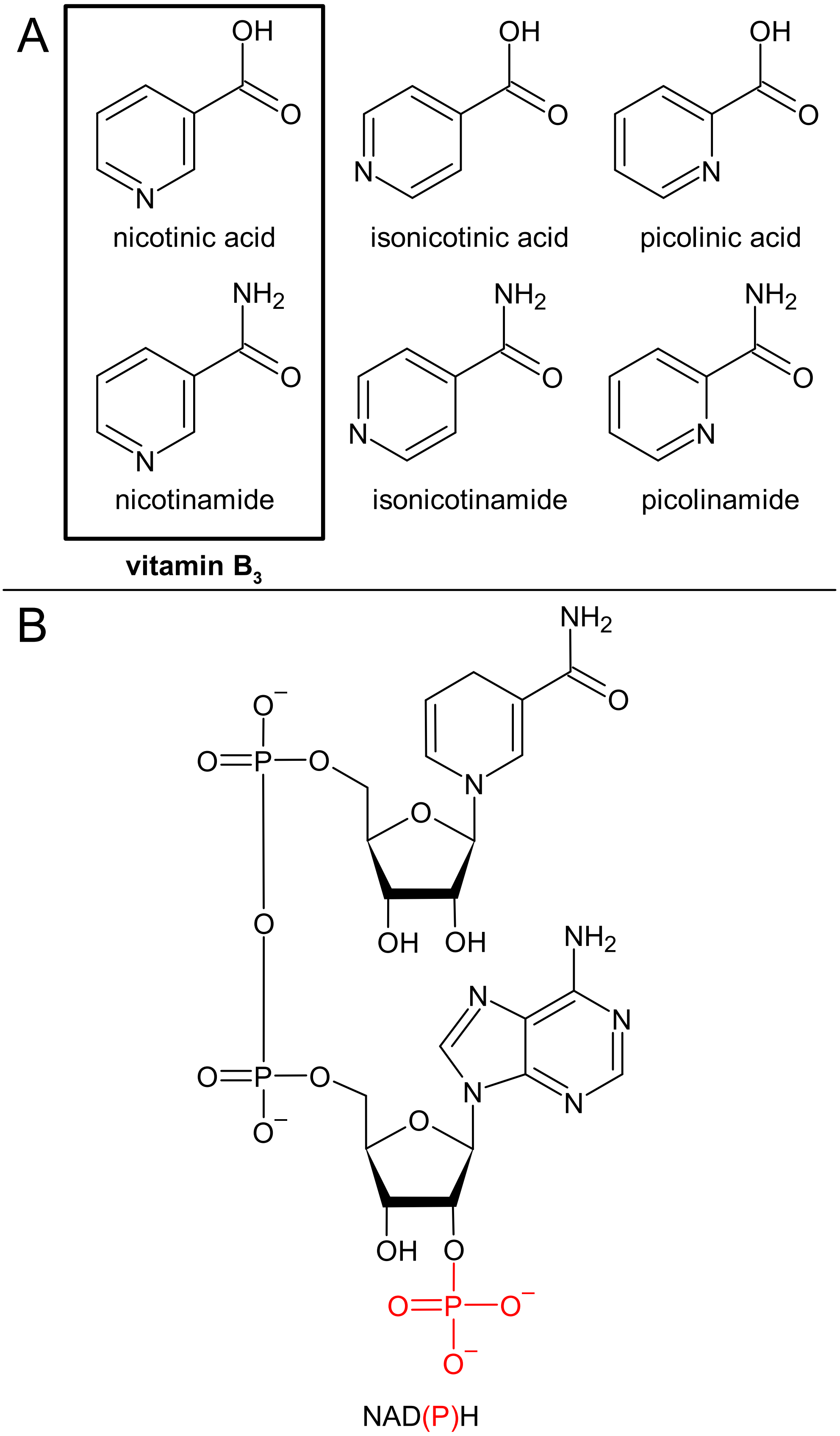

Figure 17.1: Structures of **A** vitamin B_3 (in box) and its isomers, and **B** the coenzyme nicotinamide adenine dinucleotide (phosphate), abbreviated as NAD(P)H, in its reduced form. The phosphorylated form is indicated in red.

jocaru and Unrau 2021; Kristoffersen et al. 2022). These are also called “ribozymes” and are thought to have played a crucial role in the origins of life.

Replacing a canonical nucleobase in a ribonucleotide dimer with nicotinamide leads to NAD. It has been suggested that many coenzymes, including NAD, FAD, acetyl-CoA, and F420, comprise ribonucleotide moieties that may be surviving remnants of covalently bound coenzymes in an RNA world (Shen and Ji 2011). Thus, nicotinamide and its role in NAD might be intimately linked to the origins of life in general, possibly as a critical link in an “RNA-first-proteins-second world” or an “RNA-and-proteins-side-by-side world” hypotheses.

The different forms of NAD are essential for various metabolic reactions in the cell throughout life. Examples include cellular redox reactions, energy production (synthesis of ATP, adenosine triphosphate, Friedkin and Lehninger 1949; P. Rich 2003), protection from oxidative stress (Rush et al. 1985; Couto et al. 2013), DNA repair (Wilkinson et al. 2001; Bürkle 2005), cell signaling (Clapper et al. 1987; Ziegler 2000; Berger et al. 2004; Guse 2004), 5’ modification of cellular RNA (Y. G. Chen et al. 2009), among others.

All of these examples highlight the immense biological relevance of vitamin B_3 as a crucial precursor of NAD in the RNA world. The other necessary building blocks for NAD have also been found in meteorites (Stoks and Schwartz 1981; Callahan et al. 2011; Pearce and Pudritz 2015; Furukawa et al. 2019), and their synthesis mechanisms have already been explored in the aqueous environment of the interior of meteorite parent bodies (Pearce and Pudritz 2016; Paschek, Kohler, et al. 2022; Paschek, Semenov, et al. 2023). The nucleobase adenine was found in carbonaceous chondrites (Stoks and Schwartz 1981; Callahan et al. 2011; Pearce and Pudritz 2015) and its synthesis has been explained by previous models that agree with the measured values (Pearce and Pudritz 2016; Paschek, Semenov, et al. 2023). The same is true for ribose, which was also found in carbonaceous chondrites (Furukawa et al. 2019), and its synthesis was investigated in a previous study (Paschek, Kohler, et al. 2022). Furthermore, the mineral schreibersite, which is capable of providing phosphate groups and phosphorylating nucleosides (Gull et al. 2015), is present in enstatite iron meteorites (Pasek and Lauretta 2005; Bryant and Kee 2006; Pirim et al. 2014). This makes nicotinamide the only piece needed for a complete building kit of NAD that could have been delivered to the early Earth by meteorites.

By pushing to understand its synthesis in space, this study aims to complete our knowledge of this meteoritic NAD building kit in order to better understand how meteorites might have contributed to the origins of life. All the ingredients could have been readily available in the early solar system and only needed to be assembled upon exogenous delivery onto the early Earth. With NAD as a subbranch in an emerging RNA world (Shen and Ji 2011), vitamin B_3 in carbonaceous chondrites might have supported the origins of life itself. Moreover, by considering the role of meteorites in delivering essential organic matter to the warm little ponds and hydrothermal vents, as well as the potential role of vitamin B_3 in prebiotic chemistry, we can also better understand the conditions that are necessary for life to emerge, either on the early Earth or rocky exoplanets.

17.1 Carbonaceous chondrites

Carbonaceous chondrites are widely recognized as the most interesting subclass of rocky meteorites in the context of prebiotic chemistry. They are undifferentiated and pristine bodies in character, close to their parent body material (Trigo-Rodríguez et al. 2019), and have early solar-like chemical compositions (minus the highly volatile elements, Weisberg et al. 2006). The name was coined due to their high carbon content $\sim 5\,\%$ by weight, and they all have a preponderantly dark appearance (Botta and Bada 2002; Glavin, Callahan, et al. 2010; A. K. Cobb and Pudritz 2014a). They contain up to $20\,\%$ water and have an average porosity of typically 0.2 (Mason 1963; Flynn et al. 1999; Macke et al. 2011).

Carbonaceous chondrites are divided into subgroups of distinctive composition. It is assumed that all members of a subgroup are descended from the same parent body or several very similar parent bodies formed in the same region in the early solar system (Bermingham, Füri, et al. 2020). Some fragments resulting from mutual planetesimal collisions have been impacting the proto-Earth, carrying organics with them (Pearce, Pudritz, et al. 2017). Some of these parent bodies might have remained asteroids in the solar system to this day (Burbine, McCoy, et al. 2002).

Each subgroup of meteorites is named after the first letter of the name of the first recovered fall. An example subgroup is CM (Mighei-like), which comprises carbonaceous chondrites that contain around $9\,\%$ water by weight (Rubin et al. 2007), as well as aqueously altered minerals (Palmer and Lauretta 2011), with many classified as petrologic type 2. The distribution and associations of these hydrated phases provide insight into the role of water in the early solar system (Palmer and Lauretta 2011). CM chondrites are metal-deficient compared to other subgroups, such as CO (Ornans-like) chondrites, since metals are highly susceptible to aqueous alteration (Kimura et al. 2011). Nevertheless, CM chondrites contain an array of metals in near-solar abundances, especially a significant amount of nickel (A. K. Cobb and Pudritz 2014a). Palmer and Lauretta (2011) and Kimura et al. (2011) discovered that CM chondrites contain an alloy of Fe-Ni and that kamacite grains are common in the Murchison and Murray meteorites.

CI (Ivuna-type) chondrites closely resemble the composition of the solar photosphere compared to other types of meteorites, and are thus generally accepted as the most pristine meteoritic material in the solar system (Weisberg et al. 2006; Anders and Grevesse 1989). Cb-type asteroids, e.g., (162173) Ryugu, are considered to originate from the same parent body as CI chondrites, such as the Orgueil meteorite (Yada et al. 2022; Nakamura et al. 2022; Pilorget et al. 2022; Yokoyama et al. 2022; Oba, Koga, et al. 2023).

17.2 Initial Concentrations of Reactants

Understanding the initial molecular content and concentrations of reactive species inside carbonaceous chondrite' parent bodies is challenging because the original source material that formed these planetesimals no longer exists. A. K. Cobb, Pudritz, and Pearce (2015) and Pearce and Pudritz (2016) used abundances derived from spectroscopic observations of comets in their modeling studies aimed to explain the synthesis of amino acids and nucleobases. Comets are thought to have well-preserved reservoirs of volatiles that existed in the outer early solar system at ∼5–20 au that are still accessible today (Rauer 2008; Mumma and Charnley 2011).

Nonetheless, comets are not representative of the reservoir of source material of carbonaceous chondrite parent bodies that formed in the solar system at ∼2–3 au. For example, (13) Egeria and (19) Fortuna are regarded as potential CM chondrite parent bodies (Burbine 1998). They are located close to the 3 : 1 resonance with Jupiter at ∼ 2.5 au (Burbine, McCoy, et al. 2002) and likely formed there. This was a warmer region of the solar nebula right outside the water snowline, as opposed to the outer cometary formation zone that was colder.

This follows from state-of-the-art planet formation theories, explaining planet formation by accretion of pebbles, which migrate to the inner regions and form the first planetesimals due to streaming instabilities (Johansen, Oishi, Low, et al. 2007; Ormel and Klahr 2010; Johansen, J. Blum, et al. 2014b; Klahr and Schreiber 2020b). These icy pebbles might originate from the formation region of comets and drift inwards closer to the proto-Sun. As they heat up, volatile species, e.g., CO or O_2, start to desorb through the pores of the icy pebbles and are lost to space. Therefore, these volatiles are expected to be heavily depleted in the pebbles making up the source material of carbonaceous chondrite parent bodies. This means that one has to be careful when using the measured composition of comets (Mumma and Charnley 2011) directly as a proxy for the initial composition of reactants involved in the prebiotic syntheses inside carbonaceous asteroids.

This depletion of volatiles was explored in a previous study (Paschek, Semenov, et al. 2023). The findings were based on experimental studies of mixtures of volatiles and water ice, as well as a review of the existing theoretical literature on the collapse of the solar nebula into the present solar system and the tracking of volatile ices.

Molecule i	Name	Concentration $[\mathrm{mol}_i \cdot \mathrm{mol}_{\mathrm{H_2O}}^{-1}]$
H_2O	water	1
NH_3	ammonia	7×10^{-3}
HCN	hydrogen cyanide	2.5×10^{-6}
H_2CO	formaldehyde	6.6×10^{-4}
$HOCH_2CHO$	glycolaldehyde	$(0.05\text{-}4)\times10^{-4}$
CH_3CH_2CHO	propanal	$(0.00125\text{-}1)\times10^{-4}$

Table 17.1: Initial concentrations of reactants used in the model (A. K. Cobb, Pudritz, and Pearce 2015; Goesmann et al. 2015; Paschek, Semenov, et al. 2023). Concentrations are normalized to water.

The predicted initial concentrations for reactants are listed in Table 17.1.

The abundances for volatile species (HCN and formaldehyde) are adopted from our previous study (Paschek, Semenov, et al. 2023), while abundances for non-volatile reactants (NH_3 and glycolaldehyde) necessary for the present study were adopted from another study (A. K. Cobb, Pudritz, and Pearce 2015) about amino acid synthesis in carbonaceous planetesimals, citing spectroscopic measurements in the comet C/1995 O1 (Hale-Bopp) (Mumma and Charnley 2011). The only newly added abundance is for propanal, also known as propionaldehyde. This aldehyde was detected in situ by the lander Philae (Goesmann et al. 2015), part of the ROSETTA mission, visiting and landing on comet 67P/Churyumov–Gerasimenko. It is important to note that Hale-Bopp and 67P belong to different classes of comets. Hale-Bopp originated in the Oort cloud very far outside the solar system, whereas 67P is part of the Jupiter family, orbiting closer to the Sun (Altwegg, Balsiger, and Fuselier 2019). Therefore, volatiles such as CO or water should be more depleted in 67P compared to Hale-Bopp. More refractory ices, e.g., glycolaldehyde or propanal, should have remained more intact, but their abundance normalized to water might have changed, as water started to be lost to space. Therefore, we adjusted the initial concentrations of propanal by using the one for glycolaldehyde measured for Hale-Bopp (Mumma and Charnley 2011) and using the ratio of 1/4 between the two measured by the Philae lander on 67P (Goesmann et al. 2015, see Table 17.1).

18

Results and Discussion

18.1 Reaction Pathway

In their experiments, Cleaves and Miller (2001) demonstrated the synthesis of nicotinic acid by combining aspartic acid with glyceraldehyde or dihydroxyacetone. This mixture of an amino acid and a sugar precursor is highly feasible to be present in carbonaceous planetesimals, as their respective synthesis mechanisms were shown to operate in these environments (A. K. Cobb, Pudritz, and Pearce 2015; Paschek, Kohler, et al. 2022).

The favored mechanism for amino acid synthesis in planetesimals is the Strecker synthesis (A. K. Cobb, Pudritz, and Pearce 2015), which involves aldehydes, HCN, ammonia, and water (see previous Section on Initial Concentrations and Table 17.1). Likely resulting from this Strecker synthesis, aspartic acid was detected in a wide range of carbonaceous chondrites, and thus was also available for chemical reactions (A. K. Cobb and Pudritz 2014a; Kaplan et al. 1963; Glavin, Elsila, et al. 2021).

The sugar precursors glyceraldehyde and dihydroxyacetone are easily formed via the formose reaction, which was shown to successfully describe the synthesis of ribose inside carbonaceous planetesimals (Paschek, Kohler, et al. 2022). Other necessary reactants, formaldehyde and glycolaldehyde, are also available (see Table 17.1). The formose reaction requires catalysts providing an alkaline environment, e.g., hydroxides or carbonates (Iqbal and Novalin 2012), which have also been found in carbonaceous chondrites (Barber 1981). Therefore, all the necessary reactants have been available, and the reaction pathway leading to vitamin B_3 was operational in our environment of interest.

We propose a new reaction pathway, shown in Figure 18.1, parts of which were developed in a private communication with O. Trapp (Department of Chemistry, Ludwig-Maximilians-University Munich, May 2023). It is a version of the proposal by Cleaves and Miller (2001) adapted to the conditions inside carbonaceous planetesimals. In their experiments, they mainly formed quinolinic acid **9**, and nicotinic

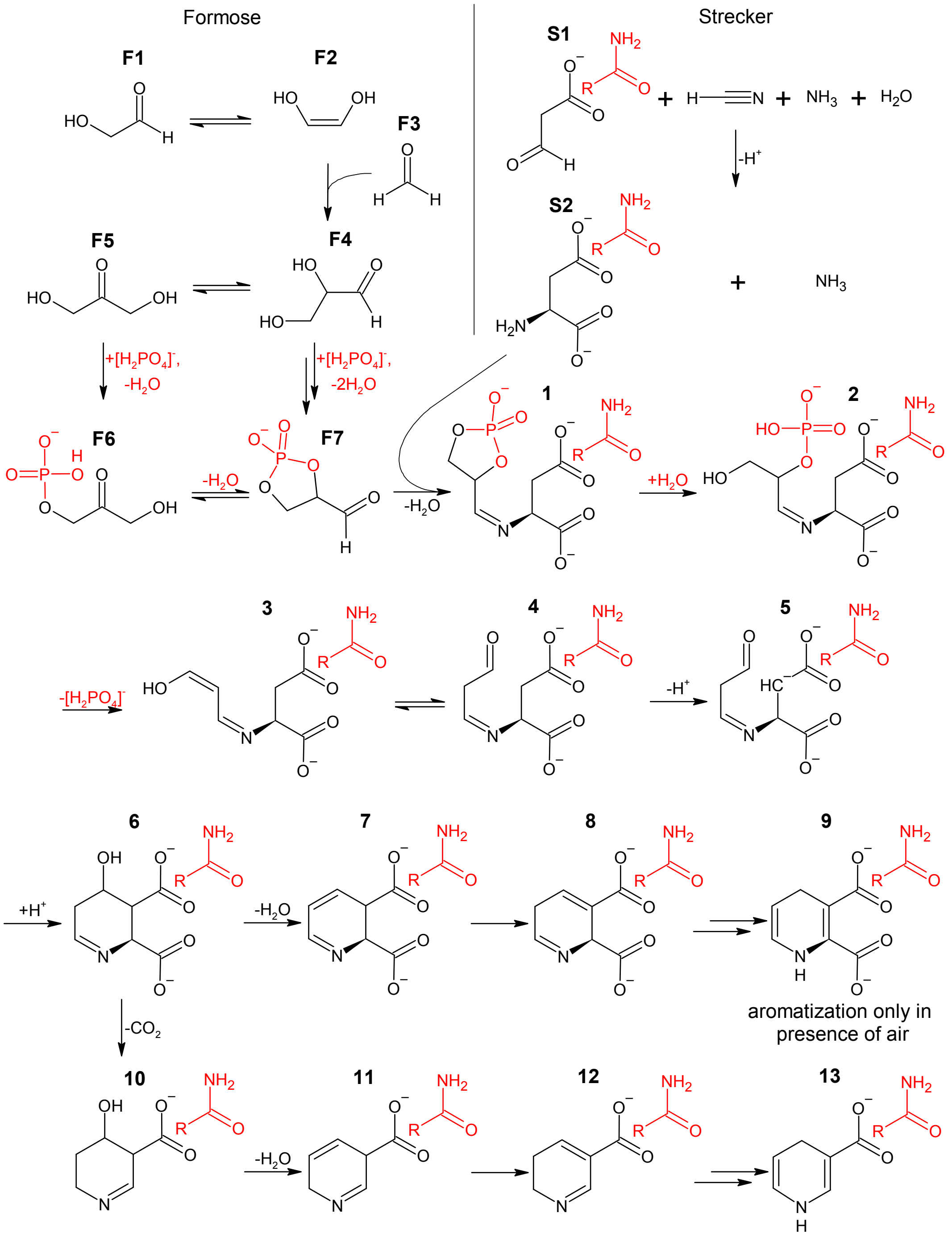

Figure 18.1: Newly proposed reaction mechanism inspired by experimental studies by Cleaves and Miller (2001). The phosphate and associated reaction steps are shown in red to indicate that phosphorylation increased the yield in the experiments; however, the synthesis of nicotinic acid was successful even without it, indicating it might be optional. Phosphates might not be readily available in meteorite parent bodies, but the reaction mechanism might still operate. The amide group serves as an alternative to the carboxyl group and is therefore also highlighted in red. Depending on the side chain of the starting aldehyde, either nicotinic acid or nicotinamide is formed in the Strecker synthesis.

acid and nicotinamide in smaller yields **13**, depending on whether aspartic acid or asparagine **S2** were used, respectively. When starting with phosphorylated glyceraldehyde **F7** or dihydroxyacetone **F6**, the yield of these products increased significantly in comparison to starting with nonphosphorylated reactants. Therefore, we presume that phosphates act as a catalyst here.

The amino acids can be synthesized in the Strecker synthesis, starting from an aldehyde **S1**. Depending on which aldehyde the Strecker synthesis starts with, one or the other amino acid is formed. This is indicated in Figure 18.1 with the alternative side chain colored in red, and R as a placeholder for the remaining molecule given in its full structure in black.

Cleaves & Miller suggested that the phosphate is immediately split off in the first step from dihydroxyacetone **F6**, leading to methylglyoxal in their proposed reaction mechanism. On the other hand, they showed that dihydroxyacetone phosphate yields more nicotinic acid than methylglyoxal does, which might favor dihydroxyacetone phosphate as the more likely intermediate in the reaction. This motivated us to propose a new mechanism, in which the phosphate group is removed later after reacting with the amino acid and allows closing the N-heterocycle.

After the formation of the imine **1**, the dephosphorylation allows the removal of an oxygen atom of **2**. Further, this new reaction step prepares for the tautomerization of the enol **3** to the aldehyde group of **4**. This allows the deprotonated carbon of the enolate in **5** to attack the electrophilic carbon in the aldehyde group on the opposite side of the ring, initiating the closure of the N-heterocycle **6**. Cleaves & Miller explain this step with the reaction of this enolate with an alkene group on the opposite side of the ring. Nevertheless, since the nucleophile enolate reacts better with the aldehyde group in **5**, our new proposal seems more feasible.

It should be noted that the experiments were also yielding products using nonphosphorylated reactants. It is an open question whether carbonaceous planetesimals contained enough minerals to allow this phosphorylation. Iron meteorites contain the phosphate-rich mineral schreibersite (Pasek and Lauretta 2005; Bryant and Kee 2006; Pirim et al. 2014), but carbonaceous chondrites do not. Whitlockite, a form of calcium phosphate, was detected in the carbonaceous chondrites Ningqiang (Hsu et al. 2006, anomalous CV condrite) and Yamato-82094 (Shibata and Matsueda 1994; Pravdivtseva et al. 2007, CO3.5). This mineral might potentially be able to initiate phosphorylation in carbonaceous planetesimals. In Figure 18.1, the phosphate and involved reaction steps are highlighted in red to indicate that the phosphorylation might be optional.

Charge migration in **6** allows for its decarboxylation to **10** and branching off from the path **7**, **8** to quinolinic acid **9**. This allows for a direct aromatization of the N-heterocycle, pushing the synthesis directly toward nicotinic acid or nicotinamide **13**. After the elimination of H_2O from **6**/**10** to **7**/**11**, quinolinic acid likely stays non-aromatized in the absence of air. Cleaves & Miller performed their experiment under vacuum conditions. Following our mechanistic proposal, this would mean that in their experiments they either detected this non-aromatized form of quinolinic acid **9** or they had air leaking in. They did not provide a mechanistic explanation of how the decarboxylation that leads to the nicotinic acid detected in the experiment occurs. However, they suggested that this decarboxylation might occur prior to aromatization because they tested whether quinolinic acid is stable under the conditions investigated. This observation is consistent with our proposal where the charge migration and decarboxylation directly lead to the aromatization.

The presence of O_2 in meteorite parent bodies is unclear, as it was only found in 67P (Bieler et al. 2015), not representing a pristine comet, making the assessment of its depletion throughout the early solar system's evolution challenging. The high reactivity of free oxygen in the environment of planetesimals containing many potential reaction partners, e.g., metals (van Kooten et al. 2022), makes it hard to assess how long oxygen might remain available there. In carbonaceous chondrites, iron is mostly in its oxidized ferrous and ferric forms, with metallic iron in minor (often zero) amounts (Garenne et al. 2019). This might hint that oxygen is mostly bound in iron and other metal oxides. Further, we are unaware of any detection of HCO_3. Vitamin B_3 synthesis pathways inspired by industrial processes (Lisicki et al. 2022) require either oxygen or HCO_3 as reactants. Therefore, these pathways are unfeasible to explain synthesis in meteorite parent bodies. It also remains an open question if alternatives proposed to the Strecker synthesis involving oxygen (Koga and Naraoka 2022) are plausible in meteorite parent bodies. Dowler et al. (1970) and Friedmann et al. (1971) demonstrated prebiotic pathways toward vitamin B_3 involving precursors formed by electrical discharges. We did not consider this mechanism further, as the reaction conditions seem unfeasible for the interior of meteorite parent bodies (electrical discharges seem unfeasible inside rocks), and to our knowledge, key reactants involved were not found in comets.

In the potential absence of free oxygen in carbonaceous planetesimals, the synthesis of vitamin B_3 in its aromatized form might even be favored over quinolinic acid (following Figure 18.1). The aromatic vitamin B_3 derivatives **10-13** have enhanced thermodynamic stability (McNaught and Wilkinson 2019) compared to the non-aromatized quinolinic acid derivatives **6-9**, whose piperideine ring is highly reactive (Shvekhgeimer 1998). Therefore, the final non-aromatized quinolinic acid derivative **9** might be less stable and more likely to decompose to other organics than vitamin B_3 **13**. Some planetesimals, which have the right balance of a big enough size $\gtrsim 10\,\mathrm{km}$ and late enough time of formation $\gtrsim 2.5\,\mathrm{Myr}$, can maintain aqueous conditions in their porous interiors for hundreds of thousands to millions of years (Paschek, Semenov, et al. 2023). When considering these long time scales, this might explain why quinolinic acid was indeed not found in carbonaceous chondrites. Smith et al. (2014) explicitly searched for quinolinic acid in carbonaceous chondrites and did not detect it, while both forms of vitamin B_3 were found in the same study. The decarboxylation itself (**6** $\longrightarrow$ **10**) might be how to aromatize the N-heterocycle in the experiments by Cleaves & Miller, leading automatically toward vitamin B_3 synthesis. This might confirm that our proposed reaction mechanism is appropriate to explain vitamin B_3 synthesis in carbonaceous planetesimals.

It is interesting to note that in the experiments by Cleaves and Miller (2001) alkaline conditions strongly favored the vitamin B_3 synthesis, which is in agreement with the conditions necessary for the formose reaction (Iqbal and Novalin 2012; Barber 1981), as mentioned above. Due to the hydroxides and carbonates found in carbonaceous chondrites (Barber 1981), the aqueous interior of meteorite parent bodies might provide alkaline conditions favorable for the complete set of reactions in our proposed mechanism (see Figure 18.1).

In the Strecker synthesis, we are targeting the amino acids aspartic acid and asparagine (indicated as black and red structures **S2**, respectively). The requisite aldehydes in the reaction are 3-oxopropanoic acid and 3-oxopropanamide, respectively (black and red structure **S1**, respectively). As abundances for these specific aldehydes are not known in comets, we use propanal as a proxy for their abundances as the closest structural equivalent (see Table 17.1). The detection of a plethora of different amino acids in carbonaceous chondrites (A. K. Cobb and Pudritz 2014a) might implicate that the specific aldehydes might actually be present in the source material of carbonaceous chondrites and be available to the Strecker synthesis. It might be that the aldehydes were either not explicitly looked for or their abundances were below the detection limits of ex situ spectroscopic observations of comets.

In our newly proposed pathway (Figure 18.1), vitamin B_3 is formed in its reduced form **13**. This is the same form of nicotinamide as in the coenzyme NAD in its reduced state NADH (see Figure 17.1**B**). The oxygen-poor environment of meteorite parent bodies might favor this pathway, and thus the prebiotic synthesis of vitamin B_3 in its reduced form, over the others mentioned above. It is a contentious debate how reduced or oxidized the early Earth's mantle and atmosphere were (Zahnle, Lupu, et al. 2020; Rollinson et al. 2017; Kuwahara, Nakada, et al. 2023; J. Wang et al. 2019; Nicklas et al. 2019; Kuwahara and Nakada 2023; Trail, Bruce Watson, et al. 2012; Armstrong et al. 2019; Matsui and Abe 1986). It might be that carbonaceous chondrites falling to the early Earth provided a high reducing power. This might have been necessary for the emergence of this important coenzyme and the origins of life by powering metabolic reduction reactions in the perhaps otherwise oxidizing environment of the early Earth.

18.2 Simulated Vitamin B_3 Abundances

18.2.1 Testing the Thermodynamic Favorability

To test if the newly proposed pathway in Figure 18.1 is thermodynamically favorable, we performed thermochemical equilibrium calculations. The difference in Gibbs free energies of formation between products and reactants determines the favorability of a chemical reaction (see Computational Methods for more details). For that, an overall summarized reaction equation of Figure 18.1 leads to

$$\begin{aligned}&\text{formaldehyde} + \text{glycolaldehyde}\\&+ \text{3-oxopropanoic acid} \,/\, \text{3-oxopropanamide}\\&+ \text{hydrogen cyanide} + \text{ammonia} + \text{water}\\&\longrightarrow \text{nicotinic acid} \,/\, \text{nicotinamide} + \text{carbon dioxide}\\&+ \text{ammonia} + \text{water},\end{aligned} \tag{18.1}$$

or

$$\begin{aligned}&H_2CO + C_2H_4O_2\\&+ C_3H_4O_3 \,/\, C_3H_5NO_2\\&+ HCN + NH_3 + H_2O\\&\longrightarrow C_5H_4NCOOH \,/\, C_5H_4NCONH_2 + CO_2\\&+ NH_3 + H_2O,\end{aligned} \tag{18.2}$$

which we use in our thermochemical equilibrium calculations. Only if the difference between products and reactants is negative, does the reaction proceed spontaneously under the given environmental conditions inside meteorite parent bodies.

To test if the pathway is feasible, we formulate the following null hypothesis assuming the pathway is not able to explain the vitamin B_3 abundances measured in meteorites: if the vitamin B_3 abundances resulting from the calculations are zero or smaller than the measured ones, the pathway in Figure 18.1 is unsuitable for the environment of meteorite parent bodies.

First, we need to define the physical conditions prevailing inside the parent bodies of carbonaceous chondrites. Thermodynamic simulations in a previous study (Paschek, Semenov, et al. 2023) and hydrothermal simulations by Travis and Schubert (2005) of carbonaceous chondrite parent bodies predicted the physical conditions allowing for liquid water in their porous interiors. The decay of radioactive isotopes, in particular, ^{26}Al as the dominant energy source in the early solar system, significantly heats up the planetesimal interiors. When assuming a pressure of 100 bar, typical for a 100 km-sized planetesimal (Pearce and Pudritz 2016), the

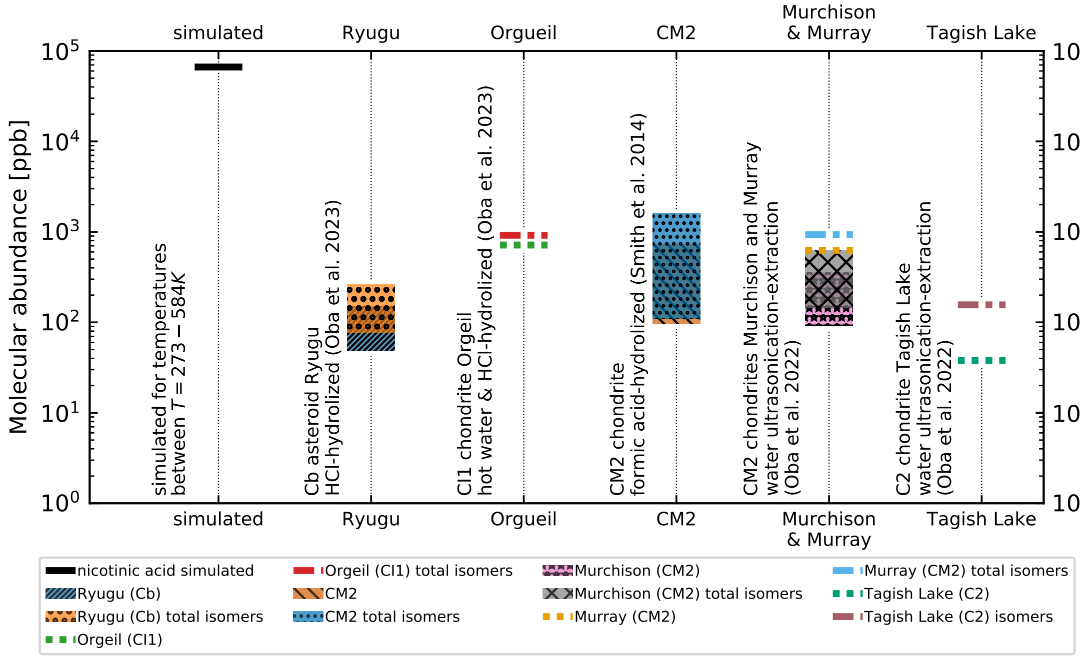

Figure 18.2: Simulated nicotinic acid abundances compared to measured values in carbonaceous chondrites and asteroid (162173) Ryugu. A rock density of $3\,\mathrm{g\,cm^{-3}}$, a porosity of 0.2 (Mason 1963; Flynn et al. 1999; Macke et al. 2011), and an ice density of $0.917\,\mathrm{g\,cm^{-3}}$ completely filling the pores (after all radionuclides have decayed and aqueous activity has ceased) were assumed as the properties of the planetesimal/carbonaceous chondrite hosting the chemical synthesis. The simulations were run at a pressure of 100 bar. From left to right, the plotted bars show the simulated molecular abundance of nicotinic acid (solid black line on the very left) for the whole temperature range of liquid water, as well as the abundances measured in samples of Cb asteroid (162173) Ryugu collected during the Hayabusa2 spacecraft mission (Oba, Koga, et al. 2023), in the CI chondrite Orgeil (Oba, Koga, et al. 2023), several Antarctic CM2 chondrites (Smith et al. 2014), the CM2 chondrites Murchison and Murray, and the ungrouped C2 chondrite Tagish Lake (Oba, Takano, Furukawa, et al. 2022) as lines and shaded ranges described in the legend. Each time, the measured nicotinic acid abundance and the sum of all isomers (nicotinic acid, isonicotinic acid, picolinic acid) are given, since thermochemical equilibrium simulations cannot distinguish between isomers. The type of extraction method used (hot water, cold water ultrasonication, HCl-hydrolyzed, formic acid) is denoted next to each panel. A tabulated version of the data presented here is available in the Supporting Information in Table S1.

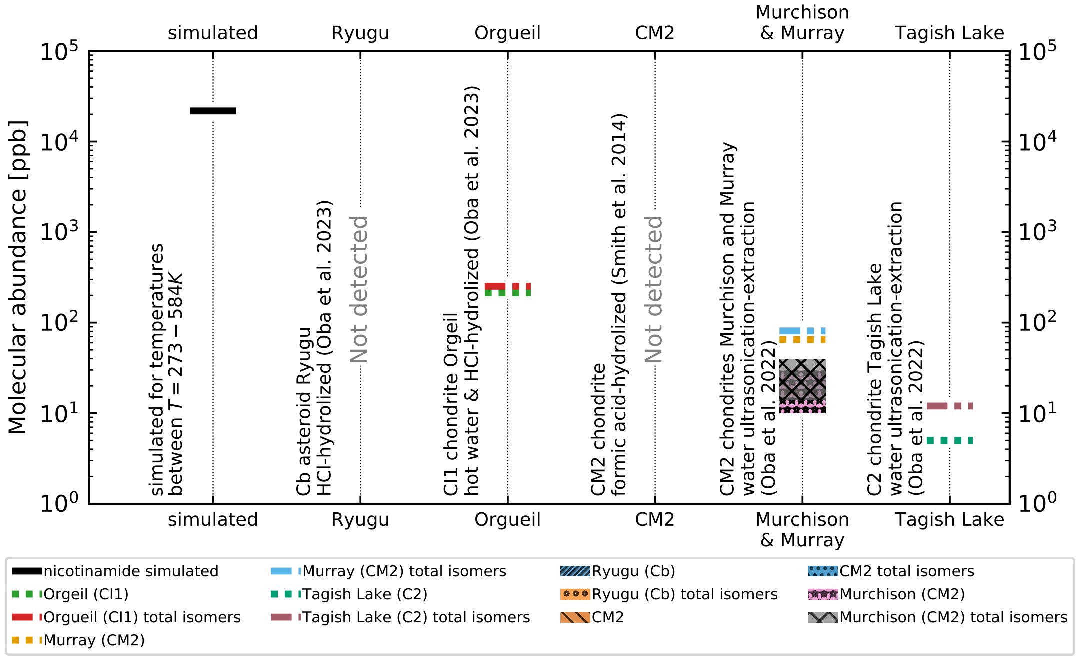

Figure 18.3: Simulated nicotinamide abundances compared to measured values in carbonaceous chondrites and asteroid (162173) Ryugu. A rock density of $3\,\mathrm{g\,cm^{-3}}$, a porosity of 0.2 (Mason 1963; Flynn et al. 1999; Macke et al. 2011), and an ice density of $0.917\,\mathrm{g\,cm^{-3}}$ completely filling the pores (after all radionuclides have decayed and aqueous activity has ceased) were assumed as the properties of the planetesimal/carbonaceous chondrite hosting the chemical synthesis. The simulations were run at a pressure of 100 bar. From left to right, the plotted bars show the simulated molecular abundance of nicotinamide (solid black line on the very left) for the whole temperature range of liquid water, as well as the abundances measured in samples of Cb asteroid (162173) Ryugu collected during the Hayabusa2 spacecraft mission (Oba, Koga, et al. 2023), in the CI chondrite Orgeil (Oba, Koga, et al. 2023), several Antarctic CM2 chondrites (Smith et al. 2014), the CM2 chondrites Murchison and Murray, and the ungrouped C2 chondrite Tagish Lake (Oba, Takano, Furukawa, et al. 2022) as lines and shaded ranges described in the legend. Each time, the measured nicotinamide abundance and the sum of all isomers (nicotinamide, isonicotinamide, picolinamide) are given, since thermochemical equilibrium simulations cannot distinguish between isomers. The type of extraction method used (hot water, cold water ultrasonication, HCl-hydrolyzed, formic acid) is denoted next to each panel. If nicotinamide was not detected in the respective samples, this is noted in the respective panel. A tabulated version of the data presented here is available in the Supporting Information in Table S2.

whole temperature range of liquid water of 273–584 K (0–311 °C) can be reached inside the planetesimal. In a previous study (Paschek, Semenov, et al. 2023), we presented model planetesimals of radii between 3–150 km and times of formation after the formation of the solar system of 0.5–3.5 Myr. The bigger or the earlier formed a planetesimal is, the higher the reached temperatures can be. Bigger planetesimals can retain the energy generated by radioactive decay better. Earlier formed planetesimals contain a higher content of the short-lived ^{26}Al isotope dominating the early solar system (Cameron and Truran 1977; Gaches et al. 2020).

In the previous study (Paschek, Semenov, et al. 2023), we explored the impact on the prebiotic chemistry of different temperature structures inside model planetesimals with different formation and evolution histories. We refrain from coupling the planetesimal models directly with the thermochemical equilibrium calculations in the present study, as we found no significant temperature dependence of the proposed reaction mechanism (see below). Nevertheless, higher temperatures used in the calculations presented here can be interpreted as representing either more central regions inside a planetesimal, or a generally bigger or earlier formed planetesimal at the same radial distance to its center.

Due to the high temperatures and pressure present in potential meteorite parent bodies, the pores in the whole central volume are filled with liquid water. This aqueous volume lies under a frozen layer at the surface of the planetesimal, shielding it from space. The water can remain liquid for several million to hundreds of millions of years (Paschek, Semenov, et al. 2023). This is consistent with simulations of equivalent model planetesimals by Travis and Schubert (2005) and Lichtenberg, Golabek, et al. (2016). Rapid convection through the whole liquid volume allows for chemical equilibration and well-mixing of the entire system (Travis and Schubert 2005). Hence, thermochemical equilibrium calculations based on Gibbs free energies of formation as performed in the present study are a well-suited approach for this environment.

As already mentioned, the typical properties of carbonaceous chondrites and therefore likely also their parent bodies are a porosity of ~ 0.2 (Mason 1963; Flynn et al. 1999; Macke et al. 2011). We assumed a general rock density of $3\,\mathrm{g\,cm^{-3}}$ and water ice density of $0.917\,\mathrm{g\,cm^{-3}}$ completely filling the rock pores of the frozen planetesimal (after the ceasing of radiogenic heating). This allows converting the molecular abundance resulting from the thermochemical equilibrium calculations into values comparable to measurements in real carbonaceous chondrites, usually given in parts per billion (ppb).

Figures 18.2 and 18.3 show the vitamin B_3 abundances resulting from the thermochemical equilibrium simulations. The leftmost black solid line shows the simulation result for the whole temperature range of liquid water. To compare this with the abundances found in carbonaceous chondrites, the bars and lines on the right show the measured abundances in different carbonaceous chondrites and the asteroid (162173) Ryugu. The simulation results in abundances of 6.64×10^4 ppb nicotinic acid and 2.18×10^4 ppb nicotinamide, which are stable over the whole temperature range of liquid water at 100 bar. These simulated abundances are around two orders of magnitude higher than the measured abundances in carbonaceous chondrites and asteroids.

As we do not see simulated abundances below the measured ones in carbonaceous chondrites, we conclude that the null hypothesis is rejected; the proposed pathway can not be ruled out and might explain how parts of the prebiotic vitamin B_3 synthesis in meteorite parent bodies proceeds. Only if the simulation had yielded lower abundances than measured, it would be completely unfit to explain the prevailing synthesis, as there would have to be another more dominating chemical process. We deduce that the pathway is well within the means of possibility.

18.2.2 Undetermined Initial Aldehyde Concentrations

It is important to note that there is no information on the initial abundances for the reactants 3-oxopropanoic acid or 3-oxopropanamide (**S1** in Figure 18.1) measured in comets or predicted by solar nebula models. As already mentioned, we used the concentration of propanal measured in the comet 67P (Goesmann et al. 2015, see Table 17.1) as the aldehyde with the closest structural resemblance instead. Propanal might be the most general representative of this class of aldehydes with the lowest complexity. Thus, we would expect that this is most likely a strong overestimate of the actual concentrations of **S1** in the source material of carbonaceous chondrite parent bodies. Therefore, the resulting vitamin B_3 abundances presented here constitute the absolute upper limit possible.

To explore this further, we ran the same simulations for varying initial concentrations of 3-oxopropanoic acid and 3-oxopropanamide. The results are presented in Figure 18.4. At very low initial aldehyde concentrations (on the right in Figure 18.4), the resulting vitamin B_3 abundances are on a plateau because the thermodynamic favorability determines the balance of the reaction, not the initial reactant concentration. As the initial aldehyde concentration is increased, the resulting abundances begin to increase linearly. This corresponds to a regime where the increased supply of the aldehyde directly affects the balance of the reaction, leading to an increase in yield. It determines how much the synthesis yields and becomes completely depleted in the process. At even higher aldehyde concentrations, the resulting abundances level off at a saturation plateau because another reactant limits the synthesis by becoming exhausted.

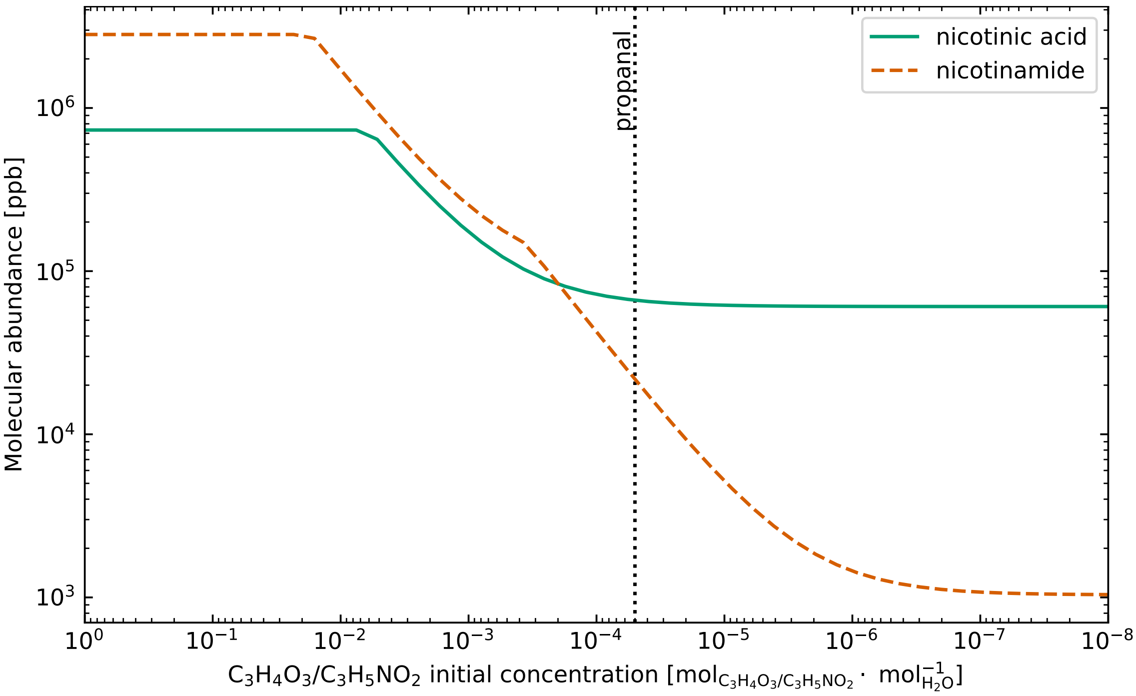

Figure 18.4: Simulated vitamin B_3 abundances depending on variable initial concentrations of the aldehydes 3-oxopropanoic acid ($C_3H_4O_3$) and 3-oxopropanamide ($C_3H_5NO_2$), which are reactants in the Strecker synthesis (**S1** in Figure 18.1). All simulations were performed at 0 °C and 100 bar. The vertical dotted black line indicates the initial concentration of propanal (mean of the range given in Table 17.1), which was used in the simulations as a surrogate for these aldehydes that have not yet been detected in comets.

For nicotinic acid, assuming the cometary abundance of propanal does not significantly affect the resulting abundance, since a lower expected initial concentration of 3-oxopropanoic acid would change the resulting abundance in minor amounts moving further into the right plateau region (see Figure 18.4). A lower initial 3-oxopropanamide concentration in comets has the potential to reduce the simulated nicotinamide abundance by about an order of magnitude. We conclude that using the cometary propanal abundance as a surrogate gives a good approximation for the achievable nicotinic acid abundance in this reaction mechanism, while for nicotinamide it is only an upper limit.

18.2.3 Comparison to Measured Abundances in Meteorites and Asteroid (162173) Ryugu

One possible explanation for why the measured abundances are below the simulated ones (see Figures 18.2 and 18.3) is that vitamin B_3 synthesis competes with the synthesis of other organic molecules drawing from the same initially available pool of reactants. As shown in previous studies, prebiotic synthesis of amino acids (A. K.

Cobb, Pudritz, and Pearce 2015), nucleobases (Pearce and Pudritz 2016; Paschek, Semenov, et al. 2023), and sugars (Paschek, Kohler, et al. 2022) draw from the same reactants in meteorite parent bodies. The autocatalytic formose reaction produces a plethora of complex sugars and decomposition products (Cleaves 2015), competing for the glyceraldehyde **F4**/**F7** needed for vitamin B_3 formation.

The previous study of ribose synthesis (Paschek, Kohler, et al. 2022) also did not consider the competition of the formose reaction for reactants with other pathways, and we were not yet aware of the pathway presented here. The result was that ribose was slightly overproduced in the simulations by factors of ∼1.04–100 (Paschek, Kohler, et al. 2022), depending on if the minimum or maximum initial glycolaldehyde abundance in comets was assumed in the simulations (see also Table 17.1 as this reactant also participates in the pathway of the present study). Knowing that the formose reaction is interlocked with vitamin B_3 synthesis via glycolaldehyde **F1** in Figure 18.1 might explain why ribose was overproduced in these past simulations, as the difference between the simulated and measured ribose amounts in meteorites might actually account for the not yet known and not yet considered synthesis of vitamin B_3 operating in parallel. The formose reaction is much faster due to its autocatalytic nature in comparison to vitamin B_3 synthesis. The formose reaction completed in ∼20–180 min in our past laboratory experiments (Paschek, Kohler, et al. 2022) depending on the used catalyst and temperatures of ≤60 °C. After this time, the maximum sugar abundances were reached and the decomposition of the products started to dominate. Cleaves and Miller (2001) showed that vitamin B_3 synthesis was completed after around 6 h, also at a temperature of 60 °C. This might indicate that the autocatalytic formose reaction is much faster than vitamin B_3 synthesis, presumably resulting in most of the glycolaldehyde forming sugars, and only a minor fraction ending up as vitamin B_3 in the simultaneous synthesis. Nevertheless, both laboratory studies did not provide any kinetic parameters. Other factors, e.g., the initial concentrations of reactants or unknown rates of decomposition reactions play a role in the completion times of the reactions. Therefore, determining the reaction rates and comparing them directly would allow to test this hypothesis.

This might explain the overproduction in the present study (see Figures 18.2 and 18.3), as this difference is actually forming an equivalent amount of sugars, including their decomposition products. There are many effective decomposition mechanisms active in the formose reaction, e.g., β-elimination, benzilic acid rearrangement, oxidation, etc. (De Bruijn et al. 1986). Due to the presumably faster reaction rate of the formose reaction, the overproduction in the present study might be significantly larger in comparison to the previous investigations of ribose. Sugars and their decomposition products are major “side products” in vitamin B_3 synthesis, leading to the overproduction in the simulations, because competition with the formose reaction was not included in the model.

For a complete evaluation of the coupled formose reaction, its notoriously complex product mixture (Cleaves 2015) would need to be included. In the previous study (Paschek, Kohler, et al. 2022), we compensated for this by running the formose reaction in the laboratory and focusing only on ribose in relation to all formed pentoses. To fully understand the interlocking with vitamin B_3 synthesis, a complete analysis of all compounds forming in a combined formose and vitamin B_3 synthesis would need to be performed in experiments, which could then be used to tweak the simulations. This is beyond the scope of the present study. Our aim is to establish a first pathway of vitamin B_3 synthesis suitable for the environment of planetesimal interiors and to check its thermodynamic feasibility. In future studies, a simultaneous evaluation of the formose and vitamin B_3 synthesis might show if this can account for the overproduction seen in both the present and past models. If not, other yet unknown interlocked synthesis mechanisms producing other prebiotic molecules might exist. The newly proposed pathway in Figure 18.1 is a first step in exploring the complex network of pathways governing the aqueous synthesis of the prebiotic organics found in carbonaceous chondrites.

Hexamethylenetetramine (HMT) was detected in carbonaceous meteorites and can be degraded to formaldehyde and ammonia upon hydrothermal treatment (Oba, Takano, Naraoka, Furukawa, et al. 2020). HMT was shown to be formed by photochemical reactions and warming of interstellar ice analogs (Bernstein et al. 1995; Muñoz Caro et al. 2004; Vinogradoff et al. 2011). Since formaldehyde and ammonia are reactants in our proposed vitamin B_3 synthesis pathway (see Figure 18.1 and Equations (18.1) and (18.2)), HMT decomposing in the aqueous interiors of carbonaceous planetesimals could be another potential source of vitamin B_3 not included in the present model. If the presence of HMT in the interstellar medium is detected by observations, future studies might be able to estimate the initial concentration of HMT in the solar nebula and explore whether it has the potential to contribute significantly to vitamin B_3 synthesis in meteorite parent bodies.

Aspartic acid, which is one of the intermediate amino acids **S2** in Figure 18.1, was found in meteorites (Kaplan et al. 1963; Glavin, Elsila, et al. 2021). This indicates that a part of the available stock of amino acids participated in the vitamin B_3 synthesis and the rest remained in the parent body until after its phase of aqueous activity. Pearce and Pudritz (2016) showed that simulating the formation of several different prebiotic organics in thermochemical equilibrium models simultaneously often results in zero abundances or fails to reproduce the measurements in meteorites, as the model does not converge correctly due to its increased complexity. This limitation of the model means that we always obtain the upper possible limit using the whole pool of reactants for one specific pathway. The actual abundances are a weighted combination of the results for the synthesis of different organic molecules in parallel and partially yet unknown chemical mechanisms, drawing from overlapping sets of reactants, as mentioned above. This limitation of the thermochemical models would also be a challenge in future combined formose and vitamin B_3 models.

Not only the amount and allocation of the available reactants (which still needs to be explored further), but also processes involving the products might explain the overestimates in the simulations. In comparison to other vitamins, B_3 is relatively stable. On the other hand, B_3 is one of the least complex vitamins. Compared to the stability of other prebiotic molecules found in meteorites, e.g., nucleobases (Levy and Miller 1998), vitamin B_3 (in this case nicotinamide) decomposes orders of magnitude faster (Yessaad et al. 2018), especially under hot ($\geq 80\,^{\circ}\mathrm{C}$) and alkaline conditions as presumed for carbonaceous parent body interiors, as mentioned earlier. This follows from comparing the pH-dependent decomposition rates and Arrhenius plots of nucleobases (Levy and Miller 1998) with the percentage of vitamin B_3 degradation at 80 °C over 60 min (Yessaad et al. 2018), and might explain the overproduction in the present simulations. Potential destruction mechanisms of aqueous vitamin B_3 have not been included in the model but might reduce its final abundance found in meteoritic samples, especially over the long periods of radiogenic heating inside parent bodies (Paschek, Semenov, et al. 2023). It is difficult to quantify the exact pH and duration of aqueous activity in the parent body of a specific meteorite and therefore was not included in the model. Nevertheless, Smith et al. (2014) found a clear correlation between increasing aqueous alteration of the studied CM2 meteorites and a decreasing vitamin B_3 abundance, confirming that decomposition by hydrolysis plays a role in meteorite parent bodies.

Smith et al. (2014) also studied the hydrolysis of nicotinamide under the procedures employed to extract the organics from the meteorites. When using acid-hydrolyzed hot water (6 M HCl, 150 °C, 3 h) for extraction, a common method also used by Oba, Koga, et al. (2023), purchased nicotinamide was 100 % converted to nicotinic acid. This might also explain why nicotinamide could only be detected by the more gentle method by Oba, Takano, Furukawa, et al. (2022), using water extraction and ultra-sonication for 10 min at room temperature without involving high temperatures or acids. In their other study Oba, Koga, et al. (2023), they could only find it in hot water extracts of the Orgueil CI meteorite at 105 °C over 20 h, which is at a lower temperature and over a shorter period in comparison to hot water extraction performed by Smith et al. (2014). In the same study Oba, Koga, et al. (2023), acid-hydrolyzed extraction (6 M HCl, same as acid-hydrolyzed extraction by Smith et al. 2014) of the same sample yielded no nicotinamide, but a slightly higher nicotinic acid abundance. This might indicate that in the acidic conditions of the extraction, nicotinamide was partially decomposed (Yessaad et al.

2018) and partially converted to nicotinic acid (Smith et al. 2014). The method of extraction in meteorites itself seems to reduce the amount of organic material recovered, and hence might explain the discrepancy between the presented simulations and measurements.

In Figures 18.2 and 18.3, we also included the sum of all isomers of nicotinic acid (isonicotinic acid, picolinic acid) and nicotinamide (isonicotinamide, picolinamide) found in meteorites (Smith et al. 2014; Oba, Takano, Furukawa, et al. 2022; Oba, Koga, et al. 2023). This is due to the fact that thermochemical equilibrium simulations can not distinguish between isomers (Paschek, Kohler, et al. 2022; Paschek, Semenov, et al. 2023). Following from this limitation it might be that the simulated abundances actually represent the sum of all isomers.

In all the carbonaceous meteorite and asteroid extracts of Oba, Takano, Furukawa, et al. (2022) and Oba, Koga, et al. (2023), no picolinic acid was detected. Picolinamide was not detected in the Ryugu asteroid samples and the CI meteorite Orgueil, and in very minor amounts ($\leq 10\,\mathrm{ppb}$), which is similar to the background noise, in the CM2 meteorites Murchison and Murray as well as the ungrouped C2 meteorite Tagish Lake. Dominance of the nicotin- and isonicotin- isomers over picolin- isomers might be a direct consequence of the newly proposed mechanism in Figure 18.1. The decarboxylation by charge migration from **6** to **10** excludes that a carboxyl/amide group is at the 2-position of the pyridine ring of the final molecule. However, this is the case for the picolin- isomers or quinolinic acid mentioned above. On the other hand, starting with 4-oxobutanoic acid/4-oxobutanamide instead of **S1** results in glutamic acid/glutamine in the Strecker reaction. Combining this directly with glycolaldehyde **F1** (instead of glyceraldehyde **F4**/**F7**) to form an imine equivalent to **1** in Figure 18.1 yields the isonicotin- isomers, following the same newly proposed mechanism. This is supported by the fact that glutamic acid was also found in meteorites (Kaplan et al. 1963; Glavin, Elsila, et al. 2021).

Nevertheless, Smith et al. (2014) found picolinic acid in their extracts from several CM2 meteorites, which is in direct contradiction to the missing detection in Murchison and Murray by Oba, Takano, Furukawa, et al. (2022), all members of the same meteorite group CM2 and potentially sharing the same parent body. They also performed proton-irradiation experiments of pyridine and CO_2 ice mixtures. The underlying idea is that prebiotic organics formed in the interstellar and interplanetary medium on ice grains at low temperatures, and were incorporated into the source material of planetesimals. Meteorites might have inherited these organics and not (only) formed them in situ by aqueous chemistry, as presented here. Smith et al. (2014) claim to have found more picolin- than other isomers in these experiments, similar to the pyridine carboxylic acids detected in the extract of their most aqueously unaltered meteorite LEW 85311 studied. However, no respective chromatography-mass spectroscopy data were provided to support these findings. It is questionable if pyridine is readily available on ice grains, as this rather complex molecule was never detected in the interstellar medium (Charnley et al. 2005; Barnum et al. 2022; Heitkämper et al. 2022; Rap et al. 2023).

Anyway, there needs to be an explanation as to why Smith et al. (2014) found picolin- isomers in dominating amounts in meteorites, and Oba, Takano, Furukawa, et al. (2022) and Oba, Koga, et al. (2023) did not. They might be inherited from ice grain processes and either very heterogeneously distributed in the same parent body, or the CM2 chondrites originate from several different bodies with different chemical histories. Another reason could be the contamination of the meteorite samples before their retrieval. At the same time, the asteroid material studied by Oba, Koga, et al. (2023) might have the highest chance of evading Earth's biosphere. Oba, Takano, Furukawa, et al. (2022) also refer to previous experiments on photon-irradiated H_2O, CO, NH_3, and CH_3OH ice mixtures (Oba, Takano, Naraoka, N. Watanabe, et al. 2019) to explain the synthesis of the N-heterocycles found in their meteoritic samples. The measured acid/amide ratios in the photochemical products were 0.8–1.0, and 9.3–72.8 in the meteorite extracts (Oba, Takano, Furukawa, et al. 2022). Oba et al. explained the high ratios in meteorites with aqueous processing of photochemical products inherited from interstellar ice grains into the meteorite parent bodies. As an alternative to in situ aqueous chemistry, we recognize reactions on and inheritance from ice grains as another possible source of the vitamin B_3 in extraterrestrial carbonaceous material. More experimental work is needed here to find pathways feasible for vitamin B_3 synthesis in the interstellar medium. The same is true for aqueous pathways other than demonstrated by Cleaves and Miller (2001) to study their interconnection with the mechanisms in Figure 18.1. This is necessary to better understand the origin of vitamin B_3 and its isomers in these extreme environments very different from the typical conditions studied in most chemical laboratories (extreme temperatures, no free oxygen available, etc.). It is an open question whether inheritance from ice grains or in situ aqueous synthesis is the primary source of vitamin B_3 and other prebiotic organics in meteorites.

19

Conclusion

Aqueous chemistry inside the warm porous rock of carbonaceous chondrite parent body planetesimals is a promising candidate for the prebiotic synthesis of vitamin B_3 in the early solar system. This could be a way to provide prebiotic molecules that are fundamental to all life as we know it and universal to all forming (exo)planetary systems. For the first time, we provide a detailed reaction mechanism suitable for this environment without any obvious caveats. Neither free oxygen nor electrical discharges are required, and the availability of necessary reactants is plausible. The origin of meteoritic organics and their contribution to the origins of life can only be understood by carefully assessing the physical setting and applying it to detailed chemical reaction mechanisms in an interdisciplinary approach.

We tested the thermodynamic favorability of our newly proposed reaction (see Figure 18.1) and evaluated the resulting abundances in comparison to measurements in carbonaceous chondrites and asteroids. We conclude that it fits well into the complex network of other prebiotic pathways, e.g., Strecker (A. K. Cobb and Pudritz 2014a; A. K. Cobb, Pudritz, and Pearce 2015), Fischer-Tropsch (Pearce and Pudritz 2015; Pearce and Pudritz 2016; Lai et al. 2019; Paschek, Semenov, et al. 2023), or formose (Paschek, Kohler, et al. 2022) reactions active in the aqueous phase of planetesimals. More detailed modeling of competition between these pathways is needed, e.g., the interplay with the formose reaction. Additionally, decomposition reactions of vitamin B_3 either by hydrolysis in planetesimals or meteorite extraction in the laboratory need to be explored further to fully understand the abundances found by measurements in meteorites.

Inheritance of organics formed on the surface of ice grains by irradiation in the interstellar medium (often including reactions between radicals) is another promising synthesis pathway that needs to be acknowledged (Smith et al. 2014). After inheritance into meteoritic material, this might influence the final available organic reservoir brought to the early Earth by impacts, but this is beyond the scope of the present study.

It might be interesting to make 3-oxopropanoic acid, 3-oxopropanamide, 4-oxobutanoic acid, and 4-oxobutanamide new targets in surveys hunting for organics in comets. We hope the present work emphasizes the importance of these aldehydes for prebiotic synthesis in the early solar system and is able to stimulate cometary surveys to search for them despite their rather high complexity and specificity. If future surveys can detect these key reactants, this might bring us closer to understanding the prebiotic synthesis of the vital vitamin B_3 as well as proteinogenic amino acids in the interplanetary space of the arising solar system.

We hope the newly proposed mechanism in Figure 18.1, building on the previous work of Cleaves and Miller (2001), might encourage more research into prebiotic vitamin B_3. In the context of prebiotic synthesis, little attention seems to be given to it. This is despite the fact that it has the potential to connect the competing “RNA first” and “metabolism first” hypotheses in a unifying scenario, much like the central dogma of molecular biology in present life.

20

Computational Methods

20.1 Thermochemical Calculations and Data

The software ChemApp (version 740) provided by GTT Technologies was used to perform the thermochemical equilibrium calculations (Petersen and Hack 2007). As inputs this software requires Gibbs free energies of formation for the molecules involved in the reaction (see also next Section on Gibbs Free Energy of Formation). These were mostly obtained from the database CHNOSZ (version 1.3.6, 2020 March 16), providing a huge library of consistent Gibbs free energies of formation, obtained from a large set of experimental and theoretical studies (Dick 2019).

The source code to set up and run the simulations, excluding the proprietary software ChemApp, is openly available on Zenodo (Paschek 2021) and as a Git repository (`https://github.com/klauspaschek/prebiotic_synthesis_planetesimal`). More details can be found in our previous study (Paschek, Semenov, et al. 2023).

20.2 Gibbs Free Energy of Formation

Each chemical molecule that takes part in a reaction as a reactant or product has a Gibbs free energy of formation ΔG_f that depends on temperature and pressure. The lower the value of ΔG_f the higher the probability that the molecule will form. The molecules should form spontaneously in the case of negative ΔG_f when the required reactants are available.

The ΔG_f as a function of temperature T and pressure p can be calculated by fitting the corresponding thermodynamic data ΔG_f from the CHNOSZ database to the function

$$G_f(T, P) = a + bT + cTln(T) + dT^2 + eT^3 + f/T + gP. \tag{20.1}$$

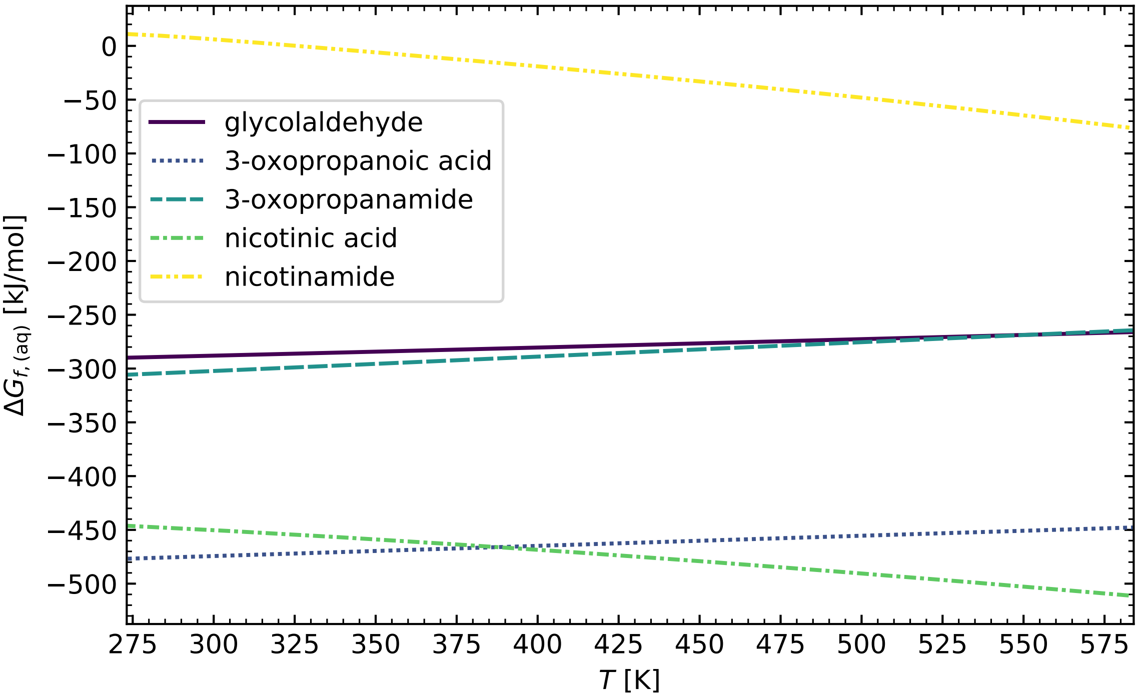

Figure 20.1: Gibbs free energies of formation $\Delta G_{f,\mathrm{(aq)}}$ as a function of temperature T for the molecules not included in the CHNOSZ database. All energies are given in an aqueous solution at a pressure of 100 bar, assuming an ideal infinite dilution.

The Gibbs coefficients a through g are necessary inputs for the equilibrium chemistry software ChemApp, which is used for the chemical reaction simulations.

As shown in previous studies (A. K. Cobb, Pudritz, and Pearce 2015; Pearce and Pudritz 2016; Paschek, Semenov, et al. 2023), in the temperature range of liquid water the Gibbs free energies are independent of pressure. This independence of pressure allows the pressure of the thermodynamic system to be set to a constant 100 bar, making temperature and initial reactant concentrations the only dynamic simulation variables. This value is chosen as it is typically representing the conditions in porous planetesimals of up to hundreds of kilometers in radius due to lithospheric pressure (Pearce and Pudritz 2016; Travis and Schubert 2005).

As the pressure dependence of ΔG_f is negligible, the Gibbs coefficient g can be neglected (Pearce and Pudritz 2016). Nevertheless, the boiling point of water remains the only pressure-dependent parameter of the model that needs to be considered. Our modeled reactions operate in the aqueous phase. It is assumed that when water evaporates, the prebiotic synthesis ceases, and lately formed organic molecules retain their present abundance. Each reaction must have a negative Gibbs free energy of reaction ΔG_r to be thermodynamically favorable, expressed as

$$\Delta G_r = \sum_{\text{products}} \Delta G_f - \sum_{\text{reactants}} \Delta G_f . \tag{20.2}$$

Conversely, reactions with positive ΔG_r require activation energy to progress. This means that this would increase the total Gibbs free energy of the system ΔG.

When the system reaches equilibrium, the chemical reactions cease, as at the current concentrations there is no longer a set of reactions that results in a negative ΔG_r. This highlights the overall concept of thermodynamic chemical reaction simulation, which involves establishing initial concentrations of reactant molecules in the system and then calculating the resulting reactant and product concentrations that minimize ΔG. The total Gibbs free energy of the system ΔG can be written as the combination of the Gibbs free energy of formation ΔG_f of each molecule

$$\Delta G = \sum_{\text{all}} \Delta G_f. \tag{20.3}$$

Catalysts have no role in minimizing Gibbs free energy computations because they do not commit molecules to the reaction. Catalysts only accelerate the reaction time by reducing the activation energy, which is a variable not used in equilibrium calculations.

20.3 Gibbs Free Energies of Formation for Species Missing in CHNOSZ

The CHNOSZ database contains only the Gibbs energy of formation for nicotinamide in its solid form $\Delta G_{f,\text{(s)}}$. To obtain the Gibbs energy in an aqueous solution $\Delta G_{f,\text{(aq)}}$, we used the formula

$$\Delta G_{f,\text{(aq)}}(T) = \Delta G_{f,\text{(s)}}(T) + RT \ln(s_{\text{sat}}(T)), \tag{20.4}$$

where T is the temperature, R is the ideal gas constant, and s_{sat} is the ideal saturated solubility in water in units of $\text{mol}\,\text{L}^{-1}$, assuming infinite dilution and that Henry's law applies (Toure and Dussap 2016). We used measured temperature-dependent solubilities of nicotinamide in water (Cysewski et al. 2021) and fit the data with a polynomial of second degree as a simple approximation of the temperature dependence. This allows us to extrapolate the measured data points for $s_{\text{sat}}(T)$ over the whole considered temperature range. Figure 20.1 shows the resulting temperature dependence of the aqueous Gibbs energies of formation, using Equation (20.4).

Nicotinic acid is missing in CHNOSZ. We used measured literature values for the thermodynamic properties at standard conditions (Knyazev et al. 2015; Di et al. 2017) and imported them into CHNOSZ. This allowed to calculate the Gibbs energies of formation over the whole considered temperature range.

Glycolaldehyde is also missing in the database, but we performed quantum chemistry calculations in a previous study (Paschek, Kohler, et al. 2022) to obtain its Gibbs energies of formation. The same techniques were used to calculate the Gibbs energies of formation for the aldehydes 3-oxopropanoic acid and 3-oxopropanamide for the first time in a private communication with B. K. D. Pearce (Department of Earth and Planetary Science, Johns Hopkins University, July 2023).

Using the software package Gaussian 09 (Frisch et al. 2009), the atomic and molecular energies and entropies were determined to calculate the Gibbs free energy of formation. The Becke-3–Lee–Yang–Parr (B3LYP) hybrid density functional (Stephens et al. 1994; Becke 1993; C. Lee et al. 1988) and the polarizable continuum model (PCM) for aqueous solution effects (Miertuš et al. 1981; Cammi and Tomasi 1995) were used, with geometry optimizations conducted using the 6-31G(d,p) basis set. Single-point energies and frequency were calculated using the 6-311++G(2df,2p) basis set. The Gibbs free energy of formation was determined using Ochterski's three-step method (Ochterski 2000), incorporating enthalpy and entropy calculations at different temperatures. Some values were obtained from experiments (Curtiss et al. 1997) and thermodynamic tables (Wagman et al. 1982), while an adjustment was made to the entropy of carbon (graphite) based on similar calculations for hydrogen and oxygen. A small error was introduced due to the use of gas-state carbon instead of carbon (graphite) for an enthalpy correction. More details can be found in the previous study (Paschek, Kohler, et al. 2022) and the given references. Figure 20.1 shows all the Gibbs energies of formation used in our simulation that are not available in the CHNOSZ database.

Acknowledgements

The authors would like to thank Oliver Trapp for helping to understand the chemical reactions toward vitamin B_3 and deriving parts of the candidate prebiotic pathway. We would also like to thank Ben K. D. Pearce for performing quantum chemistry calculations to obtain Gibbs free energies of formation for some molecules missing in the CHNOSZ database. We thank Christelle Hiemstra for the stylistic review of the manuscript. K.P. acknowledges financial support by the Deutsche Forschungsgemeinschaft (DFG, German Research Foundation) under Germany's Excellence Strategy EXC 2181/1 - 390900948 (the Heidelberg STRUCTURES Excellence Cluster). K.P. is a fellow of the International Max Planck Research School for Astronomy and Cosmic Physics at the University of Heidelberg (IMPRS-HD). D.A.S. and T.K.H. acknowledge financial support by the European Research Council under the Horizon 2020 Framework Program via the ERC Advanced Grant Origins 83 24 28.

Part V

DEEP MANTLE-ATMOSPHERE COUPLING AND CARBONACEOUS BOMBARDMENT: OPTIONS FOR BIOMOLECULE FORMATION ON AN OXIDIZED EARLY EARTH

Klaus Paschek, Thomas K. Henning, Karan Molaverdikhani, Yoshinori Miyazaki,
Ben K. D. Pearce, Ralph E. Pudritz, Dmitry A. Semenov

This following Part is based on the work *"Deep Mantle-Atmosphere Coupling and Carbonaceous Bombardment: Options for Biomolecule Formation on an Oxidized Early Earth"*, accepted for publication in *The Astrophysical Journal* (Paschek, Henning, et al. 2025) as part of the Ph.D. thesis.

The paper has been reformatted to fit the format of this thesis. The work on the paper was divided as follows: I composed the different scenarios considered in the work (geological processes, bombardment from space of different types, and combinations of these), defining the sets of parameters necessary for the simulations. Karan Molaverdikhani ran the simulations using these parameter sets for the different scenarios, using the pre-existing code published by Molaverdikhani, Henning, et al. (2019), Mollière et al. (2019), Pearce, Ayers, et al. (2019), Molaverdikhani, Helling, et al. (2020), Pearce, Ayers, et al. (2020), Pearce, Molaverdikhani, Pudritz, Henning, and Hébrard (2020), and Pearce, Molaverdikhani, Pudritz, Henning, and Cerrillo (2022). I analyzed the simulation results. For the wet-dry cycling pond model I used and adapted the pre-existing code published by Pearce, Pudritz, et al. (2017). Kai Kohler performed the formose reaction in the laboratory of Prof. Dr. Oliver Trapp and provided the yields for ribose synthesis from H_2CO used in the analysis of the simulation results, and was also mentioned in the acknowledgments for that.

I drafted the first version of the whole manuscript, except Yoshinori Miyazaki contributed edits to Section 27. The other co-authors contributed by commenting on at least one version of the draft.

Abstract

Understanding what environmental conditions prevailed on early Earth during the Hadean eon, and how this set the stage for the origins of life, remains a challenge. Geologic processes such as serpentinization and bombardment by chondritic material during the late veneer might have been very active, shaping an atmospheric composition reducing enough to allow efficient photochemical synthesis of HCN, one of the key precursors of prebiotic molecules. HCN can rain out and accumulate in warm little ponds (WLPs), forming prebiotic molecules such as nucleobases and the sugar ribose. These molecules could condense to nucleotides, the building blocks of RNA molecules, one of the ingredients of life. Here, we perform a systematic study of potential sources of reducing gases on Hadean Earth and calculate the concentrations of prebiotic molecules in WLPs based on a comprehensive geophysical and atmospheric model. We find that in a reduced H_2-dominated atmosphere, carbonaceous bombardment can produce enough HCN to reach maximum WLP concentrations of $\sim$1–10 mM for nucleobases and, in the absence of seepage, $\sim$10–100 µM for ribose. If the Hadean atmosphere was initially oxidized and CO_2-rich (90 %), we find serpentinization alone can reduce the atmosphere, resulting in WLP concentrations of an order of magnitude lower than the reducing carbonaceous bombardment case. In both cases, concentrations are sufficient for nucleotide synthesis, as shown in experimental studies. RNA could have appeared on Earth immediately after it became habitable (about 100 Myr after the Moon-forming impact), or it could have (re)appeared later at any time up to the beginning of the Archean.

21

Introduction

At the beginning of Earth's evolution, the surface of our nascent planet was a rather hostile environment, not hospitable to life. Volcanic activity and meteorite bombardment was likely high, and the hydrosphere still had to settle. The formation of the first primordial global ocean allowed liquid water, the basis for all life as we know it (Westall and Brack 2018), to appear on the Earth's surface for the first time. However, this was likely disturbed several times by large impactors, causing the ocean to evaporate and the water to be lifted back into the atmosphere (Chyba, Thomas, et al. 1990; Nisbet and Sleep 2001; Zahnle and Sleep 2006).

The question of what the atmosphere above this ocean might have been like after it had finally settled at the end of the sterilizing giant impacts is an important one. Accretion during planet formation could have produced a primary H_2-rich atmosphere (Oparin 1924; Urey 1951; Urey 1952; Young et al. 2023), which was eroded into space by the solar wind (timescale of around 100 Myr, Owen and Wu 2017) and subsequently replaced by a CO_2-rich atmosphere of several hundred bars, which was outgassed by the magma ocean (Zahnle, Arndt, et al. 2007; Miyazaki and Korenaga 2022; Johansen, Ronnet, Schiller, et al. 2023; Johansen, Camprubi, et al. 2024). Rare earth element signatures in Hadean zircons at ~ 4.35 Gyr indicate the presence of an already oxidized mantle (Trail, E. B. Watson, et al. 2011). The redox state of the mantle was already close to the quartz-fayalite-magnetite mineral buffer, which describes the chemical state of reactions between minerals containing ferrous (Fe^{2+}) and ferric (Fe^{3+}) iron in the mantle. As on modern Earth, this state of the mantle results in the emission of mostly oxidized gases such as CO_2 into the atmosphere during silicate volcanism.

The famous Urey-Miller experiments and many modern versions of them show that in a reducing atmosphere rich in H_2, CH_4 is abundant and leads to the formation of HCN, whereas a more neutral atmosphere dominated by CO_2 is less favorable for the formation of organic molecules, including HCN (Haldane 1929; Oparin 1924; Urey 1952; Miller 1957a; Schlesinger and Miller 1983; Stribling and Miller 1987;

Oró, Miller, et al. 1990; Miyakawa et al. 2002; Cleaves, Chalmers, et al. 2008; Benner, Bell, et al. 2019). When dissolved in aqueous solution, this HCN is able to react further to form many building blocks of life, such as amino acids, nucleobases, formaldehyde, sugars, and even nucleosides, the monomers of RNA (Miller 1953; Miller 1955; Miller 1957b; Miller and Urey 1959; Oró and Kamat 1961; Cleaves, Chalmers, et al. 2008; Johnson et al. 2008; Powner et al. 2009; Bada 2013; Sutherland 2016; S. Becker, Schneider, et al. 2018; Benner, Bell, et al. 2019; Yadav et al. 2020). RNA is of great interest for the origins of life, as its capabilities to store information and simultaneously self-catalyze its polymerization is one of the suggested starting points for chemical evolution and finally life in the so-called RNA world hypothesis (A. Rich 1962; Gilbert 1986; Kruger et al. 1982; Guerrier-Takada, Gardiner, et al. 1983; Guerrier-Takada and Altman 1984; Zaug and Cech 1986; Cech 1986; Johnston et al. 2001; Vaidya et al. 2012; Attwater et al. 2018; Cojocaru and Unrau 2021; Kristoffersen et al. 2022). It could also have been formed while being encapsulated in a primitive cell membrane and interacted with peptides in a more inclusive RNA-peptide world hypothesis (Di Giulio 1997; Müller et al. 2022).

This raises the seeming contradiction of how the ingredients for life could have been formed on Hadean Earth, which likely had an oxidized CO_2-rich atmosphere in the early Hadean, while reducing conditions are required for prebiotic synthesis. To solve this problem, additional sources of reducing gases have been suggested.

In Figure 21.1, we provide an overview over these sources of reducing gases, and subsequent chemical processes operating together to form precursors of prebiotic molecules on the Hadean Earth. This begins with internal geological processes in the deep mantle, including the reaction between minerals derived from mantle magma and surface water (A), creating the emission of reducing and oxidizing gases from undersea volcanoes (B). These processes are joined by meteorites, which degas reducing species upon impact (C). It continues with photochemical reactions driven by UV irradiation in the proto-atmosphere (D). And it ends with the synthesis of biomolecules by wet-dry cycling in the first reservoirs of water on the emerging islands and land masses (E), which are fed by rain-out of the compounds formed in the atmosphere.

This Hadean Earth was likely dominated by a global ocean. Here, the first volcanic islands rise to the surface (Bada and Korenaga 2018; Korenaga 2021; Chowdhury et al. 2023). These are pushed together by plate tectonics to form the first basaltic land masses. These black land masses and island arcs populate the surface, visible on the day side of the Hadean Earth in the upper half of Figure 21.1.

Because of this very active volcanism on this Hadean Earth, one source of reducing gases might haven been extensive serpentinization (Russell et al. 2010; Holm et al. 2015; Preiner et al. 2018; Miyazaki and Korenaga 2022) in the Earth's crust.

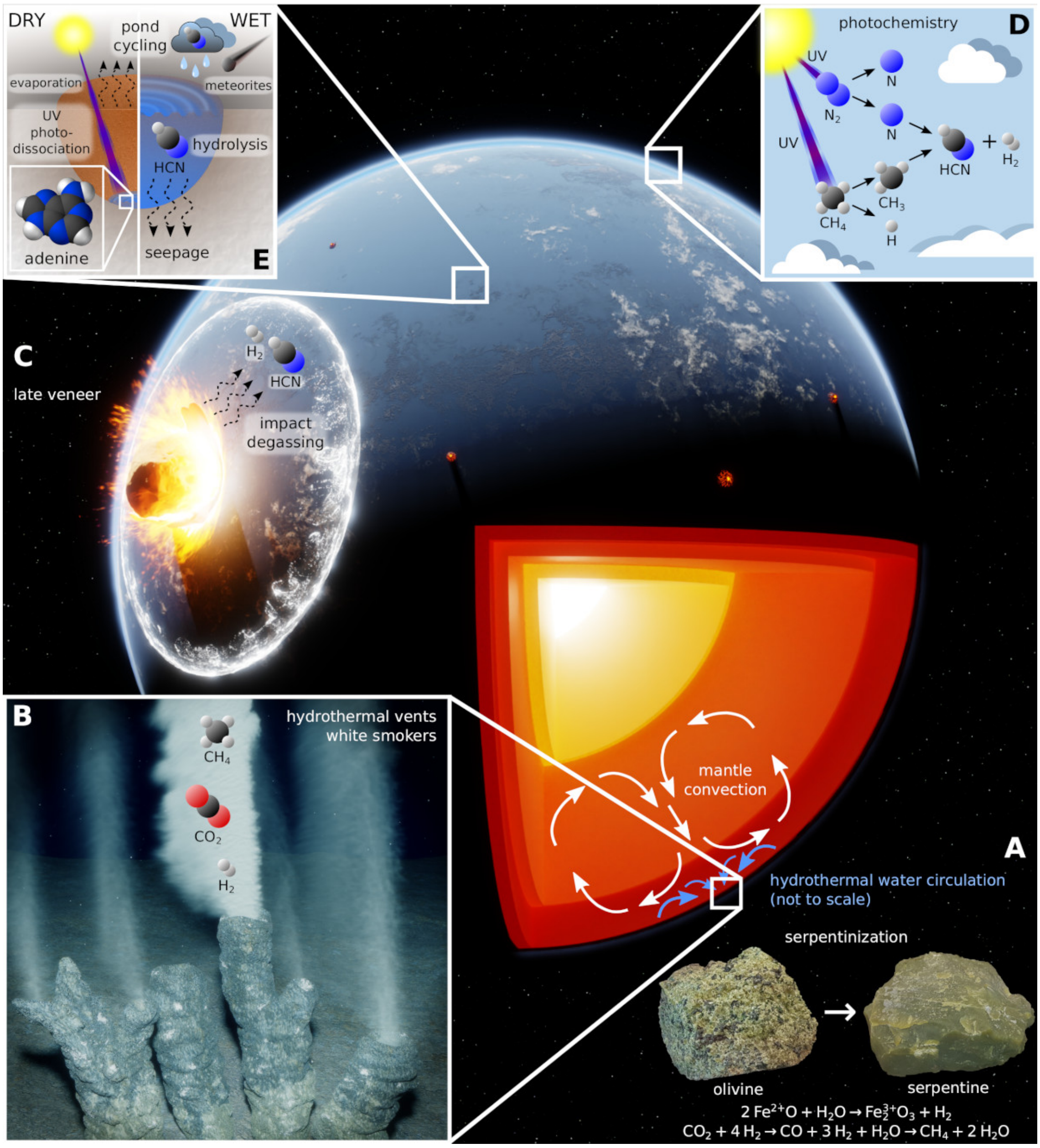

Figure 21.1: The "***HCN machine***": Geological, atmospheric, meteoritic, and chemical processes synthesizing the building blocks of life on the Hadean Earth (artist's impression, own creation, © Klaus Paschek). Panel **A** (lower right): Serpentinization and mantle processes lead to the efficient synthesis of H_2 and CH_4, including reactions with water and CO_2. Panel **B** (lower left): Emission of H_2, CH_4, and CO_2 from hydrothermal vents at volcanically active mid-ocean ridges. Panel **C** (center left): Degassing of H_2 and HCN by giant impacts. Panel **D** (top right): Synthesis of HCN from CH_4 and N_2 by UV photochemistry in the atmosphere. Panel **E** (top left): Atmospheric HCN rains out to the Earth's surface and enters lakes, ponds, and the ocean. In ponds, wet-dry cycling and aqueous chemistry convert HCN into nucleobases, sugars, and ultimately RNA (oligo)nucleotides, key ingredients of life.

After the magma ocean froze out, plate tectonics emerged, but it is still debated how and when it first appeared on Earth, and if it was present in the Hadean (Chowdhury et al. 2023) or not (Tarduno et al. 2023). Before the onset of plate tectonics, the Earth may have been undergoing stagnant lid convection (Debaille et al. 2013; Tosi et al. 2017; Tarduno et al. 2023). In any case, material convecting in the mantle rises and melts, causing magma to rise up through cracks in the crust and participate in further crust formation. This created ridges where the magma erupts at the bottom of the oceans.

In Figure 21.1(A), the geological cross-section of the Earth in the lower right shows that here the magma comes into contact with the ocean water, which enters the crust through fissures in a process called hydrothermal circulation. The Hadean crust was likely very different from today's crust, being thinner than today and undergoing rapid plate tectonic motion (Sleep, Zahnle, and Neuhoff 2001; Zahnle, Arndt, et al. 2007; Sleep, Zahnle, and Lupu 2014; Miyazaki and Korenaga 2019; Miyazaki and Korenaga 2022), influenced by early mantle differentiation. This early mantle was heterogeneous, containing iron-rich blobs that continuously supplied ferrous material to the surface (Miyazaki and Korenaga 2019; Miyazaki and Korenaga 2022). Such ferrous iron forms the iron-rich mineral group olivine, which comes into contact with ocean water through the hydrothermal circulation.

This olivine reacts with the water in the serpentinization reaction, converting the ferrous iron to more oxidized ferric iron in the mineral group serpentine, and reducing the water to H_2 (Klein et al. 2013). One of the most important factors controlling the amount of H_2 released is the hydrothermal circulation depth (HCD). With increasing depth, water penetrates further into the crust, leading to more extensive iron oxidation and consequently greater hydrogen production. This geochemical process is illustrated by the example rocks peridotite (containing olivine minerals) and serpentinite (containing serpentine minerals) and the corresponding generalized chemical reaction equations in the lower right of Figure 21.1(A).

Serpentinization is the most stable and continuous source of reducing gases to be considered here, as mantle convection provides a continuous supply of ferrous iron to the reaction.

H_2 further reacts with CO_2 dissolved in the magma to form CH_4 (Kasting 2005; McCollom and Seewald 2007; Thompson et al. 2022). These gases erupt in white smokers, a type of hydrothermal vent, and rise to the ocean surface and enter the atmosphere, as shown in the zoomed-in inset (B) in the lower left of Figure 21.1. Underwater volcanoes are driven purely by chemical reactions, not by direct eruption of silicate magma, creating a kind of "chemical volcanism".

Figure 21.1(C), in the center left, shows one of the many meteorites that struck the early Earth during the late veneer (Urey 1952). These impacts have been proposed as another source of reducing gases. The late veneer refers to the last layer of material, composed mainly of chondritic meteorites, that was late accreted to the Earth's mantle after core formation (Morbidelli and B. J. Wood 2015; Li 2022). Meteorites carry additional elements, such as metals and siderophiles (iron-loving elements), that could contribute to the release of reducing gases. This might explain why the Earth has an excess of highly siderophile elements (HSEs) in its crust and mantle, revealing the presence of the late veneer.

Enstatite chondrites, a type of iron-rich meteorites, and the siderophile fraction of ordinary and carbonaceous chondrites are expected to produce large amounts of H_2 during impact, as the reduced iron in the meteorite reacts with water, similar to the serpentinization process discussed above (Kasting 1990; Hashimoto et al. 2007; Schaefer and Fegley 2007; Schaefer and Fegley 2010; Schaefer and Fegley 2017; Kuwahara and Sugita 2015; Pearce, Molaverdikhani, Pudritz, Henning, and Cerrillo 2022; Zahnle, Lupu, et al. 2020; Wogan, Catling, et al. 2023).

There is, however, another important mechanism leading to direct HCN production by meteoritic impact. Carbonaceous chondrites could have generated HCN during impact, as the carbon reacts with an ambient N_2 and water atmosphere in a reaction induced by the energy and heat released in the impact shock (Kurosawa et al. 2013). Even without the metal component in some types of carbonaceous chondrites, HCN might be formed due to the vaporization and reaction of carbon alone.

The exact composition of the late veneer material, in particular the ratio between enstatite and carbonaceous impactors, has long been debated. Recent evidence from isotopic signatures of the primitive Earth's mantle and chondritic meteorite populations points to a mixed late veneer, although a pure enstatite or a pure carbonaceous bombardment remain valid possibilities (Fischer-Gödde and Kleine 2017; Varas-Reus et al. 2019; Budde et al. 2019; Hopp et al. 2020; Fischer-Gödde, Elfers, et al. 2020; Bermingham, Tornabene, et al. 2025).

All of these source terms inject the gases H_2, CH_4, HCN, and CO_2 into the atmosphere. There they can react further to form prebiotic molecular precursors, such as HCN and H_2CO.

The zoomed-in inset (D) in the upper right of Figure 21.1 shows that the molecules at the top of the atmosphere are exposed to UV radiation, which allows the molecules, e.g. N_2 and CH_4, to split into radicals that can recombine to form new stable molecules. In this process, the reaction likely passes through H_2CN as an intermediate (Pearce, Ayers, et al. 2019, not shown). In this photochemical reaction network (Pearce, Molaverdikhani, Pudritz, Henning, and Cerrillo 2022), there is a constant competition between reactions that produce oxidized gases such as CO_2, O_2, H_2O, etc. and reduced gases such as H_2, CH_4, HCN, etc. H_2CO can also be formed in weakly reducing atmospheres (J. P. Pinto et al. 1980; Benner, Kim, et al. 2019).

The outcome of the photochemical reaction network is primarily influenced by three key parameters. These parameters include: i) the general atmospheric composition at the start of the simulation, which may be either reducing or oxidizing, ii) the HCD of the primordial ocean penetrating into the Earth's crust, and iii) the composition of the late veneer material, which might consist of either iron-rich enstatite or carbon-rich carbonaceous chondrites, or both. We explore these various possibilities in a parameter study with several model scenarios.

The species that formed were rained out to the surface. This allowed these prebiotic precursors to accumulate on the Earth's surface, e.g., in the first water reservoirs, lakes and ponds on the first continental crust, which could have formed very early in the Earth's history, possibly as early as 4.2 Gyr ago (McCulloch and Bennett 1993; Pearce, Pudritz, et al. 2017; Chowdhury et al. 2023). Charles Darwin suggested so-called warm little ponds (WLPs) as a possible location for the origin of life. The zoomed-in inset (E) in the upper left of Figure 21.1 gives an illustration of the various active processes that drive the chemical dynamics in these WLPs. HCN in aqueous solution allows the synthesis of biomolecules such as amino acids and nucleobases as in the Urey-Miller experiments discussed above (Johnson et al. 2008; Bada 2013). H_2CO can form sugars such as ribose in the formose reaction (Breslow 1959; Butlerow 1861; Cleaves 2015). These WLPs can undergo wet-dry cycling, which allows for the synthesis of nucleotides (Powner et al. 2009; S. Becker, Thoma, et al. 2016; Sutherland 2016; S. Becker, Schneider, et al. 2018; Yadav et al. 2020) and their polymerization into RNA (Benner, Bell, et al. 2019; Da Silva et al. 2015). This involves condensation reactions that split off water, which is thermochemically inhibited in aqueous solution, but the dry phase of the WLP allows this process (Ponnamperuma et al. 1963; Fuller et al. 1972b; Powner et al. 2009; Saladino, Bizzarri, et al. 2017; Nam et al. 2018). Prebiotic molecules can be further concentrated and nucleotides can be polymerized to RNA and DNA oligomers in cracks within rocks under the influence of geothermal heat flows (Dirscherl et al. 2023; Matreux et al. 2024) caused by thermophoresis and convection processes corresponding to wet-dry cycling.

This wet-dry cycling synthesis includes source terms such as HCN and H_2CO rain-out from the atmosphere and exogenous supply by carbonaceous chondrites, which contain a plethora of biomolecules (see Figure 21.1(E), Velden and Schwartz 1977; Stoks and Schwartz 1979; Stoks and Schwartz 1981; Shimoyama et al. 1990; Callahan et al. 2011; Gilmour 2003; Pizzarello, Cooper, et al. 2006; Smith et al. 2014; Furukawa et al. 2019; Oba, Takano, Furukawa, et al. 2022; Paschek, Kohler, et al. 2022; Oba, Koga, et al. 2023; Paschek, Semenov, et al. 2023; Paschek, M.

Lee, et al. 2024c) that they might have released into the WLP (Pearce, Pudritz, et al. 2017). Sinks are destruction of the biomolecules by UV photodissociation, hydrolysis, and seepage through pores at the bottom of the pond (Pearce, Pudritz, et al. 2017; Pearce, Molaverdikhani, Pudritz, Henning, and Cerrillo 2022).

Here we build on the previous models by Pearce, Molaverdikhani, Pudritz, Henning, and Cerrillo (2022) and take a closer look at different sources of reducing gases appropriate in the context of the Hadean Earth. We take an agnostic approach and perform a systematic parameter study including different combinations of the contributing mechanisms outlined above to fully explore what might be feasible for prebiotic synthesis on the Hadean Earth.

The goal of this work is to bridge different scientific fields, ranging from geosciences to chemistry to astrophysics. Our idea and approach is to model several plausible scenarios and compare their results to get a more complete picture of what the Hadean Earth might have been like. Our goal is not to have a specific preference for any of the various hypotheses discussed in the scientific community, but to evaluate several possible scenarios, contributing mechanisms, and their interplay, given the scarce evidence available from the Hadean.

Section 22 provides a short description of the models used in this paper. Details can be found in Sections 29-31. In Section 23, we give a summary of the computational methods and the implementation of the models. The results across the whole parameter space, including photochemistry and resulting atmopheric compositions, rain-out, WLP cycling, and resulting biomolecule concentrations, are presented in Section 24. Discussion and conclusions follow in Sections 25 and 26. In Section 27, we discuss the processes in the Hadean Earth's mantle and crust, including serpentinization, in more detail. Next, in Section 28, we outline the current evidence for the composition of the late veneer, and how an enstatite and/or carbonaceous bombardment might have influenced the Hadean atmosphere. In Section 29, we place the available evidence into the timeline of the Hadean, resulting in the two main environmental scenarios into which we will place our models. Then, in Section 30, we discuss which surface gas fluxes emitted by the mantle and by impact degassing are feasible for the Hadean. These are summarized into two sets of fluxes representing the scenarios modeled in the present study in Section 31. Supplementary results are presented in the Sections 32 and 33.

22

Models

In this Section, we provide an outline of our models. First, we fit the available evidence into the timeline of the Hadean eon to come up with appropriate environmental scenarios in which to place our simulations. Here, we give a brief summary of the available evidence and the assumptions made to arrive at these scenarios, and a more in-depth discussion of this can be found in Section 29.

The formation and evolution of Earth's early atmosphere during the Hadean eon are influenced by mantle composition, tectonic activity, and volcanic outgassing. Initially, the Earth's mantle might have released large amounts of CO_2, resulting in a dense, CO_2-rich atmosphere (Zahnle, Arndt, et al. 2007; Miyazaki and Korenaga 2022; Johansen, Ronnet, Schiller, et al. 2023; Johansen, Camprubi, et al. 2024). Tectonic processes may have rapidly sequestered much of this CO_2 in the mantle, potentially causing a shift to a hydrogen-dominated atmosphere about 4.4 Gyr ago. Whether or not plate tectonics was active as the necessary process in the Hadean is still debated (Chowdhury et al. 2023; Tarduno et al. 2023). The presence of H_2 and other reducing gases likely resulted from primordial gas accretion, serpentinization of mantle materials, and outgassing from hydrothermal vents that influenced early prebiotic chemistry.

In contrast, extrapolation of the Archean rock record toward the end of the Hadean (about 4.0 Gyr ago) suggests a shift toward more oxidizing conditions, as indicated by redox-sensitive elements (Holland 1984; Aulbach and Stagno 2016; Catling and Kasting 2017; Wogan, Krissansen-Totton, et al. 2020) and oxidation states of the mineral zircon (Trail, E. B. Watson, et al. 2011) at 4.35 Gyr. However, zircons crystallize at temperatures above 600 °C (Harrison et al. 2007), reflecting deep mantle conditions, while serpentinization in the near-surface crust operates independently of this redox state. Hydrothermal vent outgassing from serpentinization could thus produce a reducing atmosphere, potentially out of equilibrium with the more oxidized state of the deep mantle.

Our simulations examine two primary scenarios, each capturing conditions at two

Parameter		Mid-Hadean (MH)	End-Hadean (EH)
t	[Gyr]	4.4	4.0
p_{surface}	[bar]	1.5	2
H_2	[%]	90	0
CO_2	[%]	0	90
N_2	[%]	10	10
CH_4	[ppm]	2	10
H_2O	[%] (surface layer)	1	1
T	[°C]	78	51

Table 22.1: Initial atmosphere compositions and parameters of the two considered epochs (see also Pearce, Molaverdikhani, Pudritz, Henning, and Cerrillo 2022). Details can be found in Section 29.

critical Hadean epochs: the mid-Hadean (MH) at 4.4 Gyr ago and the end-Hadean (EH) at 4.0 Gyr ago. The MH scenario considers an initially reducing atmosphere (90 % H_2), while the EH scenario begins with an oxidizing atmosphere (90 % CO_2), reflecting the potential changes in redox state and atmospheric composition. These models test whether geological processes, such as serpentinization and impact degassing, could convert the atmosphere to a reduced state favorable for the synthesis of prebiotic molecules. The detailed parameters for these epochs are provided in Table 22.1. Here, t is the time of the epoch in units of Gyr from today, p_{surface} is the surface pressure in bar, atmospheric gases are given in their initial molar mixing ratios (the molar mixing ratio is defined as the ratio between the amount of the respective atmospheric gas and the total amount of all gases, all in units of moles) at the beginning of the simulations in either % or parts per million (ppm), and T is the surface temperature in °C. More discussions about these two epochs and how these parameter sets were calculated are presented in Section 29.

As a next step, we explore a range of cases to simulate the atmospheric evolution in the MH and EH, distinguishing between the geological and impact-driven sources that contributed to the emission of reducing gases in the Hadean.

We consider geological sources alone and refer to them as the "geology" case G, where H_2, CO_2, and CH_4 are released by volcanic activity and serpentinization driven by hydrothermal circulation. Recent models by Miyazaki and Korenaga (2022) propose a heterogeneous Hadean mantle resulting in iron-rich upwelling and a thin crust. This fosters rapid plate tectonics, very active hydrothermal circulation from the surface ocean into the crust, extensive serpentinization (Russell et al. 2010; Klein et al. 2013; Preiner et al. 2018), and Fischer-Tropsch reactions (Kasting 2005; McCollom and Seewald 2007; Holm et al. 2015; Thompson et al. 2022) generating volcanic H_2 and CH_4 emissions. Detailed explanations of serpentinization and related mechanisms in the Hadean Earth's mantle and crust are provided in Section 27.

To assess how the HCD affects the release of these gases and influences atmospheric chemistry, we vary the HCD between 0.5 km, 1.0 km, and 2.0 km, with cases named accordingly as G0.5, G1, and G2. The corresponding calculations, extending the models by Miyazaki and Korenaga (2022) and determining the emission of these gases, and details of this modification of the HCD are presented in Section 30.1.

In scenarios focused on exogenous impacts, we consider both pure enstatite (referred to as case E) and pure carbonaceous (referred to as case C) bombardments. Details on the late veneer and possible bombardment scenarios in the Hadean can be found in Section 28. In the main results in Section 24, we consider intermediate bombardment rates based on the lunar cratering record (Pearce, Pudritz, et al. 2017; Chyba, Thomas, et al. 1990), and in the supplementary results in Section 33, we explore what would happen if there was a maxed-out and short-lived bombardment, and how this would affect the Hadean atmosphere and prebiotic synthesis in WLPs in both the MH and EH epochs.

An enstatite bombardment provides H_2 by impact degassing, as the iron-rich impact ejecta react with the impact-vaporized ocean (Sekine et al. 2003; Genda, Iizuka, et al. 2017; Genda, Brasser, et al. 2017; Benner, Bell, et al. 2019; Zahnle, Lupu, et al. 2020; Citron and Stewart 2022; Itcovitz et al. 2022; Wogan, Catling, et al. 2023), which might counteract the oxidizing effects of volcanic CO_2 outgassing. Meanwhile, a carbonaceous bombardment additionally generates HCN emissions during impacts, as the impact shock allows the carbon-rich impact material to react with the surrounding N_2-H_2O atmosphere (Kurosawa et al. 2013). Section 30.2 contains detailed information on the considered bombardment rates in the Hadean and gas emission processes during impact events.

We also examine combinations of geological and impact sources by coupling the geological fluxes (using an HCD of 2 km as a standard depth) with enstatite only, carbonaceous only, or mixed (50 % enstatite, 50 % carbonaceous) bombardments, referred to as cases G2E, G2C, and G2EC, respectively. This combined approach allows us to explore the interplay of both endogenous and exogenous contributions. Details of all considered cases are available in Section 31, and the corresponding surface gas fluxes resulting from the respective cases in both MH and EH epochs are given in Tables 31.1 and 31.2.

23

Computational Methods: Atmosphere Model and Warm Little Pond Cycling

To study the effect of the source fluxes of gases in the Hadean atmosphere, we use the 1D disequilibrium chemical kinetics model previously developed by Pearce, Molaverdikhani, Pudritz, Henning, and Cerrillo (2022). This model combines the atmospheric chemistry code ChemKM (Molaverdikhani, Henning, et al. 2019; Molaverdikhani, Helling, et al. 2020) with the chemical network CRAHCN-O (Pearce, Ayers, et al. 2019; Pearce, Ayers, et al. 2020; Pearce, Molaverdikhani, Pudritz, Henning, and Hébrard 2020), which comprises 259 one-, two-, and three-body reactions. It also includes the production of molecules by lightning in the lowest atmospheric layer of the model and the escape of hydrogen to space (Zahnle, Gacesa, et al. 2019). The *P*-*T* profiles of the atmosphere were calculated using the radiative transfer code petitRADTRANS (Mollière et al. 2019). It is important to note that the current model does not include the day/night cycle and its influence on atmospheric chemistry, as it is expected that some of the HCN would be removed from the atmosphere by rain-out overnight. For a comprehensive breakdown of the atmospheric model used, see Section A in Pearce, Molaverdikhani, Pudritz, Henning, and Cerrillo (2022).

The atmosphere model calculates rain-out rates for the key prebiotic precursors HCN and H_2CO, removing these products of the photochemical network from the atmosphere. This allows these prebiotic precursors to accumulate on the Earth's surface in the first reservoirs of water on land, e.g., WLPs. Through seasonal wet-dry cycling, the prebiotic precursors HCN and H_2CO can form prebiotic molecules such as RNA building blocks and their precursors such as nucleobases, the sugar ribose, and 2-aminooxazole (Butlerow 1861; Breslow 1959; Oró and Kimball 1961; Larowe and Regnier 2008; Powner et al. 2009; Ferus, Pietrucci, Saitta, Ivanek, et al. 2019; Yi et al. 2020).

To explore this further, we follow the study by Pearce, Molaverdikhani, Pudritz, Henning, and Cerrillo (2022) and couple the atmospheric rain-out rates with the WLP cycling model developed by Pearce, Pudritz, et al. (2017). This WLP model combines experimentally determined yields of prebiotic molecules from HCN and H_2CO with multiple sinks due to photodestruction by UV light, seepage through pores at the base of the WLPs, and hydrolysis. H_2CO can enter the ponds either directly by rain-out from the atmosphere or by aqueous synthesis from deposited HCN. In the present study, we have added experimental yields for ribose from H_2CO. Using the hydroxide $Ca(OH)_2$ as a catalyst in the formose reaction, the way to make sugars from aqueous mixtures of H_2CO and trace-amounts of glycolaldehyde (Butlerow 1861; Breslow 1959), the yield of ribose from H_2CO reached up to 1.22×10^{-3} (K. Kohler, O. Trapp private communication; Teichert et al. 2019; Paschek, Kohler, et al. 2022). This allows estimates of the possible concentrations of these prebiotic molecules in WLPs on the Hadean Earth.

24

Results

24.1 Atmosphere Compositions

24.1.1 Serpentinization and Volcanism

Figure 24.1 shows the effect of geological gas fluxes on the evolving atmosphere of the Hadean Earth. The surface fluxes for H_2, CO_2, and CH_4 used in our atmosphere model come from the global upwelling of mantle material as simulated in newly calculated models that build on and extend the mantle model established by Miyazaki and Korenaga (2022). See Section 30.1 and Figure 30.1 for details. These mantle upwelling motions bring ferrous iron-rich magma and dissolved CO_2 close to the surface. In contact with the surface hydrosphere, a combination of serpentinization, reverse gas-shift, and Fischer-Tropsch reactions (see Equations 27.2 and 27.6) results in the surface fluxes given in Tables 31.1 and 31.2. Cases MH/EH_G0.5, MH/EH_G1, and MH/EH_G2 represent these fluxes for HCDs of 0.5 km, 1.0 km, and 2.0 km, respectively. See Section 31 for details.

Table 24.1 lists the maximum reached atmospheric molar mixing rations for key prebiotic precursors of interest achieved across all modeled scenarios in the present work. To determine these maximum values, only the time evolution of these molar mixing ratios after 1000 yr is considered, due to the fact that many chemical species in the atmosphere initially show large fluctuations over many orders of magnitude, and by 1000 yr at the latest begin to stabilize and reach their first plateau, resembling something close to steady state behavior (cf. Figure 24.1 and following). We focus on these stabilized abundances because long-term atmospheric concentrations are most relevant for further implications of prebiotic synthesis in WLPs on geological time scales. We consider this a reasonable measure to ensure that Table 24.1 reflects characteristic values representative of geologically relevant time spans in the Hadean of millions of years and longer.

Maximum H_2 levels are a good proxy for how much the atmosphere is reduced,

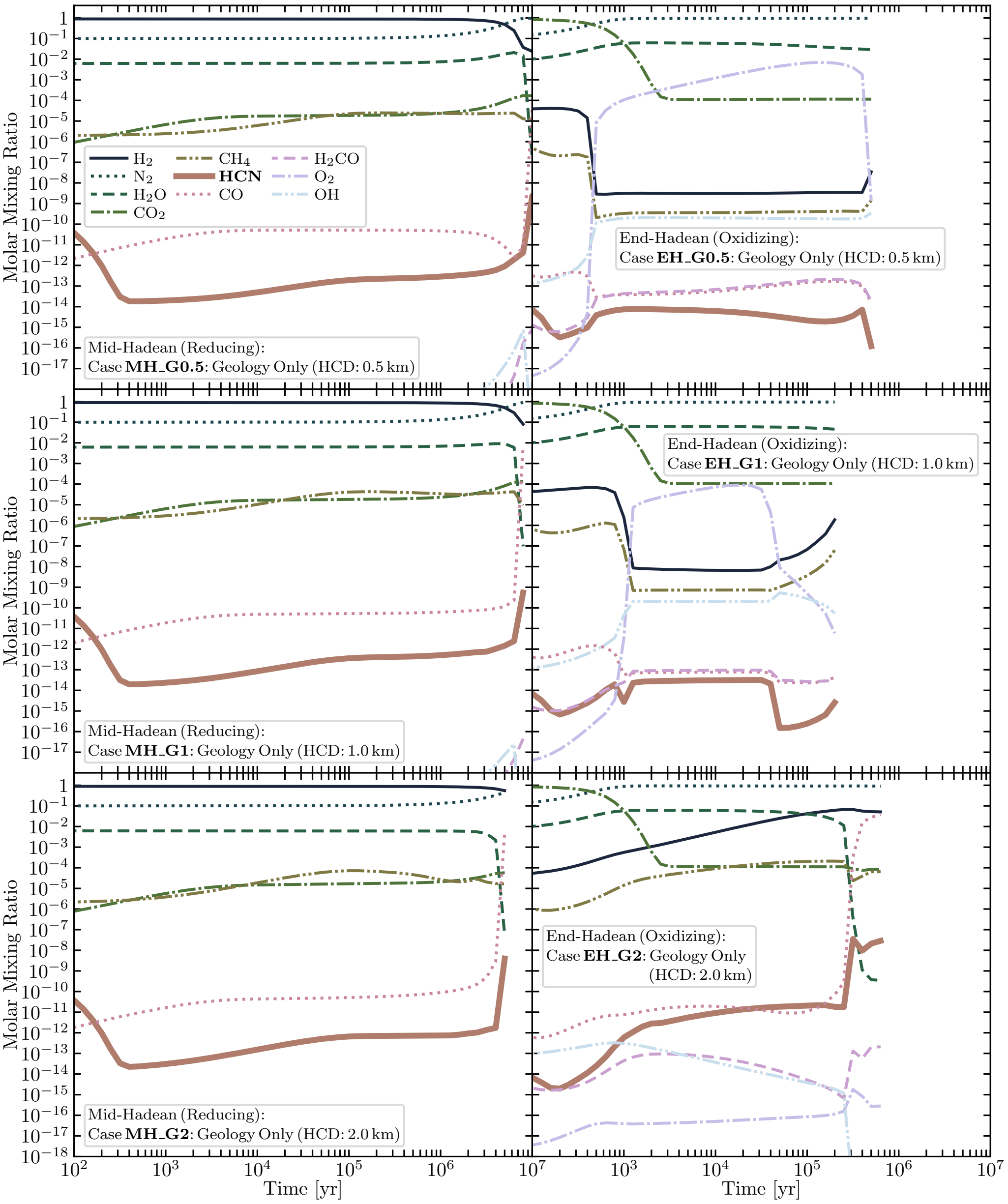

Figure 24.1: Effect of varying the hydrothermal circulation depth (HCD) during serpentinization on the atmospheric evolution. Shown is the simulated atmospheric composition of key species in the layer closest to the surface as a function of time. Only geological surface fluxes from extended models by Miyazaki and Korenaga (2022) are considered as sources for H_2, CO_2, and CH_4 (see cases MH/EH_G0.5, MH/EH_G1, and MH/EH_G2 in Tables 31.1 and 31.2). The two epochs of the mid-Hadean (MH) at 4.4 Gyr with reducing initial conditions and the end-Hadean (EH) at 4.0 Gyr with oxidizing initial conditions are compared (left vs. right column; Panels **MH_G0.5**, **MH_G1**, **MH_G2** vs. **EH_G0.5**, **EH_G1**, **EH_G2**). For each epoch, different HCDs of the primordial ocean penetrating the crustal rock are considered (top row (**MH_G0.5**, **EH_G0.5**): 0.5 km, middle row (**MH_G1**, **EH_G1**): 1.0 km, bottom row (**MH_G2**, **EH_G2**): 2.0 km). The initial conditions for the reducing and oxidizing models are summarized in Table 22.1, closely following the established atmosphere models developed by Pearce, Molaverdikhani, Pudritz, Henning, and Cerrillo (2022).

	Max. Molar Mixing Ratio							
	H_2		CH_4		HCN		H_2CO	
Case	MH (red.)	EH (ox.)	MH (red.)	EH (ox.)	MH (red.)	EH (ox.)	MH (red.)	EH (ox.)
G0.5	8.94×10^{-1}	3.44×10^{-8}	2.49×10^{-5}	1.41×10^{-9}	2.38×10^{-9}	7.19×10^{-15}	1.13×10^{-14}	2.09×10^{-13}
G1	8.94×10^{-1}	1.86×10^{-6}	4.29×10^{-5}	6.25×10^{-8}	5.51×10^{-10}	3.19×10^{-14}	4.50×10^{-17}	9.61×10^{-14}
G2	8.94×10^{-1}	6.69×10^{-2}	7.22×10^{-5}	2.11×10^{-4}	3.96×10^{-9}	3.53×10^{-8}	3.10×10^{-19}	2.08×10^{-13}
E	8.94×10^{-1}	3.06×10^{-8}	1.76×10^{-6}	5.36×10^{-24}	1.45×10^{-14}	6.97×10^{-19}	2.55×10^{-23}	8.89×10^{-26}
C	8.94×10^{-1}	1.96×10^{-7}	1.76×10^{-6}	3.04×10^{-24}	1.23×10^{-7}	7.96×10^{-19}	2.55×10^{-23}	5.48×10^{-26}
G2E	8.94×10^{-1}	8.03×10^{-2}	7.23×10^{-5}	2.16×10^{-4}	1.06×10^{-8}	3.23×10^{-8}	3.46×10^{-17}	1.66×10^{-13}
G2C	8.94×10^{-1}	1.67×10^{-2}	7.22×10^{-5}	1.57×10^{-4}	7.54×10^{-8}	2.01×10^{-10}	3.10×10^{-19}	5.89×10^{-12}
G2EC	8.94×10^{-1}	5.78×10^{-2}	7.43×10^{-5}	2.13×10^{-4}	4.35×10^{-8}	7.07×10^{-9}	2.49×10^{-16}	4.25×10^{-13}

Table 24.1: Maximum resulting atmosphere concentrations of prebiotic precursors.

especially for the initially oxidized models at 4.0 Gyr. CH_4 is a major intermediate in the synthesis of HCN in the computed photochemical reactions (Pearce, Molaverdikhani, Pudritz, Henning, and Cerrillo 2022). HCN is our key prebiotic precursor molecule. Moreover, H_2CO is of interest as the key reactant in the formation of sugars.

Case MH_G0.5 with an HCD of 0.5 km in an initially reducing atmosphere is presented in Figure 24.1. The temporal evolution of key atmospheric species shows that the molar mixing ratios for the main prebiotic precursor HCN, as well as CH_4 as one of its main reactants, stabilize at ~ 500 yr at levels of 1.8×10^{-14} and 2.2×10^{-6}, respectively. Over the next million years, they rise steadily and moderately to levels of 4.7×10^{-13} and 2.3×10^{-5} at 3 million years, respectively. Finally, over the next 7 million years, the abundance of HCN rises steeply to a maximum of 2.4×10^{-9}. In addition, oxidizing species such as OH, O_2, and the prebiotic precursor H_2CO begin to be produced, reaching a maximum of 1.1×10^{-14} of H_2CO.

In the process, water and H_2 are consumed in the photochemical reactions in the atmosphere and decrease by several orders of magnitude. CO levels rise sharply, while CH_4 and H_2O levels decrease. This can be explained by the oxidation of methane by OH radicals formed by photolysis of water to form H_2CO, which can be split by UV photolysis to form CO, O_2, and other oxidized radicals. In addition, the decrease in CH_4 can be further explained by the steep increase in HCN, which is formed by reaction with atomic nitrogen from photolysis and likely passes through H_2CN as an intermediate (Pearce, Ayers, et al. 2019), as also visualized in simplified form in Figure 21.1(D).

Similar trends can be identified in cases MH_G1 and MH_G2 in Figure 24.1 with increased HCDs. The increased surface fluxes of H_2 and CH_4 due to more productive serpentinization leave most of the reducing atmospheric species unchanged at similar levels as in the case of MH_G0.5, but the synthesis of oxidizing species including H_2CO is strongly suppressed. In summary, the elevated surface fluxes of reducing gases do not significantly increase the atmospheric levels of reducing constituents, but substantially extend the time over which the atmosphere remains reducing from millions to at least 10 million years.

Simulations of an initially oxidizing atmosphere at 4.0 Gyr are presented in Figure 24.1. In scenario EH_G0.5 with an HCD of 0.5 km, it can be seen that a moderately reduced state of the atmosphere cannot be sustained for the first hundred years. After about 300 yr, the levels of reducing gases, e.g., H_2 and CH_4, drop due to an abrupt rise of O_2 and OH in the atmosphere. This prevents effective formation of HCN, leaving it at levels of 7.2×10^{-15} and below, over 5 orders of magnitude less than the initially reducing model (see Figure 24.1(MH_G0.5)). This is not surprising, as oxidizing conditions are not a suitable environment for the effective synthesis of HCN and other key reduced prebiotic molecules. Obviously, the supply of the necessary reducing reactants H_2 and CH_4 by serpentinization is insufficient at an HCD of 0.5 km.

Increasing this HCD to 1.0 km, as shown in Figure 24.1(EH_G1), allows to delay the growth of O_2 in the atmosphere for several hundred years. The HCN level reaches a maximum of 3.2×10^{-14}, which is roughly 4 times higher than in case EH_G0.5. After the steep rise of O_2 at 1000 yr, the period during which the atmosphere remains fully oxidized is shortened compared to case EH_G0.5, and is partially reverted after about 40 000 yr. This allows the levels of H_2 and CH_4 to partially recover. Nevertheless, HCN levels are not able to grow significantly and remain very low compared to the initially reducing models MH_G0.5/1/2 at 4.4 Gyr.

This situation changes drastically when the HCD is increased to 2.0 km, as shown in Figure 24.1(EH_G2). Because of increased serpentinization, the levels of H_2 and CH_4 grow over several hundred thousand years, suppressing and evading major oxidation of the atmosphere. This allows for peak HCN abundances of 3.5×10^{-8}, which is an order of magnitude higher than in the initially reducing scenario in Figure 24.1(MH_G2). The initial buildup of HCN between 200–2000 yr coincides with a decline in CO_2, which is reduced in large amounts mainly by CH_4 (and also by H_2) from serpentinization and acts as a carbon source for HCN. *This makes an initially oxidized atmosphere (i.e., high CO_2) the most suitable environment for HCN synthesis in the presence of highly active serpentinization, a rather surprising finding.*

At the same time, the levels of O_2 and OH in the atmosphere are significantly suppressed in case EH_G2. H_2CO levels are quite stable over all cases EH_G0.5/1/2, with maximum levels around 10^{-14}. On the other hand, in the initially reducing MH models (Figures 24.1(MH_G0.5/1/2)), the H_2CO levels drop with increasing HCD due to suppressed availability of oxygen sources. An initially oxidized state of the atmosphere thus favors atmospheric H_2CO levels as another promising prebiotic precursor.

The final sharp increase of HCN in case EH_G2 at about 300 000 yr coincides with a steep increase of CO and a decrease of CH_4 and H_2O, which again can be explained by the formation process of H_2CO and the in parallel occurring reactions shown in Figure 21.1(D), as already mentioned above when explaining the steep increases at the very end in cases MH_G0.5/1/2. This means that this behavior in the initially oxidizing case EH_G2 is equivalent to the behavior in the initially reducing cases, allowing a similarly extensive HCN synthesis, and pushing the HCN levels even above the initially reducing scenario. *This underscores our striking finding that extensive serpentinization leads to the most HCN in an initially oxidized atmosphere, not a reduced one.*

24.1.2 Late Veneer in the Mid-Hadean

Figure 24.2 shows and compares the results for cases MH_G2/E/C/G2E/G2C/G2EC in Table 31.1 in the initially reducing scenario in the MH at 4.4 Gyr. Cases E and C correspond to scenarios including a bombardment of enstatite or carbonaceous composition, respectively. The geological contributions of H_2 and CH_4 are deactivated to examine the reducing potential of the late veneer alone, but the CO_2 degassed from the mantle remains in the model. The purpose is to investigate whether the bombardment with meteorites of enstatite composition is capable of reducing the atmosphere while counteracting the oxidizing gases emitted by volcanism. The same holds for case C, where a purely carbonaceous bombardment and HCN synthesis competes with the geological CO_2 emission from volcanoes. See Section 31 for details. Finally, we examined the combination of these source terms by combining the geology with an HCD of 2 km with the enstatite-only bombardment in case G2E, with the carbonaceous-only bombardment in case G2C, and perhaps the most agnostic assumption of a mixed bombardment of half and half composition in case G2EC. For comparison, case MH_G2 (geology only) is again shown in Figure 24.2(MH_G2).

In case MH_E, a late veneer of pure enstatite composition is the only source of reducing gases, in this case only H_2. Its reduction capacity competes with the geological source flux of CO_2 emitted from the Earth's mantle. For about 10 000 yr, the enstatite bombardment is able to keep the CH_4 and HCN levels stable at 1.8×10^{-6} and 1.5×10^{-14}, respectively. For CH_4 this is close to its initial abundance at the beginning of the simulation (see Table 22.1). After that, the levels of all reducing gases begin to drop steeply. This suggests that enstatite bombardment, as we have included it here in the model with a continuous intermediate impact rate (see Section 30.2), is not able to drive significant reducing chemistry in the

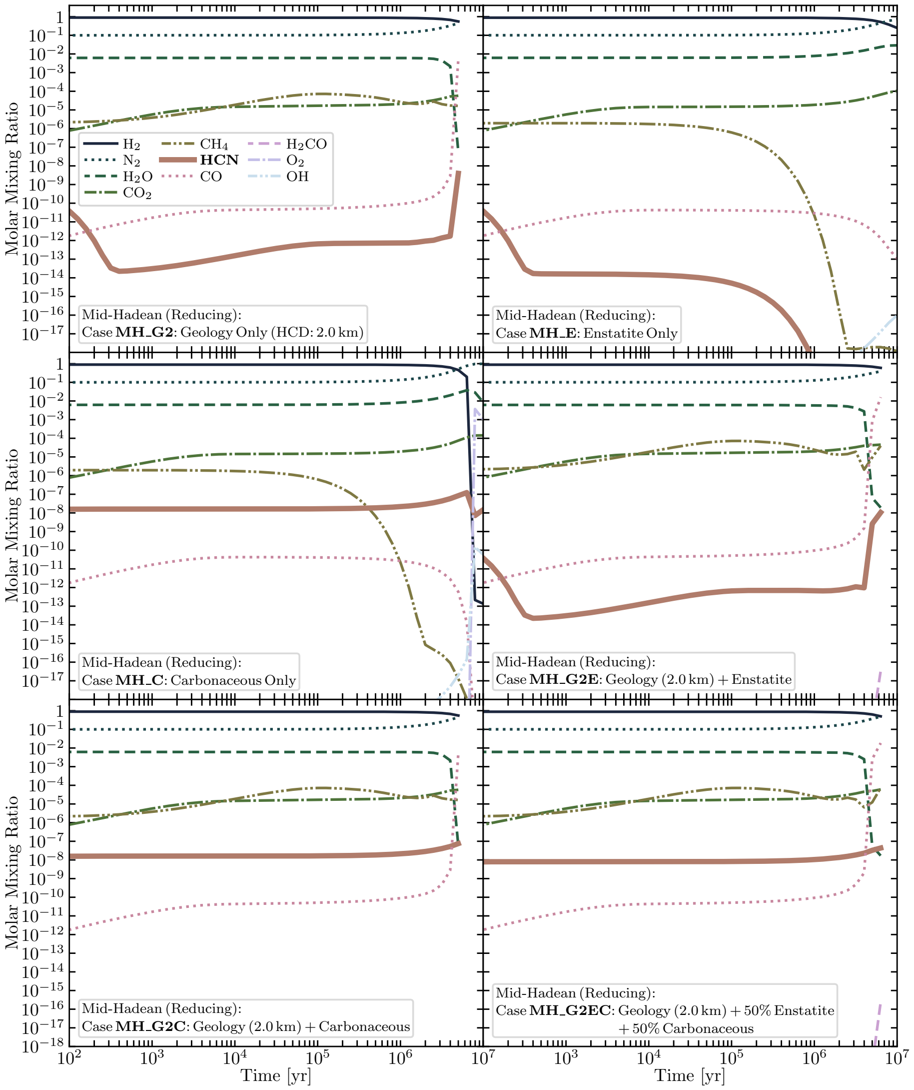

Figure 24.2: Testing whether exogenous chondritic bombardment is capable of keeping the atmosphere reduced while counteracting the oxidizing gases emitted by volcanism, as well as exploring its interplay with serpentinization. Shown is the simulated atmospheric composition of key species in the layer closest to the surface as a function of time starting at 4.4 Gyr. The atmosphere is initially set to a reducing state (H_2: 90 %, N_2: 10 %, CH_4: 1 ppm) and a temperature of 78 °C (Table 22.1), closely following the reducing case considered by Pearce, Molaverdikhani, Pudritz, Henning, and Cerrillo (2022). Panel/case **MH_G2** corresponds to a model driven by serpentinization alone (geology only) and is identical to Figure 24.1(MH_G2). It is shown here again for reference to facilitate comparison with the other cases. Cases E and C correspond to scenarios without any contribution from serpentinization, but with the reduction capacity of the late veneer alone competing with the CO_2 flux emitted from the Earth's mantle. Panel **MH_E** corresponds to a scenario with a bombardment of pure enstatite composition, and panel **MH_C** instead corresponds to a pure carbonaceous composition. Panels **MH_G2E**, **MH_G2C**, and **MH_G2EC** present the results corresponding to scenarios combining geological and late veneer source flux contributions, with case MH_G2E combining the geology with an enstatite bombardment (cases MH_G2 and MH_E), case MH_G2C combines the geology instead with a carbonaceous bombardment (MH_G2 and MH_C), and case MH_G2EC combines all three with a half-half split bombardment composition (MH_G2, 50 % of MH_E, and 50 % of MH_C).

atmosphere. It is able to delay the oxidation of the atmosphere from the mantle CO_2 for about 10 000 yr, but it cannot stop the inevitable decline of reducing gases and thus has no potential to enable effective prebiotic synthesis.

It is important to note that an increased supply of H_2 alone is not sufficient to fuel an effective HCN synthesis in the atmosphere. Comparing the H_2 surface fluxes for serpentinization and enstatite bombardment in Table 31.1, the H_2 flux for enstatite bombardment in case MH_E is actually higher than that generated by serpentinization in case MH_G2. However, the resulting HCN levels in the atmosphere are higher for serpentinization despite the lower H_2 flux compared to enstatite bombardment. Instead, it is the additional CH_4 flux resulting from serpentinization and subsequent reactions that makes the big difference here, raising HCN levels significantly, while the enstatite bombardment is not a source of CH_4. The maximum HCN levels reached in case MH_G2 are more than five orders of magnitude higher than in case MH_E (see Table 24.1).

This does not mean that an enstatite bombardment with more singular cataclysmic events is not capable of providing significant amounts of prebiotic precursors in the atmosphere. For example, the models by Wogan, Catling, et al. (2023) and Zahnle, Lupu, et al. (2020) assume that a major fraction or even all of the HSE excess in the Earth's crust and mantle was delivered to Earth by one enstatite impact. They have shown that this allows for significant CH_4 and HCN synthesis in the post-impact atmosphere. We explore what would happen if our models experienced the same maxed-out bombardment and its effect on atmospheric photochemistry and prebiotic synthesis in WLPs in the supplementary results in Section 33.

However, in what is one of the most important findings of this paper, our results indicate that enstatite bombardment is clearly outcompeted by serpentinization and is not able to drive any reducing chemistry, but only delays the decay of reducing gases.

In case MH_C, a pure carbonaceous bombardment, this becomes even clearer. Figure 24.2(MH_C) shows that the absence of any H_2 flux leads to a drop in atmospheric CH_4 only slightly earlier than for the enstatite bombardment. This means that the H_2 flux from the enstatite bombardment is nearly negligible in the formation of CH_4 in this context.

The direct synthesis of HCN during the impact of carbonaceous meteorites (see Figure 24.2(MH_C)) is able to increase the HCN levels in the atmosphere to a maximum of 1.2×10^{-7}, which is almost 2 orders of magnitude more than serpentinization alone (case MH_G2) and nearly seven orders of magnitude more than enstatite bombardment (case MH_E). Furthermore, the HCN abundance is stable over the entire time evolution at a molar mixing ratio in the atmosphere above 10^{-8}.

As another major result of this study, this makes a carbonaceous bombardment the most promising candidate for contributing the most HCN to the Hadean Earth's atmosphere.

Figure 24.2(MH_G2E) explores the possibility of a combination of very active serpentinization (case MH_G2) and pure enstatite bombardment (case MH_E). When compared to Figure 24.2(MH_G2), the evolution of reducing gases matches very closely. This confirms the findings above that serpentinization has a stronger potential to feed the production of reducing gases in the atmosphere than enstatite bombardment. Nevertheless, the enstatite bombardment pushes up the maximum HCN molar mixing ratio by a factor of ~ 2.7 compared to serpentinization alone (compare cases MH_G2 and MH_G2E in Table 24.1).

The combination of serpentinization and carbonaceous bombardment (see Figure 24.2(MH_G2C)) shows that the CH_4 level in the atmosphere is dominated by serpentinization. In contrast, HCN closely follows the same behavior as in case MH_C with carbonaceous bombardment alone. In case MH_G2C, the maximum CH_4 level matches case MH_G2, and the maximum HCN level is close to case MH_C (see Table 24.1).

Finally, Figure 24.2(MH_G2EC) shows the most agnostic case with all source terms active. Serpentinization is set to the highest efficiency with an HCD of 2.0 km, and the late veneer consists of equal amounts of enstatite and carbonaceous impactors. Looking at the trends in all of the previous cases, one would expect the CH_4 levels to be dominated by serpentinization and the HCN levels by carbonaceous bombardment, and this is indeed the behavior seen in Figure 24.2(MH_G2EC). It appears that the direct supply of CH_4 and HCN dominates over their synthesis by photochemistry. Nevertheless, the entire network of photochemical reactions helps to keep the abundances of oxidizing gases low.

24.1.3 Late Veneer in the End-Hadean

Figure 24.3 gives an overview of the different cases and the influence of impacts on the initial oxidizing atmosphere in the EH at 4.4 Gyr. Figure 24.3(EH_G2) is identical to Figure 24.1(EH_G2) and is shown again for easy comparison with the other cases EH_E/C/G2E/G2C/G2EC.

The pure enstatite bombardment with serpentinization turned off in Figure 24.3(EH_E) shows that the H_2 flux from impact degassing is not sufficient to stabilize the H_2 level in the atmosphere. After about 300 yr, its abundance begins to drop sharply and remains at a level of 3.1×10^{-8} for the next million years. The level of CH_4 shows the same decline from about 100 yr and HCN never reaches a significant amount. This coincides with a sharp increase in O_2 and OH, indicating that the enstatite bombardment is not able to reduce the atmosphere, while its own

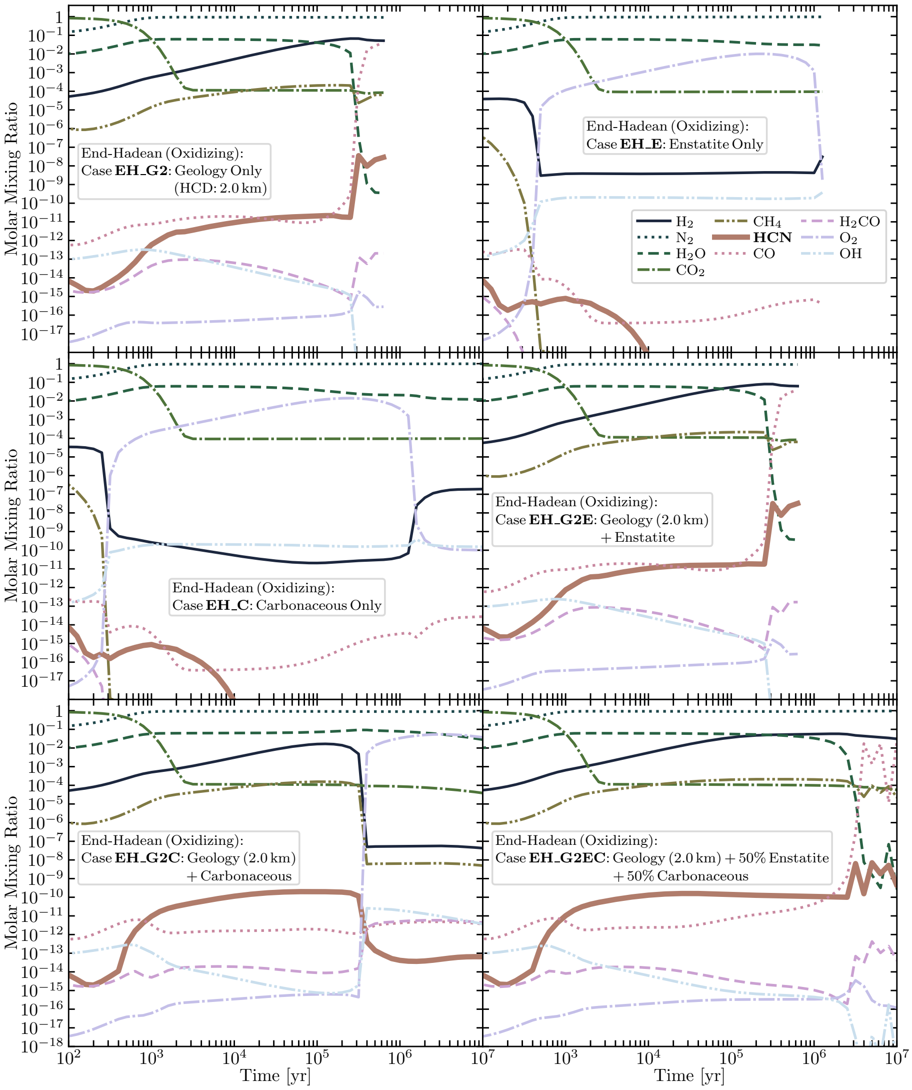

Figure 24.3: Testing whether exogenous chondritic bombardment is capable of reducing an initially oxidized atmopshere while counteracting the oxidizing gases emitted by volcanism, as well as exploring its interplay with serpentinization. Shown is the simulated atmospheric composition of key species in the layer closest to the surface as a function of time starting at 4.0 Gyr. The atmosphere is initially set to an oxidizing state (CO_2: 90 %, N_2: 10 %, CH_4: 10 ppm) and a temperature of 51 °C (Table 22.1), closely following the oxidizing case considered by Pearce, Molaverdikhani, Pudritz, Henning, and Cerrillo (2022). Panel/case **EH_G2** corresponds to a model driven by serpentinization alone (geology only) and is identical to Figure 24.1(EH_G2). It is shown here again for reference to facilitate comparison with the other cases. Cases E and C correspond to scenarios without any contribution from serpentinization, but with the reduction capacity of the late veneer alone competing with the CO_2 flux emitted from the Earth's mantle. Panel **EH_E** corresponds to a scenario with a bombardment of pure enstatite composition, and panel **EH_C** instead corresponds to a pure carbonaceous composition. Panels **EH_G2E**, **EH_G2C**, and **EH_G2EC** present the results corresponding to scenarios combining geological and late veneer source flux contributions, with case EH_G2E combining the geology with an enstatite bombardment (cases EH_G2 and EH_E), case EH_G2C combines the geology instead with a carbonaceous bombardment (EH_G2 and EH_C), and case EH_G2EC combines all three with a half-half split bombardment composition (EH_G2, 50 % of EH_E, and 50 % of EH_C).

H_2 flux is even suppressed after the onset of the formation of oxidized species in the atmosphere.

The fact that HCN is not stable and cannot be effectively produced in an oxidized atmosphere becomes clear in Figure 24.3(EH_C). The direct synthesis of HCN by carbonaceous impacts is switched on after 1000 yr, because at this time N_2 starts to exceed the atmospheric abundance of CO_2 and the ratio N_2/CO_2 is high enough to allow the formation of HCN (Kurosawa et al. 2013, see Section 28.2). Nevertheless, this is too late, as the full oxidation of the atmosphere already happens at about 300 yr with a steep decrease of H_2 and an increase of O_2 in the atmosphere. Despite the high flux of HCN due to a purely carbonaceous bombardment, it is not able to build up significantly in the atmosphere and remains at molar mixing ratios of 8.0×10^{-19} and below. Between 1 and 2 million years, H_2 levels increase and O_2 levels decrease, partially reversing the oxidation of the atmosphere, but HCN levels have already dropped drastically. It might take much more time than the 10 million years shown for them to recover.

Figure 24.3(EH_G2E) shows that the combination of serpentinization and enstatite bombardment increases the levels of H_2 in the atmosphere, but not significantly for CH_4 and HCN (see Table 24.1). Apparently, the H_2 flux from enstatite degassing does not contribute substantially to the budget of formed HCN, whereas CH_4 emitted from hydrothermal vents does. The main trends in the temporal evolution here are dictated by serpentinization (cf. Figure 24.3(EH_G2)).

Yet enstatite bombardment does not destabilize the reducing effect of serpentinization, whereas carbonaceous bombardment does. For the first 30 000 yr in Figure 24.3(EH_G2C), the atmosphere is significantly reduced. In particular, the activation of direct HCN synthesis by carbonaceous impactors around 1000 yr pushes its atmospheric abundance significantly to maximum values of 2.0×10^{-10}. However, around 300 000 yr there is a sudden increase in O_2 and a sudden decrease in reducing gas levels. The high HCN abundance leads to a relative decrease in the molar mixing ratio of H_2, keeping it below values of 1.7×10^{-2}. This is slightly too low to prevent the growth of oxidizing gases in the photochemical network.

In a mixed bombardment scenario, as assumed in Figure 24.3(EH_G2EC), this stabilizing effect of the enstatite bombardment becomes very apparent, as the additional H_2 flux from enstatite impactors keeps the reduced state of the atmosphere stable for tens of millions of years. The final increase in HCN, H_2CO, and CO at 3 million years again coincides with a decrease in CH_4 and H_2O, which can be explained as above by the oxidation of methane to H_2CO and the formation of HCN by methane and nitrogen radicals reacting through the H_2CN intermediate.

In summary, for both MH and EH models, if serpentinization is active according to the extended Hadean mantle models (Section 30.1, Miyazaki and Korenaga 2022), it dominates the levels of CH_4 in the atmosphere. Since HCN levels are closely correlated with CH_4 as its major chemical intermediate (cf. Pearce, Molaverdikhani, Pudritz, Henning, and Cerrillo 2022), serpentinization is the most important and reliable driving force in HCN synthesis. In addition, when present, carbonaceous bombardment clearly dominates the abundance of HCN by direct synthesis during impacts (Kurosawa et al. 2013).

In EH models, however, carbonaceous bombardment requires support from serpentinization. Due to its delayed activation in an initially CO_2-rich atmosphere, it either emerges in a highly oxidized atmosphere (see case EH_C) or destabilizes the H_2 levels and thus the reduced state of the atmosphere (see case EH_G2C). An enstatite component in the bombardment allows to prevent this (see case EH_G2EC). However, strongly active serpentinization with its CH_4 surface flux is by far the most effective way not only to reduce an initially oxidizing atmosphere, but also to exploit the initially high CO_2 levels as a carbon source for an effective HCN synthesis. The resulting HCN yields are comparable in magnitude to its synthesis in an initially reducing atmosphere.

After evaluating the various scenarios, we can summarize that serpentinization, and this is the most important finding in this study, might resolve one of the most widely debated issues in the origins of life research community, namely that an initially oxidized atmosphere on Hadean Earth would prevent sufficiently effective synthesis of prebiotic molecules.

24.2 Rain-out

Our atmospheric model can provide rain-out of chemical species from the lowest layer of the atmosphere closest to the surface. This effectively removes these molecules from the atmosphere at each time step and affects the balance between atmospheric gases in the photochemical network, which is already included in the calculation of the atmospheric mixing ratios as shown in the previous Sections. The rain can accumulate on the surface of the first volcanic islands and continental crust emerging from the global ocean. The calculated rain-out rates define an influx of these chemical species into the first small water bodies forming on these landmasses, e.g., small lakes and WLPs, which allow the concentration of key prebiotic precursors, e.g., the water-soluble molecules HCN and H_2CO. These rain-out rates are directly correlated with and follow the time evolution of the molar mixing ratio of the respective species, as already seen in a previous study (Pearce, Molaverdikhani, Pudritz, Henning, and Cerrillo 2022).

As an example, Figure 24.4 shows the time evolution of the rain-out rates for CO_2, HCN, and H_2CO for case EH_G2EC, incorporating all the different processes

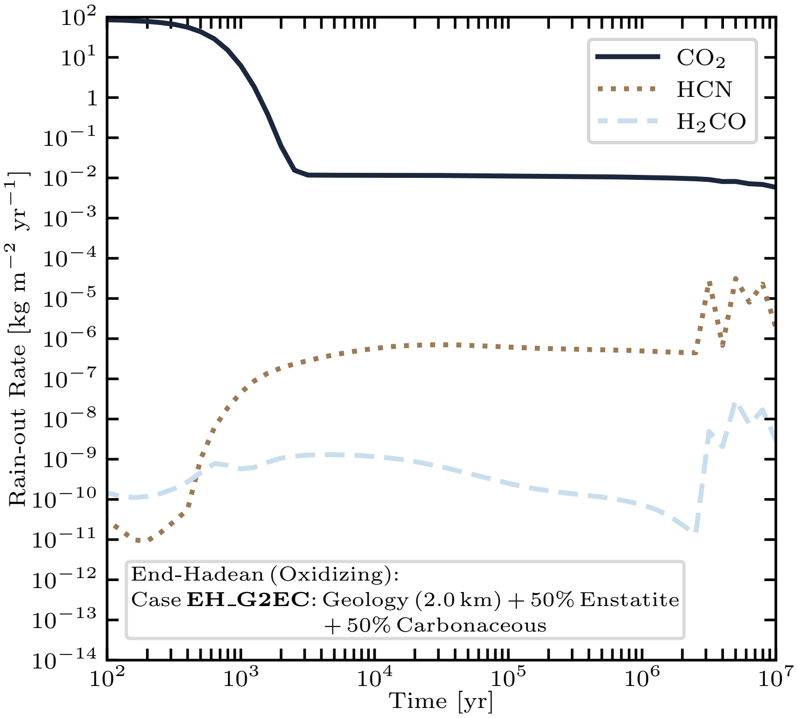

Figure 24.4: Rain-out rates of CO_2, HCN, and H_2CO from the lowest atmospheric layer closest to the surface as a function of time for case EH_G2EC.

providing reducing gases as well as CO_2 from volcanic outgassing on the Hadean Earth. It also corresponds to one of the highest rain-out rates reached across all simulations in the EH models (see Table 24.2).

HCN and H_2CO rain-out peaks around 3–5 Myr with rates of $3.1 \times 10^{-5}\,\mathrm{kg\,m^{-2}\,yr^{-1}}$ and $3.0 \times 10^{-8}\,\mathrm{kg\,m^{-2}\,yr^{-1}}$, respectively. To get a rough feel of the magnitudes involved, the average global (water) precipitation from 1983–2023 on Earth was $2.81\,\mathrm{mm\,d^{-1}}$ (Adler and Gu 2024), equivalent to $\sim 1000\,\mathrm{kg\,m^{-2}\,yr^{-1}}$. In tropical coastal areas, even over $3500\,\mathrm{mm\,yr^{-1}}$ and more can be reached locally (Ogino et al. 2016), equivalent to $3500\,\mathrm{kg\,m^{-2}\,yr^{-1}}$ and more. The shape of the time evolution of the rain-out rates in Figure 24.4 is very similar to the corresponding atmospheric molar mixing ratios in Figure 24.3(EH_G2EC).

Comparing the rain-out rates in Table 24.2 shows that the highest HCN rain-out rate is reached in case MH_C and the highest H_2CO rain-out rate is reached in case EH_G2C. The initially reducing atmosphere does not always lead to the highest HCN rain-out rates. In general it is advantageous to have initially reducing conditions for HCN formation and rain-out, but for the cases including serpentinization at an HCD of 2.0 km (cases G2, G2E, G2C, G2EC) the initially oxidizing conditions allow similar or even higher rates (cases G2 and G2E) compared to the reducing conditions. The reason is that the initially present CO_2 can be exploited as an abundant carbon source for HCN synthesis, as already discussed for the atmospheric abundances in the previous Sections. In addition, carbonaceous bombardment and

	Max. Rain-out Rate [$\mathrm{kg\,m^{-2}\,yr^{-1}}$]					
	CO_2		HCN		H_2CO	
Case	MH (red.)	EH (ox.)	MH (red.)	EH (ox.)	MH (red.)	EH (ox.)
G0.5	1.86×10^{-2}	1.20×10^{-2}	1.11×10^{-5}	3.19×10^{-11}	8.38×10^{-10}	1.47×10^{-8}
G1	1.49×10^{-2}	1.12×10^{-2}	2.57×10^{-6}	1.41×10^{-10}	3.34×10^{-12}	6.77×10^{-9}
G2	6.26×10^{-3}	1.17×10^{-2}	1.85×10^{-5}	1.57×10^{-4}	2.30×10^{-14}	1.46×10^{-8}
E	1.27×10^{-2}	9.81×10^{-3}	6.79×10^{-11}	3.09×10^{-15}	1.89×10^{-18}	6.26×10^{-21}
C	1.56×10^{-2}	9.99×10^{-3}	5.76×10^{-4}	3.53×10^{-15}	1.89×10^{-18}	3.86×10^{-21}
G2E	4.96×10^{-3}	1.17×10^{-2}	4.95×10^{-5}	1.43×10^{-4}	2.57×10^{-12}	1.17×10^{-8}
G2C	6.25×10^{-3}	1.17×10^{-2}	3.53×10^{-4}	8.91×10^{-7}	2.30×10^{-14}	4.15×10^{-7}
G2EC	6.53×10^{-3}	1.17×10^{-2}	2.03×10^{-4}	3.14×10^{-5}	1.84×10^{-11}	2.99×10^{-8}

Table 24.2: Maximum resulting rain-out rates of prebiotic precursors.

subsequent direct HCN synthesis during impacts significantly enhances HCN rain-out if the atmosphere is either non-oxidized or only moderately oxidized.

When serpentinization is included in the model, H_2CO rain-out rates are systematically higher by about 12–14 orders of magnitude in the initially oxidizing scenario, making atmospheric photochemistry a potentially significant source of H_2CO in EH WLP settings.

24.3 Prebiotic Molecules in Warm Little Ponds

One way for rained-out HCN and H_2CO to accumulate and concentrate on Hadean Earth is to enter the first emerging WLPs, small reservoirs of water about a meter in diameter that formed on the first landmasses to emerge from the global ocean. Due to the seasonal cycles of the environment, these ponds can go through repeated states of desiccation and rewetting by precipitation. Rainwater containing the prebiotic precursors HCN and H_2CO resulting from atmospheric photochemistry can accumulate in these WLPs. Experimental studies have shown that these precursor molecules are able to form complex prebiotic molecules such as RNA-building blocks during wet-dry cycling (Oró and Kimball 1961; Larowe and Regnier 2008; Ferus, Pietrucci, Saitta, Ivanek, et al. 2019; Butlerow 1861; Breslow 1959; Yi et al. 2020). To simulate this process in the context of our atmospheric models, we developed a WLP wet-dry cycling model (Pearce, Pudritz, et al. 2017; Pearce, Molaverdikhani, Pudritz, Henning, and Cerrillo 2022), which uses experimentally determined yields of prebiotic molecules formed from HCN and H_2CO, and used the determined rain-out rates in Table 24.2 as influx terms supplying the prebiotic synthesis.

Figure 24.5 shows as an example the resulting abundances for key RNA building

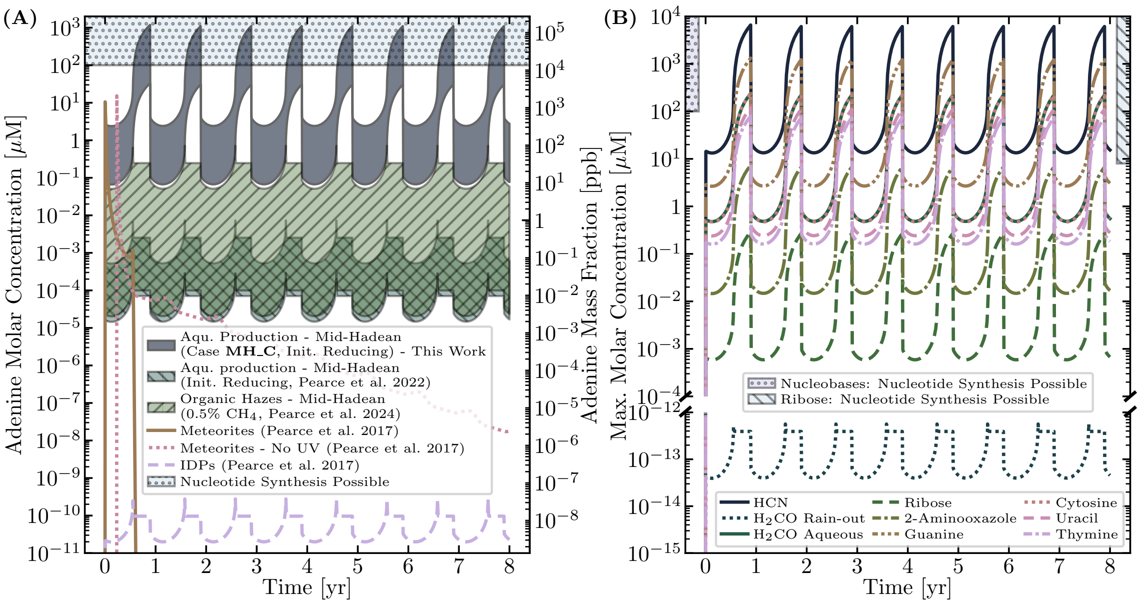

Figure 24.5: Concentrations of prebiotic molecules over time resulting from the warm little pond (WLP) cycling model (Pearce, Pudritz, et al. 2017; Pearce, Molaverdikhani, Pudritz, Henning, and Cerrillo 2022). Inflow fluxes for HCN and H_2CO are derived from atmospheric rain-out as a result of photochemistry in case MH_C (Table 24.2). Panel **A** shows a comparison of the resulting adenine concentrations in this work with the previous atmospheric model with some assumptions based on the present Earth that might be less suitable for the Hadean Earth (Pearce, Molaverdikhani, Pudritz, Henning, and Cerrillo 2022), an organic haze experiment with particles containing biomolecules formed in an atmosphere with 5 % CH_4, which fall into the pond (Pearce, Hörst, et al. 2024), delivery from meteorites and interplanetary dust particles (IDPs) (Pearce, Pudritz, et al. 2017), and the amounts required for nucleotide synthesis as determined by experimental studies (Ponnamperuma et al. 1963; Fuller et al. 1972b; Powner et al. 2009; S. Becker, Thoma, et al. 2016; Saladino, Bizzarri, et al. 2017; S. Becker, Schneider, et al. 2018; Nam et al. 2018; Teichert et al. 2019). Aqueous production is sourced from atmospheric rain-out of HCN multiplied by experimental yields of adenine (Oró and Kimball 1961; Wakamatsu et al. 1966; A. Hill and Orgel 2002; Pearce, Molaverdikhani, Pudritz, Henning, and Cerrillo 2022). The pond cycles through 6 months of wet and 6 months of dry conditions. Sinks for concentration are photodissociation by UV light, hydrolysis, and seepage through pores at the bottom of the pond. Panel **B** shows concentrations for several prebiotic molecules, including accumulating HCN and H_2CO from rain-out in case MH_C, and subsequently formed nucleobases, the sugar ribose, required amounts of nucleobases and ribose for nucleotide synthesis in experiments, and 2-aminooxazole, which is a key intermediate in the Powner-Sutherland pathway (Powner et al. 2009).

blocks and intermediates using the rain-out rates for case MH_C. The left panel shows the evolution of the prebiotic molecule adenine, one of the genetic letters in RNA and DNA molecules, over time. One year corresponds to a full cycle of 6 months of filling the pond with rain and 6 months of dry conditions (no rain), allowing evaporation to dry the pond to a minimum of 1 mm and concentrating the molecules in the process. This concentration process is what allows these complex prebiotic biomolecules to form from HCN and H_2CO.

In the left panel (A), the shaded blue area shows the range between the minimum and maximum yields of adenine formed by prebiotic synthesis from HCN. This HCN was supplied by rain-out from the atmosphere, and the influx rates correspond to the values shown in Table 24.2. The maximum yield for adenine is a concentration of 1.2 mM in the WLP. It is summarized together with the maximum reached concentrations of other prebiotic molecules relevant for the origins of life, including all considered cases, in Table 24.3. For comparison, several WLP adenine concentrations from previous studies are also plotted in Figure 24.5(A).

The dark green area with "\\"-hatching shows the resulting concentrations for the initially reduced MH from the previous study by Pearce, Molaverdikhani, Pudritz, Henning, and Cerrillo (2022). The computational methods and workflow used in that earlier study were very similar to those used in this work. Atmospheric photochemistry, rain-out rates, and prebiotic synthesis in the WLP were calculated using the same approach. It considered the same initially reducing atmosphere in the MH at 4.4 Gyr (see Table 22.1). This happened to be the most productive scenario for prebiotic molecule synthesis in the WLPs considered in this earlier study by Pearce, Molaverdikhani, Pudritz, Henning, and Cerrillo (2022).

The only difference is that Pearce, Molaverdikhani, Pudritz, Henning, and Cerrillo (2022) used different fluxes for the source terms of reducing gases. In particular, the CH_4 fluxes from serpentinization are more representative of the present-day Earth (Guzmán-Marmolejo et al. 2013), and H_2 emitted by serpentinization was omitted. Additionally, a carbonaceous late veneer was not considered, excluding the possibility of direct HCN synthesis during impact (Kurosawa et al. 2013). The maximum adenine yield in the present work is more than five orders of magnitude higher than the yield of 7.3 nM calculated by Pearce, Molaverdikhani, Pudritz, Henning, and Cerrillo (2022).

The light green area with "//"-hatching shows the resulting concentrations from an organic haze experiment with particles containing biomolecules formed in an atmosphere with 5 % CH_4, which fall into the pond (Pearce, Hörst, et al. 2024). The maximum adenine yield in the present work was more than three orders of magnitude higher than the yield of 0.7 µM obtained by Pearce, Hörst, et al. (2024).

Delivery of biomolecules by carbonaceous chondrites and interplanetary dust

	Max. Warm Little Pond Concentration [µM]							
	HCN from Rain-out		H_2CO from Rain-out		H_2CO from Aqueous Synth.[a]		Ribose	
Case	MH (red.)	EH (ox.)	MH (red.)	EH (ox.)	MH (red.)	EH (ox.)	MH (red.)	EH (ox.)
G0.5	3.66	1.05×10^{-5}	2.49×10^{-4}	4.38×10^{-3}	1.32×10^{-1}	3.79×10^{-7}	1.61×10^{-4} [b]	5.35×10^{-6} [c]
G1	8.48×10^{-1}	4.66×10^{-5}	9.93×10^{-7}	2.01×10^{-3}	3.06×10^{-2}	1.68×10^{-6}	3.73×10^{-5} [b]	2.46×10^{-6} [c]
G2	6.11	1.21×10^{3}	6.85×10^{-9}	4.36×10^{-3}	2.20×10^{-1}	4.34×10^{1}	2.69×10^{-4} [b]	5.30×10^{-2} [b]
E	2.24×10^{-5}	1.02×10^{-9}	5.62×10^{-13}	1.86×10^{-15}	8.07×10^{-7}	3.67×10^{-11}	9.84×10^{-10} [b]	4.48×10^{-14} [b]
C	6.59×10^{3}	1.16×10^{-9}	5.64×10^{-13}	1.15×10^{-15}	2.37×10^{2}	4.19×10^{-11}	2.90×10^{-1} [b]	5.12×10^{-14} [b]
G2E	1.64×10^{1}	1.03×10^{3}	7.64×10^{-7}	3.48×10^{-3}	5.90×10^{-1}	3.72×10^{1}	7.20×10^{-4} [b]	4.54×10^{-2} [b]
G2C	3.72×10^{3}	2.94×10^{-1}	6.84×10^{-9}	1.23×10^{-1}	1.34×10^{2}	1.06×10^{-2}	1.64×10^{-1} [b]	1.63×10^{-4} [c]
G2EC	1.81×10^{3}	1.03×10^{1}	5.49×10^{-6}	8.91×10^{-3}	6.51×10^{1}	3.73×10^{-1}	7.94×10^{-2} [b]	4.66×10^{-4} [b]

	Max. Warm Little Pond Concentration [µM]					
	2-Aminooxazole		Adenine		Guanine	
Case	MH (red.)	EH (ox.)	MH (red.)	EH (ox.)	MH (red.)	EH (ox.)
G0.5	3.99×10^{-3}	1.14×10^{-8}	6.47×10^{-1}	1.86×10^{-6}	7.24×10^{-1}	2.08×10^{-6}
G1	9.23×10^{-4}	5.07×10^{-8}	1.50×10^{-1}	8.23×10^{-6}	1.68×10^{-1}	9.21×10^{-6}
G2	6.65×10^{-3}	1.33	1.08	2.17×10^{2}	1.21	2.41×10^{2}
E	2.44×10^{-8}	1.11×10^{-12}	3.95×10^{-6}	1.80×10^{-10}	4.43×10^{-6}	2.01×10^{-10}
C	7.25	1.27×10^{-12}	1.19×10^{3}	2.05×10^{-10}	1.32×10^{3}	2.30×10^{-10}
G2E	1.80×10^{-2}	1.14	2.95	1.86×10^{2}	3.27	2.07×10^{2}
G2C	4.10	3.20×10^{-4}	6.70×10^{2}	5.19×10^{-2}	7.45×10^{2}	5.81×10^{-2}
G2EC	1.99	1.13×10^{-2}	3.25×10^{2}	1.85	3.62×10^{2}	2.06

	Max. Warm Little Pond Concentration [µM]					
	Cytosine		Uracil		Thymine	
Case	MH (red.)	EH (ox.)	MH (red.)	EH (ox.)	MH (red.)	EH (ox.)
G0.5	1.26×10^{-1}	3.63×10^{-7}	6.49×10^{-2}	1.86×10^{-7}	4.31×10^{-2}	1.24×10^{-7}
G1	2.93×10^{-2}	1.61×10^{-6}	1.50×10^{-2}	8.26×10^{-7}	9.97×10^{-3}	5.48×10^{-7}
G2	2.11×10^{-1}	4.34×10^{1}	1.08×10^{-1}	2.17×10^{1}	7.18×10^{-2}	1.45×10^{1}
E	7.73×10^{-7}	3.52×10^{-11}	3.97×10^{-7}	1.81×10^{-11}	2.63×10^{-7}	1.20×10^{-11}
C	2.37×10^{2}	4.02×10^{-11}	1.19×10^{2}	2.06×10^{-11}	7.91×10^{1}	1.37×10^{-11}
G2E	5.72×10^{-1}	3.72×10^{1}	2.95×10^{-1}	1.86×10^{1}	1.97×10^{-1}	1.24×10^{1}
G2C	1.34×10^{2}	1.01×10^{-2}	6.70×10^{1}	5.21×10^{-3}	4.47×10^{1}	3.45×10^{-3}
G2EC	6.50×10^{1}	3.59×10^{-1}	3.25×10^{1}	1.85×10^{-1}	2.17×10^{1}	1.24×10^{-1}

[a] Formaldehyde synthesized aqueously from rained-out HCN.

[b] Most ribose is synthesized in formose reaction starting from formaldehyde, which in turn is synthesized aqueously from rained-out HCN.

[c] Most ribose is synthesized in formose reaction starting from formaldehyde rained-out directly from the atmosphere.

Table 24.3: Maximum yields of prebiotic organic molecules in warm little ponds (WLPs).

particles (IDPs) was considered using the same wet-dry cycling model by Pearce, Pudritz, et al. (2017). In the present study, the maximum adenine yield was about two orders of magnitude higher than the yield of 10.6 µM in this previous work. The exogenous delivery of biomolecules by meteorites might still be a way to enhance the concentrations of prebiotic molecules for a limited time during the wet phase of the pond, facilitating the synthesis of RNA building blocks.

The light blue area with dotted hatching shows the range of nucleobase abundances that was required to successfully synthesize nucleotides in experiments (Ponnamperuma et al. 1963; Fuller et al. 1972b; Powner et al. 2009; S. Becker, Thoma, et al. 2016; Saladino, Bizzarri, et al. 2017; S. Becker, Schneider, et al. 2018; Nam et al. 2018; Teichert et al. 2019). Only our models (here, e.g., case MH_C) were able to generate the required nucleobases concentrations and for the first time enter the regime of feasible nucleotide synthesis in WLPs, unlike the models by Pearce, Pudritz, et al. (2017), Pearce, Molaverdikhani, Pudritz, Henning, and Cerrillo (2022), and Pearce, Hörst, et al. (2024).

Figure 24.5(B) shows concentrations for several prebiotic molecules, including accumulating HCN and H_2CO from rain-out in case MH_C, and the subsequent formation of the nucleobases guanine, cytosine, uracil, and thymine, the sugar ribose, and 2-aminooxazole as a key intermediate in the Powner-Sutherland pathway (Powner et al. 2009). The required nucleobase concentrations for nucleotide synthesis in experiments are shown again, here as a vertical bar with dotted hatching in the top left corner. In addition, the required ribose concentrations are indicated by a vertical bar with "\\"-hatching in the top right corner. The simulated ribose abundances do not reach high enough concentrations to allow nucleotide synthesis in experiments. However, by turning off the seepage at the bottom of the WLP, the required ribose concentrations can be reached, see the following Sections 24.3.1 and 25.

Figure 24.6 gives a concise overview of the most productive scenarios considered in this study. It can be seen that significantly high concentrations of prebiotic biomolecules in WLPs are possible even in an initially oxidizing environment. In case EH_G2, serpentinization provides high enough fluxes of H_2 and CH_4 to exploit the initially CO_2-rich atmosphere for its carbon and subsequent HCN synthesis. This highlights that an initially oxidizing atmosphere is a favorable scenario for highly active serpentinization in the Hadean. The resulting pond concentrations are more than two orders of magnitude higher than an initially reducing scenario (case MH_G2) and less than one order of magnitude lower than the most effective scenario overall, a purely carbonaceous bombardment in the MH (case MH_C).

Another interesting phenomenon can be clearly observed in Figure 24.6(A) if one takes a closer look at the shape of the curves in cases MH_C and EH_G2 and compares them with case MH_G2. The vertical dotted lines indicate the phase in

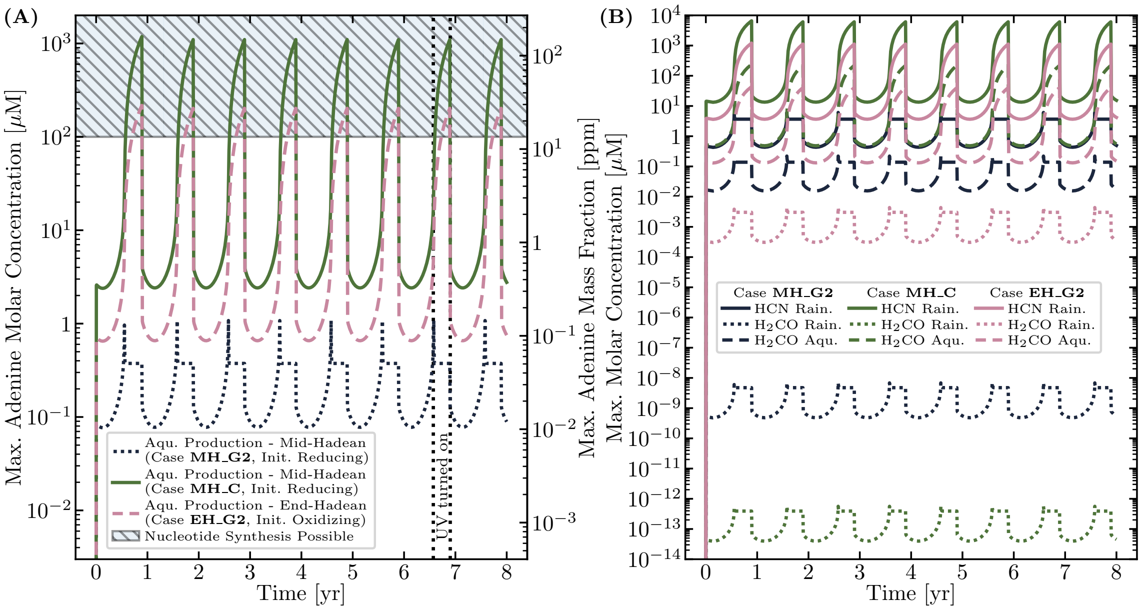

Figure 24.6: Concentrations of prebiotic molecules over time resulting from the warm little pond (WLP) cycling model (Pearce, Pudritz, et al. 2017; Pearce, Molaverdikhani, Pudritz, Henning, and Cerrillo 2022). Inflow fluxes for HCN and H_2CO are derived from atmospheric rain-out as a result of the photochemistry model. Panel **A** shows a comparison of the maximum resulting adenine concentrations for some of the most productive cases considered in this work, MH_G2, MH_C, and EH_G2. In several of these cases, sufficient amounts of adenine are reached for nucleotide synthesis, as shown by experimental studies (Ponnamperuma et al. 1963; Fuller et al. 1972b; Powner et al. 2009; S. Becker, Thoma, et al. 2016; Saladino, Bizzarri, et al. 2017; S. Becker, Schneider, et al. 2018; Nam et al. 2018; Teichert et al. 2019). Aqueous production is sourced from atmospheric rain-out of HCN multiplied by experimental yields of adenine (Oró and Kimball 1961; Wakamatsu et al. 1966; A. Hill and Orgel 2002; Pearce, Molaverdikhani, Pudritz, Henning, and Cerrillo 2022). The pond cycles through 6 months of wet and 6 months of dry conditions. Sinks for the concentration are photodissociation by UV light, hydrolysis, and seepage through pores at the bottom of the pond. Between the two vertical dotted lines is the phase of the cycles where UV irradiation is turned on while the pond is dried out. Panel **B** shows concentrations for several prebiotic molecules including accumulating HCN and H_2CO from rain-out and subsequent aqueous synthesis of H_2CO for the same three cases. Please note that the maximum pond concentrations of prebiotic biomolecules in case EH_G2 in an initially oxidizing atmosphere are comparable to the other two cases shown with initially reducing conditions.

which UV irradiation is turned on as the pond has dried out. In case MH_G2, at the beginning of this phase, the concentrations reach their maximum in a sharp peak as the pond dries down to its minimum level of 1 mm. Then UV irradiation is turned on and the concentration drops to a plateau in a steady state where production from HCN influx and destruction from UV dissociation equilibrate. This behavior was always observed in the previous studies (Pearce, Pudritz, et al. 2017; Pearce, Molaverdikhani, Pudritz, Henning, and Cerrillo 2022; Pearce, Hörst, et al. 2024, see also Figure 24.5).

In contrast, in cases MH_C and EH_G2, we reach for the first time concentrations high enough to prevent this equilibration of influx and dissociation, and the concentration continues to rise in the nearly dry pond. The rate of adenine photodestruction was measured to be $1 \times 10^{-4}\,\mathrm{photon}^{-1}$ (Poch et al. 2015; Pearce, Molaverdikhani, Pudritz, Henning, and Cerrillo 2022). This sink rate is exceeded by synthesis from HCN in cases MH_C and EH_G2 (see Figure 24.6(A)) as well as in cases MH_G2C, MH_G2EC, and EH_G2E (not shown) in the present study. The remaining sink terms that cap biomolecule abundances are seepage through pores at the bottom of the pond and hydrolysis. This effectively renders destruction by UV light negligible in the context of prebiotic synthesis in WLPs if high enough synthesis rates can be achieved.

24.3.1 No Seepage

It might be possible that after some time the pores at the bottom of the pond became clogged due to adsorption of biomolecules on the mineral surfaces or deposition of amphiphiles and mineral gels (Hazen and Sverjensky 2010; Deamer 2017; Damer and Deamer 2020a). In the wet-dry pond cycling model, this situation can be represented by turning off the seepage sink term. Table 32.1 summarizes the resulting maximum yields of prebiotic biomolecules following from such a model after allowing the molecules to accumulate for 10 000 yr.

For adenine, guanine, and cytosine, pond concentrations do not increase significantly. This is due to their relatively high rates of hydrolysis, which has become the dominant sink term without seepage (for details, see Table A6 in Pearce, Molaverdikhani, Pudritz, Henning, and Cerrillo 2022). On the other hand, in the most productive case MH_C, uracil reaches a maximum concentration of 0.89 mM (less than an order of magnitude increase over the scenario with seepage), and thymine reaches 1.8 mM (more than an order of magnitude increase). Since hydrolysis rates for 2-aminooxazole and ribose are not provided in the Pearce, Molaverdikhani, Pudritz, Henning, and Cerrillo (2022) model, their more than an order of magnitude increased concentrations of 9.6 µM and 0.24 mM in comparison to the simulations with seepage, respectively, represent potential maximum values in case MH_C without seepage.

25

Discussion

When trying to estimate whether the Hadean Earth as modeled here was able to generate conditions suitable for the origins of life, the key question to answer is whether the concentrations of biomolecules such as nucleobases, ribose, and 2-aminooxazole are high enough to promote the synthesis of nucleotides, the monomers of RNA molecules. Experimental studies that have successfully demonstrated the formation of nucleotides from solutions of nucleobases, ribose, and phosphates required minimum nucleobase concentrations of $\sim 100\,\mu\mathrm{M} - 100\,\mathrm{mM}$ for nucleobases and $\sim 8\,\mu\mathrm{M} - 15\,\mathrm{mM}$ for ribose (Ponnamperuma et al. 1963; Fuller et al. 1972b; Powner et al. 2009; S. Becker, Thoma, et al. 2016; Saladino, Bizzarri, et al. 2017; S. Becker, Schneider, et al. 2018; Nam et al. 2018; Teichert et al. 2019).

The maximum abundances for the most productive case MH_C in Table 24.3 reach the mM range for the purines adenine and guanine, and reach the 100 µM range for the pyrimidines cytosine, uracil, and thymine. Furthermore, in the case of EH_G2 in an initially oxidizing scenario, purines reach the 100 µM range and pyrimidines reach the 10 µM range. In the absence of seepage, the concentrations for the pyrimidines uracil and thymine can even reach the 100 µM range in case EH_G2 (see Table 32.1). These concentrations are well within the range required for successful nucleotide synthesis in the experiments discussed above. Assuming maximum bombardment rates as presented in the supplementary results in Section 33, these maximum nucleobase concentrations can be enhanced by about an order of magnitude (see Table 33.3).

With seepage turned on, ribose concentrations reach the 100 nM range in case MH_C and the 10 nM range in case EH_G2 (see Table 24.3), which is one to two orders of magnitude below the concentrations required for successful nucleotide synthesis. Without seepage, however, the concentrations reach almost the 10 µM range in case MH_C and the µM range in case EH_G2 (see Table 32.1). These concentrations are sufficient to allow nucleotide synthesis, as shown in the experiments by Saladino, Bizzarri, et al. (2017), but it must be noted that in these experiments ribose was not dissolved in water but in formamide.

At maxed-out bombardment rates and without seepage, as assumed for the supplementary results in Section 33, ribose concentrations reach the 100 µM range (see Table 33.4), which is close to, but still falls short of, the mM concentrations required for nucleotide synthesis in *aqueous* solution as performed in laboratory experiments (Ponnamperuma et al. 1963; Fuller et al. 1972b; Nam et al. 2018; Powner et al. 2009). It should also be noted that reaching these 100 µM ribose concentrations would require a bombardment intensity comparable to impacts the size of present-day dwarf planets (2×10^{25} g, 2300 km diameter), as suggested by Zahnle, Lupu, et al. (2020) and Wogan, Catling, et al. (2023).

This is the first model to show that the nucleobase and, without seepage, also the ribose concentrations generated by aqueous *in situ* synthesis are potentially sufficient for nucleotide synthesis in WLPs.

25.1 A New Hope: HCN Production in Initially Oxidizing Environments

We demonstrated for the first time that the synthesis of sufficiently high concentrations of nucleoside building blocks is possible even in an initially oxidized atmosphere rich in CO_2. Furthermore, in case EH_G2, these concentrations are replenished by serpentinization and subsequent photochemistry in a continuous and stable manner, rather than relying on singular cataclysmic events as in the studies by Wogan, Catling, et al. (2023) and Zahnle, Lupu, et al. (2020) and others, who considered very large enstatite impacts as the source of reducing gases on the Hadean Earth. Further increases in ribose concentrations might be necessary, however, as it is not yet certain that nucleotide synthesis in aqueous rather than formamide solution in WLPs would be successful with the current results.

Comparing the initially reducing and oxidizing models in the geology only scenario in Figures 24.1(MH_G2) and (EH_G2) leads to the conclusion that an initially oxidized and therefore CO_2-rich atmosphere might be necessary to fuel an effective HCN synthesis. The critical point is when the Earth begins to develop an effective upwelling of ferrous iron-rich mantle material and simultaneously the first hydrosphere settles on the surface, forming liquid water oceans. The contact of this liquid water with the ferrous iron from the mantle provides a large reducing potential, which in turn can utilize the carbon in atmospheric CO_2 when reacting with H_2 and CH_4, promoting the formation of HCN. This results in an order of magnitude higher HCN level compared to the initially reducing situation. In cases MH_G0.5/1/2 there is a lack of CO_2, and the HCN level is directly correlated with the CH_4 level as the main precursor and carbon source. This is consistent with previous models and the findings by Pearce, Molaverdikhani, Pudritz, Henning, and Cerrillo (2022).

This paper has elucidated a new and hitherto unknown regime that allows CO_2 to be exploited for its carbon and HCN synthesis to reach new levels. We have discovered that it is serpentinization that produces the required high H_2 and CH_4 fluxes that make this possible.

These high fluxes might also more realistically represent the situation prevailing in the Hadean. Over most of the time evolution in model EH_G2, CH_4 and HCN levels are still loosely correlated. However, in the time span of ∼200–2000 yr, HCN levels experience a brief but strong boost, as much of the carbon in the initial CO_2 atmosphere is converted directly into HCN via CH_4.

As a novel insight, our results suggest that a primary CO_2-rich atmosphere might even be beneficial as a carbon source if hydrothermal circulation reached deep enough into the crust in the Hadean. This might open the possibility of shifting the scenario in case EH_G2 from the EH at 4.0 Gyr to the very beginning of the Hadean even before 4.4 Gyr, but only if the hydrosphere was already (at least temporarily) present then. Strongly active serpentinization might have already occurred in the earliest Hadean, when the very first primordial CO_2-rich atmosphere was still present. This would create an additional scenario, not considered in the present work, that predates even the MH models. The very first atmosphere on Earth might have been a primordial CO_2-dominated one, which formed by CO_2 outgassing from the magma ocean of the forming Earth (Zahnle, Arndt, et al. 2007; Miyazaki and Korenaga 2022; Johansen, Ronnet, Schiller, et al. 2023; Johansen, Camprubi, et al. 2024).

The time window of the most effective HCN production would then be limited by the time when liquid water forms on the surface and the time scale of the subduction of atmospheric CO_2 into the Earth's mantle. According to Miyazaki and Korenaga (2022) this can be as short as 160 million years after the onset of plate tectonics. In extended models with HCD up to 2.0 km (see Figure 30.1), CO_2 was flushed into the mantle in only 82.75 Myr. If most of the prebiotic precursors for the origins of life in a scenario analogous to case EH_G2 were prepared before 4.4 Gyr, a rapid settling of the hydrosphere (Abe 1993; Korenaga 2021) after the onset of plate tectonics is required. This would allow a CO_2 atmosphere to be exploited for its carbon before it is flushed into the mantle. In contrast, the new models by Guo and Korenaga (2025) employ a different scenario with a linearly decreasing plate velocity throughout the Hadean, which would allow for only 90 bar of CO_2 to be removed from the atmosphere into the mantle (this specific information is only available in the preprint version of the article: Guo and Korenaga 2024).

There is no need to wait until the CO_2-rich atmosphere is gone to have an efficient prebiotic synthesis, as it might even be a favorable environment now to set the stage and the right conditions for the origins of life. This might make it possible to set the time for the emergence of the RNA world to only hundreds of millions of years or even much less after the formation of the Earth or $> 4.4\,\mathrm{Gyr}$ from today. It might be interesting to explore this idea further with in-depth modeling in future work.

Assuming a HCD of 2 km in the Hadean, serpentinization of upwelling mantle material at mid-ocean ridge spreading zones results in a CH_4 flux of $1.12 \times 10^{10}\,\mathrm{molecules\,cm^{-2}\,s^{-1}}$ (see Table 30.1), which corresponds to a global CH_4 flux of $\sim 3\,\mathrm{Tmol\,yr^{-1}}$. Thompson et al. (2022) compiled an extensive list of abiotic CH_4 sources and compared them to the present-day flux caused by biological activity to assess the potential of CH_4 to serve as a biosignature if detected in exoplanet atmospheres using the James Webb Space Telescope. Kasting (2005) estimated for serpentinization at spreading zones a global CH_4 flux of $1.5\,\mathrm{Tmol\,yr^{-1}}$ during the Hadean, and Catling and Kasting (2017) a flux of $0.03\,\mathrm{Tmol\,yr^{-1}}$ for the present-day Earth, using a similar estimation method as in the present study (see Section 30.1.1), starting with an expected H_2 flux and combining it with a measured CH_4/H_2 ratio in vent fluids.

For the slightly different scenario of serpentinization located at subduction zones, Fiebig et al. (2007) estimated an Archean flux of 40–80 $\mathrm{Mt\,yr^{-1}}$, equivalent to 2.5–5 $\mathrm{Tmol\,yr^{-1}}$. It is expected that subduction-related serpentinization will result in higher CH_4 fluxes than spreading zone-related serpentinization, since the subducting oceanic plate drags a lot of water deep into the mantle, and serpentine has been found to be present at depths of $\sim 5 - -200\,\mathrm{km}$ by seismic velocity measurements on present-day Earth (Reynard 2013; S. Guillot et al. 2015). However, since the presence and extent of plate tectonics and related subduction activity as found on the present-day Earth is still in question for the Hadean Earth (Chowdhury et al. 2023; Tarduno et al. 2023), we consider spreading zone serpentinization to be a more robust scenario for estimating CH_4 fluxes on the Hadean Earth.

Our considered flux of $\sim 3\,\mathrm{Tmol\,yr^{-1}}$, about twice the flux estimated by Kasting (2005), fits well within the order of magnitude of the estimated global CH_4 fluxes in the other studies, and thus appears to be a robust estimate valid for the Hadean Earth. Biological activity on Earth today results in $30\,\mathrm{Tmol\,yr^{-1}}$ of CH_4 emission (Jackson et al. 2020; Thompson et al. 2022), and therefore CH_4 remains a valid biosignature even for a Hadean Earth with a rather large HCD as considered here.

It must be acknowledged that the new models by Guo and Korenaga (2025) (more comprehensive information can be found in the preprint version of the article: Guo and Korenaga 2024) introduce a linearly decreasing plate velocity throughout the Hadean, in contrast to the Miyazaki and Korenaga (2022) models used in the present work, which use a constantly high plate velocity throughout the Hadean.

Guo and Korenaga (2024) argue that a decreasing plate velocity results from a three times higher surface heat flux, and consider it more reasonable because convective mixing gradually destroys the initial chemical heterogeneities, allowing the rapid and constant plate velocities as used by Miyazaki and Korenaga (2022). This would imply that CO_2 would be flushed into the mantle more slowly by seafloor weathering, and that ferrous iron would well up at a slower rate at mid-ocean ridges, possibly leading to lower surface fluxes of H_2, and consequently CH_4, in the Hadean. Due to the lost rock record, there is almost no way to validate which plate velocities better represent the Hadean and how the gas fluxes might have evolved. It could be interesting to model how these lower surface fluxes of reducing gases affect atmospheric photochemistry, rain-out, and biomolecule concentrations in WLPs, and see if there is a difference from current models in future studies.

The Miyazaki and Korenaga (2022) model suggests that a heterogeneous mantle composition and active serpentinization in the Hadean could provide abundant H_2. This in turn might create a strong reducing potential and enable the formation of prebiotic molecules inside hydrothermal vents (see, e.g., W. Martin and Russell 2006). However, in the context of atmospheric HCN synthesis and rain-out, oceanic dilution makes it difficult to achieve sufficiently high concentrations of HCN and H_2CO from atmospheric sources for significant prebiotic synthesis in hydrothermal vent environments.

Serpentinization is the most stable and continuous source of reducing gases considered in our models. It is fed by a steady stream of iron-rich mantle material. Our model assumes steady fluxes and continuous evolution of the atmosphere. Therefore, the effect of serpentinization should be well captured in our simulations. We consider it to be the most continuous and reliable way to supply reducing gases to the Hadean atmosphere.

25.2 Comparison with Impact Scenarios

Impacts, on the other hand, although we have treated them as continuous in our models for simplicity, might actually represent singular cataclysmic events that cause sudden bursts of prebiotic synthesis in the atmosphere and ponds. Furthermore, they can completely reshape the composition of the atmosphere and even evaporate the hydrosphere.

Comprehensive and detailed models considering single impacts and their aftermath in the Hadean Earth's atmosphere have been published, e.g., by Zahnle, Lupu, et al. (2020) and Wogan, Catling, et al. (2023), Citron and Stewart (2022) and Itcovitz et al. (2022), Benner, Bell, et al. (2019), Genda, Iizuka, et al. (2017) and Genda, Brasser, et al. (2017), and Sekine et al. (2003). These studies all focus on an enstatite bombardment and are able to generate significant amounts of prebiotic molecules in the atmosphere and HCN rain-out. The models by Wogan, Catling, et al. (2023) resulted in maximum HCN rain-out rates of 10^9 molecules $\mathrm{cm^{-2}\,s^{-1}}$, which is equivalent to $\sim 1.4 \times 10^{-5}\,\mathrm{kg\,m^{-2}\,yr^{-1}}$ of HCN. This required an impactor larger than 5×10^{21} kg (diameter of ~ 1330 km). This would mean that most of the HSE excess was delivered to the Hadean Earth's crust and mantle in just this single impact.

In the cases MH_C (reducing, carbonaceous bombardment) and EH_G2 (oxidizing, serpentinization with 2 km of HCD), our model reached maximum rain-out rates of $5.8 \times 10^{-4}\,\mathrm{kg\,m^{-2}\,yr^{-1}}$ and $1.6 \times 10^{-4}\,\mathrm{kg\,m^{-2}\,yr^{-1}}$, respectively (see Table 24.2). With a very concentrated bombardment in case EH_G2EC_HSE_max (oxidizing, maxed-out bombardment rates) in the supplementary results in Section 33, even $1.4 \times 10^{-2}\,\mathrm{kg\,m^{-2}\,yr^{-1}}$ of rain-out were reached. This is one to three orders of magnitude higher than the models by Wogan, Catling, et al. (2023). However, the enstatite bombardment cases MH/EH_E resulted in rain-out rates of $6.8 \times 10^{-11}\,\mathrm{kg\,m^{-2}\,yr^{-1}}$ and $3.1 \times 10^{-15}\,\mathrm{kg\,m^{-2}\,yr^{-1}}$, respectively, which is over 5–9 orders of magnitude lower than in the models by Wogan, Catling, et al. (2023). This is to be expected, since our model treats this bombardment only as a continuous background source of H_2, and we have chosen only a moderate bombardment intensity (see Section 30.2, Pearce, Molaverdikhani, Pudritz, Henning, and Cerrillo 2022) in the main results.

Wogan, Catling, et al. (2023) specifically point out that these high HCN rain-out rates in their model require high levels of H_2 and CH_4 in the atmosphere, leading to strong greenhouse warming reaching surface temperatures > 360 K. This might be a problem for the longevity of the first forming RNA molecules. In the present work, the carbonaceous bombardment might be a less drastic alternative to avoid too high atmospheric H_2 and CH_4 concentrations while still providing the highest HCN rain-out of all modeled scenarios, even in the initially oxidizing scenario EH_G2EC_HSE_max in the supplementary results (Section 33).

26

Conclusions

To provide an overview of the potential for prebiotic synthesis in the many scenarios considered here, and to make this visually easy to grasp, Figure 26.1 shows the peak concentrations of HCN in the atmosphere and WLPs, as well as the biomolecule adenine in WLPs, in a heatmap comparing all cases considered. It clearly shows that serpentinization with an HCD of 2 km is productive in prebiotic synthesis regardless of the initial conditions. In the initially reducing conditions of scenario MH (mid-Hadean), carbonaceous bombardment is able to promote the most productive prebiotic synthesis, while enstatite bombardment alone, as modeled here, leads to significantly lower HCN and biomolecule concentrations of up to five orders of magnitude less. In the initially oxidizing conditions of scenario EH (end-Hadean), serpentinization with an HCD of 2 km is required to achieve comparable biomolecule concentrations as in the MH scenario.

For the first time, our model of the Hadean Earth has been able to justify sufficiently high abundances of nucleobases and the sugar ribose in WLPs, in the range used by experiments showing successful formation of nucleotides, the monomers of RNA. Nevertheless, the notoriously low yield of ribose in the formose reaction, even when using very effective catalysts such as $Ca(OH)_2$, remains a challenge, and further advanced theoretical modeling efforts and experimental studies are needed to make a confident statement that ribose abundances are sufficient, as this study finds that they are not yet.

We find that between 1.0 and 2.0 km of HCD, serpentinization becomes capable of reducing even a highly oxidized atmosphere (initially 90 % CO_2). This is the requirement to allow for an effective synthesis of the building blocks of life, i.e., to start from atmospheric HCN and seed the early Earth with the ingredients for the origins of life. This eliminates the need for a primary reducing atmosphere, since serpentinization is a continuous and stable source of reducing gases over long timescales. An initial CO_2-rich atmosphere might even be advantageous, since it can be exploited for its carbon in photochemical HCN synthesis in the atmosphere,

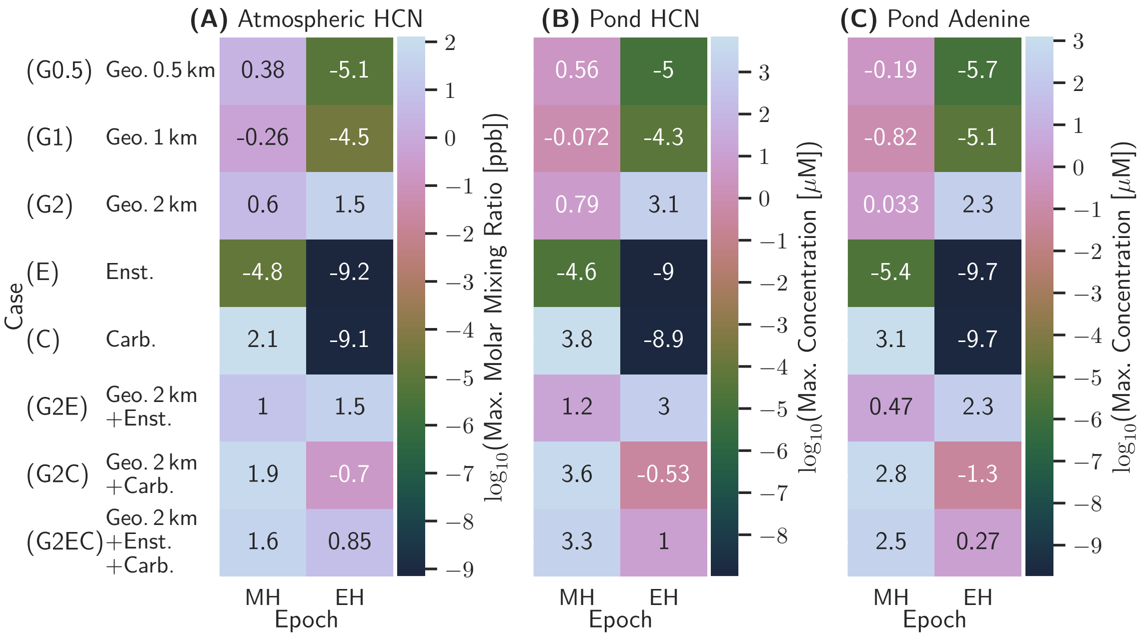

Figure 26.1: Heatmap showing a visual representation of the maximum simulated HCN atmospheric mixing ratios and biomolecule pond concentrations in Tables 24.1 and 24.3. Panel **A** shows the logarithm of the maximum molar mixing ratio of HCN reached in the Hadean atmosphere over all considered cases and both epochs of the mid-Hadean (MH) with an initially reducing atmosphere at 4.4 Gyr as well as the end-Hadean (EH) with an initially oxidizing atmosphere at 4.0 Gyr. Panel **B** shows the logarithm of the maximum concentration of HCN and panel **C** shows the logarithm of the maximum concentration of the biomolecule adenine reached in the pond cycling model over all scenarios. A heatmap plot is a graphical representation that uses color to show the magnitude of values. The representation helps visualize patterns, correlations, and distributions within our dataset across both epochs and all cases considered, where brighter colors represent higher values, and darker colors represent lower values.

as shown in the simulation of case EH_G2. It is crucial to assume serpentinization in a manner appropriate for the Hadean Earth, as estimates of its activity based on the present-day Earth might severely underestimate its potential.

UV irradiation is usually considered a threat to the stability of biomolecules formed by prebiotic synthesis and an argument against considering WLPs as one of the possible sites for the origins of life. With this model, we are able for the first time to achieve rates of biomolecule formation by prebiotic synthesis in WLPs that are high enough to make the influence of UV photodissociation negligible. Despite the fact that water bodies on the first land masses on Earth are exposed to UV, it might not pose a significant threat to the synthesis of the building blocks of the RNA world in the most productive scenarios considered here.

Exogenous delivery of biomolecules by meteorites from space resulted in maximum pond concentrations about two orders of magnitude lower (Pearce, Pudritz, et al. 2017) than the most productive scenario considered in this work. A meteorite falling into a pond during its wet phase, or into ponds that do not completely dry out, might still be an interesting way to temporarily boost biomolecule concentrations and increase yields for nucleoside/-tide synthesis and polymerization, pushing toward the emergence of the RNA world.

Formation of atmospheric HCN by lightning has been included in the model (see Section 23), but produces negligible amounts compared to UV radiation (as also shown in Pearce, Molaverdikhani, Pudritz, Henning, and Cerrillo 2022).

Furthermore, rain-out of H_2CO is negligible, and ribose is predominantly formed by H_2CO synthesized aqueously from HCN in WLPs. These results confirm the findings of Pearce, Molaverdikhani, Pudritz, Henning, and Cerrillo (2022).

Carbonaceous bombardment and immediate HCN synthesis during impact (Kurosawa et al. 2013) might be the most potent source of biomolecules and the building block of life in WLPs. Recent evidence that the HSE excess of the Earth's crust and mantle might have a significant contribution from carbonaceous chondrites (Varas-Reus et al. 2019; Budde et al. 2019; Hopp et al. 2020; Fischer-Gödde, Elfers, et al. 2020) brings this type of impactor back into the picture as a contributor to the reducing inventory of the Hadean atmosphere. In an initially reducing atmosphere (90 % H_2) carbonaceous impactors can fully unfold their potential to provide HCN to the atmosphere and WLPs, whereas in an initially oxidizing atmosphere the N_2/CO_2 ratio in the atmosphere rises too slowly and an already advanced oxidation with high O_2 levels prevents this. Another advantage of the carbonaceous bombardment scenario is that high atmospheric H_2 and CH_4 levels are not required to achieve high biomolecule concentrations in WLPs, potentially preventing a strong greenhouse effect and allowing habitable temperatures on Hadean Earth, setting the stage for the emergence of the RNA world and the origins of life.

The authors would like to thank Kai Kohler and Oliver Trapp for performing formose sugar synthesis experiments for us and providing yields for ribose synthesis from H_2CO. We thank Wolfgang Bach and Mario Trieloff for very fruitful discussions on geological processes, which were instrumental in properly discussing and implementing plausible conditions for the Hadean Earth. A big thank you goes to all the developers of the open-source software Blender, a 3D computer graphics tool, Inkscape, a vector graphics editor, and GIMP, a raster graphics editor, as well as countless creators of tutorials on YouTube for allowing K.P. to render Figure 21.1. We thank the referee for a constructive report that helped to clarify the manuscript. K.P. acknowledges financial support by the Deutsche Forschungsgemeinschaft (DFG, German Research Foundation) under Germany's Excellence Strategy EXC 2181/1 – 390900948 (the Heidelberg STRUCTURES Excellence Cluster). K.P. is a fellow of the International Max Planck Research School for Astronomy and Cosmic Physics at the University of Heidelberg (IMPRS-HD). T.K.H. and D.A.S. acknowledge financial support by the European Research Council under the Horizon 2020 Framework Program via the ERC Advanced Grant Origins 83 24 28. B.K.D.P. is supported by the 51 Pegasi b Postdoctoral Fellowship. R.E.P. is supported by an NSERC Discovery Grant. R.E.P. also gratefully acknowledges the Max Planck Institute for Astronomy for partial support of his sabbatical leave in 2022/23 when this work was started. Funding from Vector Stiftung is greatly acknowledged under project ID P2023-0152.

27

Background: Early Earth's Mantle

The structure, composition, and mechanism active in the Hadean Earth's mantle and crust are mostly unknown, as there is only little in the rock record that survived until today. The rocks embedded in the oldest cratons have been metamorphosed and lost over time, but the highly resistant mineral zircon has been preserved from the Hadean to the present (Harrison 2009). Nevertheless, the conclusions drawn from their investigation can vastly differ. For example, when trying to understand if plate tectonics was active on the Hadean Earth, studies on zircons differing in their methodologies conclude either in favor of active tectonics (Chowdhury et al. 2023) or the opposite (Tarduno et al. 2023). The evidence for active plate tectonics in the Hadean eon (>4 Gyr ago) seems scarce and elusive, and only in the Eoarchean (4–3.6 Gyr ago) it seems certain that subduction was operational (Hastie et al. 2023).

Miyazaki and Korenaga (2022) predict a Hadean Earth with a heterogeneous mantle composition and a thin crust as a consequence of mantle differentiation during magma ocean solidification. Because of the high solubility of water in magma, the primordial mantle was wet, possibly resulting in low melt viscosity and fractional crystallization of the cooling magma ocean (Miyazaki and Korenaga 2019; Dorn and Lichtenberg 2021; Luo et al. 2024). During magma ocean solidification, Mg and SiO_2-rich material would accumulate in the lower mantle, whereas Fe-rich and denser blobs would accumulate in the upper mantle and crust. Since the scale length of re-mixing is shorter than 100 km (Miyazaki and Korenaga 2019), this leads to a heterogeneous structure with a mostly depleted mantle and creates a thin crust and lithosphere. Conversely, a more homogeneous (pyrolitic) composition would lead to a very thick crust and lithosphere, decreasing the likelihood of active plate tectonics.

The heterogeneous Hadean mantle predicted by Miyazaki and Korenaga (2022) allows for active plate tectonics and rapid crustal subduction with velocities around $50\,\mathrm{cm\,yr^{-1}}$ (see also Sleep, Zahnle, and Neuhoff 2001; Zahnle, Arndt, et al. 2007; Sleep, Zahnle, and Lupu 2014). It should be noted that, in contrast, the new models by Guo and Korenaga (2025) employ a linearly decreasing plate velocity throughout the Hadean. In the case of today's Earth, crustal velocities measured as the spreading rates of mid-ocean ridges are much slower, with average values of ∼2–5 cm yr^{-1} (Parsons 1982; Cogné and Humler 2004). Subduction allows the efficient sequestration of large amounts of carbonates, flushing CO_2 out of the atmosphere. This might also be necessary to remove a CO_2 atmosphere of 110–290 bar at the beginning of the Hadean (after the Moon-forming impact). This massive atmosphere might have been outgassed from the global magma ocean with an initial CO_2 mantle concentration of 200–500 ppm, based on present-day volatile budgets (Hirschmann and Dasgupta 2009; Korenaga et al. 2017). Converting this earliest oxidizing atmosphere to the more reducing conditions necessary for an effective prebiotic synthesis might require fast subduction rates, as in the heterogeneous mantle model by Miyazaki and Korenaga (2022). This scenario of a thick CO_2 atmosphere in the earliest Hadean, flushed into the mantle within the first ~ 100 Myr, is also supported in the review by Zahnle, Arndt, et al. (2007).

The iron-enriched Hadean crust formed more olivine than the present-day oceanic crust, which in turn gives rise to a higher potential for the occurrence of the serpentinization reaction. This is a reaction of rocks in contact with water within hydrothermal vent systems. Olivine $(\mathrm{Mg,Fe})_2\mathrm{SiO}_4$ reacts with water to form the minerals serpentine $(\mathrm{Mg,Fe})_{3-\mathrm{Fe}^{3+}}(\mathrm{Si,Fe})_{2-\mathrm{Fe}^{3+}}\mathrm{O}_5(\mathrm{OH})_4$, magnetite $\mathrm{Fe}_3\mathrm{O}_4$, brucite $(\mathrm{Mg,Fe})(\mathrm{OH})_2$, and releases H_2. The ratio between the product minerals depends on the iron content of the olivine as well as the temperature, and Klein et al. (2013) describe it with the following general reaction:

$$\begin{aligned}(\mathrm{Mg,Fe})_2\mathrm{SiO}_4 + \mathrm{vH_2O} &\longrightarrow \mathrm{w(Mg,Fe)(OH)_2}\\ &+ \mathrm{x(Mg,Fe)}_{3-\mathrm{Fe}^{3+}}(\mathrm{Si,Fe})_{2-\mathrm{Fe}^{3+}}\mathrm{O}_5(\mathrm{OH})_4\\ &+ \mathrm{yFe_3O_4} + \mathrm{zH}_{2(\mathrm{aq})},\end{aligned} \tag{27.1}$$

with the generalized stoichiometric coefficients v, w, x, y, and z. Effectively, this reaction oxidizes ferrous (Fe^{2+}) to ferric (Fe^{3+}) iron, and reduces water to H_2. According to Klein et al. (2013), the effective reaction can be summarized as

$$2\,\mathrm{Fe}^{2+}\mathrm{O} + \mathrm{H_2O} \longrightarrow \mathrm{Fe}_2^{3+}\mathrm{O}_3 + \mathrm{H}_{2(\mathrm{aq})}. \tag{27.2}$$

Miyazaki and Korenaga (2022) used the following simplification of Equation 27.1 in their calculation of the H_2 output from the serpentinization reaction:

$$\begin{aligned}3\,\mathrm{Fe_2SiO_4} + 2\,\mathrm{H_2O} &\longrightarrow 2\,\mathrm{Fe_3O_4} + 3\,\mathrm{SiO_2} + 2\,\mathrm{H_2},\\ 3\,\mathrm{Mg_2SiO_4} + \mathrm{SiO_2} + 4\,\mathrm{H_2O} &\longrightarrow 2\,\mathrm{Mg_3Si_2O_5(OH)_4}.\end{aligned} \tag{27.3}$$

The H_2 resulting from the serpentinization reaction can further react to CH_4 by combining it with CO_2. The methane is produced in a combination of the reverse water-gas shift reaction

$$CO_2 + H_2 \longrightarrow CO + H_2O \tag{27.4}$$

and the Fischer-Tropsch reaction

$$CO + 3\,H_2 \longrightarrow CH_4 + H_2O, \tag{27.5}$$

effectively following (McCollom and Seewald 2007):

$$CO_2 + 4\,H_2 \longrightarrow CH_4 + 2\,H_2O. \tag{27.6}$$

Another possibility is to form CH_4 by direct reduction of CO_2 with H_2, facilitated by mineral catalysts in the so-called Sabatier (methanation) reaction, a special case of the Fischer-Tropsch reaction (Holm et al. 2015). The chemical reaction is identical to Equation 27.6, except for the additional participation of catalysts, e.g. the minerals awaruite and chromite (Bradley 2016).

These reactions only operate within the hydrothermal system at high pressures and temperatures inside the smokers. Therefore, the CO_2 involved in the reaction must be be supplied to the reaction inside the hydrothermal vent system, coming directly from the crust and mantle, not from the atmosphere. This mantle CO_2 is either left over from the original inventory in the forming mantle or has been added by subduction from the atmosphere.

The prediction is to have smokers, active undersea volcanoes, "at most of the seafloor" in the early Hadean (Miyazaki and Korenaga 2022). This possibly led to a reduced Hadean atmosphere due to the outgassed reaction products in the serpentinization and Fischer-Tropsch reactions (Equations 27.2 and 27.6).

Another model of serpentinization and subsequent H_2 and methane formation was simulated by Guzmán-Marmolejo et al. (2013). Their study used present-day crustal spreading rates and FeO oceanic crustal content to calculate the H_2 production from serpentinization. They identified the abundance of CO_2 as a limiting reactant due to its limited abundance in aqueous hydrothermal vent systems on present-day Earth. The resulting CH_4 flux from Guzmán-Marmolejo et al. (2013) was used by Pearce, Molaverdikhani, Pudritz, Henning, and Cerrillo (2022). Since the Hadean Earth's mantle and crust might have been very different from the present-day case represented in the study by Guzmán-Marmolejo et al. (2013), Pearce, Molaverdikhani, Pudritz, Henning, and Cerrillo (2022) might have underestimated the geological influence on the Hadean Earth's atmosphere. The ultramafic composition rich in fayalite (Fe^{2+}-rich olivine group) of the Hadean Earth's crust in both homogeneous and heterogeneous cases by Miyazaki and Korenaga (2022) might be more representative of the situation prevailing on the young Earth.

Klein et al. (2013) showed in simulations that olivine-rich rocks (peridotite) produce higher amounts of $H_{2(aq)}$ during serpentinization than pyroxene-rich rocks (pyroxenite). Therefore, the iron-rich Hadean mantle predicted by Miyazaki and Korenaga (2022) entails a higher potential in reducing the Hadean atmosphere than the present-day scenario by Guzmán-Marmolejo et al. (2013).

McCollom and Seewald (2007) reviewed *in situ* measurements of hydrocarbons including CH_4 in hydrothermal vent fluids. They concluded that isotopic studies of $\delta^{13}C$ and $\delta^{2}H$ for CH_4 in combination with compositional studies allow distinguishing sites with abiotic emissions from those dominated by methanogenic organisms. Unsedimented mid-ocean ridges such as "Lost City" or "Rainbow" are assumed to be free of any biological communities or sedimented biological material. Otherwise, these organisms and their remains emit biotic CH_4 resulting from metabolic activity or thermogenic decomposition of biological material. These sites are hosted in serpentinites and are most likely dominated by abiotic CH_4 emission due to serpentinization. Smokers with and without biological activity are clearly distinguishable from one another. This allows getting *in situ* measured emission rates of abiotic CH_4 in the natural environment, which might be representative of smokers active on the Hadean Earth prior to abiogenesis. Cannat et al. (2010) conclude that the most feasible value for the CH_4/H_2 ratio is $\sim 15\,\%$ as derived from *in situ* measurements in fluids emitted from hydrothermal vents off-axis to the Mid-Atlantic Ridge (Charlou et al. 2002; Kelley et al. 2005), representing these uninhabited smokers.

Thompson et al. (2022) have compiled an impressive list of geological methane production processes and corresponding studies comparing various abiotic sources. We refer the reader to this comprehensive compilation, but note that their own calculations, and many of those cited, assumed present-day Earth conditions. The focus of Thompson et al. (2022) was on methane as a biosignature on exoplanets, not on the evolutionary state of the Hadean Earth. Nevertheless, some of the cited studies make predictions for the Hadean Earth and were also used in the discussion Section above for comparison with the present work.

The prebiotic synthesis of biomolecules in WLPs depends on the presence of land masses, which depend on the growth of continental crust and sea level in the Hadean. There is evidence that already in the Hadean the first volcanic islands might have formed near subduction zones between oceanic plates, and these were pushed together by plate tectonics to form the first continental crust (McCulloch and Bennett 1993; Menneken et al. 2007; Keller and Schoene 2018; McCoy-West et al. 2019; Guo and Korenaga 2020; Chowdhury et al. 2023; Guo and Korenaga 2023). The question is whether or not these volcanic islands and continents rose to the surface above sea level. This depends on the volume of the oceans, which depends on the de- and regassing of water from the mantle over time. Evidence from zircons to constrain the behavior of the Hadean mantle and its interaction with water is scarce and limited to a single site (Jack Hills in Western Australia), so one must rely mostly on theoretical models. However, some proposed scenarios include at least temporary volcanic islands (Bada and Korenaga 2018) or possibly even continents (Korenaga 2021) above sea level in the Hadean, which might be sufficient for the presence of Hadean WLPs. Conversely, Russell (2021) argues that the Hadean Earth was a water world.

It must be acknowledged that there is still no consensus found in the geoscientific community regarding the exact characteristics and course of magma ocean solidification, the onset of plate tectonics, plate velocities, water budgets within the mantle, water degassing, and continental growth in the Hadean (Korenaga 2021, and refs. therein). The rock record provides reliable evidence only for the Archean, which might or might not have been very different from the Hadean. Theoretical models of the Hadean Earth depend on many assumptions, leading to large variations within a model, and can lead to very different results between models.

28

Background: Late Veneer/Late Heavy Bombardment/Late Accretion

During its formation, the Earth's interior was molten and differentiated. During this differentiation process, metallic and siderophile elements sink to the core, while lithophile elements remain in the mantle. Therefore, HSEs should be entirely absent in the Earth's mantle, following the metal-silicate equilibrium in the Earth's interior (H. Becker et al. 2006; Brenan and McDonough 2009). However, the HSE concentration in the upper mantle is much higher than predicted by their partitioning behavior. Since experiments have shown that differentiation and equilibration in the Earth's interior cannot explain this HSE excess (Mann et al. 2012), external delivery by impactors is proposed to explain this excess. It is assumed that impactors delivered these HSEs to the upper crust and mantle in the Hadean and Archean. In particular, chondritic material, which unlike Earth is undifferentiated and therefore siderophile-rich, could have composed the impactors, which remained in the upper mantle to explain this HSE excess.

In the geosciences, the term "late veneer" is commonly used to refer to the late delivery of chondritic material to explain this HSE excess in the Earth's mantle, while in planet formation theory, the terms "late accretion" or "late heavy bombardment" refer to a period of impacts distinct from the formation of the Earth (Morbidelli and B. J. Wood 2015), sometimes between $\sim 4.5 - -3.5\,\mathrm{Gyr}$ ago (Chyba, Thomas, et al. 1990; Chyba and Sagan 1992). Based on the lunar cratering record, the term "late heavy bombardment" or "lunar cataclysm" was coined to address the possibility that this period of impacts could have been as short as $\sim 150\,\mathrm{Myr}$ or less (Strom et al. 2005) around $\sim 3.8 - -3.9\,\mathrm{Gyr}$, but this is debated (Zahnle, Arndt, et al. 2007). A combination of a more continuous "late veneer" together with a distinct "late heavy bombardment" phase is also considered (Morbidelli and B. J. Wood 2015). Whether or not this later addition of material is distinct from the Moon-forming impact is unclear (Morbidelli and B. J. Wood 2015; Hopp et al. 2020), but the term "late accretion" is defined as all the material added after the Moon-forming impact.

After a long period in which the scientific community favored a carbonaceous late veneer (see, e.g., Chou et al. 1983), many studies concluded in a late veneer with a composition similar to enstatite chondrites (see, e.g., Fischer-Gödde and Kleine 2017; Dauphas 2017; Bermingham and R. Walker 2017). Enstatite chondrites are rich in iron, poor in volatiles and carbon and might originate from the innermost region of the solar system. An estimate for the amount of accreted enstatite material necessary to explain the HSE excess in the Earth's mantle is about $0.34\,\% M_\oplus$ (R. J. Walker 2009).

Conversely, recent isotope ratio measurements of Ru in Eoarchean rocks support a significant contribution of carbonaceous chondrites to the late veneer (Fischer-Gödde, Elfers, et al. 2020). These rocks are from southwest Greenland and might comprise pre-late veneer material of > 3.7 Gyr age, which might not have fully equilibrated with the rest of the upper mantle. The combination of this pre-late veneer mantle material with carbonaceous chondrites is consistent with the composition of the modern mantle. To explain the full HSE excess in the modern mantle, an upper bound of $0.3\,\% M_\oplus$ of carbonaceous chondritic material of class CM is sufficient, without the need for enstatite impactors. Varas-Reus et al. (2019) come to the same conclusion of a potentially carbonaceous late veneer, but looking at Se isotopes. They give upper bounds of $0.15\,\%\ M_\oplus$ for CI, and $0.26\,\%\ M_\oplus$ for CM chondritic material to explain the full HSE excess. Further studies considering the relative abundances of Se, Te, and S also concluded in a carbonaceous chondrite-like late veneer (CI and CM chondrites, Z. Wang and H. Becker 2013; Braukmüller, Wombacher, Funk, et al. 2019).

Finally, a combined Mo-Ru isotope analysis favors a heterogeneous late veneer with a contribution from both reservoirs (Hopp et al. 2020). In particular, the examination of the Mo isotope ^{94}Mo across all meteorite populations leads to the conclusion that i) the late veneer had a mixed composition and/or ii) a giant impactor, possibly the Moon-forming one, was carbonaceous and/or iii) of mixed enstatite-carbonaceous composition Hopp et al. (2020). All three scenarios are consistent with the Mo-Ru isotope signatures found. Hopp et al. (2020) ruled out a pure carbonaceous chondrite-like late veneer due to the ε^{100}Ru ≈ 0 isotope excess of the bulk silicate Earth (BSE) and ε^{100}Ru < 0 of carbonaceous chondrites. However, the newly found positive ε^{100}Ru of the Eoarchean mantle by Fischer-Gödde, Elfers, et al. (2020) relaxes this constraint, as this positive Eoarchean mantle signature might have been mixed with the negative signature of carbonaceous chondrites in the modern BSE mantle. Therefore, a purely carbonaceous late veneer is a possibility. Bermingham, Tornabene, et al. (2025) also cannot exclude a contribution from carbonaceous material.

28.1 Enstatite Iron-Rich Impactors

If the late veneer was composed of a significant fraction of iron-rich impactors, the idea is that the exogenously introduced iron is able to reduce oxidized atmospheric gases, especially water. The reduced products of the reaction, mainly H_2, are outgassed and are able to convert the atmosphere to a more reduced state, which is beneficial for many prebiotic synthesis mechanisms.

A simple representation of this reduction reaction, where iron reduces water to hydrogen, according to Zahnle, Lupu, et al. (2020), is given by

$$\mathrm{Fe} + \mathrm{H_2O} \longrightarrow \mathrm{FeO} + \mathrm{H_2}. \tag{28.1}$$

In combination with the water-gas shift and the Fisher-Tropsch reactions in Equations 27.4 and 27.5, this allows for the synthesis of methane if the temperature is high enough. These reactions are inhibited at low temperatures in the gas phase (Zahnle, Lupu, et al. 2020), but the energy dissipated at impact might allow for efficient synthesis of methane. Sekine et al. (2003) suggest that the impactor material leaves the atmosphere after impact and might re-enter it in the form of iron and nickel condensates. On the huge collective surface of these fine-grained condensates, a catalyzed version of the Fisher-Tropsch reaction might increase the yield of outgassed CH_4. Peters et al. (2023) showed in experiments that iron meteorites and iron-rich chondritic meteorites as well as volcanic ash can also catalyze these reactions.

28.2 Carbonaceous Impactors

Kurosawa et al. (2013) showed in laboratory experiments that HCN is synthesized during the impact of carbonaceous meteorites. They used hypervelocity impacts of a polycarbonate projectile fired from a gas gun and laser ablation experiments on graphite to study HCN synthesis in an atmosphere of N_2, H_2O, and CO_2 in varying mixing ratios at about 1bar total pressure. As the carbon is vaporized, it reacts to form short hydrocarbons and CN radicals, which recombine to form several nitrile compounds and HCN, according to the simplified reaction equation

$$\mathrm{C} + \mathrm{N_2} + \mathrm{H_2O} \longrightarrow \mathrm{HCN} + \text{nitriles} + \text{hydrocarbons}. \tag{28.2}$$

As the CO_2 mixing ratio is increased, the synthesis of these products becomes more and more suppressed, but is still productive as long as the molar mixing ratio N_2/CO_2 is greater than one. As soon as $N_2/CO_2 < 1$, HCN synthesis stops completely. This can be seen in the data by Kurosawa et al. (2013, Table 3), where at a partial pressure of 500 mbar of N_2 and 530 mbar of CO_2 ($500\,\mathrm{mbar}/530\,\mathrm{mbar} < 1$) no HCN could be detected anymore. Therefore, this process is only feasible for impactors entering a CO_2-poor atmosphere. For $N_2/CO_2 > 35.4$, up to 2.8 mol% of the carbon is converted into HCN, making it an interesting source term for a carbon-rich bombardment. This threshold of 35.4 results from experimental runs with partial pressures of 920 mbar of N_2 and 26 mbar of CO_2 ($920\,\mathrm{mbar}/26\,\mathrm{mbar} = 35.4$), approaching the maximum carbon to HCN conversion as seen in experiments without any CO_2 in the experiment (Kurosawa et al. 2013, Table 3).

29

Model: Timeline

The formation history and composition of the early mantle determined the composition and temperature of the first primordial atmosphere in the early Hadean. The main greenhouse gases of interest are CO_2 and water vapor, which depend on their partitioning between the atmosphere and the mantle. There seems to be a consensus that at the beginning of Earth's history, enormous amounts of CO_2 were released from the mantle, resulting in several 100 bar in the atmosphere (Zahnle, Arndt, et al. 2007; Miyazaki and Korenaga 2022). However, this thick CO_2 atmosphere might not have lasted long, depending on how quickly and efficiently it was deposited as carbonates and subducted into the mantle by plate tectonics. If and when plate tectonics was active in the Hadean is hotly debated, as noted in Section 27 (Chowdhury et al. 2023; Tarduno et al. 2023). If active, all the CO_2 could have been flushed into the mantle within 10–200 Myr (Zahnle, Arndt, et al. 2007; Miyazaki and Korenaga 2022), resulting in a strongly reduced atmosphere dominated by H_2 at ~ 4.4 Gyr.

This H_2 might be the remnant of the first primordial atmosphere accreted from the solar nebula that gave birth to the solar system. Serpentinization of ultramafic material upwelling in the mantle or the reduction by exogenously delivered chondrites further supplied this H_2 atmosphere. This atmosphere might have been further reduced by the emission of CH_4 in hydrothermal vents (see Equation 27.6) and the synthesis of HCN by the carbonaceous portion of the late veneer (see Equation 28.2), which is always productive as the ratio $N_2/CO_2 > 1$.

There seems to be no consensus on whether water was efficiently degassed as the magma ocean solidified on the surface of the nascent Earth. For example, Zahnle, Arndt, et al. (2007) suggested that most of the water was partitioned into surface reservoirs of the magma ocean and degassed from the freezing mantle into the atmosphere. This is based on the assumption that the solidified region of the mantle contained very little hydrated minerals. Oxygen isotope signatures in zircons formed at ~ 4.4 Gyr and younger confirm that they were chemically altered by liquid water (Wilde et al. 2001; Mojzsis et al. 2001; Valley et al. 2005; Cavosie et al. 2005).

Whether this evidence means that the mantle is mostly dry is not clear.

On the other hand, Miyazaki and Korenaga (2022) draw another scenario where most of the water remained in the mantle, assuming that the percolation of volatiles through the porous melt of the freezing magma was too slow and trapped most of them (Hier-Majumder and Hirschmann 2017). This has strong implications for the viscosity of the Hadean mantle. Low viscosity and thus early active plate tectonics promoted very fast renewal of the Hadean Earth's crust, which enhanced the ability of serpentinization to reduce surface water to H_2 and CH_4 (in combination with CO_2 in the mantle), as well as the rapid sequestration of atmospheric CO_2 into the Hadean mantle.

Pearce, Molaverdikhani, Pudritz, Henning, and Cerrillo (2022) constructed a corresponding atmospheric composition under the assumption of maintaining habitability at the surface (0–100 °C). To achieve this, a P-T profile was generated with the 1D radiative transfer code petitRADTRANS (T. Guillot 2010; Mollière et al. 2019). The corresponding set of parameters for a habitable atmosphere with an exemplary temperature of 78 °C in the MH at 4.4 Gyr is summarized in Table 22.1.

Later, toward the end of the Hadean, the rock record indicates more oxidizing conditions again, although it does not date all the way back to 4.0 Gyr ago. For example, redox-sensitive elements in the greenstone belt at 3.8 Gyr seem to indicate that the mantle was as oxidized as it is today (Aulbach and Stagno 2016), resulting in volcanic emission of mostly oxidizing gases (Holland 1984; Catling and Kasting 2017; Wogan, Krissansen-Totton, et al. 2020; Wogan, Catling, et al. 2023). However, Archean metamorphosed mid-ocean ridge basalts and picrites (up to 3.0 Gyr old) show lower oxidation states (Aulbach and Stagno 2016). Thermodynamic calculations also show a decreasing reducing power of serpentinization reactions in upwelling ultramafic rocks over the Archean (3.5 Gyr and younger), setting the stage for the Great Oxidation Event (Leong et al. 2021). Constraints on atmospheric H_2 levels in detrital magnetites in Archean riverbeds (3.0 Gyr) indicate pressures of $< 10^{-2}$ bar (Kadoya and Catling 2019).

Zircons dated back to 4.35 Gyr show oxygen fugacities, indicating that they crystallized in magmatic melts with oxidation states similar to present-day conditions (Trail, E. B. Watson, et al. 2011). This state of the Hadean mantle would be consistent with the quartz-fayalite-magnetite mineral buffer, suggesting that volcanic outgassing would contribute mainly oxidized gases. The assumption that volcanic outgassing strongly influenced the Hadean atmosphere leads to the conclusion that the Hadean atmosphere was oxidized as early as 4.35 Gyr (Trail, E. B. Watson, et al. 2011). However, it is questionable whether fluxes of oxidizing gases from volcanic outgassing might not be outcompeted by secondary geologic processes such as serpentinization. Hadean zircons crystallize at temperatures above 600 °C (Harrison et al. 2007) and therefore probe conditions deep in the Earth's mantle. However, serpentinization of rocks in the near-surface crust is a chemical process that operates independently of the redox state of these deeper regions. Outgassing from hydrothermal vent fields off-axis to the mid-ocean ridges, driven by serpentinization, might result in a Hadean atmosphere out of equilibrium with the Hadean mantle. The present work aims to explore this scenario.

An extrapolation of the rock record to the end of the Hadean, combined with the redox state of the late Hadean mantle, motivates the consideration of an atmosphere in an initially oxidizing state. This might describe a potential scenario of the late Hadean Earth atmosphere in an oxidized state, assuming that serpentinization and the late veneer were not yet able to produce fluxes of reducing gases that significantly affected the Earth's atmosphere. After this point in time, about 4.0 Gyr ago, these sources of reducing gases might have finally begun to contribute significantly, potentially altering this initial state toward more reducing conditions. Starting the simulation with this initially oxidized atmosphere allows us to test whether or not our considered source terms of reducing gases (serpentinization and impact degassing) are capable of transforming the atmosphere into a sufficiently reducing state favorable for the synthesis of HCN and other key precursors of prebiotic organics. This might lead to a reduced Hadean atmosphere out of equilibrium with the more oxidized state of the mantle. Even if this reducing atmosphere begins to equilibrate with the upper parts of the crust and mantle, near-surface zircon crystals might be too inert to be affected. This might explain why 4.35 Gyr old Hadean zircons do not reflect this in their oxygen fugacities. Thus, these oxidized zircons do not necessarily rule out a reduced atmosphere throughout the late Hadean.

A corresponding set of parameters for an initially oxidized and habitable atmosphere with a temperature of 51 °C in the EH at 4.0 Gyr from Pearce, Molaverdikhani, Pudritz, Henning, and Cerrillo (2022) is given in Table 22.1. We build on these two epochs of potential Hadean atmospheres from the previous study by Pearce, Molaverdikhani, Pudritz, Henning, and Cerrillo (2022) and introduce our newly determined source terms of reducing gases plausible in these epochs. The oxidizing atmosphere in the EH starts with a ratio of $N_2/CO_2 \ll 1$. Therefore, the direct synthesis of HCN by the carbonaceous portion of the late veneer (see Equation 28.2) is not operational until the composition of the atmosphere is not inverted by the supply of reducing gases from other considered sources (serpentinization and enstatite bombardment) or by photochemistry in the atmosphere.

30

Model: Sources of Atmospheric Gases

An overview of the source terms for atmospheric gases, including H_2, CO_2, CH_4, and HCN, is summarized in Table 30.1. These include emissions from hydrothermal vents on a global scale in the Hadean, impact degassing from enstatite impacts, and HCN synthesis from carbonaceous impacts. Each source is discussed in more detail in the following Sections.

30.1 Hadean Earth's Mantle Model

The geophysical Hadean mantle model developed by Miyazaki and Korenaga (2022) examines different regimes of mantle convection, as well as the dissolution and degassing of volatiles. The overall budgets of volatiles such as water and CO_2 follow present-day values, but their initial values are based on partitioning between the atmosphere and magma ocean based on solubilities to the silicate melt (see also Dorn and Lichtenberg 2021; Luo et al. 2024).

Overall, the model results in a flux of H_2 to the atmosphere due to serpentinization in hydrothermal vent systems. Upwelling ferrous iron comes into contact with water penetrating the crust through fissures around these submarine volcanic systems. During this process, the iron is oxidized to ferric iron and the water is reduced to H_2. The main parameter that determines how much H_2 is released is the HCD. The deeper the water can penetrate the crust, the more iron can be oxidized.

The most direct way to determine the HCD is to look at the serpentinites left in the crust after contact with water. In particular, the depth of serpentinization in young oceanic crust formed from mid-oceanic ridges is of interest, as we expect the hydrothermal circulation to be prevalent in this environment on the Hadean Earth. Serpentinite formed in subduction zones beneath continental crust, as found on the present Earth, might not be representative of the Hadean Earth, where subduction might be active but massive continental plates are not yet present.

Lissenberg et al. (2024) drilled 1269 m into the Mid-Atlantic Ridge and found

	Flux [$cm^{-2}\,s^{-1}$]			
	Smokers/Mantle		Impacts	
Gas	Hadean	Today	Enstatite	Carbonaceous
H_2	1.87×10^{10} (0.5 km)^{a,b}	6.25×10^{7b}	2.30×10^{11} (4.4 Gyr)^{f}	
	3.74×10^{10} (1.0 km)^{a,b}	$8.6\ \times10^{9c}$	2.30×10^{10} (4.0 Gyr)^{f}	
	7.48×10^{10} (2.0 km)^{a,b}	2.10×10^{9d}		
CO_2	5.17×10^{10} (0.5 km)^{a,b}	$7\ \times10^{-1c}$		
	4.89×10^{10} (1.0 km)^{a,b}	3.00×10^{11e}		
	4.33×10^{10} (2.0 km)^{a,b}			
CH_4	2.77×10^{9} (0.5 km)^{a,b}	9.35×10^{7b}		
	5.61×10^{9} (1.0 km)^{a,b}	$6.8\ \times10^{8c}$		
	1.12×10^{10} (2.0 km)^{a,b}			
HCN				3.35×10^{9}(4.4 Gyr)^{g}
				3.35×10^{8}(4.0 Gyr)^{g}

[a] Miyazaki and Korenaga (2022): Extended model with varying hydrothermal circulation depth (HCD, see Figure 30.1).
[b] Charlou et al. (2002), Kelley et al. (2005), and Cannat et al. (2010): Used methane/hydrogen ratio measured in hydrothermal fluids (≈ 15 %).
[c] Guzmán-Marmolejo et al. (2013)
[d] Liu et al. (2023): Globally up-scaled from smokers at North Atlantic mid-ocean ridge.
[e] Hu et al. (2012)
[f] Pearce, Pudritz, et al. (2017) and Pearce, Molaverdikhani, Pudritz, Henning, and Cerrillo (2022): Complete oxidation of incoming iron ($Fe + H_2O \longrightarrow FeO + H_2$, Zahnle, Lupu, et al. 2020) based on a model of the late veneer using the lunar cratering record.
[g] Kurosawa et al. (2013): For $N_2/CO_2 > 35.4$.

Table 30.1: Atmospheric source fluxes in the Hadean eon due to geological processes and impacts.

serpentinization of the recovered peridotite over the full depth of the drill core. Changes in seismic wave velocities measured in the oceanic crust around slow to ultra-slow spreading ridges indicate the presence of serpentinites to at least 3–4 km below the seafloor (S. Guillot et al. 2015). The degree of serpentinization varies somewhere between $> 97\,\%$ near the surface and $\sim 20\,\%$ in deep regions. Along cracks in the crust, it cannot be excluded that serpentinization might locally extend as far as 8 km below the seafloor, as has been found by seismic measurements of microearthquakes along the Mid-Atlantic Ridge (Toomey et al. 1988; Tilmann et al. 2004; S. Guillot et al. 2015). Computational modeling suggests that thermal cracking of oceanic crust could lead to hydration and subsequent serpentinization of rocks down to depths of 30–50 km (Korenaga 2007). In addition, this might have ruptured the first stagnant lid crust formed on the Hadean Earth, initiating the first plate tectonic convection in the early history of the Earth.

Another way to determine how deep the ocean water penetrates the oceanic

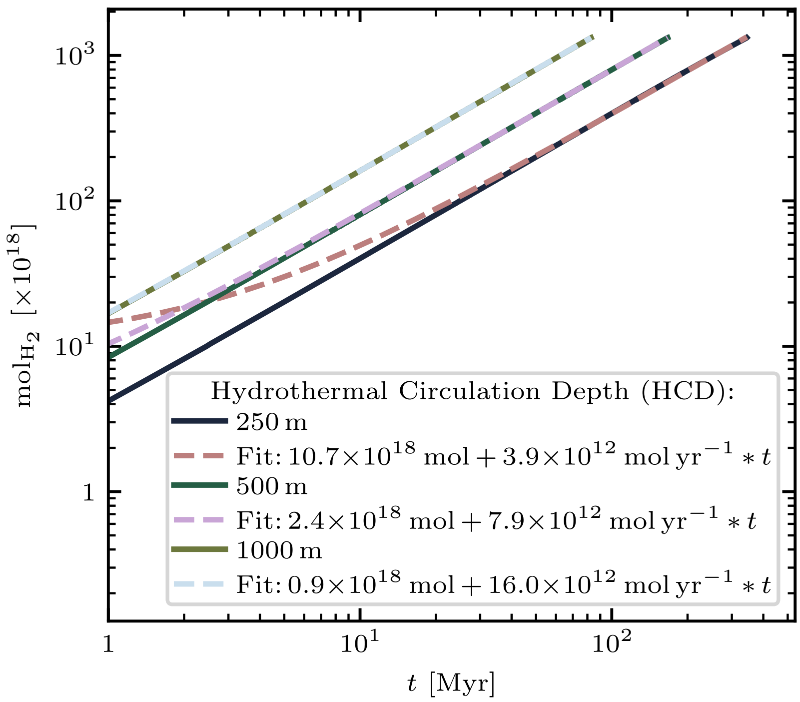

Figure 30.1: Global emissions of H_2 over time from serpentinization in white smokers, hydrothermal vents located off-axis to mid-ocean ridges, in the Hadean. The hydrothermal circulation depth (HCD) was varied in extended calculations of the Hadean mantle model by Miyazaki and Korenaga (2022). Linear fitting allows H_2 surface fluxes to be derived in units of mol yr^{-1}. A doubling of the HCD results in a doubling of the H_2 flux, as more upwelling ferrous iron comes in contact with seawater, promoting the serpentinization reaction.

crust is to look at carbonate deposition. It indicates the alteration of rocks by hydrothermal fluids that enter the cracks and carry dissolved CO_2, which is deposited as carbonates in the cracks. Carbonate deposits can be observed in drill cores taken from the ocean floor. Alteration of the oceanic crust occurs up to 5 km below the seafloor, but the degree of alteration is significantly lower below 500 m and is almost negligible below 2 km (see, e.g., Staudigel et al. 1981; Alt and Teagle 1999).

30.1.1 Mantle Model Assumptions

Miyazaki and Korenaga (2022)'s original model used an HCD of 500 m as a conservative estimate based on the drilling records of carbonate deposits. We used this existing model and extend it to include HCDs of 1 and 2 km. Some exemplary data are shown in Figure 30.1. This is motivated by the fact that an HCD of 2 km is consistent with still rather conservative constraints from both seismic measurements of serpentinization and carbonate deposits in drill cores as described above.

All resulting H_2 surface fluxes were introduced into the photochemical atmosphere model to investigate the impact of HCD on prebiotic synthesis. This approach might better represent Hadean conditions and is supported by the fact that hydrothermal alteration can occur at these depths today. What distinguishes the present model from others is that it is specifically tailored to the Hadean and extends beyond the present-day situation commonly assumed as the basis for calculations in similar models (cf., e.g., Guzmán-Marmolejo et al. 2013; Thompson et al. 2022).

In addition to the H_2 fluxes, the geophysical mantle model also provides a surface degassing flux of $6.53 \times 10^{11}\,\mathrm{kg\,yr^{-1}}$ of CO_2 (Miyazaki and Korenaga 2022), based on the mantle processing rate. In addition, under the high temperatures and pressures of hydrothermal fluids, H_2 and CO_2 can react to form CH_4 according to Equation 27.6. For the most realistic representation of this in our model, we have used the measurements from submersible missions that have sampled the fluid composition emitted from uninhabited hydrothermal vents *in situ* (Charlou et al. 2002; Kelley et al. 2005; Cannat et al. 2010). The CH_4/H_2 ratio is about 15 %.

This ratio can now be combined with Equation 27.6, which states that the production of one mole of CH_4 consumes one mole of CO_2 and four moles of H_2. The model by Miyazaki and Korenaga (2022) provides the initial fluxes Φ_{H_2} and Φ_{CO_2} emitted by the mantle for H_2 and CO_2, respectively, prior to this reaction. As a result, the effectively emitted gas fluxes after this reaction is complete are

$$\Phi_{H_2,\mathrm{eff}} = 0.625 * \Phi_{H_2}, \tag{30.1}$$

$$\Phi_{CH_4,\mathrm{eff}} = 0.09375 * \Phi_{H_2}, \tag{30.2}$$

$$\Phi_{CO_2,\mathrm{eff}} = \Phi_{CO_2} - \Phi_{CH_4}. \tag{30.3}$$

These effective surface fluxes are listed in the second column of Table 30.1. The third column lists surface fluxes predicted or extrapolated from current Earth measurements that differ from those representative of the Hadean.

V

30.2 Bombardment

To quantify the contribution of meteorite impacts in reducing the atmosphere and allowing for prebiotic synthesis during the late veneer, it is first necessary to estimate the rates of meteorite bombardment in the Hadean. For the two scenarios at 4.4 Gyr and 4.0 Gyr, we applied the bombardment rates determined by Pearce, Molaverdikhani, Pudritz, Henning, and Cerrillo (2022) of $1.2 \times 10^{25}\,\mathrm{g\,Gyr^{-1}}$ and $1.2 \times 10^{24}\,\mathrm{g\,Gyr^{-1}}$, respectively, based on exponentially decaying fits to the lunar cratering record analyzed by the Apollo program (Pearce, Pudritz, et al. 2017; Chyba, Thomas, et al. 1990, see Figure 30.2). Comparable bombardment models have also been used in other studies of prebiotic synthesis and the favorable conditions that set the stage for the origins of life on early Earth (Chyba and Sagan 1992; Laneuville et al. 2018; Kadoya, Krissansen-Totton, et al. 2020).

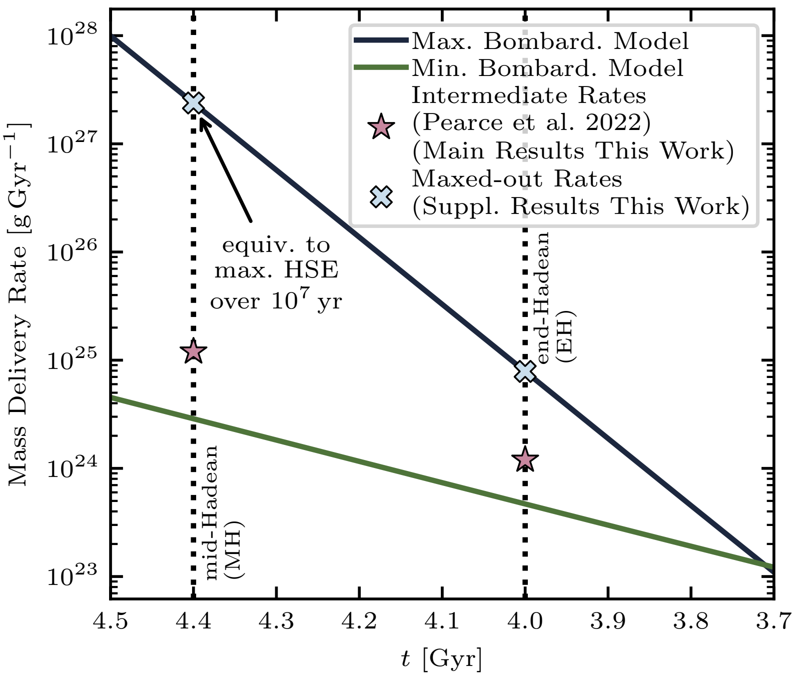

Figure 30.2: Early Earth bombardment models by Pearce, Pudritz, et al. (2017) derived from exponentially decaying fits to the lunar cratering record (Chyba, Thomas, et al. 1990). The red stars represent the intermediate mass delivery rates in the mid-Hadean (MH) at 4.4 Gyr and the end-Hadean (EH) at 4.0 Gyr used by Pearce, Molaverdikhani, Pudritz, Henning, and Cerrillo (2022) and in the main results of this work (Section 24). The maxed-out rates marked with blue crosses were used in the supplementary results of this work (Section 33). The maxed-out rate at 4.4 Gyr roughly corresponds to the total excess of highly siderophile elements (HSEs) of the late veneer spread over a time span of 10 million years, the maximum duration of our atmospheric models. This is equivalent to a single impactor of 2×10^{25} g hitting Earth during the late veneer (Zahnle, Lupu, et al. 2020; Wogan, Catling, et al. 2023).

Red stars in Figure 30.2 mark these intermediate rates, which were used in the main results of this work in Section 24. We assume that these rates do not change substantially over the maximum duration of 10 million years in our atmospheric models and are therefore assumed to be constant in the respective epochs MH or EH, which simplifies the implementation of our simulations.

Blue crosses mark the maxed-out rates in the MH and EH of $2.4 \times 10^{27}\,\mathrm{g\,Gyr^{-1}}$ and $7.9 \times 10^{24}\,\mathrm{g\,Gyr^{-1}}$, respectively, which were used in the supplementary results in Section 33. The maxed-out rate at 4.4 Gyr roughly corresponds to the total excess of HSEs of the late veneer spread over a time span of 10 million years, the maximum duration of our atmospheric models. This is equivalent to a single impactor of 2×10^{25} g (2300 km diameter) hitting Earth during the late veneer (Zahnle, Lupu, et al. 2020; Wogan, Catling, et al. 2023, $2 \times 10^{25}\,\mathrm{g}/10^{7}\,\mathrm{yr} = 2 \times 10^{27}\,\mathrm{g\,Gyr^{-1}} \approx 2.4 \times 10^{27}\,\mathrm{g\,Gyr^{-1}}$).

We then combined this with the rates of reducing gases emitted per impactor

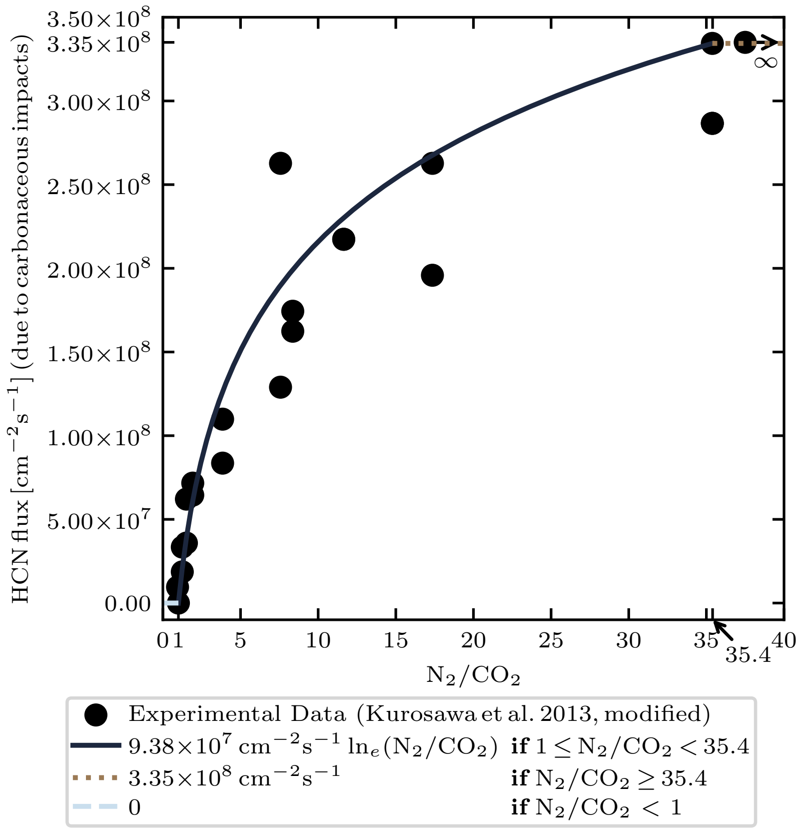

Figure 30.3: Impact degassing of HCN by impacts of carbonaceous chondrites in the EH. The yields of carbon to HCN conversion in the experimental data of Kurosawa et al. (2013, Table 3) were multiplied by the bombardment rate determined by Pearce, Molaverdikhani, Pudritz, Henning, and Cerrillo (2022). The partial pressures of N_2 and CO_2 used in the experiments were divided, and are represented by the plotted ratio N_2/CO_2. By fitting the functions given in the figure legend to the respective ranges of N_2/CO_2, HCN surface fluxes can be derived in units of molecules $\mathrm{HCN\,cm^{-2}\,s^{-1}}$. The data point in the upper right corner represents a measurement without any CO_2 in the atmosphere employed in the experiment. Therefore, this point would have to be at an infinite ratio of N_2/CO_2, since the amount of CO_2 in this measurement was zero.

mass. For enstatite meteorites, equilibrium chemistry calculations of Equation 28.1 by Zahnle, Lupu, et al. (2020) resulted in a rate of $\sim 10^{-21}\,\mathrm{mol\,H_2\,cm^{-2}\,g^{-1}}$ impactor.

Carbonaceous impacts could have facilitated the direct synthesis of HCN in a N_2-H_2O atmosphere. This hypothesis is supported by experiments performed by Kurosawa et al. (2013) and summarized in Equation 28.2. The experiments showed that up to 2.8 mol% of the impacting carbon is converted into HCN when the N_2/CO_2 ratio exceeds 35.4 (as described in Section 28.2). For the carbonaceous component of the bombardment we assumed a carbon content of 3.2 wt%, similar to CI chondrites (Wasson et al. 1988). This amount corresponds to a carbon content of $2.66 \times 10^{-3}\,\mathrm{mol\,C\,g^{-1}}$. Combined this gives a maximum possible HCN production rate of $7.45 \times 10^{-5}\,\mathrm{mol\,HCN\,g^{-1}}$ impactor.

Figure 30.3 shows the performed fits of the experimental data by Kurosawa et al. (2013, Table 3) used to determine the surface flux of HCN generated by impact degassing of carbonaceous chondrites in the Hadean. If the atmosphere contains more CO_2 than N_2 ($N_2/CO_2 < 1$), no HCN formation was detected in the experiments. As soon as more N_2 then CO_2 is in the atmosphere ($N_2/CO_2 > 1$), HCN production during impact starts to increase logarithmically. It reaches a maximum as soon as the amount of N_2 is more than 35.4 times the amount of CO_2 in the surrounding atmosphere.

Overall, this allowed us to infer the global degassing rates of these reducing gases injected into the photochemical atmosphere model. To accomplish this, we combined the bombardment rates of exogenous iron and carbon delivery at a given epoch with the synthesis rates of H_2 and HCN. The results are given in Table 30.1 in the two rightmost columns. The different bombardment rates in the different epochs have been taken into account. In the EH, the initial CO_2 level in the atmosphere was too high to allow HCN synthesis by carbonaceous impacts. Therefore, the HCN flux is not valid until the N_2/CO_2 ratio exceeds 35.4 as the atmospheric composition evolves in the model. To account for different possible compositions of the late veneer (enstatite vs. carbonaceous, see Section 28), we will consider several cases with either a pure enstatite, a pure carbonaceous, or a mixed bombardment.

31

Model: Hadean Earth Scenarios

In a parameter study, we explore different scenarios and their interplay in multiple cases, which serve as the basis for several model runs. The goal is to explore as much of the parameter space as possible.

Table 31.1 presents the different cases analyzed in the reducing scenario during the MH at 4.4 Gyr, while Table 31.2 represents the oxidizing scenario in the EH, 4.0 Gyr ago. Each case listed represents a set of initial parameters that we used in a separate run of the atmosphere model. The parameters are combinations of the source fluxes specified in Table 30.1.

First, in both the reducing and oxidizing cases, we examine how the HCD affects the injection of H_2, CO_2, and methane by the geophysical mantle processes of the early Earth. We will refer to this as the "geology" case G. We examined three specific sub-cases, each with a different HCD of 0.5 km, 1 km, and 2 km, to explore the range that is potentially feasible for the Hadean (see Section 30.1). These sub-cases are designated G0.5, G1, and G2, respectively.

Additionally, we explore the effects of either a purely enstatite or a purely carbonaceous bombardment in cases E and C, respectively. The geological contributions of H_2 and CH_4 are deactivated to examine the reducing potential of the late veneer alone, but the CO_2 emitted by the mantle remains in the model. The purpose is to investigate whether the bombardment is capable of reducing the atmosphere while counteracting the oxidizing gases emitted by volcanism. Numerous models have examined the same interplay between the reducing effect of an exogenous enstatite bombardment and the oxidizing effect of endogenous volcanism in competition with each other (Wogan, Catling, et al. 2023; Zahnle, Lupu, et al. 2020; Itcovitz et al. 2022; Citron and Stewart 2022). Case E will be used to compare our results with these previous studies. We have assumed an HCD of 2 km, which results in the lowest net CO_2 release from the geological model by Miyazaki and Korenaga (2022). Therefore, this represents the best case scenario for the successful reduction of the atmosphere by the late veneer. The same holds for case C, where a purely carbona-

Case	Flux [cm^{-2} s^{-1}]			
	H_2	CO_2	CH_4	HCN
MH_G: Geology only				
MH_G0.5: 0.5 km HCD[a]	1.85×10^{10}	5.17×10^{10}	2.77×10^{9}	
MH_G1: 1.0 km HCD[a]	3.74×10^{10}	4.89×10^{10}	5.61×10^{9}	
MH_G2: 2.0 km HCD[a]	7.48×10^{10}	4.33×10^{10}	1.12×10^{10}	
MH_E: 100 % enstatite bombardment only	2.30×10^{11}	4.33×10^{10}	0	
MH_C: 100 % carbonaceous bombardment only	0	4.33×10^{10}	0	3.35×10^{9}
MH_G2E: Geology (2.0 km) + 100 % enstatite	3.05×10^{11}	4.33×10^{10}	1.12×10^{10}	
MH_G2C: Geology (2.0 km) + 100 % carbonaceous	7.48×10^{10}	4.33×10^{10}	1.12×10^{10}	3.35×10^{9}
MH_G2EC: Geology (2.0 km) + 50 % enstatite + 50 % carbonaceous	1.90×10^{11}	4.33×10^{10}	1.12×10^{10}	1.68×10^{9}

[a] HCD: hydrothermal circulation depth

Table 31.1: Different scenarios considered for the mid-Hadean Earth (MH) in the initially *reducing* scenario at 4.4 Gyr.

Case	Flux [cm^{-2} s^{-1}]			
	H_2	CO_2	CH_4	HCN
EH_G: Geology only				
EH_G0.5: 0.5 km HCD[a]	1.85×10^{10}	5.17×10^{10}	2.77×10^{9}	
EH_G1: 1.0 km HCD[a]	3.74×10^{10}	4.89×10^{10}	5.61×10^{9}	
EH_G2: 2.0 km HCD[a]	7.48×10^{10}	4.33×10^{10}	1.12×10^{10}	
EH_E: 100 % enstatite bombardment only	2.30×10^{10}	4.33×10^{10}	0	
EH_C: 100 % carbonaceous bombardment only	0	4.33×10^{10}	0	3.35×10^{8}
EH_G2E: Geology (2.0 km) + 100 % enstatite	9.78×10^{10}	4.33×10^{10}	1.12×10^{10}	
EH_G2C: Geology (2.0 km) + 100 % carbonaceous	7.48×10^{10}	4.33×10^{10}	1.12×10^{10}	3.35×10^{8}
EH_G2EC: Geology (2.0 km) + 50 % enstatite + 50 % carbonaceous	8.63×10^{10}	4.33×10^{10}	1.12×10^{10}	1.68×10^{8}

[a] HCD: hydrothermal circulation depth

Table 31.2: Different scenarios considered for the end-Hadean Earth (EH) in the initially *oxidizing* scenario at 4.0 Gyr.

ceous bombardment and HCN synthesis competes with the geological CO_2 emission from volcanoes.

Finally, we examined the combination of these source terms by combining the geology with an HCD of 2 km with the enstatite-only bombardment in case G2E, with the carbonaceous-only bombardment in case G2C, and perhaps the most agnostic assumption of a mixed bombardment of half and half composition in case G2EC.

The same cases were considered for the oxidizing scenario summarized in Table 31.2 in the EH at 4.0 Gyr. The main difference is a reduced bombardment rate due to the decline of the late veneer over time, while the geologic mantle fluxes remain unchanged. Since the oxidizing scenario starts with a ratio $N_2/CO_2 < 1$ (see Table 22.1), the source fluxes of reducing gases due to carbonaceous impacts are initially inactive (see Section 28.2). They only become active when this ratio exceeds 1, due to the effects of geology and enstatite bombardment, as well as photochemistry changing the atmospheric composition. This highlights the need to study all these processes and their interactions in combined models, as done in the present study.

32

Supplementary Results: No Seepage

Table 32.1 shows the maximum yields of prebiotic organic molecules reached in the simulation of WLPs in the *absence* of seepage after a simulation period of 10 000 yr. This could be a reasonable scenario if the pores at the bottom of the pond are clogged due to adsorption of biomolecules on the mineral surfaces or deposition of amphiphiles and mineral gels (Hazen and Sverjensky 2010; Deamer 2017; Damer and Deamer 2020a).

	Max. Warm Little Pond Concentration [µM]							
	HCN from Rain-out		H_2CO from Rain-out		H_2CO from Aqueous Synth.[a]		Ribose	
Case	MH (red.)	EH (ox.)	MH (red.)	EH (ox.)	MH (red.)	EH (ox.)	MH (red.)	EH (ox.)
G0.5	4.22×10^{3}	1.21×10^{-2}	2.87×10^{-1}	5.04	1.52×10^{2}	4.37×10^{-4}	1.86×10^{-1}[b]	6.14×10^{-3} [c]
G1	9.78×10^{2}	5.37×10^{-2}	1.14×10^{-3}	2.32	3.52×10^{1}	1.93×10^{-3}	4.30×10^{-2}[b]	2.83×10^{-3} [c]
G2	7.04×10^{3}	5.95×10^{4}	7.87×10^{-6}	5.01	2.54×10^{2}	2.14×10^{3}	3.09×10^{-1}[b]	2.62 [b]
E	2.58×10^{-2}	1.17×10^{-6}	6.46×10^{-10}	2.14×10^{-12}	9.29×10^{-4}	4.23×10^{-8}	1.13×10^{-6}[b]	5.16×10^{-11}[b]
C	2.19×10^{5}	1.34×10^{-6}	6.48×10^{-10}	1.32×10^{-12}	7.88×10^{3}	4.83×10^{-8}	9.61 [b]	5.89×10^{-11}[b]
G2E	1.88×10^{4}	5.44×10^{4}	8.78×10^{-4}	4.00	6.77×10^{2}	1.96×10^{3}	8.26×10^{-1}[b]	2.39 [b]
G2C	1.34×10^{5}	3.39×10^{2}	7.86×10^{-6}	1.42×10^{2}	4.82×10^{3}	1.22×10^{1}	5.89 [b]	1.88×10^{-1} [c]
G2EC	7.73×10^{4}	1.19×10^{4}	6.31×10^{-3}	1.02×10^{1}	2.78×10^{3}	4.29×10^{2}	3.40 [b]	5.36×10^{-1} [b]

	Max. Warm Little Pond Concentration [µM]					
	2-Aminooxazole		Adenine		Guanine	
Case	MH (red.)	EH (ox.)	MH (red.)	EH (ox.)	MH (red.)	EH (ox.)
G0.5	4.65	1.33×10^{-5}	4.85	1.39×10^{-5}	5.59	1.61×10^{-5}
G1	1.08	5.91×10^{-5}	1.12	6.17×10^{-5}	1.29	7.11×10^{-5}
G2	7.75	6.55×10^{1}	8.09	6.84×10^{1}	9.32	7.88×10^{1}
E	2.84×10^{-5}	1.29×10^{-9}	2.97×10^{-5}	1.35×10^{-9}	3.42×10^{-5}	1.56×10^{-9}
C	2.41×10^{2}	1.48×10^{-9}	2.51×10^{2}	1.54×10^{-9}	2.90×10^{2}	1.78×10^{-9}
G2E	2.07×10^{1}	5.99×10^{1}	2.16×10^{1}	6.25×10^{1}	2.49×10^{1}	7.20×10^{1}
G2C	1.47×10^{2}	3.73×10^{-1}	1.54×10^{2}	3.89×10^{-1}	1.77×10^{2}	4.49×10^{-1}
G2EC	8.50×10^{1}	1.31×10^{1}	8.88×10^{1}	1.37×10^{1}	1.02×10^{2}	1.58×10^{1}

	Max. Warm Little Pond Concentration [µM]					
	Cytosine		Uracil		Thymine	
Case	MH (red.)	EH (ox.)	MH (red.)	EH (ox.)	MH (red.)	EH (ox.)
G0.5	4.10×10^{-2}	1.18×10^{-7}	1.72×10^{1}	4.95×10^{-5}	3.38×10^{1}	9.71×10^{-5}
G1	9.50×10^{-3}	5.22×10^{-7}	3.99	2.19×10^{-4}	7.83	4.30×10^{-4}
G2	6.84×10^{-2}	5.78×10^{-1}	2.88×10^{1}	2.43×10^{2}	5.64×10^{1}	4.76×10^{2}
E	2.51×10^{-7}	1.14×10^{-11}	1.05×10^{-4}	4.80×10^{-9}	2.07×10^{-4}	9.40×10^{-9}
C	2.13	1.30×10^{-11}	8.94×10^{2}	5.48×10^{-9}	1.75×10^{3}	1.07×10^{-8}
G2E	1.83×10^{-1}	5.29×10^{-1}	7.68×10^{1}	2.22×10^{2}	1.50×10^{2}	4.35×10^{2}
G2C	1.30	3.29×10^{-3}	5.47×10^{2}	1.38	1.07×10^{3}	2.71
G2EC	7.51×10^{-1}	1.16×10^{-1}	3.16×10^{2}	4.87×10^{1}	6.19×10^{2}	9.55×10^{1}

[a] Formaldehyde synthesized aqueously from rained-out HCN.

[b] Most ribose is synthesized in formose reaction starting from formaldehyde, which in turn is synthesized aqueously from rained-out HCN.

[c] Most ribose is synthesized in formose reaction starting from formaldehyde rained-out directly from the atmosphere.

Table 32.1: Maximum yields of prebiotic organic molecules in warm little ponds (WLPs) with turned off seepage after 10 000 yr.

33

Supplementary Results: Increased Impact Rates

Table 33.1 presents three additional models that explore what happens when the mass delivery rates in Figure 30.2 are at their maximum possible values, in contrast to all the models presented before using intermediate rates of impacting material.

In naming these three cases, *G2EC* refers to a mixed scenario in which serpentinization driven by an HCD of 2 km, 50 % enstatite, and 50 % carbonaceous bombardment are active at the same time. *HSE_max* refers to a bombardment that delivered the entire excess of HSEs to the Hadean Earth spread over a time span of only 10 million years, the maximum duration of our atmospheric models. This means that the late veneer was deposited in only this relatively short period of time in truly cataclysmic events of dwarf planet-sized impacts (2×10^{25} g, 2300 km diameter), as suggested by Zahnle, Lupu, et al. (2020) and Wogan, Catling, et al. (2023). This is equivalent to the maximum rate of impacting material at 4.4 Gyr ago, derived from the lunar cratering record, and fitted with an exponentially decaying bombardment model spanning from 4.5 Gyr to 3.9 Gyr ago (Chyba, Thomas, et al. 1990; Pearce, Pudritz, et al. 2017, see Figure 30.2), denoted *lunar_max*. Therefore, case MH_G2EC_HSE/lunar_max got its name due to this equivalence.

Figures 33.1(MH_G2EC_HSE/lunar_max) and (EH_G2EC_HSE_max) explore what would happen to the atmosphere if the entire late veneer was delivered to the Hadean Earth during the simulated time, either to an initially reducing or oxidizing atmosphere, respectively. In both cases, atmospheric HCN concentrations are mainly driven by direct synthesis during carbonaceous impacts, and their levels reach the 10^{-6} range, two orders of magnitude higher than in the most productive case MH_C (see Table 24.1) using intermediate mass delivery rates in the main results Section 24. In case EH_G2EC_lunar_max, HCN levels reach the 10^{-8} range, comparable to the most productive cases in the main results. This means that even without assuming that dwarf planet-sized impactors struck Earth, the

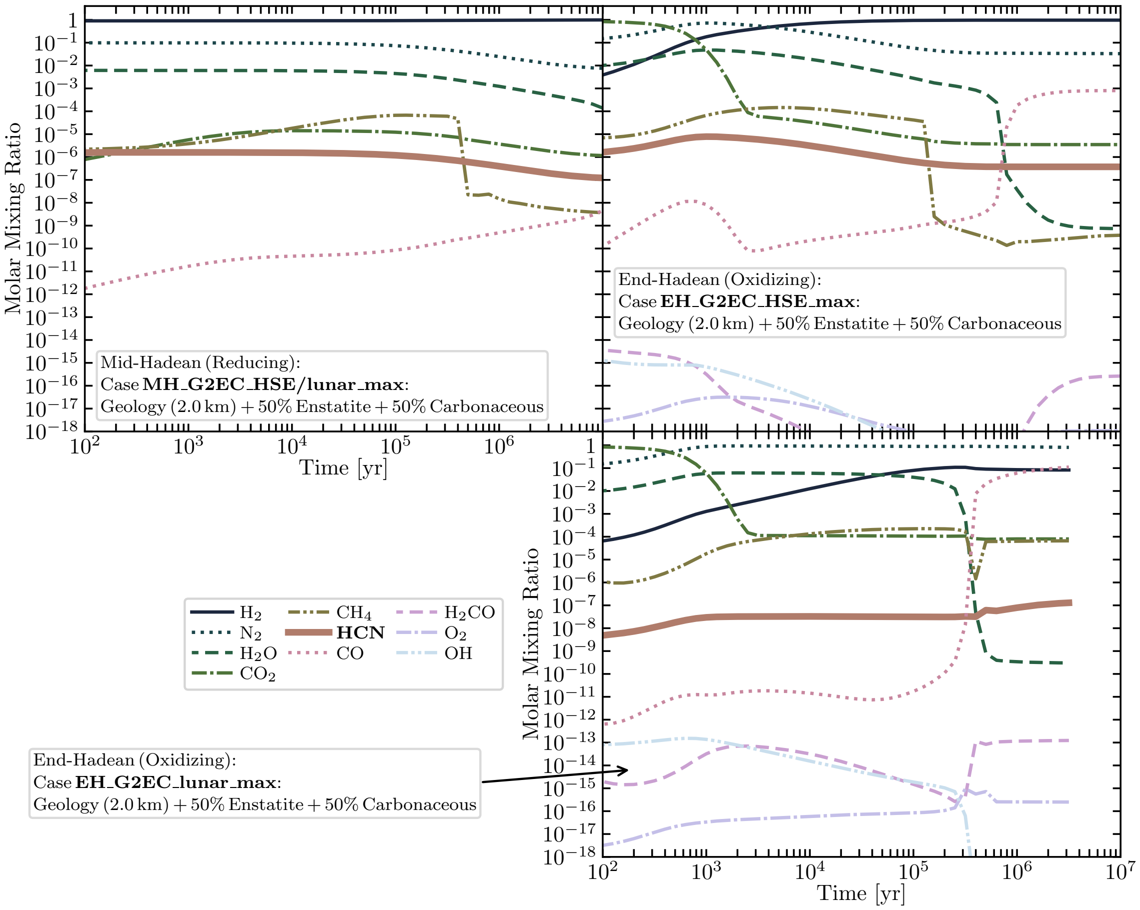

Figure 33.1: Exploring the effect of maxed-out exogenous chondritic bombardment. Shown is the simulated atmospheric composition of key species in the layer closest to the surface as a function of time. All cases consider the combination of geologic and late veneer source terms of atmospheric gases (referred to as *G2EC*), with serpentinization driven by an hydrothermal circulation depth (HCD) of 2 km, and maxed-out bombardment with a composition split half-half between enstatite and carbonaceous chondrites (see Table 33.1). The two epochs of the mid-Hadean (MH) at 4.4 Gyr with reducing initial conditions and the end-Hadean (EH) at 4.0 Gyr with oxidizing initial conditions are compared (left vs. right column). The initial conditions for the reducing and oxidizing models are summarized in Table 22.1, closely following the established atmosphere models developed by Pearce, Molaverdikhani, Pudritz, Henning, and Cerrillo (2022). *HSE_max* refers to a bombardment that delivered the entire excess of highly siderophile elements (HSEs) to the Hadean Earth spread over a time span of only 10 million years, the maximum duration of our atmospheric models. This is equivalent to the maximum rate of impacting material at 4.4 Gyr derived from the lunar cratering record, termed *lunar_max*. Panel **MH_G2EC_HSE/lunar_max** shows the effect of a maxed-out bombardment, comprising the whole late veneer, on the initially reducing atmosphere in the MH. Panel **EH_G2EC_HSE_max** shows the effect of this maxed-out bombardment on the initially oxidized atmosphere in the EH. And panel **EH_G2EC_lunar_max** shows the effect of the maximum bombardment rate derived from the lunar cratering record at this time (4.0 Gyr).

Case	Flux [cm^{-2} s^{-1}]			
	H$_2$	CO$_2$	CH$_4$	HCN
MH_G2EC_HSE/lunar_max @ 4.4 Gyr:	2.29×10^{13}	4.33×10^{10}	1.12×10^{10}	3.35×10^{11}
EH_G2EC_HSE_max (equiv. to lunar_max @ 4.4 Gyr):	2.29×10^{13}	4.33×10^{10}	1.12×10^{10}	3.35×10^{11}
EH_G2EC_lunar_max @ 4.0 Gyr:	1.50×10^{11}	4.33×10^{10}	1.12×10^{10}	1.10×10^{9}

Table 33.1: Additional scenarios considered with maximum impact rates (see Figure 30.2) in the mixed case G2EC (serpentinization driven by an hydrothermal circulation depth (HCD) of 2 km, 50 % enstatite, 50 % carbonaceous bombardment) for both the mid-Hadean (MH) and end-Hadean (EH).

	Max. Rain-out Rate [$\mathrm{kg\,m^{-2}\,yr^{-1}}$]		
Case	CO_2	HCN	H_2CO
MH_G2EC_HSE/lunar_max	1.55×10^{-3}	7.23×10^{-3}	1.35×10^{-10}
EH_G2EC_HSE_max	3.47×10^{-3}	1.40×10^{-2}	1.88×10^{-11}
EH_G2EC_lunar_max	1.15×10^{-2}	5.73×10^{-4}	8.68×10^{-9}

Table 33.2: Maximum resulting rain-out rates of prebiotic precursors with maxed-out bombardment rates.

maximum bombardment model based on the lunar cratering record 4.0 Gyr ago (see Figure 30.2) is capable of producing enough atmospheric HCN to motivate nucleotide synthesis in WLPs, despite the initially CO_2-rich atmosphere.

Table 33.2 presents the maximum rain-out rates for CO_2, HCN, and H_2CO with maxed-out bombardment rates. In particular, the HCN rain-out in case EH_G2EC_HSE_max is very high, reaching the $10^{-2}\,\mathrm{kg\,m^{-2}\,yr^{-1}}$ range, more than an order of magnitude higher than in the most productive case MH_C (see Table 24.2) using intermediate mass delivery rates in the main results Section 24. This shows that if the late veneer was formed in a very short time in a concentrated bombardment in the EH, it might have been able to transform the initially CO_2-rich atmosphere into a reducing state. This is a very promising result to justify a robust prebiotic synthesis throughout the Hadean.

Table 33.3 summarizes the maximum concentrations of prebiotic molecules in WLPs resulting from these three additional cases with maxed-out impact rates, and Table 33.4 shows the corresponding WLP concentrations with seepage turned off due to clogged pores at the bottom of the pond. With seepage, purine concentrations reach the 10 mM range, pyrimidine concentrations reach the mM range, and ribose concentrations reach the µM range. Without seepage, pyrimidine concentrations also reach the 10 mM range, and ribose concentrations reach the 100 µM range. These nucleobase concentrations are about an order of magnitude higher than the intermediate impact rates (see Tables 24.3 and 32.1) and are sufficient for nucleotide synthesis. Even with maxed-out bombardment rates and without seepage, ribose concentrations are close to, but still fall short of, the mM concentrations required for nucleotide synthesis in aqueous solution as performed in laboratory experiments (Ponnamperuma et al. 1963; Fuller et al. 1972b; Nam et al. 2018; Powner et al. 2009).

	Max. Warm Little Pond Concentration [µM]			
Case	HCN from Rain-out	H_2CO from Rain-out	H_2CO from Aqueous Synth.[a]	Ribose
MH_G2EC_HSE/lunar_max	9.22×10^{4}	4.01×10^{-5}	3.32×10^{3}	4.05[b]
EH_G2EC_HSE_max	1.79×10^{5}	5.60×10^{-6}	6.43×10^{3}	7.84[b]
EH_G2EC_lunar_max	6.56×10^{3}	2.59×10^{-3}	2.36×10^{2}	2.88×10^{-1}[b]

	Max. Warm Little Pond Concentration [µM]					
Case	2-Aminooxazole	Adenine	Guanine	Cytosine	Uracil	Thymine
MH_G2EC_HSE/lunar_max	1.01×10^{2}	1.66×10^{4}	1.84×10^{4}	3.32×10^{3}	1.66×10^{3}	1.11×10^{3}
EH_G2EC_HSE_max	1.96×10^{2}	3.21×10^{4}	3.57×10^{4}	6.42×10^{3}	3.21×10^{3}	2.14×10^{3}
EH_G2EC_lunar_max	7.21	1.18×10^{3}	1.31×10^{3}	2.36×10^{2}	1.18×10^{2}	7.87×10^{1}

[a] Formaldehyde synthesized aqueously from rained-out HCN.

[b] Most ribose synthesized in formose reaction starting from formaldehyde, which in turn was aqueously synthesized from rained-out HCN.

Table 33.3: Maximum yields of prebiotic organic molecules in warm little ponds (WLPs) with maxed-out bombardment rates.

Case	Max. Warm Little Pond Concentration [µM]			
	HCN from Rain-out	H_2CO from Rain-out	H_2CO from Aqueous Synth.[a]	Ribose
MH_G2EC_HSE/lunar_max	2.75×10^{6}	4.61×10^{-2}	9.90×10^{4}	1.21×10^{2}[b]
EH_G2EC_HSE_max	5.31×10^{6}	6.44×10^{-3}	1.91×10^{5}	2.33×10^{2}[b]
EH_G2EC_lunar_max	2.18×10^{5}	2.97	7.84×10^{3}	9.57×10^{0}[b]

Case	Max. Warm Little Pond Concentration [µM]					
	2-Aminooxazole	Adenine	Guanine	Cytosine	Uracil	Thymine
MH_G2EC_HSE/lunar_max	3.03×10^{3}	3.16×10^{3}	3.64×10^{3}	2.67×10^{1}	1.12×10^{4}	2.20×10^{4}
EH_G2EC_HSE_max	5.84×10^{3}	6.10×10^{3}	7.02×10^{3}	5.15×10^{1}	2.17×10^{4}	4.25×10^{4}
EH_G2EC_lunar_max	2.40×10^{2}	2.50×10^{2}	2.88×10^{2}	2.12	8.89×10^{2}	1.74×10^{3}

[a] Formaldehyde synthesized aqueously from rained-out HCN.

[b] Most ribose synthesized in formose reaction starting from formaldehyde, which in turn was aqueously synthesized from rained-out HCN.

Table 33.4: Maximum yields of prebiotic organic molecules in warm little ponds (WLPs) with maxed-out bombardment rates and with turned off seepage after 10 000 yr.

Part VI

SUMMARY AND OUTLOOK

34

Summary

The goal of this thesis was to understand prebiotic synthesis as a phenomenon occurring in meteorite parent bodies in space as well as on the Hadean Earth, including their joint contribution to providing the building blocks of life. Crucial to this was an assessment of the environmental conditions governing the efficiency of the chemical reactions in terms of availability of reactants and thermodynamic favorability due to temperature appropriate to various settings, including interplanetary space with icy pebbles drifting inward in the early solar system, the first forming planetesimals and their interiors, or the early Earth's atmosphere and mantle interior. Simulations of prebiotic synthesis for key building blocks of life in these different scenarios were performed. This was based on the remarkable previous work by Pearce and Pudritz (2016), Pearce, Pudritz, et al. (2017), and Pearce, Molaverdikhani, Pudritz, Henning, and Cerrillo (2022) and extended its application to as appropriate as possible scenarios for the environments of protoplanetary disks and the Hadean Earth. This was further extended by a careful quantitative comparison of the meteoritic and geological contributions to the prebiotic inventory of the early Earth, potentially allowing the emergence of the RNA world and ultimately the origins of life.

Compared to meteoritic abundances, the simulated nucleobase and ribose abundances in Parts II and III agree well. For vitamin B_3 in Part IV, the simulated abundances were too high, but this can be explained by the fact that the underlying chemical reaction pathways are intertwined with the sugar formation in the formose reaction. A new reaction pathway to vitamin B_3 has been proposed that involves sugar precursors as intermediates and shares the same pool of reactants. Therefore, some of the intermediates might actually be involved in the formation of sugars such as ribose in Part III. The resulting vitamin B_3 abundances in the simulations are therefore overestimates because the concurrent sugar synthesis was not included in the model due to the high complexity of the autocatalytic formose reaction. It is very difficult to account for all the sugar ”by-products” formed in the notoriously complex product mixture of the formose reaction.

The key improvement to obtain simulated biomolecule abundances consistent with those found in meteorites was to introduce a proper understanding of the volatile depletion in the icy pebbles as they approach the formation region of the planetesimal, before it warms up after its formation due to radiogenic heating before and the chemical reactions start. This allowed to improve the overestimation in the previous study by Pearce and Pudritz (2016) by several orders of magnitude and to accurately fit the meteoritic abundances for the first time. This could be interpreted as a verification that the modeled reaction pathways and the estimation of the initial volatile content realistically describe the processes occurring inside meteorite parent bodies. The majority of the prebiotic molecules found in the carbonaceous asteroids Ryugu and Bennu, and all carbonaceous meteorites, could have been formed by aqueous in situ formation inside their parent planetesimals.

This makes aqueous alteration much less a destructive mechanism, as otherwise often perceived in the literature (see, e.g., Smith et al. 2014; Oba, Takano, Furukawa, et al. 2022), and an important, if not the dominant, productive mechanism forming a rich set of prebiotic molecules, explaining the much richer organic content of the rocky material of asteroids and meteorites compared to comets. Comets are also likely to inherit prebiotic molecules formed in the ISM and protoplanetary disks, but show far less complex organic molecules, with the most complex found being the simplest amino acid glycine (Altwegg, Balsiger, Bar-Nun, et al. 2016). No nucleobases, complex sugars, complex carboxylic acids, etc. have been found in comets to date. So aqueous chemistry might make the difference.

Fujiya et al. (2012) determined the age of carbonates inside CM chondrites by radiometric dating using the ratio of ^{53}Mn and ^{53}Cr isotopes. The idea is to determine when these meteorites, including Murchison, experienced aqueous activity as part of their parent bodies. All meteoritic carbonates studied turned out to have the same age of 4.563 Gyr, which means that the parent bodies of the CM chondrites formed 3.5 Gyr after the formation of the solar system. This fits perfectly with the simulated planetesimal used in Parts II and III and shown in Figures 7.1c and 14.2 with the same assumed formation age of 3.5 Gyr and a radius of 150 km.

Carbonaceous meteorites rich in prebiotic organics might therefore be derived from parent bodies just like the one shown in Figures 9.1 to 9.3, 15.2 and 15.3 in the results Sections of Parts II and III, including the simulated nucleobase and ribose abundances that follow from our theoretical models. Since our calculated molecular abundances agree well with the ranges found in carbonaceous meteorites, these larger planetesimals seem to be a better fit as parent bodies of organic-rich meteorites. The smaller planetesimals also considered in Parts II and III with radii as small as 4 km (see Figures 7.1a and 14.1) would have had to form already much earlier at 1 Myr to remain at temperatures low enough for aqueous synthesis of prebiotic molecules. This conclusion has not yet been discussed in Parts II and III and the corresponding published papers (Paschek, Semenov, et al. 2023; Paschek, Kohler, et al. 2022), and is another compelling confirmation of the ability of our theoretical thermochemical models to accurately model and explain the formation of prebiotic molecules in meteorite parent bodies.

This makes large carbonaceous planetesimals with diameters over 200 km, formed 3.5 Gyr after the birth of our solar system, ideal chemical reactors floating through space and possibly preparing the ingredients for the origins of life on Earth. The later formation of these large bodies prevents them from reaching the boiling point of water, which would stop the formation of prebiotic molecules and destroy them. It also prevents the differentiation of their rocks. These planetesimals could perhaps also seed the building blocks of life on other planets and moons in our solar system, as well as in exoplanetary systems that could host similar prebiotic reactors, waiting to seed the ingredients of alien worlds.

In Part V, we found that the geological processes as well as a carbonaceous bombardment alone are sufficient to reach the necessary biomolecule concentrations in WLPs, potentially sustaining the emergence of the RNA world. In combination, geological processes and impacts can further increase WLP concentrations. But only by assuming the most short-lived and highest bombardment intensity that can be justified by the available evidence for the late veneer, could enstatite bombardment potentially lead to sufficiently high biomolecule concentrations for the emergence of RNA in WLPs.

Serpentinization alone can reduce an atmosphere, even if initially highly reducing with 90 % CO_2, if the hydrothermal circulation of ocean water into the crust is deep enough, up to 2 km, and comes into contact with the much more ferrous iron-rich upwelling magma specific to the Hadean eon compared to present-day Earth. This invalidates the claim of, e.g., Zahnle, Lupu, et al. (2020) and Wogan, Catling, et al. (2023) that volcanic activity only supplied oxidized gases to the Hadean atmosphere, while they only consider the geophysical process of silicate volcanism and completely ignore the chemical processes governing serpentinization. The findings of this thesis emphasize the fact that the geological processes active in the Hadean might have been significantly different from today. Scientific studies of the Hadean Earth cannot rely on extrapolations of conditions indicated by the available evidence from the Archean to the present Phanerozoic eons during the past 3.8 Gyr (Aulbach and Stagno 2016; Rollinson et al. 2017).

As shown in Figure 24.6, the simulations of WLP biomolecule concentrations at the highest maximum HCN rain-out rates across the different scenarios simulated in Part V showed that the destruction of formed biomolecules by UV irradiation inside the pond becomes negligible at these high HCN influx rates. The destruction of prebiotic molecules by UV light is a common concern (see, e.g., Cleaves and Miller 1998; Todd et al. 2021) and is even used as an argument for the origins of life in the deep oceans. In our simulations with UV fluxes appropriate for the Hadean and experimentally verified destruction rates of nucleobases, we found that in the most productive scenarios, including serpentinization with hydrothermal circulation reaching 2 km deep and carbonaceous bombardment, nucleobases formation rates outweigh UV destruction rates by several orders of magnitude. UV light might not be as detrimental to prebiotic synthesis as previously thought.

The delivery of biomolecules formed in space by carbonaceous meteorites is clearly outcompeted by the maximum WLP concentrations reached due to atmospheric photochemistry and rain-out, but during the wet phase of the WLP, the release of these exogenously formed biomolecules can increase the concentrations and enhance nucleotide formation. Therefore, this nicely incorporates the idea that biomolecules formed in space contributed to the origins of life on Earth, as explored in Parts II to IV.

However, the most important finding in Part V and the thesis as a whole is that even in an initially CO_2-rich and therefore oxidizing atmosphere, these geological and meteoritic processes are able to lead to sufficiently high biomolecules concentrations in WLPs. Considering only serpentinization and excluding bombardment, the high initial CO_2 level in the atmosphere acts as a carbon source for atmospheric HCN formation and rain-out. This makes an initially oxidizing atmosphere the most suitable environment for nucleotide formation in WLPs with serpentinization alone. This is a striking finding, as it challenges and might resolve one of the most widely debated dogmas in the origins of life research community, namely that an initially oxidized atmosphere on Hadean Earth would prevent sufficiently effective synthesis of prebiotic molecules (see Section 2.3.1). This goes all the way back to the discussion about the validity of the Miller-Urey experiments.

We find for the first time that this might not be the case, provided that the emission of reducing gases by serpentinization is strong enough in a primordial oxidizing atmosphere, as predicted by countless studies across the planetary and geosciences (see, e.g., Solomatova and Caracas 2021; Johansen, Camprubi, et al. 2024). It might even be the desirable initial state of the atmosphere, as it can provide the carbon necessary for the organic matter formed by prebiotic synthesis. This makes the system of the Hadean Earth a better machinery for the production of, e.g., HCN and biomolecules than previously thought.

Putting all the results of this thesis together, and seeing in the simulations how well all these different mechanisms work together to push the concentrations in WLPs above the threshold necessary for the synthesis of RNA building blocks, it seems almost trivial how the stage was set for the origins of life on our home planet.

It is important to recognize that there are other prebiotic synthesis mechanisms capable of contributing building blocks to the early Earth in addition to those studied in this thesis. Examples include the emergence of life and its building blocks in hydrothermal vents (see, e.g., W. Martin, Baross, et al. 2008), or organic synthesis in the ISM and protoplanetary disks (see, e.g., Sandford et al. 2020), which could have been delivered to Earth by comets, meteorites, and interstellar dust particles. These other theories and contributing mechanisms make it even more promising that the origins of life are a natural mechanism occurring within planetary systems and the universe as a whole, advancing our understanding of how life, and ultimately we, came to be.

35

Outlook

The importance of the interconnection of chemical pathways within parent bodies is an important lesson from the simulations performed in Parts III and IV. In future studies, it might be interesting to attempt to simulate pathways that form several classes of prebiotic molecules simultaneously, to explore what pools of reactants they might share. Since some prebiotic molecules can be formed by different reactions, this might also allow us to deduce which type of reaction is more dominant for a particular type of molecule when checking which pathway allows for a better match with the abundances found in meteorites.

Currently, work is underway to implement a similar simulation for the formation of carboxylic acids in meteorite parent bodies (M. Lee et al. 2025, in prep.), based on a previous review of meteoritic abundances of carboxylic acids and potential aqueous formation pathways suitable for the conditions present inside meteorite parent bodies (Lai et al. 2019).

Malamud et al. (2022) performed theoretical simulations of the redistribution of volatile ices inside comets due to radiogenic heating. The idea is that comets also incorporate short-lived isotopes during their accretion, which leads to their internal heating similar to that of planetesimals. This effect is predicted to be already present in very small comets with radii above a kilometer due to their exceptionally low thermal conductivity, effectively trapping the dissipated heat inside. Comets are loose aggregates of small icy pebbles formed on the outskirts of the forming solar system, and experience only moderate compression due to their low surface gravity. This leads to a high porosity of the comet, with very small contact areas between the pebbles inside the comet. Experimental results have been used to simulate this compression and to obtain an effective thermal conductivity that is realistic for comets.

As a result, it is expected that highly volatile ices, e.g., CO ice, will begin to desorb in the interior of the comet due to warming, initiating the movement of these volatiles, now in gaseous form, radially outward through the interior and refreezing at shallower near-surface layers of the comet. This effectively results in a redistribution of these volatile ices to the surface layers of the comet and a depletion of these volatiles in the core. This means that for larger comets, the abundance of volatile ices measured by observational surveys should increase due to their enrichment near the surface. In compiling a database of measured volatile abundances by reviewing the existing literature, Robinson et al. (2024) found a statistically significant correlation between measured CO/H_2O abundances and the size of the cometary nuclei. For a size distribution of 0.25–30 km this abundance ratio increases by three orders of magnitude.

This means that the abundances of volatiles in icy pebbles, such as those found in the early solar system, are expected to be similar to the composition of small comets. This could make small, pristine comets a good proxy for the composition of icy pebbles as they formed in the early solar system. On the other hand, larger comets have elevated volatile abundances compared to their source material.

In Parts II to IV, cometary abundances of volatiles were used to estimate the initial composition of icy pebbles in the early solar system. Due to radial drift, these icy pebbles move inward within the protoplanetary disk form which they formed, moving closer to the proto-Sun. TPD experiments were used to estimate the volatile loss of the pebbles as they warmed up during the migration process. This volatile loss was then used to estimate the volatile abundances remaining in the icy pebbles as they moved close to the snow line, where they formed into 100 km-sized planetesimals by accretion. Inside the porous rocky interior of the planetesimal, these volatiles then participate in the prebiotic synthesis of biomolecules by aqueous chemistry.

The comets used to estimate the volatile abundances in icy pebbles in Parts II to IV were at the upper end of the size distribution of comets analyzed by Robinson et al. (2024), e.g., comet C/1995 O1 (Hale-Bopp) with a mean radius of 30 km. This means that the volatile enrichment measured in these large comets must be corrected before applying the volatile loss derived from the TPD experimental data. The cometary abundances used in Parts II to IV might be overestimates of the composition of pristine icy pebbles.

A first attempt to account for this was already made, as presented in Figure 35.1. Similar to Figure 10.1, the initial CO concentration is varied according to the volatile depletion estimates discussed above, resulting in nucleobase abundances that agree exceptionally well with meteoritic abundances measured in carbonaceous chondrites. A manuscript for publication is in preparation (Paschek, Malamud, et al. 2025, in prep.).

In recent years, there has been a growing consensus that a significant fraction of water is mixed into the mantle of Earth-sized terrestrial planets, as well as super-Earth's and sub-Neptunes, during their formation (see, e.g., Miyazaki and Korenaga

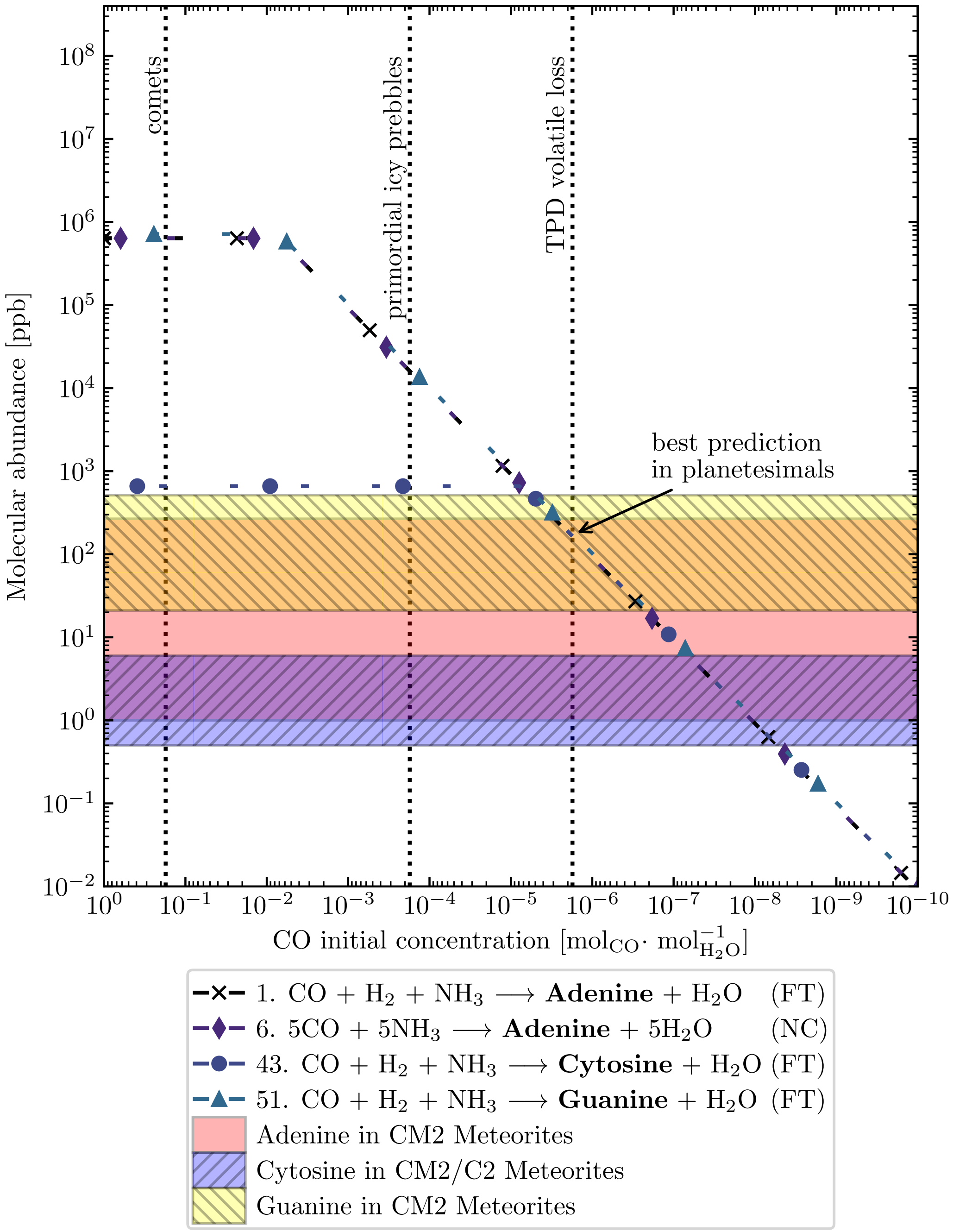

Figure 35.1: Simulated nucleobase abundances in a meteorite parent body as a function of initial CO abundance (normalized to water). The resulting nucleobase abundances are shown for several different simulated reaction pathways involving CO as a reactant, as established in Part II and Table 7.1. The shaded areas show the ranges of measured nucleobase abundances in carbonaceous chondrites. From left to right, the vertical dotted lines indicate the CO abundances as measured in comets, estimated for icy pebbles according to Robinson et al. (2024), and estimated as initially present in meteorite parent bodies using results from temperature programmed desorption (TPD) experiments. An arrow points to the best prediction for nucleobase abundances from prebiotic synthesis simulations, resulting from taking all these volatile depletion estimates into account. Plot from Paschek, Malamud, et al. (2025, in prep.).

2019; Dorn and Lichtenberg 2021; Luo et al. 2024). The geophysical model of the Hadean Earth's mantle by Miyazaki and Korenaga (2022) and used in Part V is based on exactly this highly hydrated mantle, resulting in a heterogeneous composition that allows ferrous iron-rich upwelling of mantle material, which significantly enhances serpentinization on young planets. Due to the increasing number of super-Earth and sub-Neptunian exoplanets discovered, there is also a growing interest in these exoplanets in the scientific community. It might be interesting to apply the geophysical model by Miyazaki and Korenaga (2022) to exoplanets of these larger sizes to estimate the potential for serpentinization and the resulting H_2 and CH_4 emission. Applying this to the atmosphere model in Part V might allow us to assess their potential for prebiotic synthesis of the building blocks of life, as well as to estimate the upper limits of gases emitted by abiotic sources in the hunt for biosignatures in their atmospheres (cf., e.g., Thompson et al. 2022).

List of Figures

List of Tables

References

Abe, Y. (**1993**). 'Physical State of the Very Early Earth'. *Lithos.* The Evolving Earth 30.3, pp. 223–235. DOI: `10.1016/0024-4937(93)90037-D` (cit. on p. 209).

Adler, R. F. and G. Gu (**2024**). 'Global Precipitation for the Year 2023 and How It Relates to Longer Term Variations and Trends'. *Atmosphere* 15.5, p. 535. DOI: `10.3390/atmos15050535` (cit. on p. 198).

Alexander, C. M. O. (**2011**). 'The Molecular Universe'. *IAU Symp. 280.* Ed. by J. Cernicharo and R. Bachiller. Cambridge, UK: Cambridge University Press, p. 288 (cit. on pp. 48, 52).

Alexander, C. M. O., A. P. Boss and R. W. Carlson (**2001**). 'The Early Evolution of the Inner Solar System: A Meteoritic Perspective'. *Science* 293.5527, pp. 64–69. DOI: `10.1126/science.1052872` (cit. on pp. 54, 107).

Alexander, C. M. O., G. D. Cody, B. T. De Gregorio, L. R. Nittler and R. M. Stroud (**2017**). 'The nature, origin and modification of insoluble organic matter in chondrites, the major source of Earth's C and N'. *Geoch* 77.2, pp. 227–256. DOI: `https://doi.org/10.1016/j.chemer.2017.01.007` (cit. on p. 43).

Alt, J. C. and D. A. H. Teagle (**1999**). 'The Uptake of Carbon during Alteration of Ocean Crust'. *Geochimica et Cosmochimica Acta* 63.10, pp. 1527–1535. DOI: `10.1016/S0016-7037(99)00123-4` (cit. on p. 233).

Altwegg, K., H. Balsiger, A. Bar-Nun, J.-J. Berthelier, A. Bieler, P. Bochsler, C. Briois, U. Calmonte, M. R. Combi, H. Cottin et al. (**2016**). 'Prebiotic chemicals–amino acid and phosphorus–in the coma of comet 67P/Churyumov-Gerasimenko'. *SciA* 2.5, e1600285–e1600285. DOI: `10.1126/sciadv.1600285` (cit. on pp. 20, 53, 254).

Altwegg, K., H. Balsiger and S. A. Fuselier (**2019**). 'Cometary Chemistry and the Origin of Icy Solar System Bodies: The View After Rosetta'. *Annu. Rev. Astron. Astrophys.* 57.1, pp. 113–155. DOI: `10.1146/annurev-astro-091918-104409` (cit. on p. 145).

Anders, E. and N. Grevesse (**1989**). 'Abundances of the Elements: Meteoritic and Solar'. *Geochim. Cosmochim. Acta* 53.1, pp. 197–214. DOI: `10.1016/0016-7037(89)90286-X` (cit. on p. 144).

Anglada-Escudé, G., P. J. Amado, J. Barnes, Z. M. Berdiñas, R. P. Butler, G. A. L. Coleman, I. de la Cueva, S. Dreizler, M. Endl, B. Giesers et al. (**2016**). 'A Terrestrial Planet Candidate in a Temperate Orbit around Proxima Centauri'. *Nature* 536.7617, pp. 437–440. DOI: `10.1038/nature19106` (cit. on p. 4).

Armstrong, K., D. J. Frost, C. A. McCammon, D. C. Rubie and T. Boffa Ballaran (**2019**). 'Deep magma ocean formation set the oxidation state of Earth's mantle'. *Science* 365.6456, pp. 903–906. DOI: `10.1126/science.aax8376` (cit. on p. 151).

Attwater, J., A. Raguram, A. S. Morgunov, E. Gianni and P. Holliger (**2018**). 'Ribozyme-catalysed RNA synthesis using triplet building blocks'. *eLife* 7. Ed. by A. M. Pyle, e35255. DOI: `10.7554/eLife.35255` (cit. on pp. 9, 41, 140, 174).

Aulbach, S. and V. Stagno (**2016**). 'Evidence for a Reducing Archean Ambient Mantle and Its Effects on the Carbon Cycle'. *Geology* 44.9, pp. 751–754. DOI: `10.1130/G38070.1` (cit. on pp. 181, 228, 255).

Ayotte, P., R. S. Smith, K. P. Stevenson, Z. Dohnálek, G. A. Kimmel and B. D. Kay (**2001**). 'Effect of porosity on the adsorption, desorption, trapping, and release of volatile gases by amorphous solid water'. *JGRE* 106.E12, pp. 33387–33392. DOI: `10.1029/2000JE001362` (cit. on pp. 20, 45, 55, 56, 58).

Bada, J. L. (**2013**). 'New Insights into Prebiotic Chemistry from Stanley Miller's Spark Discharge Experiments'. *Chemical Society Reviews* 42.5, pp. 2186–2196. DOI: `10.1039/C3CS35433D` (cit. on pp. 33, 174, 178).

Bada, J. L. and J. Korenaga (**2018**). 'Exposed Areas Above Sea Level on Earth >3.5 Gyr Ago: Implications for Prebiotic and Primitive Biotic Chemistry'. *Life* 8.4, p. 55. DOI: `10.3390/life8040055` (cit. on pp. 174, 221).

Bahcall, J. N., M. H. Pinsonneault and S. Basu (**2001**). 'Solar Models: Current Epoch and Time Dependences, Neutrinos, and Helioseismological Properties'. *Astrophysical Journal* 555.2, pp. 990–1012. DOI: `10.1086/321493`. arXiv: `0010346 [astro-ph]` (cit. on p. 62).

Ballotta, B., S. Nandi, V. Barone and S. Rampino (**2021**). 'Gas-Phase Formation and Isomerization Reactions of Cyanoacetaldehyde, a Prebiotic Molecule of Astrochemical Interest'. *ESC* 5.5, pp. 1071–1082. DOI: `10.1021/acsearthspacechem.1c00013` (cit. on p. 48).

Banfalvi, G. (**2021**). 'Prebiotic Pathway from Ribose to RNA Formation'. *Int. J. Mol. Sci.* 22.8. DOI: `10.3390/ijms22083857` (cit. on p. 106).

Barber, D. J. (**1981**). 'Matrix phyllosilicates and associated minerals in C2M carbonaceous chondrites'. *Geochim. Et Cosmochim. Acta* 45.6, pp. 945–970. DOI: `10.1016/0016-7037(81)90120-4` (cit. on pp. 105, 147, 151).

Barnum, T. J., M. A. Siebert, K. L. K. Lee, R. A. Loomis, P. B. Changala, S. B. Charnley, M. L. Sita, C. Xue, A. J. Remijan, A. M. Burkhardt et al. (**2022**). 'A

Search for Heterocycles in GOTHAM Observations of TMC-1'. *J. Phys. Chem. A* 126.17, pp. 2716–2728. DOI: 10.1021/acs.jpca.2c01435 (cit. on p. 162).

Basiuk, V. A. and R. Navarro-González (**1998**). 'Pyrolytic Behavior of Amino Acids and Nucleic Acid Bases: Implications for Their Survival during Extraterrestrial Delivery'. *Icarus* 134.2, pp. 269–278. DOI: 10.1006/icar.1998.5950 (cit. on p. 124).

Becke, A. D. (**1993**). 'Density-functional thermochemistry. III. The role of exact exchange'. *J. Chem. Phys.* 98.7, pp. 5648–5652. DOI: 10.1063/1.464913 (cit. on pp. 113, 168).

Becker, H., M. Horan, R. Walker, S. Gao, J.-P. Lorand and R. Rudnick (**2006**). 'Highly siderophile element composition of the Earth's primitive upper mantle: Constraints from new data on peridotite massifs and xenoliths'. *Geochimica et Cosmochimica Acta* 70.17, pp. 4528–4550. DOI: 10.1016/j.gca.2006.06.004 (cit. on p. 223).

Becker, S., J. Feldmann, S. Wiedemann, H. Okamura, C. Schneider, K. Iwan, A. Crisp, M. Rossa, T. Amatov and T. Carell (**2019**). 'Unified prebiotically plausible synthesis of pyrimidine and purine RNA ribonucleotides'. *Science* 366.6461, pp. 76–82. DOI: 10.1126/science.aax2747 (cit. on pp. 42, 102, 139).

Becker, S., C. Schneider, H. Okamura, A. Crisp, T. Amatov, M. Dejmek and T. Carell (**2018**). 'Wet-dry cycles enable the parallel origin of canonical and non-canonical nucleosides by continuous synthesis'. *Nature Communications* 9.1, pp. 1–9. DOI: 10.1038/s41467-017-02639-1 (cit. on pp. 33, 42, 102, 139, 174, 178, 200, 203, 204, 207).

Becker, S., I. Thoma, A. Deutsch, T. Gehrke, P. Mayer, H. Zipse and T. Carell (**2016**). 'A High-Yielding, Strictly Regioselective Prebiotic Purine Nucleoside Formation Pathway'. *Science* 352.6287, pp. 833–836. DOI: 10.1126/science.aad2808 (cit. on pp. 33, 178, 200, 203, 204, 207).

Bell, E. A., P. Boehnke, T. M. Harrison and W. L. Mao (**2015**). 'Potentially Biogenic Carbon Preserved in a 4.1 Billion-Year-Old Zircon'. *Proceedings of the National Academy of Sciences* 112.47, pp. 14518–14521. DOI: 10.1073/pnas.1517557112 (cit. on p. 27).

Benner, S. A. (**2010**). 'Defining Life'. *Astrobiology* 10.10, pp. 1021–1030. DOI: 10.1089/ast.2010.0524 (cit. on p. 7).

Benner, S. A., E. A. Bell, E. Biondi, R. Brasser, T. Carell, H.-J. Kim, S. J. Mojzsis, A. Omran, M. A. Pasek and D. Trail (**2019**). 'When Did Life Likely Emerge on Earth in an RNA-First Process?'. *ChemSystemsChem* 2.2, e1900035. DOI: 10.1002/syst.201900035 (cit. on pp. 33, 174, 178, 183, 211).

Benner, S. A., H.-J. Kim and E. Biondi (**2019**). 'Prebiotic Chemistry That Could Not Not Have Happened'. *Life* 9.4, p. 84. DOI: `10.3390/life9040084` (cit. on p. 178).

Bera, P. P., M. Nuevo, C. K. Materese, S. A. Sandford and T. J. Lee (**2016**). 'Mechanisms for the formation of thymine under astrophysical conditions and implications for the origin of life'. *JChPh* 144.14, p. 144308. DOI: `10.1063/1.4945745` (cit. on p. 85).

Bera, P. P., M. Nuevo, S. N. Milam, S. A. Sandford and T. J. Lee (**2010**). 'Mechanism for the abiotic synthesis of uracil via UV-induced oxidation of pyrimidine in pure H2O ices under astrophysical conditions'. *JChPh* 133.10, p. 104303. DOI: `10.1063/1.3478524` (cit. on p. 85).

Bera, P. P., T. Stein, M. Head-Gordon and T. J. Lee (**2017**). 'Mechanisms of the Formation of Adenine, Guanine, and Their Analogues in UV-Irradiated Mixed NH3:H2O Molecular Ices Containing Purine'. *AsBio* 17.8, pp. 771–785. DOI: `10.1089/ast.2016.1614` (cit. on p. 85).

Berger, F., M. H. Ramírez-Hernández and M. Ziegler (**2004**). 'The new life of a centenarian: signalling functions of NAD(P)'. *Trends Biochem. Sci.* 29.3, pp. 111–118. DOI: `10.1016/j.tibs.2004.01.007` (cit. on p. 142).

Bergin, E. A., G. A. Blake, F. Ciesla, M. M. Hirschmann and J. Li (**2015**). 'Tracing the ingredients for a habitable earth from interstellar space through planet formation'. *PNAS* 112.29, pp. 8965–8970. DOI: `10.1073/pnas.1500954112`. arXiv: `1507.04756 [astro-ph.EP]` (cit. on p. 53).

Bergner, J. B. and F. Ciesla (**2021**). 'Ice Inheritance in Dynamical Disk Models'. *Astrophys. J.* 919.1, 45, p. 45. DOI: `10.3847/1538-4357/ac0fd7` (cit. on pp. 45, 52, 54, 56, 59, 108).

Bergner, J. B., M. Rajappan and K. I. Öberg (**2022**). 'HCN Snow Lines in Protoplanetary Disks: Constraints from Ice Desorption Experiments'. *Astrophysical Journal* 933.2, p. 206. DOI: `10.3847/1538-4357/ac771e` (cit. on pp. 45, 55, 56, 58).

Bermingham, K. R., H. A. Tornabene, R. J. Walker, L. V. Godfrey, B. S. Meyer, P. Piccoli and S. J. Mojzsis (**2025**). 'The Non-Carbonaceous Nature of Earth's Late-Stage Accretion'. *Geochimica et Cosmochimica Acta* 392, pp. 38–51. DOI: `10.1016/j.gca.2024.11.005` (cit. on pp. 177, 224).

Bermingham, K. R. and R. Walker (**2017**). 'The ruthenium isotopic composition of the oceanic mantle'. *Earth and Planetary Science Letters* 474, pp. 466–473. DOI: `10.1016/j.epsl.2017.06.052` (cit. on p. 224).

Bermingham, K. R., E. Füri, K. Lodders and B. Marty (**2020**). 'The NC-CC Isotope Dichotomy: Implications for the Chemical and Isotopic Evolution of the Early

Solar System'. *Space Sci. Rev.* 216.8, p. 133. DOI: 10.1007/s11214-020-00748-w (cit. on p. 143).

Bernstein, M. P., S. A. Sandford, L. J. Allamandola, S. Chang and M. A. Scharberg (**1995**). 'Organic Compounds Produced by Photolysis of Realistic Interstellar and Cometary Ice Analogs Containing Methanol'. *Astrophys. J.* 454, p. 327. DOI: 10.1086/176485 (cit. on p. 159).

Bieler, A., K. Altwegg, H. Balsiger, A. Bar-Nun, J.-J. Berthelier, P. Bochsler, C. Briois, U. Calmonte, M. Combi, J. De Keyser et al. (**2015**). 'Abundant molecular oxygen in the coma of comet 67P/Churyumov–Gerasimenko'. *Nature* 526.7575, pp. 678–681. DOI: 10.1038/nature15707 (cit. on p. 150).

Birnstiel, T. (**2024**). 'Dust Growth and Evolution in Protoplanetary Disks'. *Annual Review of Astronomy and Astrophysics* 62.Volume 62, 2024, pp. 157–202. DOI: 10.1146/annurev-astro-071221-052705 (cit. on p. 20).

Bitz, S. M. C. and B. Nagy (**1966**). 'Ozonolysis of "polymer-type" material in coal, kerogen and in the orgueil meteorite: a preliminary report '. *PNAS* 56.5, pp. 1383–1390. DOI: 10.1073/pnas.56.5.1383 (cit. on p. 43).

Bland, P. A., O. Alard, G. K. Benedix, A. T. Kearsley, O. N. Menzies, L. E. Watt and N. W. Rogers (**2005**). 'Volatile fractionation in the early solar system and chondrule/matrix complementarity'. *Proc. Natl. Acad. Sci.* 102.39, pp. 13755–13760. DOI: 10.1073/pnas.0501885102 (cit. on pp. 54, 107).

Blokhuis, A., D. Lacoste, P. Nghe and L. Peliti (**2018**). 'Selection Dynamics in Transient Compartmentalization'. *Physical Review Letters* 120.15, p. 158101. DOI: 10.1103/PhysRevLett.120.158101 (cit. on p. 12).

Blum, R. (**2015**). 'Vitamins, 11. Niacin (Nicotinic Acid, Nicotinamide)'. *Ullmann's Encyclopedia of Industrial Chemistry.* John Wiley & Sons, Ltd. Chap. 11, pp. 1–9. ISBN: 9783527306732. DOI: 10.1002/14356007.o27_o14.pub2. eprint: https://onlinelibrary.wiley.com/doi/pdf/10.1002/14356007.o27_o14.pub2 (cit. on p. 140).

Bondeson, J. (**2014**). 'Spontaneous Generation'. *The Feejee Mermaid and Other Essays in Natural and Unnatural History.* Cornell University Press, pp. 193–249. ISBN: 978-1-5017-2227-1. DOI: 10.7591/9781501722271-009 (cit. on p. 3).

Botta, O. and J. L. Bada (**2002**). 'Extraterrestrial organic compounds in meteorites'. *Surveys in Geophysics* 23, pp. 411–467. DOI: 10.1023/A:1020139302770 (cit. on p. 143).

Bradley, A. S. (**2016**). 'The Sluggish Speed of Making Abiotic Methane'. *Proceedings of the National Academy of Sciences* 113.49, pp. 13944–13946. DOI: 10.1073/pnas.1617103113 (cit. on p. 219).

Braukmüller, N., F. Wombacher, C. Funk and C. Münker (**2019**). 'Earth's volatile element depletion pattern inherited from a carbonaceous chondrite-like source'.

Nature Geoscience 12.7, pp. 564–568. DOI: 10.1038/s41561-019-0375-x (cit. on p. 224).

Braukmüller, N., F. Wombacher, D. C. Hezel, R. Escoube and C. Münker (**2018**). ‘The chemical composition of carbonaceous chondrites: Implications for volatile element depletion, complementarity and alteration’. *Geochim. Cosmochim. Acta* 239, pp. 17–48. DOI: 10.1016/j.gca.2018.07.023 (cit. on pp. 54, 107).

Brenan, J. M. and W. F. McDonough (**2009**). ‘Core formation and metal–silicate fractionation of osmium and iridium from gold’. *Nature Geoscience* 2.11, pp. 798–801. DOI: 10.1038/ngeo658 (cit. on p. 223).

Breslow, R. (**1959**). ‘On the mechanism of the formose reaction’. *Tetrahedron Letters* 1.21, pp. 22–26. DOI: 10.1016/S0040-4039(01)99487-0 (cit. on pp. 15, 105, 178, 185, 186, 199).

Brinton, K. L. and J. L. Bada (**1996**). ‘A reexamination of amino acids in lunar soils: Implications for the survival of exogenous organic material during impact delivery’. *Geochim. Et Cosmochim. Acta* 60.2, pp. 349–354. DOI: 10.1016/0016-7037(95)00404-1 (cit. on p. 124).

Brownlee, D., P. Tsou, J. Aléon, C. M. O. Alexander, T. Araki, S. Bajt, G. A. Baratta, R. Bastien, P. Bland, P. Bleuet et al. (**2006**). ‘Comet 81P/Wild 2 Under a Microscope’. *Sci* 314.5806, pp. 1711–1716. DOI: 10.1126/science.1135840 (cit. on pp. 53, 85).

Bryant, D. E. and T. P. Kee (**2006**). ‘Direct evidence for the availability of reactive, water soluble phosphorus on the early Earth. H-Phosphinic acid from the Nantan meteorite’. *Chem. Commun. (Cambridge, U. K.)* 22, p. 2344. DOI: 10.1039/b602651f (cit. on pp. 142, 149).

Buchwald, V. F. (1975). *Handbook of Iron Meteorites – Their History, Distribution, Composition and Structure*. 2nd ed. Berkeley: University of California Press, pp. 381–407. ISBN: 0-520-02934-8 (cit. on p. 47).

Budde, G., C. Burkhardt and T. Kleine (**2019**). ‘Molybdenum isotopic evidence for the late accretion of outer Solar System material to Earth’. *Nature Astronomy* 3.8, pp. 736–741. DOI: 10.1038/s41550-019-0779-y (cit. on pp. 177, 215).

Burbine, T. H., T. J. McCoy, A. Meibom, B. Gladman and K. Keil (**2002**). ‘Meteoritic parent bodies: Their number and identification’. *Asteroids III*. Ed. by W. F. B. Jr., A. Cellino, P. Paolicchi and R. P. Binzel. Tucson, AZ: University of Arizona Press (cit. on pp. 143, 144).

Burbine, T. H., T. J. Mccoy, A. Meibom, B. Gladman and K. Keil (**2002**). ‘Meteoritic Parent Bodies: Their Number and Identification’. *Asteroids III*. Ed. by W. F. Bottke Jr., A. Cellino, P. Paolicchi and R. P. Binzel. Tucson, AZ, USA: University of Arizona Press, pp. 653–667 (cit. on pp. 22, 25, 53, 61, 107).

Burbine, T. H. (**1998**). 'Could G-class Asteroids Be the Parent Bodies of the CM Chondrites?'. *Meteorit. Planet. Sci.* 33.2, pp. 253–258. DOI: `10.1111/j.1945-5100.1998.tb01630.x` (cit. on pp. 25, 144).

Burke, D. J., F. Puletti, W. A. Brown, P. M. Woods, S. Viti and B. Slater (**2014**). 'Glycolaldehyde, methyl formate and acetic acid adsorption and thermal desorption from interstellar ices'. *Mon. Not. R. Astron. Soc.* 447.2, pp. 1444–1451. DOI: `10.1093/mnras/stu2490` (cit. on p. 109).

Burkhardt, C., F. Spitzer, A. Morbidelli, G. Budde, J. H. Render, T. S. Kruijer and T. Kleine (**2021**). 'Terrestrial planet formation from lost inner solar system material'. *Science Advances* 7.52, eabj7601. DOI: `10.1126/sciadv.abj7601` (cit. on p. 109).

Bürkle, A. (**2005**). 'Poly(ADP-ribose)'. *FEBS J.* 272.18, pp. 4576–4589. DOI: `10.1111/j.1742-4658.2005.04864.x`. eprint: `https://febs.onlinelibrary.wiley.com/doi/pdf/10.1111/j.1742-4658.2005.04864.x` (cit. on p. 142).

Burton, A. S., J. C. Stern, J. E. Elsila, D. P. Glavin and J. P. Dworkin (**2012**). 'Understanding Prebiotic Chemistry through the Analysis of Extraterrestrial Amino Acids and Nucleobases in Meteorites'. *Chemical Society Reviews* 41.16, pp. 5459–5472. DOI: `10.1039/C2CS35109A` (cit. on p. 4).

Butlerow, A. (**1861**). 'Bildung einer zuckerartigen Substanz durch Synthese'. *Justus Liebigs Ann. Der Chem.* 120.3, pp. 295–298. DOI: `10.1002/jlac.18611200308` (cit. on pp. 15, 105, 178, 185, 186, 199).

Cafferty, B. J., D. M. Fialho, J. Khanam, R. Krishnamurthy and N. V. Hud (**2016**). 'Spontaneous formation and base pairing of plausible prebiotic nucleotides in water'. *NatCo* 7.1, p. 11328. DOI: `10.1038/ncomms11328` (cit. on p. 42).

Cafferty, B. J. and N. V. Hud (**2015**). 'Was a Pyrimidine-Pyrimidine Base Pair the Ancestor of Watson-Crick Base Pairs? Insights from a Systematic Approach to the Origin of RNA'. *Israel Journal of Chemistry* 55.8, pp. 891–905. DOI: `10.1002/ijch.201400206` (cit. on p. 42).

Callahan, M. P., K. E. Smith, H. J. Cleaves, J. Ruzicka, J. C. Stern, D. P. Glavin, C. H. House and J. P. Dworkin (**2011**). 'Carbonaceous meteorites contain a wide range of extraterrestrial nucleobases'. *PNAS* 108.34, pp. 13995–13998. DOI: `10.1073/pnas.1106493108` (cit. on pp. 24, 43, 45, 66, 67, 78, 80, 142, 178).

Cameron, A. G. W. and J. W. Truran (**1977**). 'The Supernova Trigger for Formation of the Solar System'. *Icarus* 30.3, pp. 447–461. DOI: `10.1016/0019-1035(77)90101-4` (cit. on pp. 22, 155).

Cammi, R. and J. Tomasi (**1995**). 'Remarks on the use of the apparent surface charges (ASC) methods in solvation problems: Iterative versus matrix-inversion procedures and the renormalization of the apparent charges'. *J. Comput. Chem.* 16.12, pp. 1449–1458. DOI: `10.1002/jcc.540161202` (cit. on pp. 113, 168).

Cannat, M., F. Fontaine and J. EscartíN (**2010**). 'Serpentinization and Associated Hydrogen And Methane Fluxes at Slow Spreading Ridges'. *Diversity Of Hydrothermal Systems On Slow Spreading Ocean Ridges.* American Geophysical Union (AGU), pp. 241–264. ISBN: 9781118666616. DOI: 10.1029/2008GM000760 (cit. on pp. 220, 232, 234).

Cannizzaro, S. (**1853**). 'Ueber den der Benzoësäure entsprechenden Alkohol'. *Justus Liebigs Ann. Der Chem.* 88.1, pp. 129–130. DOI: 10.1002/jlac.18530880114 (cit. on pp. 17, 105).

Cassen, P. (**2001**). 'Nebular thermal evolution and the properties of primitive planetary materials'. *Meteorit. & Planet. Sci.* 36.5, pp. 671–700. DOI: 10.1111/j.1945-5100.2001.tb01908.x (cit. on pp. 54, 107).

Catling, D. C. and J. F. Kasting (2017). *Atmospheric Evolution on Inhabited and Lifeless Worlds.* Cambridge: Cambridge University Press. ISBN: 978-0-521-84412-3. DOI: 10.1017/9781139020558 (cit. on pp. 4, 31, 181, 210, 228).

Cavosie, A. J., J. W. Valley, S. A. Wilde and E.i.m.f. (**2005**). 'Magmatic δ18O in 4400–3900 Ma Detrital Zircons: A Record of the Alteration and Recycling of Crust in the Early Archean'. *Earth and Planetary Science Letters* 235.3, pp. 663–681. DOI: 10.1016/j.epsl.2005.04.028 (cit. on p. 227).

Ceccarelli, C., P. Caselli, D. Bockelée-Morvan, O. Mousis, S. Pizzarello, F. Robert and D. A. Semenov (**2014**). 'Deuterium Fractionation: The Ariadne's Thread from the Precollapse Phase to Meteorites and Comets Today'. *Protostars and Planets VI.* Ed. by H. Beuther, R. S. Klessen, C. P. Dullemond and T. K. Henning. Tucson, AZ, USA: University of Arizona Press, pp. 859–882. DOI: 10.2458/azu_uapress_9780816531240-ch037 (cit. on p. 22).

Cech, T. R. (**1986**). 'A model for the RNA-catalyzed replication of RNA'. *Proc. Natl. Acad. Sci.* 83.12, pp. 4360–4363. DOI: 10.1073/pnas.83.12.4360 (cit. on pp. 9, 41, 101, 140, 174).

Chakrabarti, A. C., R. R. Breaker, G. F. Joyce and D. W. Deamer (**1994**). 'Production of RNA by a polymerase protein encapsulated within phospholipid vesicles'. *JMolE* 39.6, pp. 555–559. DOI: 10.1007/bf00160400 (cit. on p. 42).

Charlou, J. L., J. P. Donval, Y. Fouquet, P. Jean-Baptiste and N. Holm (**2002**). 'Geochemistry of High H2 and CH4 Vent Fluids Issuing from Ultramafic Rocks at the Rainbow Hydrothermal Field (36°14′N, MAR)'. *Chemical Geology* 191.4, pp. 345–359. DOI: 10.1016/S0009-2541(02)00134-1 (cit. on pp. 220, 232, 234).

Charnley, S. B., Y.-J. Kuan, H.-C. Huang, O. Botta, H. M. Butner, N. Cox, D. Despois, P. Ehrenfreund, Z. Kisiel, Y.-Y. Lee et al. (**2005**). 'Astronomical Searches for Nitrogen Heterocycles'. *Adv. Space Res.* Space Life Sciences: Astrobiology: Steps toward Origin of Life and Titan before Cassini 36.2, pp. 137–145. DOI: 10.1016/j.asr.2005.09.005 (cit. on p. 162).

Chen, Q.-Q., Z.-R. Zhao and X. Wang (**2021**). 'A Prebiotic Ribosylation of Pyrimidine Nucleobases Enabled by Metal Cations and Clay Minerals'. *Life* 11.12. DOI: `10.3390/life11121381` (cit. on p. 128).

Chen, Y. G., W. E. Kowtoniuk, I. Agarwal, Y. Shen and D. R. Liu (**2009**). 'LC/MS analysis of cellular RNA reveals NAD-linked RNA'. *Nat. Chem. Biol.* 5.12, pp. 879–881. DOI: `10.1038/nchembio.235` (cit. on p. 142).

Chou, C.-L., D. M. Shaw and J. H. Crocket (**1983**). 'Siderophile Trace Elements in the Earth's Oceanic Crust and Upper Mantle'. *Journal of Geophysical Research: Solid Earth* 88.S02, A507–A518. DOI: `10.1029/JB088iS02p0A507` (cit. on p. 224).

Choughuley, A. S., A. S. Subbaraman, Z. A. Kazi and M. S. Chadha (**1977**). 'A possible prebiotic synthesis of thymine: Uracil-formaldehyde-formic acid reaction'. *Biosystems* 9.2-3, pp. 73–80. DOI: `10.1016/0303-2647(77)90014-4` (cit. on pp. 47, 50).

Chowdhury, W., D. Trail, M. Miller and P. Savage (**2023**). 'Eoarchean and Hadean Melts Reveal Arc-like Trace Element and Isotopic Signatures'. *Nature Communications* 14.1, p. 1140. DOI: `10.1038/s41467-023-36538-5` (cit. on pp. 27, 32, 174, 176, 178, 181, 210, 217, 220, 227).

Chyba, C. F. and C. Sagan (**1992**). 'Endogenous production, exogenous delivery and impact-shock synthesis of organic molecules: an inventory for the origins of life'. *Nature* 355.6356, pp. 125–132. DOI: `10.1038/355125a0` (cit. on pp. 14, 101, 124, 139, 223, 234).

Chyba, C. F., P. J. Thomas, L. Brookshaw and C. Sagan (**1990**). 'Cometary delivery of organic molecules to the early earth'. *Science* 249.4967, pp. 366–373. DOI: `10.1126/science.11538074` (cit. on pp. 101, 124, 173, 183, 223, 234, 235, 245).

Ciesla, F. and S. A. Sandford (**2012**). 'Organic Synthesis via Irradiation and Warming of Ice Grains in the Solar Nebula'. *Sci* 336.6080, pp. 452–454. DOI: `10.1126/science.1217291` (cit. on pp. 53, 85).

Citron, R. I. and S. T. Stewart (**2022**). 'Large Impacts onto the Early Earth: Planetary Sterilization and Iron Delivery'. *The Planetary Science Journal* 3.5, p. 116. DOI: `10.3847/PSJ/ac66e8` (cit. on pp. 183, 211, 239).

Clapper, D. L., T. F. Walseth, P. J. Dargie and H. C. Lee (**1987**). 'Pyridine nucleotide metabolites stimulate calcium release from sea urchin egg microsomes desensitized to inositol trisphosphate.'. *J. Biol. Chem.* 262.20, pp. 9561–9568. DOI: `10.1016/S0021-9258(18)47970-7` (cit. on p. 142).

Cleaves, H. J., J. H. Chalmers, A. Lazcano, S. L. Miller and J. L. Bada (**2008**). 'A Reassessment of Prebiotic Organic Synthesis in Neutral Planetary Atmospheres'. *Origins of Life and Evolution of Biospheres* 38.2, pp. 105–115. DOI: `10.1007/s11084-007-9120-3` (cit. on pp. 14, 174).

Cleaves, H. J. and S. L. Miller (**1998**). 'Oceanic Protection of Prebiotic Organic Compounds from UV Radiation'. *Proceedings of the National Academy of Sciences* 95.13, pp. 7260–7263. DOI: `10.1073/pnas.95.13.7260` (cit. on p. 256).

— (**2001**). 'The Nicotinamide Biosynthetic Pathway Is a By-Product of the RNA World'. *J. Mol. Evol.* 52.1, pp. 73–77. DOI: `10.1007/s002390010135` (cit. on pp. 147, 148, 151, 158, 162, 164).

Cleaves, H. J. (**2015**). 'Formose Reaction'. *Encyclopedia of Astrobiology*. Ed. by M. Gargaud, W. M. Irvine, R. Amils, H. J. Cleaves, D. L. Pinti, J. C. Quintanilla, D. Rouan, T. Spohn, S. Tirard and M. Viso. Berlin, Hdoielberg: Springer, pp. 877–884. ISBN: 978-3-662-44185-5. DOI: `10.1007/978-3-662-44185-5_587` (cit. on pp. 158, 159, 178).

Cobb, A. K. and R. E. Pudritz (**2014a**). 'Nature's starships. I. Observed abundances and relative frequencies of amino acids in meteorites'. *Astrophys. J.* 783.2, p. 140. DOI: `10.1088/0004-637X/783/2/140` (cit. on pp. 143, 147, 151, 163).

— (**2014b**). 'Nature's Starships. I. Observed Abundances and Relative Frequencies of Amino Acids in Meteorites'. *Astrophys. J.* 783.2, p. 140. DOI: `10.1088/0004-637x/783/2/140` (cit. on pp. 24, 25, 124).

Cobb, A. K., R. E. Pudritz and B. K. D. Pearce (**2015**). 'Nature's Starships. II. Simulating the Synthesis of Amino Acids in Meteorite Parent Bodies'. *Astrophys. J.* 809.1, p. 6. DOI: `10.1088/0004-637x/809/1/6` (cit. on pp. 26, 48, 51, 57, 59, 60, 70, 88, 107, 110, 112–114, 144, 145, 147, 157, 163, 166).

Cobb, M. and N. Comfort (**2023**). 'What Rosalind Franklin Truly Contributed to the Discovery of DNA's Structure'. *Nature* 616.7958, pp. 657–660. DOI: `10.1038/d41586-023-01313-5` (cit. on p. 3).

Cogné, J.-P. and E. Humler (**2004**). 'Temporal Variation of Oceanic Spreading and Crustal Production Rates during the Last 180 My'. *Earth and Planetary Science Letters* 227.3, pp. 427–439. DOI: `10.1016/j.epsl.2004.09.002` (cit. on p. 218).

Cojocaru, R. and P. J. Unrau (**2021**). 'Processive RNA polymerization and promoter recognition in an RNA World'. *Sci* 371.6535, pp. 1225–1232. DOI: `10.1126/science.abd9191` (cit. on pp. 9, 41, 140, 174).

Collings, M. P., M. A. Anderson, R. Chen, J. W. Dever, S. Viti, D. A. Williams and M. R. S. McCoustra (**2004**). 'A laboratory survey of the thermal desorption of astrophysically relevant molecules'. *Monthly Notices of the Royal Astronomical Society* 354.4, pp. 1133–1140. DOI: `10.1111/j.1365-2966.2004.08272.x` (cit. on pp. 20, 45, 55, 56, 58).

Couto, N., N. Malys, S. J. Gaskell and J. Barber (**2013**). 'Partition and Turnover of Glutathione Reductase from Saccharomyces cerevisiae: A Proteomic Approach'. *J. Proteome Res.* 12 (6). DOI: `10.1021/pr4001948` (cit. on p. 142).

Crick, F. H. C. (**1968**). 'The origin of the genetic code'. *Journal of Molecular Biology* 38.3, pp. 367–379. DOI: `10.1016/0022-2836(68)90392-6` (cit. on p. 42).

Cuppen, H. M., C. Walsh, T. Lamberts, D. A. Semenov, R. T. Garrod, E. M. Penteado and S. Ioppolo (**2017**). 'Grain Surface Models and Data for Astrochemistry'. *Space Sci. Rev.* 212.1-2, pp. 1–58. DOI: `10.1007/s11214-016-0319-3` (cit. on pp. 55, 107, 108).

Cuppen, H. M., H. Linnartz and S. Ioppolo (**2024**). 'Laboratory and Computational Studies of Interstellar Ices'. *Annual Review of Astronomy and Astrophysics* 62.Volume 62, 2024, pp. 243–286. DOI: `10.1146/annurev-astro-071221-052732` (cit. on pp. 19, 20).

Curtiss, L. A., K. Raghavachari, P. C. Redfern and J. A. Pople (**1997**). 'Assessment of Gaussian-2 and density functional theories for the computation of enthalpies of formation'. *J. Chem. Phys.* 106.3, pp. 1063–1079. DOI: `10.1063/1.473182` (cit. on pp. 114, 168).

Cysewski, P., M. Przybyłek, A. Kowalska and N. Tymorek (**2021**). 'Thermodynamics and Intermolecular Interactions of Nicotinamide in Neat and Binary Solutions: Experimental Measurements and COSMO-RS Concentration Dependent Reactions Investigations'. *Int. J. Mol. Sci.* 22.14. DOI: `10.3390/ijms22147365` (cit. on p. 167).

d'Ischia, M., P. Manini, Z. Martins, L. Remusat, C. M. O. Alexander, C. Puzzarini, V. Barone and R. Saladino (**2021**). 'Insoluble organic matter in chondrites: Archetypal melanin-like PAH-based multifunctionality at the origin of life?'. *PhLRv* 37, pp. 65–93. DOI: `https://doi.org/10.1016/j.plrev.2021.03.002` (cit. on p. 43).

Da Silva, L., M. C. Maurel and D. W. Deamer (**2015**). 'Salt-Promoted Synthesis of RNA-like Molecules in Simulated Hydrothermal Conditions'. *J. Mol. Evol.* 80.2, pp. 86–97. DOI: `10.1007/s00239-014-9661-9` (cit. on pp. 33, 42, 101, 102, 139, 178).

Dalrymple, G. B. (**2001**). 'The Age of the Earth in the Twentieth Century: A Problem (Mostly) Solved'. *Geological Society, London, Special Publications* 190.1, pp. 205–221. DOI: `10.1144/GSL.SP.2001.190.01.14` (cit. on p. 27).

Damer, B. and D. W. Deamer (**2020a**). 'The Hot Spring Hypothesis for an Origin of Life'. *Astrobiology* 20.4, pp. 429–452. DOI: `10.1089/ast.2019.2045` (cit. on pp. 4, 102, 139, 205, 243).

— (**2020b**). 'The Hot Spring Hypothesis for an Origin of Life'. *AsBio* 20.4, pp. 429–452. DOI: `10.1089/ast.2019.2045`. eprint: `https://doi.org/10.1089/ast.2019.2045` (cit. on pp. 32, 42).

Dance, A. (**2023**). 'How Did Life Begin? One Key Ingredient Is Coming into View'. *Nature* 615.7950, pp. 22–25. DOI: `10.1038/d41586-023-00574-4` (cit. on p. 9).

Dauphas, N. (**2017**). 'The isotopic nature of the Earth's accreting material through time'. *Nature* 541.7638, pp. 521–524. DOI: `10.1038/nature20830` (cit. on p. 224).

Dauphas, N. and B. Marty (**2002**). 'Inference on the nature and the mass of Earth's late veneer from noble metals and gases'. *JGRE* 107.12, pp. 12–1. DOI: `10.1029/2001je001617`. arXiv: `0109309 [astro-ph]` (cit. on pp. 43, 53, 88).

De Bruijn, J. M., A. P. G. Kieboom and H. Van Bekkiun (**1986**). 'Alkaline Degradation of Monosaccharides VI1: The Fhucto-Fobmose Reaction of Mixtures of D-Fructose and Formaldehyde'. *J. Carbohydr. Chem.* 5.4, pp. 561–569. DOI: `10.1080/07328308608062975` (cit. on pp. 17, 123, 158).

Deamer, D. W. and G. R. Fleischaker (1994). *Origin of Life: The Central Concepts.* Ed. by A. C. Bartlett. Boston, London: Jones and Bartlett Boston (cit. on p. 7).

Deamer, D. W. (**2007**). 'Emergent Phenomena in Biology: The Origin of Cellular Life'. *Planetary Systems and the Origins of Life.* Ed. by R. Pudritz, P. Higgs and J. Stone. Cambridge Astrobiology. Cambridge: Cambridge University Press, pp. 89–110 (cit. on p. 4).

— (**2017**). 'Darwin's prescient guess'. *PNAS* 114.43, pp. 11264–11265. DOI: `10.1073/pnas.1715433114` (cit. on pp. 32, 42, 205, 243).

Deamer, D. W., B. Damer and V. Kompanichenko (**2019**). 'Hydrothermal Chemistry and the Origin of Cellular Life'. *AsBio* 19.12, pp. 1523–1537. DOI: `10.1089/ast.2018.1979` (cit. on p. 41).

Deamer, D. W., J. P. Dworkin, S. A. Sandford, M. P. Bernstein and L. J. Allamandola (**2002**). 'The First Cell Membranes'. *Astrobiology* 2.4, pp. 371–381. DOI: `10.1089/153110702762470482` (cit. on p. 12).

Debaille, V., C. O'Neill, A. D. Brandon, P. Haenecour, Q.-Z. Yin, N. Mattielli and A. H. Treiman (**2013**). 'Stagnant-Lid Tectonics in Early Earth Revealed by 142Nd Variations in Late Archean Rocks'. *Earth and Planetary Science Letters* 373, pp. 83–92. DOI: `10.1016/j.epsl.2013.04.016` (cit. on p. 176).

Derenne, S. and F. Robert (**2010**). 'Model of molecular structure of the insoluble organic matter isolated from Murchison meteorite'. *Meteorit. & Planet. Sci.* 45.9, pp. 1461–1475. DOI: `10.1111/j.1945-5100.2010.01122.x` (cit. on pp. 43, 124).

Di, Y.-Y., D. Xu, Y.-X. Kong and C.-S. Zhou (**2017**). 'Thermochemical Properties of Dissolution of Nicotinic Acid C6H5NO2(s) in Aqueous Solution'. *J. Solution Chem.* 46.4, pp. 886–895. DOI: `10.1007/s10953-017-0607-x` (cit. on p. 167).

Di Giulio, M. (**1997**). 'On the RNA World: Evidence in Favor of an Early Ribonucleopeptide World'. *Journal of Molecular Evolution* 45.6, pp. 571–578. DOI: `10.1007/PL00006261` (cit. on pp. 13, 174).

Dick, J. M. (**2019**). 'CHNOSZ: Thermodynamic calculations and diagrams for geochemistry'. *Front. Earth Sci.* 7, p. 180. DOI: `10.3389/feart.2019.00180` (cit. on pp. 70, 89, 110, 165).

Dirscherl, C. F., A. Ianeselli, D. Tetiker, T. Matreux, R. M. Queener, C. B. Mast and D. Braun (**2023**). ‘A Heated Rock Crack Captures and Polymerizes Primordial DNA and RNA’. *Physical Chemistry Chemical Physics* 25.4, pp. 3375–3386. DOI: `10.1039/D2CP04538A` (cit. on p. 178).

Dorn, C. and T. Lichtenberg (**2021**). ‘Hidden Water in Magma Ocean Exoplanets’. *The Astrophysical Journal Letters* 922.1, p. L4. DOI: `10.3847/2041-8213/ac33af` (cit. on pp. 217, 231, 262).

Dowler, M. J., W. D. Fuller, L. E. Orgel and R. A. Sanchez (**1970**). ‘Prebiotic Synthesis of Propiolaldehyde and Nicotinamide’. *Science* 169.3952, pp. 1320–1321. DOI: `10.1126/science.169.3952.1320` (cit. on p. 150).

Drake, F. D. (**1965**). ‘Chapter IX - The Radio Search for Intelligent Extraterrestrial Life’. *Current Aspects of Exobiology*. Ed. by G. Mamikunian and M. H. Briggs. Pergamon, pp. 323–345. ISBN: 978-1-4832-0047-7. DOI: `10.1016/B978-1-4832-0047-7.50015-0` (cit. on p. 4).

Drozdovskaya, M. N., E. F. van Dishoeck, M. Rubin, J. K. Jørgensen and K. Altwegg (**2019**). ‘Ingredients for solar-like systems: protostar IRAS 16293-2422 B versus comet 67P/Churyumov-Gerasimenko’. *Monthly Notices of the Royal Astronomical Society* 490.1, pp. 50–79. DOI: `10.1093/mnras/stz2430`. arXiv: `1908.11290 [astro-ph.SR]` (cit. on p. 53).

Drozdovskaya, M. N., C. Walsh, E. F. van Dishoeck, K. Furuya, U. Marboeuf, A. Thiabaud, D. Harsono and R. Visser (**2016**). ‘Cometary ices in forming protoplanetary disc midplanes’. *Mon. Not. R. Astron. Soc.* 462.1, pp. 977–993. DOI: `10.1093/mnras/stw1632` (cit. on pp. 45, 52, 54, 56, 59, 108, 109).

Dry, M. E. (**2002**). ‘The Fischer–Tropsch Process: 1950–2000’. *Catalysis Today*. Fischer-Tropsch Synthesis on the Eve of the XXI Century 71.3, pp. 227–241. DOI: `10.1016/S0920-5861(01)00453-9` (cit. on p. 15).

Eckhardt, A. K., M. M. Linden, R. C. Wende, B. Bernhardt and P. R. Schreiner (**2018**). ‘Gas-phase sugar formation using hydroxymethylene as the reactive formaldehyde isomer’. *Nature Chemistry* 10.11, pp. 1141–1147. DOI: `10.1038/s41557-018-0128-2` (cit. on p. 105).

Eigen, M. (**1971**). ‘Selforganization of Matter and the Evolution of Biological Macromolecules’. *Naturwissenschaften* 58.10, pp. 465–523. DOI: `10.1007/BF00623322` (cit. on pp. 10, 13).

Eistrup, C., C. Walsh and E. F. van Dishoeck (**2019**). ‘Cometary compositions compared with protoplanetary disk midplane chemical evolution. An emerging chemical evolution taxonomy for comets’. *Astronomy and Astrophysics* 629, A84, A84. DOI: `10.1051/0004-6361/201935812`. arXiv: `1907.11255 [astro-ph.EP]` (cit. on p. 53).

Elbakyan, V. G., A. Johansen, M. Lambrechts, V. Akimkin and E. I. Vorobyov (**2020**). 'Gravitoviscous protoplanetary disks with a dust component. III. Evolution of gas, dust, and pebbles'. *Astronomy and Astrophysics* 637, A5, A5. DOI: 10.1051/0004-6361/201937198. arXiv: 2004.00126 [astro-ph.EP] (cit. on p. 53).

Elvehjem, C., R. J. Madden, F. Strong and D. Woolley (**1938**). 'The Isolation and Identification of the Anti-Black Tongue Factor'. *J. Biol. Chem.* 123.1, pp. 137–149. DOI: 10.1016/S0021-9258(18)74164-1 (cit. on p. 140).

Emberson, J. (**2010**). 'Amino acid synthesis in meteoritic parent bodies'. *Undergrad. Honor. Thesis Mcmaster Univ.* (cit. on pp. 113, 114).

Endres, C. P., S. Schlemmer, P. Schilke, J. Stutzki and H. S. P. Müller (**2016**). 'The Cologne Database for Molecular Spectroscopy, CDMS, in the Virtual Atomic and Molecular Data Centre, VAMDC'. *Journal of Molecular Spectroscopy.* New Visions of Spectroscopic Databases, Volume II 327, pp. 95–104. DOI: 10.1016/j.jms.2016.03.005 (cit. on p. 19).

Eschenmoser, A. (**2007a**). 'On a Hypothetical Generational Relationship between HCN and Constituents of the Reductive Citric Acid Cycle'. *Chem. & Biodivers.* 4.4, pp. 554–573. DOI: 10.1002/cbdv.200790050 (cit. on p. 106).

— (**2007b**). 'The search for the chemistry of life's origin'. *Tetrahedron* 63.52, pp. 12821–12844. DOI: 10.1016/j.tet.2007.10.012 (cit. on p. 106).

Espinosa-García, J. and S. Dóbé (**2005**). 'Theoretical enthalpies of formation for atmospheric hydroxycarbonyls'. *J. Mol. Struct. :* 713.1-3, pp. 119–125. DOI: 10.1016/j.theochem.2004.11.002 (cit. on p. 113).

Farkas-Takacs, A., C. Kiss, S. Góbi and Á. Kereszturi (**2021**). 'Serpentinization in the thermal evolution of icy Kuiper belt objects in the early Solar system'. *European Planetary Science Congress 2021*, EPSC2021-543, EPSC2021–543. DOI: 10.5194/epsc2020-651 (cit. on p. 65).

Fedoseev, G., H. M. Cuppen, S. Ioppolo, T. Lamberts and H. Linnartz (**2015**). 'Experimental evidence for glycolaldehyde and ethylene glycol formation by surface hydrogenation of CO molecules under dense molecular cloud conditions'. *Mon. Not. R. Astron. Soc.* 448.2, pp. 1288–1297. DOI: 10.1093/mnras/stu2603 (cit. on p. 105).

Fernandez, D. (**2013**). *Undergrad. Honor. Thesis Mcmaster Univ.* (cit. on pp. 113, 114).

Ferris, J. P., P. C. Joshi, E. H. Edelson and J. G. Lawless (**1978**). 'HCN: A plausible source of purines, pyrimidines and amino acids on the primitive earth'. *JMolE* 11.4, pp. 293–311. DOI: 10.1007/bf01733839 (cit. on pp. 47, 74).

Ferris, J. P., P. C. Joshi, K. J. Wang, S. Miyakawa and W. Huang (**2004**). 'Catalysis in prebiotic chemistry: Application to the synthesis of RNA oligomers'. *Adv.*

Space Res. 33.1, pp. 100–105. DOI: 10.1016/j.asr.2003.02.010 (cit. on pp. 42, 101).

Ferris, J. P., A. R. Hill, R. Liu and L. E. Orgel (**1996**). 'Synthesis of long prebiotic oligomers on mineral surfaces'. *Nature* 381.6577, pp. 59–61. DOI: 10.1038/381059a0 (cit. on pp. 42, 101, 128).

Ferris, J. P., R. A. Sanchez and L. E. Orgel (**1968**). 'Studies in prebiotic synthesis. III. Synthesis of pyrimidines from cyanoacetylene and cyanate'. *Journal of Molecular Biology* 33.3, pp. 693–704. DOI: 10.1016/0022-2836(68)90314-8 (cit. on p. 47).

Ferus, M., F. Pietrucci, A. M. Saitta, O. Ivanek, A. Knizek, P. Kubelík, M. Krus, L. Juha, R. Dudzak, J. Dostál et al. (**2019**). 'Prebiotic Synthesis Initiated in Formaldehyde by Laser Plasma Simulating High-Velocity Impacts'. *Astronomy & Astrophysics* 626, A52. DOI: 10.1051/0004-6361/201935435 (cit. on pp. 33, 185, 199).

Ferus, M., F. Pietrucci, A. M. Saitta, A. Knížek, P. Kubelík, O. Ivanek, V. Shestivska and S. Civiš (**2017**). 'Formation of Nucleobases in a Miller–Urey Reducing Atmosphere'. *Proceedings of the National Academy of Sciences* 114.17, pp. 4306–4311. DOI: 10.1073/pnas.1700010114 (cit. on p. 14).

Fiebig, J., A. B. Woodland, J. Spangenberg and W. Oschmann (**2007**). 'Natural Evidence for Rapid Abiogenic Hydrothermal Generation of CH4'. *Geochimica et Cosmochimica Acta* 71.12, pp. 3028–3039. DOI: 10.1016/j.gca.2007.04.010 (cit. on p. 210).

Fischer-Gödde, M., B. M. Elfers, C. Münker, K. Szilas, W. D. Maier, N. Messling, T. Morishita, M. Van Kranendonk and H. Smithies (**2020**). 'Ruthenium isotope vestige of Earth's pre-late-veneer mantle preserved in Archaean rocks'. *Nature* 579.7798, pp. 240–244. DOI: 10.1038/s41586-020-2069-3 (cit. on pp. 43, 53, 101, 139, 140, 177, 215, 224).

Fischer-Gödde, M. and T. Kleine (**2017**). 'Ruthenium isotopic evidence for an inner Solar System origin of the late veneer'. *Nature* 541.7638, pp. 525–527. DOI: 10.1038/nature21045 (cit. on pp. 43, 177, 224).

Flynn, G., L. Moore and W. Klöck (**1999**). 'Density and Porosity of Stone Meteorites: Implications for the Density, Porosity, Cratering, and Collisional Disruption of Asteroids'. *Icarus* 142.1, pp. 97–105. DOI: 10.1006/icar.1999.6210 (cit. on pp. 61, 143, 153–155).

Franklin, R. E. and R. G. Gosling (**1953**). 'Molecular Configuration in Sodium Thymonucleate'. *Nature* 171.4356, pp. 740–741. DOI: 10.1038/171740a0 (cit. on p. 3).

Free Software Foundation, Inc. (2020). *GNU Compiler Collection*. URL: https://gcc.gnu.org/ (visited on 17/11/2021) (cit. on p. 110).

Friedkin, M. and A. L. Lehninger (**1949**). 'Esterification of Inorganic Phosphate Coupled to Electron Transport between Dihydrodiphosphopyridine Nucleotide and Oxygen. I'. *J. Biol. Chem.* 178.2, pp. 611–623. DOI: `10.1016/S0021-9258(18)56879-4` (cit. on pp. 13, 142).

Friedmann, N., S. L. Miller and R. A. Sanchez (**1971**). 'Primitive Earth Synthesis of Nicotinic Acid Derivatives'. *Science* 171.3975, pp. 1026–1027. DOI: `10.1126/science.171.3975.1026` (cit. on p. 150).

Frisch, M. J., G. W. Trucks, H. B. Schlegel, G. E. Scuseria, M. A. Robb, J. R. Cheeseman, G. Scalmani, V. Barone, G. A. Petersson, H. Nakatsuji et al. (**2009**). '*Gaussian 09*, Revision E.01'. Wallingford, CT, USA (cit. on pp. 113, 114, 168).

Fujiya, W., N. Sugiura, H. Hotta, K. Ichimura and Y. Sano (**2012**). 'Evidence for the Late Formation of Hydrous Asteroids from Young Meteoritic Carbonates'. *Nature Communications* 3.1, p. 627. DOI: `10.1038/ncomms1635` (cit. on pp. 22, 254).

Fuller, W. D., R. A. Sanchez and L. E. Orgel (**1972a**). 'Studies in prebiotic synthesis. VII: Solid-State Synthesis of Purine Nucleosides'. *J. Mol. Evol.* 1.3, pp. 249–257. DOI: `10.1007/bf01660244` (cit. on p. 102).

Fuller, W. D., R. A. Sanchez and L. E. Orgel (**1972b**). 'Studies in Prebiotic Synthesis: VI. Synthesis of Purine Nucleosides'. *Journal of Molecular Biology* 67.1, pp. 25–33. DOI: `10.1016/0022-2836(72)90383-X` (cit. on pp. 178, 200, 203, 204, 207, 208, 248).

— (**1972c**). 'Studies in prebiotic synthesis: VI. Synthesis of purine nucleosides'. *J. Mol. Biol.* 67.1, pp. 25–33. DOI: `10.1016/0022-2836(72)90383-x` (cit. on p. 102).

Furukawa, Y., Y. Chikaraishi, N. Ohkouchi, N. O. Ogawa, D. P. Glavin, J. P. Dworkin, C. Abe and T. Nakamura (**2019**). 'Extraterrestrial ribose and other sugars in primitive meteorites'. *Proc. Natl. Acad. Sci.* 116.49, pp. 24440–24445. DOI: `10.1073/pnas.1907169116` (cit. on pp. 24, 43, 88, 101, 118–121, 124–127, 142, 178).

Gaches, B. A. L., S. Walch, S. S. R. Offner and C. Münker (**2020**). 'Aluminum-26 Enrichment in the Surface of Protostellar Disks Due to Protostellar Cosmic Rays'. *Astrophys. J.* 898.1, p. 79. DOI: `10.3847/1538-4357/ab9a38` (cit. on pp. 22, 155).

Gánti, T. (2003). *The Principles of Life*. Oxford University Press. ISBN: 978-0-19-850726-0 (cit. on p. 13).

Garenne, A., P. Beck, G. Montes-Hernandez, L. Bonal, E. Quirico, O. Proux and J. Hazemann (**2019**). 'The Iron Record of Asteroidal Processes in Carbonaceous Chondrites'. *Meteorit. Planet. Sci.* 54.11, pp. 2652–2665. DOI: `10.1111/maps.13377` (cit. on p. 150).

Garrett, E. R. and J. Tsau (**1972**). 'Solvolyses of Cytosine and Cytidine'. *Journal of Pharmaceutical Sciences* 61.7, pp. 1052–1061. DOI: `10.1002/jps.2600610703` (cit. on p. 47).

Gautier, L. (2010). *rpy2*. URL: `https://github.com/rpy2/rpy2` (visited on 17/11/2021) (cit. on p. 110).

Genda, H., R. Brasser and S. J. Mojzsis (**2017**). 'The Terrestrial Late Veneer from Core Disruption of a Lunar-Sized Impactor'. *Earth and Planetary Science Letters* 480, pp. 25–32. DOI: `10.1016/j.epsl.2017.09.041` (cit. on pp. 183, 211).

Genda, H., T. Iizuka, T. Sasaki, Y. Ueno and M. Ikoma (**2017**). 'Ejection of Iron-Bearing Giant-Impact Fragments and the Dynamical and Geochemical Influence of the Fragment Re-Accretion'. *Earth and Planetary Science Letters* 470, pp. 87–95. DOI: `10.1016/j.epsl.2017.04.035` (cit. on pp. 183, 211).

Ghesquière, P., T. Mineva, D. Talbi, P. Theulé, J. A. Noble and T. Chiavassa (**2015**). 'Diffusion of molecules in the bulk of a low density amorphous ice from molecular dynamics simulations'. *Phys. Chem. Chem. Phys.* 17 (17), pp. 11455–11468. DOI: `10.1039/c5cp00558b` (cit. on pp. 55, 107–109).

Gilbert, W. (**1986**). 'Origin of life: The RNA world'. *Nature* 319.6055, p. 618. DOI: `10.1038/319618a0` (cit. on pp. 9, 41, 101, 174).

Gilmour, I. (**2003**). 'Structural and Isotopic Analysis of Organic Matter in Carbonaceous Chondrites'. *Treatise on Geochemistry*. Vol. 1. Elsevier Inc., pp. 269–290. ISBN: 9780080548074. DOI: `10.1016/b0-08-043751-6/01146-4` (cit. on pp. 43, 124, 178).

Glassmeier, K.-H., H. Boehnhardt, D. Koschny, E. Kührt and I. Richter (**2007**). 'The Rosetta Mission: Flying Towards the Origin of the Solar System'. *Space Science Reviews* 128.1, pp. 1–21. DOI: `10.1007/s11214-006-9140-8` (cit. on p. 20).

Glavin, D. P., M. P. Callahan, J. P. Dworkin and J. E. Elsila (**2010**). 'The effects of parent body processes on amino acids in carbonaceous chondrites'. *Meteorit. Planet. Sci.* 45.12, pp. 1948–1972. DOI: `10.1111/j.1945-5100.2010.01132.x` (cit. on p. 143).

Glavin, D. P., J. P. Dworkin, C. M. O. Alexander, J. C. Aponte, A. A. Baczynski, J. J. Barnes, H. A. Bechtel, E. L. Berger, A. S. Burton, P. Caselli et al. (**2025**). 'Abundant Ammonia and Nitrogen-Rich Soluble Organic Matter in Samples from Asteroid (101955) Bennu'. *Nature Astronomy* 9.2, pp. 199–210. DOI: `10.1038/s41550-024-02472-9` (cit. on pp. 4, 21).

Glavin, D. P., J. E. Elsila, H. L. McLain, J. C. Aponte, E. T. Parker, J. P. Dworkin, D. H. Hill, H. C. Connolly Jr. and D. S. Lauretta (**2021**). 'Extraterrestrial Amino Acids and L-enantiomeric Excesses in the CM2 Carbonaceous Chondrites Aguas

Zarcas and Murchison'. *Meteor. Planet. Sci.* 56.1, pp. 148–173. DOI: `10.1111/maps.13451` (cit. on pp. 147, 159, 161).

Góbi, S. and Á. Kereszturi (**2017**). 'Role of serpentinization in the thermal and connected mineral evolution of planetesimals – evaluating possible consequences for exoplanetary systems'. *Monthly Notices of the Royal Astronomical Society* 466.2, pp. 2099–2110. DOI: `10.1093/mnras/stw3223` (cit. on p. 65).

Goesmann, F., H. Rosenbauer, J. H. Bredehöft, M. Cabane, P. Ehrenfreund, T. Gautier, C. Giri, H. Krüger, L. Le Roy, A. J. MacDermott et al. (**2015**). 'Organic compounds on comet 67P/Churyumov-Gerasimenko revealed by COSAC mass spectrometry'. *Science* 349.6247, aab0689. DOI: `10.1126/science.aab0689` (cit. on pp. 145, 156).

Gomes, R., H. F. Levison, K. Tsiganis and A. Morbidelli (**2005**). 'Origin of the cataclysmic Late Heavy Bombardment period of the terrestrial planets'. *Nature* 435.7041, pp. 466–469. DOI: `10.1038/nature03676` (cit. on pp. 42, 53, 101).

Guerrier-Takada, C. and S. Altman (**1984**). 'Catalytic activity of an RNA molecule prepared by transcription in vitro'. *Science* 223.4633, pp. 285–286. DOI: `10.1126/science.6199841` (cit. on pp. 9, 41, 101, 140, 174).

Guerrier-Takada, C., K. Gardiner, T. Marsh, N. Pace and S. Altman (**1983**). 'The RNA moiety of ribonuclease P is the catalytic subunit of the enzyme'. *Cell* 35.3, pp. 849–857. DOI: `10.1016/0092-8674(83)90117-4` (cit. on pp. 9, 41, 101, 140, 174).

Guillot, S., S. Schwartz, B. Reynard, P. Agard and C. Prigent (**2015**). 'Tectonic Significance of Serpentinites'. *Tectonophysics* 646, pp. 1–19. DOI: `10.1016/j.tecto.2015.01.020` (cit. on pp. 210, 232).

Guillot, T. (**2010**). 'On the Radiative Equilibrium of Irradiated Planetary Atmospheres'. *Astronomy & Astrophysics* 520, A27. DOI: `10.1051/0004-6361/200913396` (cit. on p. 228).

Gull, M., M. A. Mojica, F. M. Fernández, D. A. Gaul, T. M. Orlando, C. L. Liotta and M. A. Pasek (**2015**). 'Nucleoside phosphorylation by the mineral schreibersite'. *Scientific Reports* 5.1, p. 17198. DOI: `10.1038/srep17198` (cit. on pp. 43, 128, 142).

Guo, M. and J. Korenaga (**2020**). 'Argon Constraints on the Early Growth of Felsic Continental Crust'. *Science Advances* 6.21, eaaz6234. DOI: `10.1126/sciadv.aaz6234` (cit. on p. 220).

— (**2023**). 'The Combined Hf and Nd Isotope Evolution of the Depleted Mantle Requires Hadean Continental Formation'. *Science Advances* 9.12, eade2711. DOI: `10.1126/sciadv.ade2711` (cit. on p. 220).

— (**2024**). 'Rapidly Evolving Ocean pH in the Early Earth: Insights from Global Carbon Cycle Coupled with Ocean Chemistry'. DOI: `10.21203/rs.3.rs-4247090/v1` (cit. on pp. 209–211).

— (**2025**). 'Rapid Rise of Early Ocean pH under Elevated Weathering Rates'. *Nature Geoscience*, pp. 1–7. DOI: `10.1038/s41561-025-01649-9` (cit. on pp. 209, 210, 217).

Guse, A. H. (**2004**). 'Biochemistry, Biology, and Pharmacology of Cyclic Adenosine Diphosphoribose (cADPR)'. *Curr. Med. Chem.* 11.7, pp. 847–855. DOI: `10.2174/0929867043455602` (cit. on p. 142).

Guzmán-Marmolejo, A., A. Segura and E. Escobar-Briones (**2013**). 'Abiotic Production of Methane in Terrestrial Planets'. *Astrobiology* 13.6, pp. 550–559. DOI: `10.1089/ast.2012.0817` (cit. on pp. 201, 219, 220, 232, 234).

Haas, M., S. Lamour, S. B. Christ and O. Trapp (**2020**). 'Mineral-mediated carbohydrate synthesis by mechanical forces in a primordial geochemical setting'. *Communications Chemistry* 3.1, pp. 1–6. DOI: `10.1038/s42004-020-00387-w` (cit. on p. 116).

Haas, M., S. Lamour and O. Trapp (**2018**). 'Development of an advanced derivatization protocol for the unambiguous identification of monosaccharides in complex mixtures by gas and liquid chromatography'. *J. Chromatogr. A* 1568, pp. 160–167. DOI: `10.1016/j.chroma.2018.07.015` (cit. on p. 116).

Haldane, J. B. S. (**1929**). 'The Origin of Life'. *Rationalist Annual*, p. 12 (cit. on pp. 14, 173).

Hand, K. P., C. B. Phillips, A. Murray, J. B. Garvin, E. H. Maize, R. G. Gibbs, G. Reeves, A. M. S. Martin, G. H. Tan-Wang, J. Krajewski et al. (**2022**). 'Science Goals and Mission Architecture of the Europa Lander Mission Concept'. *The Planetary Science Journal* 3.1, p. 22. DOI: `10.3847/PSJ/ac4493` (cit. on p. 4).

Harris, C. R., K. J. Millman, S. J. van der Walt, R. Gommers, P. Virtanen, D. Cournapeau, E. Wieser, J. Taylor, S. Berg, N. J. Smith et al. (**2020**). 'Array programming with NumPy'. *Nature* 585.7825, pp. 357–362. DOI: `10.1038/s41586-020-2649-2` (cit. on pp. 89, 110).

Harrison, T. M. (**2009**). 'The Hadean Crust: Evidence from >4 Ga Zircons'. *Annual Review of Earth and Planetary Sciences* 37.1, pp. 479–505. DOI: `10.1146/annurev.earth.031208.100151` (cit. on pp. 27, 217).

Harrison, T. M., E. B. Watson and A. B. Aikman (**2007**). 'Temperature Spectra of Zircon Crystallization in Plutonic Rocks'. *Geology* 35.7, pp. 635–638. DOI: `10.1130/G23505A.1` (cit. on pp. 181, 228).

Hashimoto, G. L., Y. Abe and S. Sugita (**2007**). 'The Chemical Composition of the Early Terrestrial Atmosphere: Formation of a Reducing Atmosphere from CI-like Material'. *Journal of Geophysical Research: Planets* 112.E5. DOI: `10.1029/2006JE002844` (cit. on p. 177).

Hastie, A. R., S. Law, G. D. Bromiley, J. G. Fitton, S. L. Harley and D. D. Muir (**2023**). 'Deep Formation of Earth's Earliest Continental Crust Consistent with Subduction'. *Nature Geoscience* 16.9, pp. 816–821. DOI: `10.1038/s41561-023-01249-5` (cit. on pp. 27, 217).

Hayatsu, R., M. H. Studier, S. Matsuoka and E. Anders (**1972**). 'Origin of Organic Matter in Early Solar System—VI. Catalytic Synthesis of Nitriles, Nitrogen Bases and Porphyrin-like Pigments'. *Geochimica et Cosmochimica Acta* 36.5, pp. 555–571. DOI: `10.1016/0016-7037(72)90075-0` (cit. on p. 15).

Hayatsu, R. and E. Anders (**1981**). 'Organic compounds in meteorites and their origins'. *Cosmo- and Geochemistry.* Berlin, Heidelberg, Germany: Springer Berlin Heidelberg, pp. 1–37. ISBN: 978-3-540-38806-7. DOI: `10.1007/3-540-10920-X_13` (cit. on p. 48).

Hayatsu, R., M. H. Studier, A. Oda, K. Fuse and E. Anders (**1968**). 'Origin of organic matter in early solar system-II. Nitrogen compounds'. *Geochimica et Cosmochimica Acta* 32.2, pp. 175–190. DOI: `10.1016/S0016-7037(68)80003-1` (cit. on pp. 15, 47–50, 75).

Hazen, R. M. and D. A. Sverjensky (**2010**). 'Mineral Surfaces, Geochemical Complexities, and the Origins of Life'. *Cold Spring Harbor Perspectives in Biology* 2.5, a002162. DOI: `10.1101/cshperspect.a002162` (cit. on pp. 205, 243).

He, J., S. M. Emtiaz and G. Vidali (**2017**). 'Diffusion and Clustering of Carbon Dioxide on Non-porous Amorphous Solid Water'. *Astrophysical Journal* 837.1, p. 65. DOI: `10.3847/1538-4357/aa5f52` (cit. on p. 55).

— (**2018**). 'Measurements of Diffusion of Volatiles in Amorphous Solid Water: Application to Interstellar Medium Environments'. *Astrophysical Journal* 863.2, p. 156. DOI: `10.3847/1538-4357/aad227` (cit. on p. 55).

Heitkämper, J., S. Suchaneck, J. García de la Concepción, J. Kästner and G. Molpeceres (**2022**). 'The Reactivity of Pyridine in Cold Interstellar Environments: The Reaction of Pyridine with the CN Radical'. *Frontiers in Astronomy and Space Sciences* 9. DOI: `10.3389/fspas.2022.1020635` (cit. on p. 162).

Henke, S., H.-P. Gail, M. Trieloff and W. H. Schwarz (**2013**). 'Thermal evolution model for the H chondrite asteroid-instantaneous formation versus protracted accretion'. *Icarus* 226.1, pp. 212–228. DOI: `10.1016/j.icarus.2013.05.034` (cit. on p. 65).

Henke, S., H.-P. Gail, M. Trieloff, W. H. Schwarz and T. Kleine (**2012**). 'Thermal evolution and sintering of chondritic planetesimals'. *Astronomy and Astrophysics* 537, A45. DOI: `10.1051/0004-6361/201117177` (cit. on p. 65).

Henning, T. K. and D. A. Semenov (**2013**). 'Chemistry in Protoplanetary Disks'. *Chemical Reviews* 113.12, pp. 9016–9042. DOI: `10.1021/cr400128p` (cit. on p. 19).

Hier-Majumder, S. and M. M. Hirschmann (**2017**). 'The Origin of Volatiles in the Earth's Mantle'. *Geochemistry, Geophysics, Geosystems* 18.8, pp. 3078–3092. DOI: `10.1002/2017GC006937` (cit. on p. 228).

Hildenbrand, G., K. Paschek, M. Schäfer, M. Hausmann, G. Hildenbrand, K. Paschek, M. Schäfer and M. Hausmann (**2022**). 'Cryovolcanism in the Solar System and beyond: Considerations on Energy Sources, Geological Aspects, and Astrobiological Perspectives'. *Astronomy and Planetary Science - From Cryovolcanism to Black Holes and Galactic Evolution*. IntechOpen. ISBN: 978-1-80356-120-2. DOI: `10.5772/intechopen.105067` (cit. on p. x).

Hill, A. and L. E. Orgel (**2002**). 'Synthesis of Adenine from HCN Tetramer and Ammonium Formate'. *Origins of life and evolution of the biosphere* 32.2, pp. 99–102. DOI: `10.1023/A:1016070723772` (cit. on pp. 200, 204).

Hirschmann, M. M. and R. Dasgupta (**2009**). 'The H/C ratios of Earth's near-surface and deep reservoirs, and consequences for deep Earth volatile cycles'. *Chemical Geology* 262.1, pp. 4–16. DOI: `10.1016/j.chemgeo.2009.02.008` (cit. on p. 218).

Holland, H. D. (1984). *The Chemical Evolution of the Atmosphere and Oceans*. Princeton University Press (cit. on pp. 181, 228).

Holm, N., C. Oze, O. Mousis, J. Waite and A. Guilbert-Lepoutre (**2015**). 'Serpentinization and the Formation of H2 and CH4 on Celestial Bodies (Planets, Moons, Comets)'. *Astrobiology* 15.7, pp. 587–600. DOI: `10.1089/ast.2014.1188` (cit. on pp. 174, 182, 219).

Hopp, T., G. Budde and T. Kleine (**2020**). 'Heterogeneous accretion of Earth inferred from Mo-Ru isotope systematics'. *Earth and Planetary Science Letters* 534, p. 116065. DOI: `10.1016/j.epsl.2020.116065` (cit. on pp. 177, 215, 223, 224).

Hsu, W., Y. Guan, X. Hua, Y. Wang, L. Leshin and T. Sharp (**2006**). 'Aqueous alteration of opaque assemblages in the Ningqiang carbonaceous chondrite: Evidence from oxygen isotopes'. *Earth Planet. Sci. Lett.* 243.1, pp. 107–114. DOI: `10.1016/j.epsl.2005.12.021` (cit. on p. 149).

Hu, R., S. Seager and W. Bains (**2012**). 'PHOTOCHEMISTRY IN TERRESTRIAL EXOPLANET ATMOSPHERES. I. PHOTOCHEMISTRY MODEL AND BENCHMARK CASES'. *The Astrophysical Journal* 761.2, p. 166. DOI: `10.1088/0004-637X/761/2/166` (cit. on p. 232).

Hud, N. V. (**2018**). 'Searching for lost nucleotides of the pre-RNA World with a self-refining model of early Earth'. *NatCo* 9.1, p. 5171. DOI: `10.1038/s41467-018-07389-2` (cit. on p. 42).

Hunter, J. D. (**2007**). 'Matplotlib: A 2D Graphics Environment'. *Comput. Sci. & Eng.* 9.3, pp. 90–95. DOI: `10.1109/mcse.2007.55` (cit. on pp. 89, 110).

Iqbal, Z. and S. Novalin (**2012**). 'The Formose Reaction: A Tool to Produce Synthetic Carbohydrates Within a Regenerative Life Support System'. *Curr. Org. Chem.* 16.6, pp. 769–788. DOI: `10.2174/138527212799957968` (cit. on pp. 16, 105, 147, 151).

Itcovitz, J. P., A. S. P. Rae, R. I. Citron, S. T. Stewart, C. A. Sinclair, P. B. Rimmer and O. Shorttle (**2022**). 'Reduced Atmospheres of Post-impact Worlds: The Early Earth'. *The Planetary Science Journal* 3.5, p. 115. DOI: `10.3847/PSJ/ac67a9` (cit. on pp. 183, 211, 239).

Jackson, R. B., M. Saunois, P. Bousquet, J. G. Canadell, B. Poulter, A. R. Stavert, P. Bergamaschi, Y. Niwa, A. Segers and A. Tsuruta (**2020**). 'Increasing Anthropogenic Methane Emissions Arise Equally from Agricultural and Fossil Fuel Sources'. *Environmental Research Letters* 15.7, p. 071002. DOI: `10.1088/1748-9326/ab9ed2` (cit. on p. 210).

Jakob, W., J. Rhinelander and D. Moldovan (2017). *pybind11 – Seamless operability between C++11 and Python*. URL: `https://github.com/pybind/pybind11` (visited on 17/11/2021) (cit. on pp. 70, 89, 110).

Jeilani, Y. A. and M. T. Nguyen (**2020**). 'Autocatalysis in Formose Reaction and Formation of RNA Nucleosides'. *J. Phys. Chem. B* 124.50, pp. 11324–11336. DOI: `10.1021/acs.jpcb.0c07070` (cit. on p. 106).

Johansen, A., J. Blum, H. Tanaka, C. Ormel, M. Bizzarro and H. Rickman (**2014a**). 'The Multifaceted Planetesimal Formation Process'. *Protostars and Planets VI*. Ed. by H. Beuther, R. S. Klessen, C. P. Dullemond and T. K. Henning. Tucson: University of Arizona Press, p. 547. DOI: `10.2458/azu_uapress_9780816531240-ch024`. arXiv: `1402.1344 [astro-ph.EP]` (cit. on pp. 3, 20, 53).

— (**2014b**). 'The Multifaceted Planetesimal Formation Process'. *Protostars and Planets VI*. Ed. by H. Beuther, R. S. Klessen, C. P. Dullemond and T. K. Henning. Tucson, AZ: University of Arizona Press. ISBN: 9780816531240. DOI: `10.2458/azu_uapress_9780816531240-ch024` (cit. on p. 144).

Johansen, A., E. Camprubi, E. van Kooten and H. J. Hoeijmakers (**2024**). 'Self-Oxidation of the Atmospheres of Rocky Planets with Implications for the Origin of Life'. *Astrobiology* 24.9, pp. 856–880. DOI: `10.1089/ast.2023.0104` (cit. on pp. 14, 173, 181, 209, 256).

Johansen, A., J. S. Oishi, M.-M. M. Low, H. H. Klahr, T. K. Henning and A. Youdin (**2007**). 'Rapid planetesimal formation in turbulent circumstellar disks'. *Nature* 448.7157, pp. 1022–1025. DOI: `10.1038/nature06086` (cit. on p. 144).

Johansen, A., J. S. Oishi, M.-M. Mac Low, H. H. Klahr, T. K. Henning and A. Youdin (**2007**). 'Rapid planetesimal formation in turbulent circumstellar disks'. *Nature* 448.7157, pp. 1022–1025. DOI: `10.1038/nature06086` (cit. on pp. 3, 20, 53, 108).

Johansen, A., T. Ronnet, M. Bizzarro, M. Schiller, M. Lambrechts, Å. Nordlund and H. Lammer (**2021**). 'A pebble accretion model for the formation of the terrestrial planets in the Solar System'. *Science Advances* 7 (8), pp. 444–461. DOI: `10.1126/sciadv.abc0444` (cit. on pp. 42, 109).

Johansen, A., T. Ronnet, M. Schiller, Z. Deng and M. Bizzarro (**2023**). 'Anatomy of Rocky Planets Formed by Rapid Pebble Accretion - III. Partitioning of Volatiles between Planetary Core, Mantle, and Atmosphere'. *Astronomy & Astrophysics* 671, A76. DOI: `10.1051/0004-6361/202142143` (cit. on pp. 173, 181, 209).

Johnson, A. P., H. J. Cleaves, J. P. Dworkin, D. P. Glavin, A. Lazcano and J. L. Bada (**2008**). 'The Miller Volcanic Spark Discharge Experiment'. *Science* 322.5900, pp. 404–404. DOI: `10.1126/science.1161527` (cit. on pp. 33, 174, 178).

Johnston, W. K., P. J. Unrau, M. S. Lawrence, M. E. Glasner and D. P. Bartel (**2001**). 'RNA-Catalyzed RNA Polymerization: Accurate and General RNA-Templated Primer Extension'. *Science* 292.5520, pp. 1319–1325. DOI: `10.1126/science.1060786` (cit. on pp. 9, 41, 101, 140, 174).

Kadoya, S. and D. C. Catling (**2019**). 'Constraints on Hydrogen Levels in the Archean Atmosphere Based on Detrital Magnetite'. *Geochimica et Cosmochimica Acta* 262, pp. 207–219. DOI: `10.1016/j.gca.2019.07.041` (cit. on p. 228).

Kadoya, S., J. Krissansen-Totton and D. C. Catling (**2020**). 'Probable Cold and Alkaline Surface Environment of the Hadean Earth Caused by Impact Ejecta Weathering'. *Geochemistry, Geophysics, Geosystems* 21.1, e2019GC008734. DOI: `10.1029/2019GC008734` (cit. on p. 234).

Kaltenegger, L. (**2017**). 'How to Characterize Habitable Worlds and Signs of Life'. *Annual Review of Astronomy and Astrophysics* 55.Volume 55, 2017, pp. 433–485. DOI: `10.1146/annurev-astro-082214-122238` (cit. on p. 4).

Kaplan, I., E. Degens and J. Reuter (**1963**). 'Organic compounds in stony meteorites'. *Geochim. Cosmochim. Acta* 27.7, pp. 805–834. DOI: `10.1016/0016-7037(63)90045-0` (cit. on pp. 147, 159, 161).

Kasting, J. F. (**1990**). 'Bolide Impacts and the Oxidation State of Carbon in the Earth's Early Atmosphere'. *Origins of life and evolution of the biosphere* 20.3, pp. 199–231. DOI: `10.1007/BF01808105` (cit. on p. 177).

Kasting, J. F. (**2005**). 'Methane and Climate during the Precambrian Era'. *Precambrian Research*. Stable Isotopes, Life and Early Earth History 137.3, pp. 119–129. DOI: `10.1016/j.precamres.2005.03.002` (cit. on pp. 176, 182, 210).

Kasting, J. F., D. P. Whitmire and R. T. Reynolds (**1993**). 'Habitable Zones around Main Sequence Stars'. *Icarus* 101.1, pp. 108–128. DOI: `10.1006/icar.1993.1010` (cit. on p. 3).

Kauffman, S. A. (**1986**). 'Autocatalytic Sets of Proteins'. *Journal of Theoretical Biology* 119.1, pp. 1–24. DOI: `10.1016/S0022-5193(86)80047-9` (cit. on p. 13).

Kawabata, M., K. Kawashima, H. Mutsuro-Aoki, T. Ando, T. Umehara and K. Tamura (**2022**). 'Peptide Bond Formation between Aminoacyl-Minihelices by a Scaffold Derived from the Peptidyl Transferase Center'. *Life* 12.4, p. 573. DOI: `10.3390/life12040573` (cit. on p. 9).

Kebukawa, Y., Q. H. S. Chan, S. Tachibana, K. Kobayashi and M. E. Zolensky (**2017**). 'One-pot synthesis of amino acid precursors with insoluble organic matter in planetesimals with aqueous activity'. *SciA* 3.3, e1602093. DOI: `10.1126/sciadv.1602093`. eprint: `https://www.science.org/doi/pdf/10.1126/sciadv.1602093` (cit. on p. 43).

Keller, B. and B. Schoene (**2018**). 'Plate Tectonics and Continental Basaltic Geochemistry throughout Earth History'. *Earth and Planetary Science Letters* 481, pp. 290–304. DOI: `10.1016/j.epsl.2017.10.031` (cit. on p. 220).

Kelley, D. S., J. A. Karson, G. L. Früh-Green, D. R. Yoerger, T. M. Shank, D. A. Butterfield, J. M. Hayes, M. O. Schrenk, E. J. Olson, G. Proskurowski et al. (**2005**). 'A Serpentinite-Hosted Ecosystem: The Lost City Hydrothermal Field'. *Science* 307.5714, pp. 1428–1434. DOI: `10.1126/science.1102556` (cit. on pp. 220, 232, 234).

Kim, H.-J. and S. A. Benner (**2017**). 'Prebiotic stereoselective synthesis of purine and noncanonical pyrimidine nucleotide from nucleobases and phosphorylated carbohydrates'. *Proc. Natl. Acad. Sci.* 114.43, pp. 11315–11320. DOI: `10.1073/pnas.1710778114` (cit. on p. 102).

— (**2018**). 'A Direct Prebiotic Synthesis of Nicotinamide Nucleotide'. *Chem. – A Eur. J.* 24.3, pp. 581–584. DOI: `10.1002/chem.201705394` (cit. on p. 102).

Kim, H.-J., A. Ricardo, H. I. Illangkoon, M. J. Kim, M. A. Carrigan, F. Frye and S. A. Benner (**2011**). 'Synthesis of Carbohydrates in Mineral-Guided Prebiotic Cycles'. *J. Am. Chem. Soc.* 133.24, pp. 9457–9468. DOI: `10.1021/ja201769f` (cit. on p. 116).

Kimura, M., J. N. Grossman and M. Weisberg (**2011**). 'Fe-Ni metal and sulfide minerals in CM chondrites: An indicator for thermal history'. *Meteorit. Planet. Sci.* 46.3, pp. 431–442. DOI: `10.1111/j.1945-5100.2010.01164.x` (cit. on p. 143).

Klahr, H. H. and A. Schreiber (**2020a**). 'Turbulence Sets the Length Scale for Planetesimal Formation: Local 2D Simulations of Streaming Instability and Planetesimal Formation'. *Astrophys. J.* 901.1, 54, p. 54. DOI: `10.3847/1538-4357/abac58` (cit. on pp. 3, 20, 53, 108).

— (**2020b**). 'Turbulence Sets the Length Scale for Planetesimal Formation: Local 2D Simulations of Streaming Instability and Planetesimal Formation'. *Astrophys. J.* 901.1, p. 54. DOI: `10.3847/1538-4357/abac58` (cit. on p. 144).

Klein, F., W. Bach and T. M. McCollom (**2013**). 'Compositional controls on hydrogen generation during serpentinization of ultramafic rocks'. *Lithos* 178, pp. 55–69. DOI: `10.1016/j.lithos.2013.03.008` (cit. on pp. 29, 176, 182, 218, 220).

Knyazev, A., N. Smirnova, A. Shipilova, A. Shushunov, E. Gusarova and S. Knyazeva (**2015**). 'Thermodynamic properties and low-temperature X-ray diffraction of vitamin B3'. *Thermochim. Acta* 604, pp. 115–121. DOI: `10.1016/j.tca.2015.01.012` (cit. on p. 167).

Koga, T. and H. Naraoka (**2022**). 'Synthesis of Amino Acids from Aldehydes and Ammonia: Implications for Organic Reactions in Carbonaceous Chondrite Parent Bodies'. *ACS Earth Space Chem.* 6.5, pp. 1311–1320. DOI: `10.1021/acsearthspacechem.2c00008` (cit. on p. 150).

Kooten, E. van, M. Schiller, F. Moynier, A. Johansen, T. Haugbølle and M. Bizzarro (**2021**). 'Hybrid Accretion of Carbonaceous Chondrites by Radial Transport across the Jupiter Barrier'. *Astrophys. J.* 910 (1), p. 70. DOI: `10.3847/1538-4357/abd9c8` (cit. on pp. 42, 53, 101, 109).

Korenaga, J. (**2007**). 'Thermal Cracking and the Deep Hydration of Oceanic Lithosphere: A Key to the Generation of Plate Tectonics?'. *Journal of Geophysical Research: Solid Earth* 112.B5. DOI: `10.1029/2006JB004502` (cit. on p. 232).

— (**2021**). 'Was There Land on the Early Earth?'. *Life* 11.11, p. 1142. DOI: `10.3390/life11111142` (cit. on pp. 27, 174, 209, 221).

Korenaga, J., N. J. Planavsky and D. A. D. Evans (**2017**). 'Global water cycle and the coevolution of the Earth's interior and surface environment'. *Philosophical Transactions of the Royal Society A: Mathematical, Physical and Engineering Sciences* 375.2094, p. 20150393. DOI: `10.1098/rsta.2015.0393` (cit. on p. 218).

Kristoffersen, E. L., M. Burman, A. Noy and P. Holliger (**2022**). 'Rolling circle RNA synthesis catalyzed by RNA'. *eLife* 11. Ed. by T. W. Nilsen, J. L. Manley and J. Sponer, e75186. DOI: `10.7554/eLife.75186` (cit. on pp. 9, 41, 142, 174).

Krot, A. N., K. Keil, E. R. D. Scott, C. A. Goodrich and M. K. Weisberg (**2007**). '1.05 - Classification of Meteorites'. *Treatise on Geochemistry.* Ed. by H. D. Holland and K. K. Turekian. Oxford: Pergamon, pp. 1–52. ISBN: 978-0-08-043751-4. DOI: `10.1016/B0-08-043751-6/01062-8` (cit. on pp. 23, 24).

Kruger, K., P. J. Grabowski, A. J. Zaug, J. Sands, D. E. Gottschling and T. R. Cech (**1982**). 'Self-splicing RNA: Autoexcision and autocyclization of the ribosomal RNA intervening sequence of tetrahymena'. *Cell* 31.1, pp. 147–157. DOI: `10.1016/0092-8674(82)90414-7` (cit. on pp. 9, 41, 101, 140, 174).

Kruse, F. M., J. S. Teichert and O. Trapp (**2020**). 'Prebiotic Nucleoside Synthesis: The Selectivity of Simplicity'. *Chem. – A Eur. J.* 26.65, pp. 14776–14790. DOI: `10.1002/chem.202001513` (cit. on pp. 106, 116).

Kun, Á., M. Santos and E. Szathmáry (**2005**). 'Real Ribozymes Suggest a Relaxed Error Threshold'. *Nature Genetics* 37.9, pp. 1008–1011. DOI: `10.1038/ng1621` (cit. on p. 13).

Kurosawa, K., S. Sugita, K. Ishibashi, S. Hasegawa, Y. Sekine, N. O. Ogawa, T. Kadono, S. Ohno, N. Ohkouchi, Y. Nagaoka et al. (**2013**). 'Hydrogen Cyanide Production due to Mid-Size Impacts in a Redox-Neutral N2-Rich Atmosphere'. *Origins of Life and Evolution of Biospheres* 43.3, pp. 221–245. DOI: `10.1007/s11084-013-9339-0` (cit. on pp. 31, 177, 183, 196, 197, 201, 215, 225, 226, 232, 236, 237).

Kuwahara, H. and R. Nakada (**2023**). 'Partitioning of Fe2+ and Fe3+ between bridgmanite and silicate melt: Implications for redox evolution of the Earth's mantle'. *Earth Planet. Sci. Lett.* 615, p. 118197. DOI: `10.1016/j.epsl.2023.118197` (cit. on p. 151).

Kuwahara, H., R. Nakada, S. Kadoya, T. Yoshino and T. Irifune (**2023**). 'Hadean mantle oxidation inferred from melting of peridotite under lower-mantle conditions'. *Nat. Geosci.* 16.5, pp. 461–465. DOI: `10.1038/s41561-023-01169-4` (cit. on p. 151).

Kuwahara, H. and S. Sugita (**2015**). 'The Molecular Composition of Impact-Generated Atmospheres on Terrestrial Planets during the Post-Accretion Stage'. *Icarus* 257, pp. 290–301. DOI: `10.1016/j.icarus.2015.05.007` (cit. on p. 177).

Lai, J. C., B. K. D. Pearce, R. E. Pudritz and D. Lee (**2019**). 'Meteoritic abundances of fatty acids and potential reaction pathways in planetesimals'. *Icarus* 319, pp. 685–700. DOI: `10.1016/j.icarus.2018.09.028` (cit. on pp. 12, 24, 124, 163, 259).

Laneuville, M., M. Kameya and H. J. Cleaves (**2018**). 'Earth Without Life: A Systems Model of a Global Abiotic Nitrogen Cycle'. *Astrobiology* 18.7, pp. 897–914. DOI: `10.1089/ast.2017.1700` (cit. on p. 234).

Lange, K., C. P. Dullemond, M. Trieloff and J. Blum (**2022**). *in preparation* (cit. on pp. 111, 112, 118, 125).

Larowe, D. E. and P. Regnier (**2008**). 'Thermodynamic potential for the abiotic synthesis of adenine, cytosine, guanine, thymine, uracil, ribose, and deoxyribose in hydrothermal systems'. *OLEB* 38.5, pp. 383–397. DOI: 10.1007/s11084-008-9137-2 (cit. on pp. 33, 46, 47, 74, 185, 199).

Larralde, R., M. P. Robertson and S. L. Miller (**1995**). 'Rates of decomposition of ribose and other sugars: Implications for chemical evolution'. *Proc. Natl. Acad. Sci.* 92.18, pp. 8158–8160. DOI: 10.1073/pnas.92.18.8158 (cit. on pp. 123–125).

Lauretta, D. S., S. S. Balram-Knutson, E. Beshore, W. V. Boynton, C. Drouet d'Aubigny, D. N. DellaGiustina, H. L. Enos, D. R. Golish, C. W. Hergenrother, E. S. Howell et al. (**2017**). 'OSIRIS-REx: Sample Return from Asteroid (101955) Bennu'. *Space Science Reviews* 212.1, pp. 925–984. DOI: 10.1007/s11214-017-0405-1 (cit. on p. 21).

Le Roy, L., K. Altwegg, H. Balsiger, J.-J. Berthelier, A. Bieler, C. Briois, U. Calmonte, M. R. Combi, J. De Keyser, F. Dhooghe et al. (**2015**). 'Inventory of the volatiles on comet 67P/Churyumov-Gerasimenko from Rosetta/ROSINA'. *Astronomy and Astrophysics* 583, A1, A1. DOI: 10.1051/0004-6361/201526450 (cit. on p. 53).

Lee, C., W. Yang and R. G. Parr (**1988**). 'Development of the Colle-Salvetti correlation-energy formula into a functional of the electron density'. *Phys. Rev. B* 37 (2), pp. 785–789. DOI: 10.1103/PhysRevB.37.785 (cit. on pp. 113, 168).

Lee, M., K. Paschek, D. A. Semenov and T. K. Henning (**2025**). 'Prebiotic Carboxylic Acid Synthesis in Carbonaceous Planetesimals [working title]'. ***in preparation*** (cit. on pp. x, 259).

Lee, T., D. A. Papanastassiou and G. J. Wasserburg (**1977**). 'Aluminum-26 in the early solar system - Fossil or fuel'. *Astrophysical Journal* 211, p. L110. DOI: 10.1086/182351 (cit. on p. 61).

Leong, J. A. M., T. Ely and E. L. Shock (**2021**). 'Decreasing Extents of Archean Serpentinization Contributed to the Rise of an Oxidized Atmosphere'. *Nature Communications* 12.1, p. 7341. DOI: 10.1038/s41467-021-27589-7 (cit. on p. 228).

Levy, M. and S. L. Miller (**1998**). 'The stability of the RNA bases: Implications for the origin of life'. *PNAS* 95.14, pp. 7933–7938. DOI: 10.1073/pnas.95.14.7933 (cit. on pp. 48, 50, 160).

Li, C.-H. (**2022**). 'Late Veneer and the Origins of Volatiles of Earth'. *Acta Geochimica* 41.4, pp. 650–664. DOI: 10.1007/s11631-021-00517-8 (cit. on pp. 31, 177).

Lichtenberg, T., G. J. Golabek, T. V. Gerya and M. R. Meyer (**2016**). 'The effects of short-lived radionuclides and porosity on the early thermo-mechanical evolution of planetesimals'. *Icarus* 274, pp. 350–365. DOI: 10.1016/j.icarus.2016.03.004 (cit. on pp. 49, 155).

Lichtenberg, T. and S. Krijt (**2021**). 'System-level Fractionation of Carbon from Disk and Planetesimal Processing'. *Astrophys. J. Lett.* 913.2, p. L20. DOI: 10.3847/2041-8213/abfdce (cit. on pp. 45, 52, 54, 56, 59, 60, 107–109).

Lineweaver, C. H. and A. Chopra (**2012**). 'The Habitability of Our Earth and Other Earths: Astrophysical, Geochemical, Geophysical, and Biological Limits on Planet Habitability'. *Annual Review of Earth and Planetary Sciences* 40.Volume 40, 2012, pp. 597–623. DOI: 10.1146/annurev-earth-042711-105531 (cit. on p. 3).

Lisicki, D., K. Nowak and B. Orlińska (**2022**). 'Methods to Produce Nicotinic Acid with Potential Industrial Applications'. *Materials* 15.3. DOI: 10.3390/ma15030765 (cit. on p. 150).

Lissenberg, C. J., A. M. McCaig, S. Q. Lang, P. Blum, N. Abe, W. J. Brazelton, R. Coltat, J. R. Deans, K. L. Dickerson, M. Godard et al. (**2024**). 'A Long Section of Serpentinized Depleted Mantle Peridotite'. *Science* 385.6709, pp. 623–629. DOI: 10.1126/science.adp1058 (cit. on p. 231).

Liu, Z., M. Perez-Gussinye, J. García-Pintado, L. Mezri and W. Bach (**2023**). 'Mantle serpentinization and associated hydrogen flux at North Atlantic magma-poor rifted margins'. *Geology* 51.3, pp. 284–289. DOI: 10.1130/G50722.1 (cit. on p. 232).

Lodders, K. (**2003**). 'Solar System Abundances and Condensation Temperatures of the Elements'. *Astrophys. J.* 591.2, pp. 1220–1247. DOI: 10.1086/375492 (cit. on pp. 53, 54, 107).

Lorenz, R. D. (**2020**). 'Maunder's Work on Planetary Habitability in 1913: Early Use of the Term "Habitable Zone" and a "Drake Equation" Calculation'. *Research Notes of the AAS* 4.6, p. 79. DOI: 10.3847/2515-5172/ab9831 (cit. on p. 3).

Luo, H., C. Dorn and J. Deng (**2024**). 'The Interior as the Dominant Water Reservoir in Super-Earths and Sub-Neptunes'. *Nature Astronomy*, pp. 1–9. DOI: 10.1038/s41550-024-02347-z (cit. on pp. 217, 231, 262).

Macke, R. J., G. J. Consolmagno and D. T. Britt (**2011**). 'Density, porosity, and magnetic susceptibility of carbonaceous chondrites'. *Meteoritics and Planetary Science* 46.12, pp. 1842–1862. DOI: 10.1111/j.1945-5100.2011.01298.x (cit. on pp. 61, 143, 153–155).

Malamud, U., W. A. Landeck, D. Bischoff, C. Kreuzig, H. B. Perets, B. Gundlach and J. Blum (**2022**). 'Are There Any Pristine Comets? Constraints from Pebble Structure'. *Monthly Notices of the Royal Astronomical Society* 514.3, pp. 3366–3394. DOI: 10.1093/mnras/stac1535 (cit. on p. 259).

Mann, U., D. J. Frost, D. C. Rubie, H. Becker and A. Audétat (**2012**). 'Partitioning of Ru, Rh, Pd, Re, Ir and Pt between liquid metal and silicate at high pressures and high temperatures - Implications for the origin of highly siderophile element concentrations in the Earth's mantle'. *Geochimica et Cosmochimica Acta* 84, pp. 593–613. DOI: `10.1016/j.gca.2012.01.026` (cit. on p. 223).

Markvoort, A. J., N. Pfleger, R. Staffhorst, P. A. J. Hilbers, R. A. van Santen, J. A. Killian and B. de Kruijff (**2010**). 'Self-Reproduction of Fatty Acid Vesicles: A Combined Experimental and Simulation Study'. *Biophysical Journal* 99.5, pp. 1520–1528. DOI: `10.1016/j.bpj.2010.06.057` (cit. on p. 12).

Martin, R. G. and M. Livio (**2021**). 'How much water was delivered from the asteroid belt to the Earth after its formation?'. *Monthly Notices of the Royal Astronomical Society*, pp. 1–5. DOI: `10.1093/mnrasl/slab062`. arXiv: `2106.03999` (cit. on p. 53).

Martin, W., J. Baross, D. Kelley and M. J. Russell (**2008**). 'Hydrothermal vents and the origin of life'. *Nat. Rev. Microbiol.* 6.11, pp. 805–814. DOI: `10.1038/nrmicro1991` (cit. on pp. 4, 28, 140, 257).

Martin, W. and M. J. Russell (**2006**). 'On the Origin of Biochemistry at an Alkaline Hydrothermal Vent'. *Philosophical Transactions of the Royal Society B: Biological Sciences* 362.1486, pp. 1887–1926. DOI: `10.1098/rstb.2006.1881` (cit. on p. 211).

Marty, B., G. Avice, Y. Sano, K. Altwegg, H. Balsiger, M. Hässig, A. Morbidelli, O. Mousis and M. Rubin (**2016**). 'Origins of volatile elements (H, C, N, noble gases) on Earth and Mars in light of recent results from the ROSETTA cometary mission'. *E&PSL* 441, pp. 91–102. DOI: `10.1016/j.epsl.2016.02.031` (cit. on p. 53).

Mason, B. (**1963**). 'The carbonaceous chondrites'. *Space Sci. Rev.* 1.4, pp. 621–646. DOI: `10.1007/bf00212446` (cit. on pp. 43, 61, 111, 143, 153–155).

Masset, F. and M. Snellgrove (**2001**). 'Reversing type II migration: Resonance trapping of a lighter giant protoplanet'. *Monthly Notices of the Royal Astronomical Society* 320.4, pp. L55–L59. DOI: `10.1046/j.1365-8711.2001.04159.x`. arXiv: `0003421 [astro-ph]` (cit. on p. 62).

Materese, C. K., M. Nuevo, B. L. McDowell, C. E. Buffo and S. A. Sandford (**2018**). 'The Photochemistry of Purine in Ice Analogs Relevant to Dense Interstellar Clouds'. *Astrophysical Journal* 864.1, p. 44. DOI: `10.3847/1538-4357/aad328` (cit. on p. 85).

Matreux, T., P. Aikkila, B. Scheu, D. Braun and C. B. Mast (**2024**). 'Heat Flows Enrich Prebiotic Building Blocks and Enhance Their Reactivity'. *Nature* 628.8006, pp. 110–116. DOI: `10.1038/s41586-024-07193-7` (cit. on p. 178).

Matsui, T. and Y. Abe (**1986**). 'Evolution of an impact-induced atmosphere and magma ocean on the accreting Earth'. *Nature* 319.6051, pp. 303–305. DOI: `10.1038/319303a0` (cit. on p. 151).

Matsumura, S., Á. Kun, M. Ryckelynck, F. Coldren, A. Szilágyi, F. Jossinet, C. Rick, P. Nghe, E. Szathmáry and A. D. Griffiths (**2016**). 'Transient Compartmentalization of RNA Replicators Prevents Extinction Due to Parasites'. *Science* 354.6317, pp. 1293–1296. DOI: `10.1126/science.aag1582` (cit. on p. 13).

May, R. A., R. S. Smith and B. D. Kay (**2012**). 'The Molecular Volcano Revisited: Determination of Crack Propagation and Distribution During the Crystallization of Nanoscale Amorphous Solid Water Films'. *The Journal of Physical Chemistry Letters* 3.3, pp. 327–331. DOI: `10.1021/jz201648g` (cit. on p. 55).

— (**2013a**). 'The release of trapped gases from amorphous solid water films. I. "Top-down" crystallization-induced crack propagation probed using the molecular volcano'. *Journal of Chemical Physics* 138.10, p. 104501. DOI: `10.1063/1.4793311` (cit. on p. 55).

— (**2013b**). 'The release of trapped gases from amorphous solid water films. II. "Bottom-up" induced desorption pathways'. *Journal of Chemical Physics* 138.10, p. 104502. DOI: `10.1063/1.4793312` (cit. on p. 55).

Mayor, M. and D. Queloz (**1995**). 'A Jupiter-mass Companion to a Solar-Type Star'. *Nature* 378.6555, pp. 355–359. DOI: `10.1038/378355a0` (cit. on p. 4).

McCollom, T. M. and J. S. Seewald (**2007**). 'Abiotic Synthesis of Organic Compounds in Deep-Sea Hydrothermal Environments'. *Chemical Reviews* 107.2, pp. 382–401. DOI: `10.1021/cr0503660` (cit. on pp. 29, 176, 182, 219, 220).

McCoy, T. J., S. S. Russell, T. J. Zega, K. L. Thomas-Keprta, S. A. Singerling, F. E. Brenker, N. E. Timms, W. D. A. Rickard, J. J. Barnes, G. Libourel et al. (**2025**). 'An Evaporite Sequence from Ancient Brine Recorded in Bennu Samples'. *Nature* 637.8048, pp. 1072–1077. DOI: `10.1038/s41586-024-08495-6` (cit. on p. 22).

McCoy-West, A. J., P. Chowdhury, K. W. Burton, P. Sossi, G. M. Nowell, J. G. Fitton, A. C. Kerr, P. A. Cawood and H. M. Williams (**2019**). 'Extensive Crustal Extraction in Earth's Early History Inferred from Molybdenum Isotopes'. *Nature Geoscience* 12.11, pp. 946–951. DOI: `10.1038/s41561-019-0451-2` (cit. on p. 220).

McCulloch, M. T. and V. C. Bennett (**1993**). 'Evolution of the Early Earth: Constraints from 143Nd 142Nd Isotopic Systematics'. *Lithos*. The Evolving Earth 30.3, pp. 237–255. DOI: `10.1016/0024-4937(93)90038-E` (cit. on pp. 32, 178, 220).

McNaught, A. D. and A. Wilkinson (**2019**). 'aromaticity (A00442)'. *The IUPAC Compendium of Chemical Terminology: The Gold Book*. Ed. by S. J. Chalk. 2nd ed. Research Triangle Park, NC: International Union of Pure and Applied Chemistry (IUPAC), p. 110. ISBN: 0-9678550-9-8. DOI: `10.1351/goldbook.A00442` (cit. on p. 150).

Menneken, M., A. A. Nemchin, T. Geisler, R. T. Pidgeon and S. A. Wilde (**2007**). 'Hadean Diamonds in Zircon from Jack Hills, Western Australia'. *Nature* 448.7156, pp. 917–920. DOI: `10.1038/nature06083` (cit. on p. 220).

Miertuš, S., E. Scrocco and J. Tomasi (**1981**). 'Electrostatic interaction of a solute with a continuum. A direct utilizaion of AB initio molecular potentials for the prevision of solvent effects'. *Chemical Physics* 55.1, pp. 117–129. DOI: `10.1016/0301-0104(81)85090-2` (cit. on pp. 113, 168).

Miller, S. L. (**1953**). 'A Production of Amino Acids Under Possible Primitive Earth Conditions'. *Science* 117.3046, pp. 528–529. DOI: `10.1126/science.117.3046.528` (cit. on pp. 4, 14, 174).

— (**1955**). 'Production of Some Organic Compounds under Possible Primitive Earth Conditions1'. *Journal of the American Chemical Society* 77.9, pp. 2351–2361. DOI: `10.1021/ja01614a001` (cit. on p. 174).

— (**1957a**). 'The Formation of Organic Compounds on the Primitive Earth'. *Annals of the New York Academy of Sciences* 69.2, pp. 260–275. DOI: `10.1111/j.1749-6632.1957.tb49662.x` (cit. on p. 173).

— (**1957b**). 'The Mechanism of Synthesis of Amino Acids by Electric Discharges'. *Biochimica et Biophysica Acta* 23, pp. 480–489. DOI: `10.1016/0006-3002(57)90366-9` (cit. on p. 174).

Miller, S. L. and H. C. Urey (**1959**). 'Organic Compound Synthesis on the Primitive Earth'. *Science* 130.3370, pp. 245–251. DOI: `10.1126/science.130.3370.245` (cit. on pp. 14, 174).

Mills, A. A. (**1968**). 'Boron in Carbonaceous Chondrites'. *Nature* 220 (5172), pp. 1113–1114. DOI: `10.1038/2201113a0` (cit. on p. 124).

Minton, D. A. and R. Malhotra (**2010**). 'Dynamical erosion of the asteroid belt and implications for large impacts in the inner Solar System'. *Icarus* 207.2, pp. 744–757. DOI: `10.1016/j.icarus.2009.12.008`. arXiv: `0909.3875 [astro-ph.EP]` (cit. on p. 53).

Miyakawa, S., H. Yamanashi, K. Kobayashi, H. J. Cleaves and S. L. Miller (**2002**). 'Prebiotic Synthesis from CO Atmospheres: Implications for the Origins of Life'. *Proceedings of the National Academy of Sciences* 99.23, pp. 14628–14631. DOI: `10.1073/pnas.192568299` (cit. on pp. 14, 174).

Miyazaki, Y. and J. Korenaga (**2019**). 'On the Timescale of Magma Ocean Solidification and Its Chemical Consequences: 2. Compositional Differentiation Under Crystal Accumulation and Matrix Compaction'. *Journal of Geophysical Research: Solid Earth* 124.4, pp. 3399–3419. DOI: `10.1029/2018JB016928` (cit. on pp. 176, 217, 260).

— (**2022**). 'A wet heterogeneous mantle creates a habitable world in the Hadean'. *Nature* 603.7899, pp. 86–90. DOI: `10.1038/s41586-021-04371-9` (cit. on pp. 27, 28, 173, 174, 176, 181–183, 187, 188, 196, 209–211, 217–220, 227, 228, 231–234, 239, 262).

Mojzsis, S. J., T. M. Harrison and R. T. Pidgeon (**2001**). 'Oxygen-Isotope Evidence from Ancient Zircons for Liquid Water at the Earth's Surface 4,300 Myr Ago'. *Nature* 409.6817, pp. 178–181. DOI: `10.1038/35051557` (cit. on p. 227).

Molaverdikhani, K., C. Helling, B. W. P. Lew, R. J. MacDonald, D. Samra, N. Iro, P. Woitke and V. Parmentier (**2020**). 'Understanding the Atmospheric Properties and Chemical Composition of the Ultra-Hot Jupiter HAT-P-7b - II. Mapping the Effects of Gas Kinetics'. *Astronomy & Astrophysics* 635, A31. DOI: `10.1051/0004-6361/201937044` (cit. on pp. 169, 185).

Molaverdikhani, K., T. K. Henning and P. Mollière (**2019**). 'From Cold to Hot Irradiated Gaseous Exoplanets: Fingerprints of Chemical Disequilibrium in Atmospheric Spectra'. *The Astrophysical Journal* 883.2, p. 194. DOI: `10.3847/1538-4357/ab3e30` (cit. on pp. 169, 185).

Mollière, P., J. P. Wardenier, R. van Boekel, T. K. Henning, K. Molaverdikhani and I. a. G. Snellen (**2019**). 'petitRADTRANS - A Python Radiative Transfer Package for Exoplanet Characterization and Retrieval'. *Astronomy & Astrophysics* 627, A67. DOI: `10.1051/0004-6361/201935470` (cit. on pp. 169, 185, 228).

Monroe, A. A. and S. Pizzarello (**2011**). 'The soluble organic compounds of the Bells meteorite: Not a unique or unusual composition'. *Geochimica et Cosmochimica Acta* 75.23, pp. 7585–7595. DOI: `10.1016/j.gca.2011.09.041` (cit. on p. 50).

Morange, M. (**2008**). 'What History Tells Us XIII. Fifty Years of the Central Dogma'. *Journal of Biosciences* 33.2, pp. 171–175. DOI: `10.1007/s12038-008-0034-7` (cit. on p. 7).

Morbidelli, A. and B. J. Wood (**2015**). 'Late Accretion and the Late Veneer'. *The Early Earth: Accretion and Differentiation*. American Geophysical Union (AGU). Chap. 4, pp. 71–82. ISBN: 978-1-118-86035-9. DOI: `10.1002/9781118860359.ch4` (cit. on pp. 31, 139, 177, 223).

Mulkidjanian, A. Y., A. Y. Bychkov, D. V. Dibrova, M. Y. Galperin and E. V. Koonin (**2012**). 'Origin of first cells at terrestrial, anoxic geothermal fields'. *PNAS* 109.14. DOI: `10.1073/pnas.1117774109` (cit. on p. 41).

Müller, F., L. Escobar, F. Xu, E. Węgrzyn, M. Nainytė, T. Amatov, C.-Y. Chan, A. Pichler and T. Carell (**2022**). 'A Prebiotically Plausible Scenario of an RNA–Peptide World'. *Nature* 605.7909, pp. 279–284. DOI: `10.1038/s41586-022-04676-3` (cit. on pp. 13, 174).

Mumma, M. J. and S. B. Charnley (**2011**). 'The Chemical Composition of Comets—Emerging Taxonomies and Natal Heritage'. *Annu. Rev. Astron. Astrophys.* 49, pp. 471–524. DOI: `10.1146/annurev-astro-081309-130811` (cit. on pp. 45, 48, 52, 53, 57, 59, 107, 110, 144, 145).

Muñoz Caro, G. M., U. Meierhenrich, W. A. Schutte and J. M. Greenberg (**2004**). 'UV-photoprocessing of Interstellar Ice Analogs: Detection of Hexamethylenetetramine-Based Species'. *Astron. Astrophys.* 413.1, pp. 209–216. DOI: `10.1051/0004-6361:20031447` (cit. on p. 159).

Nakamura, E., K. Kobayashi, R. Tanaka, T. Kunihiro, H. Kitagawa, C. Potiszil, T. Ota, C. Sakaguchi, M. Yamanaka, D. M. Ratnayake et al. (**2022**). 'On the Origin and Evolution of the Asteroid Ryugu: A Comprehensive Geochemical Perspective'. *Proc. Jpn. Acad., Ser. B* 98.6, pp. 227–282. DOI: `10.2183/pjab.98.015` (cit. on pp. 22, 25, 144).

Nam, I., H. G. Nam and R. N. Zare (**2018**). 'Abiotic synthesis of purine and pyrimidine ribonucleosides in aqueous microdroplets'. *Proc. Natl. Acad. Sci.* 115.1, pp. 36–40. DOI: `10.1073/pnas.1718559115` (cit. on pp. 102, 178, 200, 203, 204, 207, 208, 248).

Naraoka, H., Y. Takano, J. P. Dworkin, Y. Oba, K. Hamase, A. Furusho, N. O. Ogawa, M. Hashiguchi, K. Fukushima, D. Aoki et al. (**2023**). 'Soluble Organic Molecules in Samples of the Carbonaceous Asteroid (162173) Ryugu'. *Science* 379.6634, eabn9033. DOI: `10.1126/science.abn9033` (cit. on pp. 4, 21).

Nelson, K. E., M. P. Robertson, M. Levy and S. L. Miller (**2001**). 'Concentration by Evaporation and the Prebiotic Synthesis of Cytosine'. *OLEB* 31.3, pp. 221–229. DOI: `10.1023/A:1010652418557` (cit. on p. 48).

Nicklas, R. W., I. S. Puchtel, R. D. Ash, P. M. Piccoli, E. Hanski, E. G. Nisbet, P. Waterton, D. G. Pearson and A. D. Anbar (**2019**). 'Secular mantle oxidation across the Archean-Proterozoic boundary: Evidence from V partitioning in komatiites and picrites'. *Geochim. Cosmochim. Acta* 250, pp. 49–75. DOI: `10.1016/j.gca.2019.01.037` (cit. on p. 151).

Nielsen, P. E., M. Egholm, R. H. Berg and O. Buchardt (**1991**). 'Sequence-Selective Recognition of DNA by Strand Displacement with a Thymine-Substituted Polyamide'. *Sci* 254.5037, pp. 1497–1500. DOI: `10.1126/science.1962210` (cit. on p. 42).

Niitsu, T., M. M. Ito and H. Inoue (**1992**). 'Analysis of the Formose Reaction System'. *Journal of Chemical Engineering of Japan* 25.5, pp. 480–485. DOI: `10.1252/jcej.25.480` (cit. on p. 17).

Nisbet, E. G. and N. H. Sleep (**2001**). 'The Habitat and Nature of Early Life'. *Nature* 409.6823, pp. 1083–1091. DOI: `10.1038/35059210` (cit. on p. 173).

Nissen, P., J. Hansen, N. Ban, P. B. Moore and T. A. Steitz (**2000**). 'The Structural Basis of Ribosome Activity in Peptide Bond Synthesis'. *Science* 289.5481, pp. 920–930. DOI: `10.1126/science.289.5481.920` (cit. on p. 9).

Noble, J. A., Theule, P., Mispelaer, F., Duvernay, F., Danger, G., Congiu, E., Dulieu, F. and Chiavassa, T. (**2012**). 'The desorption of H2CO from interstellar grains analogues'. *Astron. & Astrophys.* 543, A5. DOI: 10.1051/0004-6361/201219437 (cit. on p. 108).

Noller, H. F. (**2012**). 'Evolution of Protein Synthesis from an RNA World'. *Cold Spring Harbor Perspectives in Biology* 4.4, a003681. DOI: 10.1101/cshperspect.a003681 (cit. on p. 9).

Nuevo, M., C. K. Materese and S. A. Sandford (**2014**). 'THE PHOTOCHEMISTRY OF PYRIMIDINE IN REALISTIC ASTROPHYSICAL ICES AND THE PRODUCTION OF NUCLEOBASES'. *Astrophysical Journal* 793.2, p. 125. DOI: 10.1088/0004-637X/793/2/125 (cit. on p. 85).

Oba, Y., T. Koga, Y. Takano, N. O. Ogawa, N. Ohkouchi, K. Sasaki, H. Sato, D. P. Glavin, J. P. Dworkin, H. Naraoka et al. (**2023**). 'Uracil in the carbonaceous asteroid (162173) Ryugu'. *Nat. Commun.* 14.1, p. 1292. DOI: 10.1038/s41467-023-36904-3 (cit. on pp. 4, 21, 22, 25, 140, 144, 153, 154, 160–162, 178).

Oba, Y., Y. Takano, Y. Furukawa, T. Koga, D. P. Glavin, J. P. Dworkin and H. Naraoka (**2022**). 'Identifying the wide diversity of extraterrestrial purine and pyrimidine nucleobases in carbonaceous meteorites'. *NatCo* 13.1, p. 2008. DOI: 10.1038/s41467-022-29612-x (cit. on pp. 4, 24, 25, 43, 45, 50, 67, 74, 83, 84, 140, 153, 154, 160–162, 178, 254).

Oba, Y., Y. Takano, H. Naraoka, Y. Furukawa, D. P. Glavin, J. P. Dworkin and S. Tachibana (**2020**). 'Extraterrestrial Hexamethylenetetramine in Meteorites—a Precursor of Prebiotic Chemistry in the Inner Solar System'. *Nat. Commun.* 11.1, p. 6243. DOI: 10.1038/s41467-020-20038-x (cit. on p. 159).

Oba, Y., Y. Takano, H. Naraoka, N. Watanabe and A. Kouchi (**2019**). 'Nucleobase synthesis in interstellar ices'. *NatCo* 10.1, p. 4413. DOI: 10.1038/s41467-019-12404-1 (cit. on pp. 85, 162).

Öberg, K. I. and E. A. Bergin (**2021**). 'Astrochemistry and compositions of planetary systems'. *Physics Reports* 893, pp. 1–48. DOI: 10.1016/j.physrep.2020.09.004 (cit. on pp. 54, 107).

Öberg, K. I., S. Facchini and D. E. Anderson (**2023**). 'Protoplanetary Disk Chemistry'. *Annual Review of Astronomy and Astrophysics* 61.Volume 61, 2023, pp. 287–328. DOI: 10.1146/annurev-astro-022823-040820 (cit. on p. 19).

Öberg, K. I., R. Murray-Clay and E. A. Bergin (**2011**). 'The Effects of Snowlines on C/O in Planetary Atmospheres'. *The Astrophysical Journal Letters* 743.1, p. L16. DOI: 10.1088/2041-8205/743/1/L16 (cit. on p. 20).

Ochterski, J. W. (2000). *Thermochemistry in Gaussian.* Wallingford, CT, USA: Gaussian Inc., pp. 1–19 (cit. on pp. 113, 168).

Ogino, S.-Y., M. D. Yamanaka, S. Mori and J. Matsumoto (**2016**). 'How Much Is the Precipitation Amount over the Tropical Coastal Region?'. *Journal of Climate* 29.3, pp. 1231–1236. DOI: 10.1175/JCLI-D-15-0484.1 (cit. on p. 198).

Ohtomo, Y., T. Kakegawa, A. Ishida, T. Nagase and M. T. Rosing (**2014**). 'Evidence for Biogenic Graphite in Early Archaean Isua Metasedimentary Rocks'. *Nature Geoscience* 7.1, pp. 25–28. DOI: `10.1038/ngeo2025` (cit. on p. 27).

Omran, A., C. Menor-Salvan, G. Springsteen and M. Pasek (**2020**). 'The Messy Alkaline Formose Reaction and Its Link to Metabolism'. *Life* 10.8. DOI: `10.3390/life10080125` (cit. on p. 115).

OoLEN, S. Asche, C. Bautista, D. Boulesteix, A. Champagne-Ruel, C. Mathis, O. Markovitch, Z. Peng, A. Adams, A. V. Dass et al. (**2023**). 'What It Takes to Solve the Origin(s) of Life: An Integrated Review of Techniques'. DOI: `10.48550/arXiv.2308.11665`. arXiv: `2308.11665 [q-bio]` (cit. on p. x).

Oparin, A. I. (1924). *The Origin of Life [Russian: Proiskhozhdenie zhizni]*. Moscow: Izd. Moskovskii Rabochii (cit. on pp. 14, 173).

Orgel, L. E. (**2004**). 'Prebiotic Chemistry and the Origin of the RNA World'. *Crit. Rev. Biochem. Mol. Biol.* 39.2, pp. 99–123. DOI: `10.1080/10409230490460765` (cit. on pp. 9, 42, 101).

Ormel, C. W. and H. H. Klahr (**2010**). 'The effect of gas drag on the growth of protoplanets - Analytical expressions for the accretion of small bodies in laminar disks'. *Astron. & Astrophys.* 520.5, A43. DOI: `10.1051/0004-6361/201014903` (cit. on pp. 3, 20, 53, 108, 144).

Oró, J. and S. S. Kamat (**1961**). 'Amino-Acid Synthesis from Hydrogen Cyanide under Possible Primitive Earth Conditions'. *Nature* 190.4774, pp. 442–443. DOI: `10.1038/190442a0` (cit. on p. 174).

Oró, J. and A. P. Kimball (**1961**). 'Synthesis of purines under possible primitive earth conditions. I. Adenine from hydrogen cyanide'. *Archives of Biochemistry and Biophysics* 94.2, pp. 217–227. DOI: `10.1016/0003-9861(61)90033-9` (cit. on pp. 33, 47, 74, 185, 199, 200, 204).

Oró, J., S. L. Miller and A. Lazcano (**1990**). 'THE ORIGIN AND EARLY EVOLUTION OF LIFE ON EARTH'. *Annual Review of Earth and Planetary Sciences* 18.Volume 18, 1990, pp. 317–356. DOI: `10.1146/annurev.ea.18.050190.001533` (cit. on p. 174).

Owen, J. E. and Y. Wu (**2017**). 'The Evaporation Valley in the Kepler Planets'. *The Astrophysical Journal* 847.1, p. 29. DOI: `10.3847/1538-4357/aa890a` (cit. on p. 173).

Palmer, E. E. and D. S. Lauretta (**2011**). 'Aqueous alteration of kamacite in CM chondrites'. *Meteorit. Planet. Sci.* 46.10, pp. 1587–1607. DOI: `10.1111/j.1945-5100.2011.01251.x` (cit. on p. 143).

Pantaleone, S., J. Enrique-Romero, C. Ceccarelli, S. Ferrero, N. Balucani, A. Rimola and P. Ugliengo (**2021**). 'H2 Formation on Interstellar Grains and the Fate of

Reaction Energy'. *The Astrophysical Journal* 917.1, p. 49. DOI: 10.3847/1538-4357/ac0142 (cit. on p. 19).

Pappalardo, R. T., B. J. Buratti, H. Korth, D. A. Senske, D. L. Blaney, D. D. Blankenship, J. L. Burch, P. R. Christensen, S. Kempf, M. G. Kivelson et al. (**2024**). 'Science Overview of the Europa Clipper Mission'. *Space Science Reviews* 220.4, p. 40. DOI: 10.1007/s11214-024-01070-5 (cit. on p. 4).

Parker, E. T., H. L. McLain, D. P. Glavin, J. P. Dworkin, J. E. Elsila, J. C. Aponte, H. Naraoka, Y. Takano, S. Tachibana, H. Yabuta et al. (**2023**). 'Extraterrestrial Amino Acids and Amines Identified in Asteroid Ryugu Samples Returned by the Hayabusa2 Mission'. *Geochimica et Cosmochimica Acta* 347, pp. 42–57. DOI: 10.1016/j.gca.2023.02.017 (cit. on pp. 4, 21).

Parsons, B. (**1982**). 'Causes and Consequences of the Relation between Area and Age of the Ocean Floor'. *Journal of Geophysical Research: Solid Earth* 87.B1, pp. 289–302. DOI: 10.1029/JB087iB01p00289 (cit. on p. 218).

Pascal, R., A. Pross and J. D. Sutherland (**2013**). 'Towards an Evolutionary Theory of the Origin of Life Based on Kinetics and Thermodynamics'. *Open Biology* 3.11, p. 130156. DOI: 10.1098/rsob.130156 (cit. on p. 4).

Paschek, K. (2021). *prebiotic_synthesis_planetesimal (v1.0)*. Version v1.0. DOI: 10.5281/zenodo.5774880. URL: https://github.com/klauspaschek/prebiotic%5C_synthesis%5C_planetesimal (visited on 17/11/2021) (cit. on pp. 69, 89, 112, 129, 165).

Paschek, K., T. K. Henning, K. Molaverdikhani, Y. Miyazaki, B. K. D. Pearce, R. E. Pudritz and D. A. Semenov (**2025**). 'Deep Mantle-Atmosphere Coupling and Carbonaceous Bombardment: Options for Biomolecule Formation on an Oxidized Early Earth'. *The Astrophysical Journal [**in press**]*. DOI: 10.3847/1538-4357/adc39b (cit. on pp. ix, 28–31, 33, 36, 169). arXiv: 2503.15479 [astro-ph.EP].

Paschek, K., K. Kohler, B. K. D. Pearce, K. Lange, T. K. Henning, O. Trapp, R. E. Pudritz and D. A. Semenov (**2022**). 'Possible Ribose Synthesis in Carbonaceous Planetesimals'. *Life* 12.3, p. 404. DOI: 10.3390/life12030404 (cit. on pp. ix, 24, 36, 88, 95, 97, 131, 142, 147, 158, 159, 161, 163, 168, 178, 186, 255).

Paschek, K., M. Lee, D. A. Semenov and T. K. Henning (**2024a**). 'Cover Feature: Prebiotic Vitamin B3 Synthesis in Carbonaceous Planetesimals (ChemPlusChem 4/2024)'. *ChemPlusChem* 89.4, e202400008. DOI: 10.1002/cplu.202400008 (cit. on pp. 23, 131).

— (**2024b**). 'Prebiotic Vitamin B3 Synthesis in Carbonaceous Planetesimals'. *ChemPlusChem* 89.4, e202300508. DOI: 10.1002/cplu.202300508 (cit. on pp. ix, 21, 36, 131, 133).

— (**2024c**). 'Prebiotic Vitamin B3 Synthesis in Carbonaceous Planetesimals'. *ChemPlusChem* 89.4, e202300508. DOI: `10.1002/cplu.202300508` (cit. on p. 178).

Paschek, K., U. Malamud, D. A. Semenov and T. K. Henning (**2025**). 'Volatile Differentiation in Comets and Implications for Prebiotic Synthesis in Carbonaceous Planetesimals [working title]'. ***in preparation*** (cit. on pp. x, 260, 261).

Paschek, K., A. Roßmann, M. Hausmann and G. Hildenbrand (**2021**). 'Analysis of Tidal Accelerations in the Solar System and in Extrasolar Planetary Systems'. *Applied Sciences* 11.18, p. 8624. DOI: `10.3390/app11188624` (cit. on p. ix).

Paschek, K., D. A. Semenov, B. K. D. Pearce, K. Lange, T. K. Henning and R. E. Pudritz (**2022**). 'Meteorites and the RNA world II: Synthesis of Nucleobases in Carbonaceous Planetesimals and the Role of Initial Volatile Content'. *Arxiv (Revis.)* arXiv: `2112.09160 [astro-ph.EP]` (cit. on pp. 102, 106, 109–112, 118, 128, 129).

— (**2023**). 'Meteorites and the RNA World: Synthesis of Nucleobases in Carbonaceous Planetesimals and the Role of Initial Volatile Content'. *The Astrophysical Journal* 942.1, p. 50. DOI: `10.3847/1538-4357/aca27e` (cit. on pp. ix, 35, 37, 95, 131, 142, 144, 145, 151, 152, 155, 158, 160, 161, 163, 165, 166, 178, 255).

Pascucci, I., D. Apai, K. Luhman, T. K. Henning, J. Bouwman, M. R. Meyer, F. Lahuis and A. Natta (**2009**). 'The different evolution of gas and dust in disks around Sun-like and cool stars'. *The Astrophysical Journal* 696.1, pp. 143–159. DOI: `10.1088/0004-637X/696/1/143` (cit. on p. 19).

Pasek, M. A. and D. S. Lauretta (**2005**). 'Aqueous Corrosion of Phosphide Minerals from Iron Meteorites: A Highly Reactive Source of Prebiotic Phosphorus on the Surface of the Early Earth'. *Astrobiology* 5.4, pp. 515–535. DOI: `10.1089/ast.2005.5.515` (cit. on pp. 142, 149).

Paul, N. and G. F. Joyce (**2002**). 'A Self-Replicating Ligase Ribozyme'. *Proceedings of the National Academy of Sciences* 99.20, pp. 12733–12740. DOI: `10.1073/pnas.202471099` (cit. on p. 9).

Pearce, B. K. D., P. W. Ayers and R. E. Pudritz (**2019**). 'A Consistent Reduced Network for HCN Chemistry in Early Earth and Titan Atmospheres: Quantum Calculations of Reaction Rate Coefficients'. *The Journal of Physical Chemistry A* 123.9, pp. 1861–1873. DOI: `10.1021/acs.jpca.8b11323` (cit. on pp. 32, 169, 177, 185, 189).

— (**2020**). 'CRAHCN-O: A Consistent Reduced Atmospheric Hybrid Chemical Network Oxygen Extension for Hydrogen Cyanide and Formaldehyde Chemistry in CO2-, N2-, H2O-, CH4-, and H2-Dominated Atmospheres'. *The Journal of Physical Chemistry A* 124.41, pp. 8594–8606. DOI: `10.1021/acs.jpca.0c06804` (cit. on pp. 169, 185).

Pearce, B. K. D., S. M. Hörst, J. A. Sebree and C. He (**2024**). 'Organic Hazes as a Source of Life's Building Blocks to Warm Little Ponds on the Hadean Earth'. *The Planetary Science Journal* 5.1, p. 23. DOI: `10.3847/PSJ/ad17bd` (cit. on pp. 200, 201, 203, 205).

Pearce, B. K. D., K. Molaverdikhani, R. E. Pudritz, T. K. Henning and K. E. Cerrillo (**2022**). 'Toward RNA Life on Early Earth: From Atmospheric HCN to Biomolecule Production in Warm Little Ponds'. *The Astrophysical Journal* 932.1, p. 9. DOI: `10.3847/1538-4357/ac47a1` (cit. on pp. 32, 169, 177, 179, 182, 185, 188, 189, 192, 195, 197, 199–201, 203–205, 209, 212, 215, 219, 228, 229, 232, 234–236, 246, 253).

Pearce, B. K. D., K. Molaverdikhani, R. E. Pudritz, T. K. Henning and E. Hébrard (**2020**). 'HCN Production in Titan's Atmosphere: Coupling Quantum Chemistry and Disequilibrium Atmospheric Modeling'. *The Astrophysical Journal* 901.2, p. 110. DOI: `10.3847/1538-4357/abae5c` (cit. on pp. 169, 185).

Pearce, B. K. D. and R. E. Pudritz (**2015**). 'Seeding The Pregenetic Earth: Meteoritc Abundance of Nucleobases and Potential Reaction Pathways'. *Astrophys. J.* 807.1, p. 85. DOI: `10.1088/0004-637x/807/1/85` (cit. on pp. 24, 43, 45, 46, 48, 66, 67, 84, 87, 106, 124, 142, 163).

— (**2016**). 'Meteorites and the RNA World: A Thermodynamic Model of Nucleobase Synthesis within Planetesimals'. *Astrobiology* 16.11, pp. 853–872. DOI: `10.1089/ast.2015.1451` (cit. on pp. 4, 26, 37, 39, 43–51, 54, 57, 59, 60, 70, 73–76, 81, 83, 84, 87, 88, 95, 106, 107, 110, 112, 113, 129, 131, 142, 144, 152, 158, 159, 163, 166, 253, 254).

Pearce, B. K. D., R. E. Pudritz, D. A. Semenov and T. K. Henning (**2017**). 'Origin of the RNA world: The fate of nucleobases in warm little ponds'. *Proc. Natl. Acad. Sci.* 114.43, pp. 11327–11332. DOI: `10.1073/pnas.1710339114` (cit. on pp. 4, 25, 26, 32, 33, 41–43, 102, 128, 139, 143, 169, 178, 179, 183, 186, 199, 200, 203–205, 214, 232, 234, 235, 245, 253).

Pearce, B. K. D., A. S. Tupper, R. E. Pudritz and P. G. Higgs (**2018**). 'Constraining the Time Interval for the Origin of Life on Earth'. *Astrobiology* 18.3, pp. 343–364. DOI: `10.1089/ast.2017.1674` (cit. on p. 27).

Peltzer, E., J. Bada, G. Schlesinger and S. Miller (**1984**). 'The chemical conditions on the parent body of the murchison meteorite: Some conclusions based on amino, hydroxy and dicarboxylic acids'. *AdSpR* 4.12, pp. 69–74. DOI: `10.1016/0273-1177(84)90546-5` (cit. on p. 49).

Peng, Z., K. Paschek and J. C. Xavier (**2022**). 'What Wilhelm Ostwald Meant by "Autokatalyse" and Its Significance to Origins-of-Life Research'. *BioEssays* 44.9, p. 2200098. DOI: `10.1002/bies.202200098` (cit. on p. x).

Peretó, J., J. L. Bada and A. Lazcano (**2009**). 'Charles Darwin and the Origin of Life'. *Origins Life Evol. Biospheres* 39.5, pp. 395–406. DOI: `10.1007/s11084-009-9172-7` (cit. on p. 139).

Perotti, G., V. Christiaens, T. K. Henning, B. Tabone, L. B. F. M. Waters, I. Kamp, G. Olofsson, S. L. Grant, D. Gasman, J. Bouwman et al. (**2023**). 'Water in the Terrestrial Planet-Forming Zone of the PDS 70 Disk'. *Nature* 620.7974, pp. 516–520. DOI: `10.1038/s41586-023-06317-9` (cit. on p. 4).

Peters, S., D. A. Semenov, R. Hochleitner and O. Trapp (**2023**). 'Synthesis of Prebiotic Organics from CO2 by Catalysis with Meteoritic and Volcanic Particles'. *Scientific Reports* 13.1, p. 6843. DOI: `10.1038/s41598-023-33741-8` (cit. on p. 225).

Petersen, S. and K. Hack (**2007**). 'The thermochemistry library ChemApp and its applications'. *Int. J. Mater. Res.* 98, pp. 935–945. DOI: `10.3139/146.101551` (cit. on pp. 69, 89, 110, 165).

Pierazzo, E. and C. F. Chyba (**1999**). 'Amino acid survival in large cometary impacts'. *Meteorit. & Planet. Sci.* 34.6, pp. 909–918. DOI: `10.1111/j.1945-5100.1999.tb01409.x` (cit. on p. 124).

Pilorget, C., T. Okada, V. Hamm, R. Brunetto, T. Yada, D. Loizeau, L. Riu, T. Usui, A. Moussi-Soffys, K. Hatakeda et al. (**2022**). 'First Compositional Analysis of Ryugu Samples by the MicrOmega Hyperspectral Microscope'. *Nature Astronomy* 6.2, pp. 221–225. DOI: `10.1038/s41550-021-01549-z` (cit. on pp. 22, 25, 144).

Pinto, G. A., Y. Marrocchi, A. Morbidelli, S. Charnoz, M. Eugenia Varela, K. Soto, R. Martínez and F. Olivares (**2021**). 'Constraints on Planetesimal Accretion Inferred from Particle-size Distribution in CO Chondrites'. *Astrophysical Journal, Letters* 917.2, p. L25. DOI: `10.3847/2041-8213/ac17f2`. arXiv: `2107.12658` (cit. on p. 53).

Pinto, J. P., G. R. Gladstone and Y. L. Yung (**1980**). 'Photochemical Production of Formaldehyde in Earth's Primitive Atmosphere'. *Science* 210.4466, pp. 183–185. DOI: `10.1126/science.210.4466.183` (cit. on p. 178).

Pirim, C., M. Pasek, D. Sokolov, A. Sidorov, R. Gann and T. Orlando (**2014**). 'Investigation of schreibersite and intrinsic oxidation products from Sikhote-Alin, Seymchan, and Odessa meteorites and Fe3P and Fe2NiP synthetic surrogates'. *Geochim. Cosmochim. Acta* 140, pp. 259–274. DOI: `10.1016/j.gca.2014.05.027` (cit. on pp. 142, 149).

Piso, A.-M. A., K. I. Öberg, T. Birnstiel and R. A. Murray-Clay (**2015**). 'C/O and Snowline Locations in Protoplanetary Disks: The Effect of Radial Drift and Viscous Gas Accretion'. *Astrophysical Journal* 815.2, 109, p. 109. DOI: `10.1088/0004-637x/815/2/109`. arXiv: `1511.05563 [astro-ph.EP]` (cit. on p. 54).

Pizzarello, S., G. W. Cooper and G. J. Flynn (**2006**). 'The Nature and Distribution of the Organic Material in Carbonaceous Chondrites and Interplanetary Dust Particles'. *Meteorites and the Early Solar System II*. Tucson, AZ, USA: University of Arizona Press, pp. 625–651 (cit. on pp. 43, 124, 178).

Pizzarello, S. (**2012**). 'Hydrogen Cyanide in the Murchison Meteorite'. *Astrophysical Journal* 754.2, p. L27. DOI: `10.1088/2041-8205/754/2/L27` (cit. on p. 50).

Pizzarello, S. and W. Holmes (**2009**). 'Nitrogen-containing compounds in two CR2 meteorites: 15N composition, molecular distribution and precursor molecules'. *Geochimica et Cosmochimica Acta* 73.7, pp. 2150–2162. DOI: `10.1016/j.gca.2009.01.022` (cit. on p. 50).

Pizzarello, S. and E. Shock (**2010**). 'The Organic Composition of Carbonaceous Meteorites: The Evolutionary Story Ahead of Biochemistry'. *Cold Spring Harbor Perspectives in Biology* 2.3, a002105. DOI: `10.1101/cshperspect.a002105` (cit. on p. 22).

— (**2017**). 'Carbonaceous Chondrite Meteorites: The Chronicle of a Potential Evolutionary Path between Stars and Life'. *Orig. Life Evol. Biosph.* 47.3, pp. 249–260. DOI: `10.1007/s11084-016-9530-1` (cit. on p. 101).

Poch, O., M. Jaber, F. Stalport, S. Nowak, T. Georgelin, J.-F. Lambert, C. Szopa and P. Coll (**2015**). 'Effect of Nontronite Smectite Clay on the Chemical Evolution of Several Organic Molecules under Simulated Martian Surface Ultraviolet Radiation Conditions'. *Astrobiology* 15.3, pp. 221–237. DOI: `10.1089/ast.2014.1230` (cit. on p. 205).

Ponnamperuma, C., C. Sagan and R. Mariner (**1963**). 'Synthesis of Adenosine Triphosphate Under Possible Primitive Earth Conditions'. *Nature* 199.4890, pp. 222–226. DOI: `10.1038/199222a0` (cit. on pp. 178, 200, 203, 204, 207, 208, 248).

Pontoppidan, K. M., C. Salyk, E. A. Bergin, S. Brittain, B. Marty, O. Mousis and K. I. Öberg (**2014**). 'Volatiles in Protoplanetary Disks'. *Protostars and Planets VI*. Ed. by H. Beuther, R. S. Klessen, C. P. Dullemond and T. K. Henning. Tucson, AZ, USA: University of Arizona Press, pp. 363–385. DOI: `10.2458/azu_uapress_9780816531240-ch016` (cit. on p. 20).

Postberg, F., N. Khawaja, B. Abel, G. Choblet, C. R. Glein, M. S. Gudipati, B. L. Henderson, H.-W. Hsu, S. Kempf, F. Klenner et al. (**2018**). 'Macromolecular Organic Compounds from the Depths of Enceladus'. *Nature* 558.7711, pp. 564–568. DOI: `10.1038/s41586-018-0246-4` (cit. on p. 4).

Potapov, A. and M. McCoustra (**2021**). 'Physics and chemistry on the surface of cosmic dust grains: A laboratory view'. *Int. Rev. Phys. Chem.* 40.2, pp. 299–364. DOI: `10.1080/0144235x.2021.1918498` (cit. on pp. 19, 55, 108).

Powner, M. W., B. Gerland and J. D. Sutherland (**2009**). 'Synthesis of Activated Pyrimidine Ribonucleotides in Prebiotically Plausible Conditions'. *Nature*

459.7244, pp. 239–242. DOI: 10.1038/nature08013 (cit. on pp. 33, 174, 178, 185, 200, 203, 204, 207, 208, 248).

Pravdivtseva, O., C. Hohenberg and A. Meshik (**2007**). ‘I-Xe SYSTEM IN MAGNETITES SEPARATED FROM CO CHONDRITES OF DIFFERENT PETROLOGIC TYPE.’. *Meteorit. Planet. Sci., Suppl.* 42, p. 5317 (cit. on p. 149).

Preiner, M., J. C. Xavier, F. L. Sousa, V. Zimorski, A. Neubeck, S. Q. Lang, H. C. Greenwell, K. Kleinermanns, H. Tüysüz, T. M. McCollom et al. (**2018**). ‘Serpentinization: Connecting Geochemistry, Ancient Metabolism and Industrial Hydrogenation’. *Life* 8.4, p. 41. DOI: 10.3390/life8040041 (cit. on pp. 174, 182).

Rap, D. B., A. Simon, K. Steenbakkers, J. G. M. Schrauwen, B. Redlich and S. Brünken (**2023**). ‘Fingerprinting Fragments of Fragile Interstellar Molecules: Dissociation Chemistry of Pyridine and Benzonitrile Revealed by Infrared Spectroscopy and Theory’. *Faraday Discuss.* DOI: 10.1039/D3FD00015J (cit. on p. 162).

Rauchfuß, H. (2005). *Chemische Evolution und der Ursprung des Lebens.* Berlin, Heidelberg, Germany: Springer-Verlag. ISBN: 978-3-540-27666-1. DOI: 10.1007/3-540-27666-1 (cit. on pp. 17, 115).

Rauer, H. (**2008**). ‘Comets’. *Trans-Neptunian Objects and Comets.* Ed. by D. Jewitt, A. Morbidelli and H. Rauer. Berlin, Heidelberg, Germany: Springer Berlin Heidelberg, pp. 165–256. ISBN: 978-3-540-71958-8. DOI: 10.1007/978-3-540-71958-8_3 (cit. on pp. 45, 52, 144).

Reynard, B. (**2013**). ‘Serpentine in Active Subduction Zones’. *Lithos.* Serpentinites from Mid-Oceanic Ridges to Subduction 178, pp. 171–185. DOI: 10.1016/j.lithos.2012.10.012 (cit. on p. 210).

Ricardo, A., M. A. Carrigan, A. N. Olcott and S. A. Benner (**2004**). ‘Borate Minerals Stabilize Ribose’. *Science* 303.5655, pp. 196–196. DOI: 10.1126/science.1092464 (cit. on p. 124).

Rich, A. (**1962**). ‘On the problems of evolution and biochemical information transfer’. *Horizons in Biochemistry.* Ed. by M. Kasha and B. Pullman. Academic Press: New York, NY, USA, pp. 103–126 (cit. on pp. 9, 41, 101, 174).

Rich, P. (**2003**). ‘The molecular machinery of Keilin’s respiratory chain’. *Biochem. Soc. Trans.* 31.6, pp. 1095–1105. DOI: 10.1042/bst0311095. eprint: https://portlandpress.com/biochemsoctrans/article-pdf/31/6/1095/537595/bst0311095.pdf (cit. on pp. 13, 142).

Robertson, M. P. and S. L. Miller (**1995**). ‘An efficient prebiotic synthesis of cytosine and uracil’. *Nature* 375.6534, pp. 772–774. DOI: 10.1038/375772a0 (cit. on p. 47).

Robinson, J. E., U. Malamud, C. Opitom, H. Perets and J. Blum (**2024**). ‘A Link between the Size and Composition of Comets’. *Monthly Notices of the Royal*

Astronomical Society 531.1, pp. 859–883. DOI: 10.1093/mnras/stae881 (cit. on pp. 260, 261).

Rollinson, H., J. Adetunji, D. Lenaz and K. Szilas (**2017**). 'Archaean chromitites show constant Fe3+/ΣFe in Earth's asthenospheric mantle since 3.8 Ga'. *Lithos* 282-283, pp. 316–325. DOI: 10.1016/j.lithos.2017.03.020 (cit. on pp. 151, 255).

Rubin, A. E., J. M. Trigo-Rodríguez, H. Huber and J. T. Wasson (**2007**). 'Progressive aqueous alteration of CM carbonaceous chondrites'. *Geochim. Cosmochim. Acta* 71.9, pp. 2361–2382. DOI: 10.1016/j.gca.2007.02.008 (cit. on p. 143).

Rush, G. F., J. R. Gorski, M. G. Ripple, J. Sowinski, P. Bugelski and W. R. Hewitt (**1985**). 'Organic hydroperoxide-induced lipid peroxidation and cell death in isolated hepatocytes'. *Toxicol. Appl. Pharmacol.* 78.3, pp. 473–483. DOI: 10.1016/0041-008X(85)90255-8 (cit. on p. 142).

Russell, M. J., A. J. Hall and W. Martin (**2010**). 'Serpentinization as a Source of Energy at the Origin of Life'. *Geobiology* 8.5, pp. 355–371. DOI: 10.1111/j.1472-4669.2010.00249.x (cit. on pp. 29, 174, 182).

Russell, M. J. (**2021**). 'The "Water Problem"(Sic), the Illusory Pond and Life's Submarine Emergence—A Review'. *Life* 11.5, p. 429. DOI: 10.3390/life11050429 (cit. on pp. 27, 221).

Sagan, C. and B. N. Khare (**1979**). 'Tholins: Organic Chemistry of Interstellar Grains and Gas'. *Nature* 277.5692, pp. 102–107. DOI: 10.1038/277102a0 (cit. on p. 14).

Saladino, R., B. M. Bizzarri, L. Botta, J. Šponer, J. E. Šponer, T. Georgelin, M. Jaber, B. Rigaud, M. Kapralov, G. N. Timoshenko et al. (**2017**). 'Proton Irradiation: A Key to the Challenge of N-glycosidic Bond Formation in a Prebiotic Context'. *Scientific Reports* 7.1, p. 14709. DOI: 10.1038/s41598-017-15392-8 (cit. on pp. 178, 200, 203, 204, 207).

Saladino, R., E. Carota, G. Botta, M. Kapralov, G. N. Timoshenko, A. Y. Rozanov, E. Krasavin and E. Di Mauro (**2015**). 'Meteorite-catalyzed syntheses of nucleosides and of other prebiotic compounds from formamide under proton irradiation'. *Proc. Natl. Acad. Sci.* 112.21, E2746–E2755. DOI: 10.1073/pnas.1422225112 (cit. on p. 106).

Salinas, V. N., M. R. Hogerheijde, E. A. Bergin, L. Ilsedore Cleeves, C. Brinch, G. A. Blake, D. C. Lis, G. J. Melnick, O. Panić, J. C. Pearson et al. (**2016**). 'First detection of gas-phase ammonia in a planet-forming disk - NH3, N2H+, and H2O in the disk around TW Hydrae'. *Astronomy & Astrophysics* 591, A122. DOI: 10.1051/0004-6361/201628172 (cit. on p. 19).

Sandford, S. A., M. Nuevo, P. P. Bera and T. J. Lee (**2020**). 'Prebiotic Astrochemistry and the Formation of Molecules of Astrobiological Interest in Interstellar

Clouds and Protostellar Disks'. *Chemical Reviews* 120.11, pp. 4616–4659. DOI: `10.1021/acs.chemrev.9b00560` (cit. on pp. 4, 19, 257).

Schaefer, L. and B. Fegley (**2007**). 'Outgassing of Ordinary Chondritic Material and Some of Its Implications for the Chemistry of Asteroids, Planets, and Satellites'. *Icarus* 186.2, pp. 462–483. DOI: `10.1016/j.icarus.2006.09.002` (cit. on p. 177).

— (**2010**). 'Chemistry of Atmospheres Formed during Accretion of the Earth and Other Terrestrial Planets'. *Icarus* 208.1, pp. 438–448. DOI: `10.1016/j.icarus.2010.01.026` (cit. on p. 177).

— (**2017**). 'Redox States of Initial Atmospheres Outgassed on Rocky Planets and Planetesimals'. *The Astrophysical Journal* 843.2, p. 120. DOI: `10.3847/1538-4357/aa784f` (cit. on p. 177).

Schlesinger, G. and S. L. Miller (**1983**). 'Prebiotic Synthesis in Atmospheres Containing CH4, CO, and CO2'. *Journal of Molecular Evolution* 19.5, pp. 376–382. DOI: `10.1007/BF02101642` (cit. on p. 173).

Schöning, K.-U., P. Scholz, S. Guntha, X. Wu, R. Krishnamurthy and A. Eschenmoser (**2000**). 'Chemical Etiology of Nucleic Acid Structure: The α-Threofuranosyl-(3'→2') Oligonucleotide System'. *Sci* 290.5495, pp. 1347–1351. DOI: `10.1126/science.290.5495.1347` (cit. on p. 42).

Schoonen, M. A. A. and Y. Xu (**2001**). 'Nitrogen reduction under hydrothermal vent conditions: Implications for the prebiotic synthesis of C-H-O-N compounds'. *AsBio* 1.2, pp. 133–142. DOI: `10.1089/153110701753198909` (cit. on p. 41).

Schulte, M. and E. Shock (**2004**). 'Coupled organic synthesis and mineral alteration on meteorite parent bodies'. *Meteoritics and Planetary Science* 39.9, pp. 1577–1590. DOI: `10.1111/j.1945-5100.2004.tb00128.x` (cit. on pp. 48, 52).

Seita, T., K. Yamauchi, M. Kinoshita and M. Imoto (**1972**). 'Condensation polymerization of nucleotide analogues'. *MmCP* 154.1, pp. 255–261. DOI: `10.1002/macp.1972.021540123` (cit. on p. 42).

Sekine, Y., S. Sugita, T. Kadono and T. Matsui (**2003**). 'Methane production by large iron meteorite impacts on early Earth'. *Journal of Geophysical Research: Planets* 108.E7, p. 5070. DOI: `10.1029/2002JE002034` (cit. on pp. 183, 211, 225).

Semenov, D. A. and D. Wiebe (**2011**). 'Chemical Evolution of Turbulent Protoplanetary Disks and the Solar Nebula'. *Astrophys. J. Suppl.* 196.2, 25, p. 25. DOI: `10.1088/0067-0049/196/2/25` (cit. on pp. 45, 52, 54, 56, 58, 59, 108).

Shadyro, O., P. Lagutin, I. Edimecheva, S. Brinkevich and T. Kagiya (**2008**). 'Protective effects of vitamin glycosides on γ-radiation and H2O2-induced decomposition of thymine in aqueous solutions'. *JRadR* 49.4, pp. 431–435. DOI: `10.1269/jrr.08004` (cit. on pp. 74, 84).

Shapiro, R. (**1999**). 'Prebiotic cytosine synthesis: A critical analysis and implications for the origin of life'. *PNAS* 96.8, pp. 4396–4401. DOI: `10.1073/pnas.96.8.4396` (cit. on p. 48).

Shen, L. and H.-F. Ji (**2011**). 'Small Cofactors May Assist Protein Emergence from RNA World: Clues from RNA-Protein Complexes'. *PLoS ONE* 6.7. Ed. by D. J. Stekel, e22494. DOI: `10.1371/journal.pone.0022494` (cit. on p. 142).

Shibata, Y. and H. Matsueda (**1994**). 'Chemical composition of Fe-Ni metal and phosphate minerals in Yamato-82094 carbonaceous chondrite'. *Proc. NIPR Symp. Antarct. Meteorites* 7, pp. 110–124. DOI: `10.15094/00004640` (cit. on p. 149).

Shimoyama, A., S. Hagishita and K. Harada (**1990**). 'Search for nucleic acid bases in carbonaceous chondrites from Antarctica'. *GeocJ* 24.5, pp. 343–348. DOI: `10.2343/geochemj.24.343` (cit. on pp. 24, 43, 45, 66, 80, 178).

Shvekhgeimer, M.-G. A. (**1998**). '2,3,4,5-Tetrahydropyridine (Δ1-piperideine) and Its Derivatives. Synthesis and Chemical Properties'. *Russ. Chem. Rev.* 67.12, pp. 1031–1060. DOI: `10.1070/RC1998v067n12ABEH000434` (cit. on p. 150).

Sleep, N. H., K. J. Zahnle and P. S. Neuhoff (**2001**). 'Initiation of Clement Surface Conditions on the Earliest Earth'. *Proceedings of the National Academy of Sciences* 98.7, pp. 3666–3672. DOI: `10.1073/pnas.071045698` (cit. on pp. 176, 217).

Sleep, N. H., K. J. Zahnle and R. E. Lupu (**2014**). 'Terrestrial Aftermath of the Moon-forming Impact'. *Philosophical Transactions of the Royal Society A: Mathematical, Physical and Engineering Sciences* 372.2024, p. 20130172. DOI: `10.1098/rsta.2013.0172` (cit. on pp. 176, 217).

Smith, K. E., M. P. Callahan, P. A. Gerakines, J. P. Dworkin and C. H. House (**2014**). 'Investigation of pyridine carboxylic acids in CM2 carbonaceous chondrites: Potential precursor molecules for ancient coenzymes'. *Geochim. Cosmochim. Acta* 136, pp. 1–12. DOI: `10.1016/j.gca.2014.04.001` (cit. on pp. 24, 25, 140, 151, 153, 154, 160–163, 178, 254).

Socha, R. F., A. H. Weiss and M. M. Sakharov (**1980**). 'Autocatalysis in the formose reaction'. *React. Kinet. Catal. Lett.* 14.2, pp. 119–128. DOI: `10.1007/bf02061275` (cit. on pp. 15, 16, 105).

Solomatova, N. V. and R. Caracas (**2021**). 'Genesis of a CO2-rich and H2O-depleted Atmosphere from Earth's Early Global Magma Ocean'. *Science Advances* 7.41, eabj0406. DOI: `10.1126/sciadv.abj0406` (cit. on p. 256).

Šponer, J. E., J. Šponer, O. Nováková, V. Brabec, O. Šedo, Z. Zdráhal, G. Costanzo, S. Pino, R. Saladino and E. Di Mauro (**2016**). 'Emergence of the First Catalytic Oligonucleotides in a Formamide-Based Origin Scenario'. *Chem. – A Eur. J.* 22.11, pp. 3572–3586. DOI: `10.1002/chem.201503906` (cit. on p. 106).

Springsklee, C., B. Scheu, C. Seifert, M. Manga, C. Cimarelli, D. Gaudin, O. Trapp and D. B. Dingwell (**2023**). 'A Gas-Tight Shock Tube Apparatus for Laboratory Volcanic Lightning under Varying Atmospheric Conditions'. *Volcanica* 6.2, pp. 437–445. DOI: `10.30909/vol.06.02.437445` (cit. on p. 32).

Staudigel, H., S. R. Hart and S. H. Richardson (**1981**). 'Alteration of the Oceanic Crust: Processes and Timing'. *Earth and Planetary Science Letters* 52.2, pp. 311–327. DOI: `10.1016/0012-821X(81)90186-2` (cit. on p. 233).

Stephens, P. J., F. J. Devlin, C. F. Chabalowski and M. J. Frisch (**1994**). 'Ab Initio Calculation of Vibrational Absorption and Circular Dichroism Spectra Using Density Functional Force Fields'. *J. Phys. Chem.* 98.45, pp. 11623–11627. DOI: `10.1021/j100096a001` (cit. on pp. 113, 168).

Stoks, P. G. and A. W. Schwartz (**1979**). 'Uracil in carbonaceous meteorites'. *Nature* 282.5740, pp. 709–710. DOI: `10.1038/282709a0` (cit. on pp. 24, 43, 45, 66, 79, 178).

— (**1981**). 'Nitrogen-heterocyclic compounds in meteorites: significance and mechanisms of formation'. *Geochimica et Cosmochimica Acta* 45.4, pp. 563–569. DOI: `10.1016/0016-7037(81)90189-7` (cit. on pp. 24, 43, 45, 66, 78, 80, 142, 178).

Strecker, A. (**1850**). 'Ueber Die Künstliche Bildung Der Milchsäure Und Einen Neuen, Dem Glycocoll Homologen Körper;'. *Justus Liebigs Annalen der Chemie* 75.1, pp. 27–45. DOI: `10.1002/jlac.18500750103` (cit. on p. 15).

— (**1854**). 'Ueber Einen Neuen Aus Aldehyd - Ammoniak Und Blausäure Entstehenden Körper'. *Justus Liebigs Annalen der Chemie* 91.3, pp. 349–351. DOI: `10.1002/jlac.18540910309` (cit. on p. 15).

Stribling, R. and S. L. Miller (**1987**). 'Energy Yields for Hydrogen Cyanide and Formaldehyde Syntheses: The Hcn and Amino Acid Concentrations in the Primitive Ocean'. *Origins of life and evolution of the biosphere* 17.3, pp. 261–273. DOI: `10.1007/BF02386466` (cit. on p. 173).

Strom, R. G., R. Malhotra, T. Ito, F. Yoshida and D. A. Kring (**2005**). 'The Origin of Planetary Impactors in the Inner Solar System'. *Science* 309.5742, pp. 1847–1850. DOI: `10.1126/science.1113544` (cit. on p. 223).

Sutherland, J. D. (**2016**). 'The Origin of Life—Out of the Blue'. *Angewandte Chemie International Edition* 55.1, pp. 104–121. DOI: `10.1002/anie.201506585` (cit. on pp. 33, 174, 178).

— (**2017**). 'Opinion: Studies on the Origin of Life — the End of the Beginning'. *Nature Reviews Chemistry* 1.2, pp. 1–7. DOI: `10.1038/s41570-016-0012` (cit. on p. 4).

Tarduno, J. A., R. D. Cottrell, R. K. Bono, N. Rayner, W. J. Davis, T. Zhou, F. Nimmo, A. Hofmann, J. Jodder, M. Ibañez-Mejia et al. (**2023**). 'Hadaean to Palaeoarchaean Stagnant-Lid Tectonics Revealed by Zircon Magnetism'. *Nature*

618.7965, pp. 531–536. DOI: 10.1038/s41586-023-06024-5 (cit. on pp. 27, 176, 181, 210, 217, 227).

Taylor, J., M. Radica, L. Welbanks, R. J. MacDonald, J. Blecic, M. Zamyatina, A. Roth, J. L. Bean, V. Parmentier, L.-P. Coulombe et al. (**2023**). 'Awesome SOSS: Atmospheric Characterization of WASP-96 b Using the JWST Early Release Observations'. *Monthly Notices of the Royal Astronomical Society* 524.1, pp. 817–834. DOI: 10.1093/mnras/stad1547 (cit. on p. 4).

Teichert, J. S., F. M. Kruse and O. Trapp (**2019**). 'Direct Prebiotic Pathway to DNA Nucleosides'. *Angew. Chem. Int. Ed.* 58.29, pp. 9944–9947. DOI: 10.1002/anie.201903400 (cit. on pp. 106, 116, 117, 186, 200, 203, 204, 207).

Thompson, M. A., J. Krissansen-Totton, N. Wogan, M. Telus and J. J. Fortney (**2022**). 'The Case and Context for Atmospheric Methane as an Exoplanet Biosignature'. *Proceedings of the National Academy of Sciences* 119.14, e2117933119. DOI: 10.1073/pnas.2117933119 (cit. on pp. 176, 182, 210, 220, 234, 262).

Tilmann, F., E. Flueh, L. Planert, T. Reston and W. Weinrebe (**2004**). 'Microearthquake Seismicity of the Mid-Atlantic Ridge at 5°S: A View of Tectonic Extension'. *Journal of Geophysical Research: Solid Earth* 109.B6. DOI: 10.1029/2003JB002827 (cit. on p. 232).

Tinetti, G., A. Vidal-Madjar, M.-C. Liang, J.-P. Beaulieu, Y. Yung, S. Carey, R. J. Barber, J. Tennyson, I. Ribas, N. Allard et al. (**2007**). 'Water Vapour in the Atmosphere of a Transiting Extrasolar Planet'. *Nature* 448.7150, pp. 169–171. DOI: 10.1038/nature06002 (cit. on p. 4).

Todd, Z. R., J. W. Szostak and D. D. Sasselov (**2021**). 'Shielding from UV Photodamage: Implications for Surficial Origins of Life Chemistry on the Early Earth'. *ACS Earth and Space Chemistry* 5.2, pp. 239–246. DOI: 10.1021/acsearthspacechem.0c00270 (cit. on p. 256).

Toomey, D. R., S. C. Solomon and G. M. Purdy (**1988**). 'Microearthquakes beneath Median Valley of Mid-Atlantic Ridge near 23°N: Tomography and Tectonics'. *Journal of Geophysical Research: Solid Earth* 93.B8, pp. 9093–9112. DOI: 10.1029/JB093iB08p09093 (cit. on p. 232).

Toppozini, L., H. Dies, D. W. Deamer and M. C. Rheinstädter (**2013**). 'Adenosine Monophosphate Forms Ordered Arrays in Multilamellar Lipid Matrices: Insights into Assembly of Nucleic Acid for Primitive Life'. *PLoS ONE* 8.5. Ed. by H.-A. Tajmir-Riahi, e62810. DOI: 10.1371/journal.pone.0062810 (cit. on pp. 42, 101).

Tosi, N., M. Godolt, B. Stracke, T. Ruedas, J. L. Grenfell, D. Höning, A. Nikolaou, A.-C. Plesa, D. Breuer and T. Spohn (**2017**). 'The Habitability of a Stagnant-

Lid Earth'. *Astronomy & Astrophysics* 605, A71. DOI: 10.1051/0004-6361/201730728 (cit. on p. 176).

Toure, O. and C.-G. Dussap (**2016**). 'Determination of Gibbs energies of formation in aqueous solution using chemical engineering tools'. *Bioresour. Technol.* 213, pp. 359–368. DOI: 10.1016/j.biortech.2016.02.109 (cit. on p. 167).

Trail, D., E. Bruce Watson and N. D. Tailby (**2012**). 'Ce and Eu anomalies in zircon as proxies for the oxidation state of magmas'. *Geochim. Cosmochim. Acta* 97, pp. 70–87. DOI: 10.1016/j.gca.2012.08.032 (cit. on p. 151).

Trail, D., E. B. Watson and N. D. Tailby (**2011**). 'The Oxidation State of Hadean Magmas and Implications for Early Earth's Atmosphere'. *Nature* 480.7375, pp. 79–82. DOI: 10.1038/nature10655 (cit. on pp. 173, 181, 228).

Travis, B. J. and G. Schubert (**2005**). 'Hydrothermal convection in carbonaceous chondrite parent bodies'. *E&PSL* 240.2, pp. 234–250. DOI: 10.1016/j.epsl.2005.09.008 (cit. on pp. 49, 50, 66, 70, 152, 155, 166).

Trigo-Rodríguez, J. M., A. Rimola, S. Tanbakouei, V. C. Soto and M. Lee (**2019**). 'Accretion of Water in Carbonaceous Chondrites: Current Evidence and Implications for the Delivery of Water to Early Earth'. *Space Sci. Rev.* 215.1, p. 18. DOI: 10.1007/s11214-019-0583-0 (cit. on p. 143).

Urey, H. C. (**1951**). 'The Origin and Development of the Earth and Other Terrestrial Planets'. *Geochimica et Cosmochimica Acta* 1.4, pp. 209–277. DOI: 10.1016/0016-7037(51)90001-4 (cit. on p. 173).

— (**1952**). 'On the Early Chemical History of the Earth and the Origin of Life'. *Proceedings of the National Academy of Sciences* 38.4, pp. 351–363. DOI: 10.1073/pnas.38.4.351 (cit. on pp. 173, 176).

Vaidya, N., M. L. Manapat, I. A. Chen, R. Xulvi-Brunet, E. J. Hayden and N. Lehman (**2012**). 'Spontaneous network formation among cooperative RNA replicators'. *Nature* 491.7422, pp. 72–77. DOI: 10.1038/nature11549 (cit. on pp. 9, 41, 101, 140, 174).

Valley, J. W., J. S. Lackey, A. J. Cavosie, C. C. Clechenko, M. J. Spicuzza, M. A. S. Basei, I. N. Bindeman, V. P. Ferreira, A. N. Sial, E. M. King et al. (**2005**). '4.4 Billion Years of Crustal Maturation: Oxygen Isotope Ratios of Magmatic Zircon'. *Contributions to Mineralogy and Petrology* 150.6, pp. 561–580. DOI: 10.1007/s00410-005-0025-8 (cit. on p. 227).

van Kooten, E. M., E. Kubik, J. Siebert, B. D. Heredia, T. B. Thomsen and F. Moynier (**2022**). 'Metal compositions of carbonaceous chondrites'. *Geochim. Cosmochim. Acta* 321, pp. 52–77. DOI: 10.1016/j.gca.2022.01.008 (cit. on p. 150).

Van Schmus, W. R. and J. A. Wood (**1967**). 'A chemical-petrologic classification for the chondritic meteorites'. *Geochimica et Cosmochimica Acta* 31.5, 747, IN7, 755–754, IN10, 765. DOI: 10.1016/s0016-7037(67)80030-9 (cit. on p. 53).

Varas-Reus, M. I., S. König, A. Yierpan, J.-P. Lorand and R. Schoenberg (**2019**). 'Selenium isotopes as tracers of a late volatile contribution to Earth from the outer Solar System'. *Nat. Geosci.* 12.9, pp. 779–782. DOI: 10.1038/s41561-019-0414-7 (cit. on pp. 139, 140, 177, 215, 224).

Velden, W. van der and A. W. Schwartz (**1977**). 'Search for purines and pyrimidines in the Murchison meteorite'. *Geochimica et Cosmochimica Acta* 41.7, pp. 961–968. DOI: 10.1016/0016-7037(77)90155-7 (cit. on pp. 24, 43, 80, 178).

Vinogradoff, V., F. Duvernay, G. Danger, P. Theulé and T. Chiavassa (**2011**). 'New Insight into the Formation of Hexamethylenetetramine (HMT) in Interstellar and Cometary Ice Analogs'. *Astron. Astrophys.* 530, A128. DOI: 10.1051/0004-6361/201116688 (cit. on p. 159).

Virtanen, P., R. Gommers, T. E. Oliphant, M. Haberland, T. Reddy, D. Cournapeau, E. Burovski, P. Peterson, W. Weckesser, J. Bright et al. (**2020**). 'SciPy 1.0: Fundamental Algorithms for Scientific Computing in Python'. *Nature Methods* 17, pp. 261–272. DOI: 10.1038/s41592-019-0686-2 (cit. on pp. 61, 70, 89, 110).

Visser, R., E. F. van Dishoeck, S. D. Doty and C. P. Dullemond (**2009**). 'The chemical history of molecules in circumstellar disks. I. Ices'. *Astron. & Astrophys.* 495.3, pp. 881–897. DOI: 10.1051/0004-6361/200810846 (cit. on pp. 54, 108).

Vollstaedt, H., K. Mezger and Y. Alibert (**2020**). 'Carbonaceous Chondrites and the Condensation of Elements from the Solar Nebula'. *Astrophys. J.* 897.1, 82, p. 82. DOI: 10.3847/1538-4357/ab97b4 (cit. on pp. 54, 107).

Wagman, D. D., W. H. Evans, V. B. Parker, R. H. Schumm, I. Halow, S. M. Bailey, K. L. Churney and R. L. Nutall (**1982**). 'The NBS tables of chemical thermodynamic properties'. *J. Phys. Chem. Ref. Data* 11, p. 2 (cit. on pp. 114, 168).

Wai, C. M. and J. T. Wasson (**1977**). 'Nebular condensation of moderately volatile elements and their abundances in ordinary chondrites'. *Earth Planet. Sci. Lett.* 36.1, pp. 1–13. DOI: 10.1016/0012-821X(77)90182-0 (cit. on pp. 54, 107).

Wakamatsu, H., Y. Yamada, T. Saito, I. Kumashiro and T. Takenishi (**1966**). 'Synthesis of Adenine by Oligomerization of Hydrogen Cyanide'. *Journal of Organic Chemistry* 31.6, pp. 2035–2036. DOI: 10.1021/jo01344a545 (cit. on pp. 47, 74, 200, 204).

Walker, R. J. (**2009**). 'Highly siderophile elements in the Earth, Moon and Mars: Update and implications for planetary accretion and differentiation'. *Geochemistry* 69.2, pp. 101–125. DOI: 10.1016/j.chemer.2008.10.001 (cit. on p. 224).

Walsh, K. J., A. Morbidelli, S. N. Raymond, D. P. O'Brien and A. M. Mandell (**2011**). 'A low mass for Mars from Jupiter's early gas-driven migration'. *Nature*

475.7355, pp. 206–209. DOI: 10.1038/nature10201. arXiv: 1201.5177 [astro-ph.EP] (cit. on pp. 53, 62).

Wang, J., X. Xiong, E. Takahashi, L. Zhang, L. Li and X. Liu (**2019**). 'Oxidation State of Arc Mantle Revealed by Partitioning of V, Sc, and Ti Between Mantle Minerals and Basaltic Melts'. *J. Geophys. Res.: Solid Earth* 124.5, pp. 4617–4638. DOI: 10.1029/2018JB016731 (cit. on p. 151).

Wang, Z. and H. Becker (**2013**). 'Ratios of S, Se and Te in the silicate Earth require a volatile-rich late veneer'. *Nature* 499.7458, pp. 328–331. DOI: 10.1038/nature12285 (cit. on p. 224).

Wasson, J. T., G. W. Kallemeyn, S. K. Runcorn, G. Turner and M. M. Woolfson (**1988**). 'Compositions of Chondrites'. *Philosophical Transactions of the Royal Society of London. Series A, Mathematical and Physical Sciences* 325.1587, pp. 535–544. DOI: 10.1098/rsta.1988.0066 (cit. on p. 236).

Watanabe, S.-i., Y. Tsuda, M. Yoshikawa, S. Tanaka, T. Saiki and S. Nakazawa (**2017**). 'Hayabusa2 Mission Overview'. *Space Science Reviews* 208.1, pp. 3–16. DOI: 10.1007/s11214-017-0377-1 (cit. on p. 20).

Watson, J. D. and F. H. C. Crick (**1953**). 'Molecular Structure of Nucleic Acids: A Structure for Deoxyribose Nucleic Acid'. *Nature* 171.4356, pp. 737–738. DOI: 10.1038/171737a0 (cit. on p. 3).

Weber, A. L. and S. Pizzarello (**2006**). 'The peptide-catalyzed stereospecific synthesis of tetroses: A possible model for prebiotic molecular evolution'. *Proc. Natl. Acad. Sci.* 103.34, pp. 12713–12717. DOI: 10.1073/pnas.0602320103 (cit. on p. 106).

Weisberg, M. K., T. J. McCoy and A. N. Krot (**2006**). 'Systematics and Evaluation of Meteorite Classification'. *Meteorites and the Early Solar System II*. Ed. by D. S. Lauretta and H. Y. McSween Jr. Tucson, AZ: University of Arizona Press, pp. 19–52. DOI: 978-0-8165-2562-1 (cit. on pp. 143, 144).

Weiss, A. H., R. B. LaPierre and J. Shapira (**1970**). 'Homogeneously Catalyzed Formaldehyde Condensation to Carbohydrates'. *Journal of Catalysis* 16.3, pp. 332–347. DOI: 10.1016/0021-9517(70)90230-7 (cit. on p. 17).

Westall, F. and A. Brack (**2018**). 'The Importance of Water for Life'. *Space Science Reviews* 214.2, p. 50. DOI: 10.1007/s11214-018-0476-7 (cit. on p. 173).

Wilde, S. A., J. W. Valley, W. H. Peck and C. M. Graham (**2001**). 'Evidence from Detrital Zircons for the Existence of Continental Crust and Oceans on the Earth 4.4 Gyr Ago'. *Nature* 409.6817, pp. 175–178. DOI: 10.1038/35051550 (cit. on pp. 27, 227).

Wilkins, M. H. F., A. R. Stokes and H. R. Wilson (**1953**). 'Molecular Structure of Nucleic Acids: Molecular Structure of Deoxypentose Nucleic Acids'. *Nature* 171.4356, pp. 738–740. DOI: 10.1038/171738a0 (cit. on p. 3).

Wilkinson, A., J. Day and R. Bowater (**2001**). 'Bacterial DNA ligases'. *Mol. Microbiol.* 40.6, pp. 1241–1248. DOI: `10.1046/j.1365-2958.2001.02479.x`. eprint: `https://onlinelibrary.wiley.com/doi/pdf/10.1046/j.1365-2958.2001.02479.x` (cit. on p. 142).

Wogan, N., D. C. Catling, K. J. Zahnle and R. E. Lupu (**2023**). 'Origin-of-Life Molecules in the Atmosphere after Big Impacts on the Early Earth'. *The Planetary Science Journal* 4.9, p. 169. DOI: `10.3847/PSJ/aced83` (cit. on pp. 31, 177, 183, 193, 208, 211, 212, 228, 235, 239, 245, 255).

Wogan, N., J. Krissansen-Totton and D. C. Catling (**2020**). 'Abundant Atmospheric Methane from Volcanism on Terrestrial Planets Is Unlikely and Strengthens the Case for Methane as a Biosignature'. *The Planetary Science Journal* 1.3, p. 58. DOI: `10.3847/PSJ/abb99e` (cit. on pp. 181, 228).

Wolszczan, A. and D. A. Frail (**1992**). 'A Planetary System around the Millisecond Pulsar PSR1257 + 12'. *Nature* 355.6356, pp. 145–147. DOI: `10.1038/355145a0` (cit. on p. 4).

Xavier, J. C., W. Hordijk, S. Kauffman, M. Steel and W. F. Martin (**2020**). 'Autocatalytic chemical networks at the origin of metabolism'. *Proc. R. Soc. B* 287.1922, p. 20192377. DOI: `10.1098/rspb.2019.2377` (cit. on pp. 14, 140).

Yada, T., M. Abe, T. Okada, A. Nakato, K. Yogata, A. Miyazaki, K. Hatakeda, K. Kumagai, M. Nishimura, Y. Hitomi et al. (**2022**). 'Preliminary Analysis of the Hayabusa2 Samples Returned from C-type Asteroid Ryugu'. *Nature Astronomy* 6.2, pp. 214–220. DOI: `10.1038/s41550-021-01550-6` (cit. on pp. 22, 25, 144).

Yadav, M., R. Kumar and R. Krishnamurthy (**2020**). 'Chemistry of Abiotic Nucleotide Synthesis'. *Chemical Reviews* 120.11, pp. 4766–4805. DOI: `10.1021/acs.chemrev.9b00546` (cit. on pp. 33, 174, 178).

Yamada, Y., I. Noda, I. Kumashiro and T. Takenishi (**1969**). 'Synthesis of 4,8-Diaminopyrimido[5,4-d]pyrimidine from Hydrogen Cyanide in Liquid Ammonia'. *Bulletin of the Chemical Society of Japan* 42.5, pp. 1454–1456. DOI: `10.1246/bcsj.42.1454` (cit. on pp. 47, 74).

Yang, C. C. and J. Oró (**1971**). 'Synthesis of adenine, guanine, cytosine and other nitrogen organic compounds by a Fischer-Tropsch-like process'. *Chemical Evolution and the Origin of Life; Proceedings of the Third International Conference.* Ed. by J. Cernicharo and R. Bachiller. Amsterdam: North-Holland Publishing Co., pp. 152–167 (cit. on pp. 15, 47).

Yessaad, M., L. Bernard, D. Bourdeaux, P. Chennell and V. Sautou (**2018**). 'Development of a Stability Indicating Method for Simultaneous Analysis of Five Water-Soluble Vitamins by Liquid Chromatography'. *Pharmaceutical Technology in Hospital Pharmacy* 3.4, pp. 207–218. DOI: `10.1515/pthp-2018-0026` (cit. on p. 160).

Yi, R., Q. P. Tran, S. Ali, I. Yoda, Z. R. Adam, H. J. Cleaves and A. C. Fahrenbach (**2020**). 'A Continuous Reaction Network That Produces RNA Precursors'. *Proceedings of the National Academy of Sciences* 117.24, pp. 13267–13274. DOI: `10.1073/pnas.1922139117` (cit. on pp. 33, 185, 199).

Yokoyama, T., K. Nagashima, I. Nakai, E. D. Young, Y. Abe, J. Aléon, C. M. O. Alexander, S. Amari, Y. Amelin, K.-i. Bajo et al. (**2022**). 'Samples Returned from the Asteroid Ryugu Are Similar to Ivuna-type Carbonaceous Meteorites'. *Science* 379.6634, eabn7850. DOI: `10.1126/science.abn7850` (cit. on pp. 22, 25, 144).

Yomogida, K. and T. Matsui (**1983**). 'Physical properties of ordinary chondrites'. *JGRB* 88 (B11), pp. 9513–9533. DOI: `10.1029/jb088ib11p09513` (cit. on p. 65).

Young, E. D., A. Shahar and H. E. Schlichting (**2023**). 'Earth Shaped by Primordial H2 Atmospheres'. *Nature* 616.7956, pp. 306–311. DOI: `10.1038/s41586-023-05823-0` (cit. on p. 173).

Yu, H., S. Zhang and J. C. Chaput (**2012**). 'Darwinian evolution of an alternative genetic system provides support for TNA as an RNA progenitor'. *NatCh* 4.3, pp. 183–187. DOI: `10.1038/nchem.1241` (cit. on p. 42).

Zahnle, K. J., N. Arndt, C. Cockell, A. Halliday, E. Nisbet, F. Selsis and N. H. Sleep (**2007**). 'Emergence of a Habitable Planet'. *Space Science Reviews* 129.1, pp. 35–78. DOI: `10.1007/s11214-007-9225-z` (cit. on pp. 173, 176, 181, 209, 217, 218, 223, 227).

Zahnle, K. J., M. Gacesa and D. C. Catling (**2019**). 'Strange messenger: A new history of hydrogen on Earth, as told by Xenon'. *Geochimica et Cosmochimica Acta* 244, pp. 56–85. DOI: `10.1016/j.gca.2018.09.017` (cit. on p. 185).

Zahnle, K. J., R. E. Lupu, D. C. Catling and N. Wogan (**2020**). 'Creation and Evolution of Impact-generated Reduced Atmospheres of Early Earth'. *The Planetary Science Journal* 1.1, p. 11. DOI: `10.3847/PSJ/ab7e2c` (cit. on pp. 31, 151, 177, 183, 193, 208, 211, 225, 232, 235, 236, 239, 245, 255).

Zahnle, K. J. and N. H. Sleep (**2006**). 'Impacts and the Early Evolution of Life'. *Comets and the Origin and Evolution of Life*. Ed. by P. J. Thomas, R. D. Hicks, C. F. Chyba and C. P. McKay. Berlin, Heidelberg: Springer, pp. 207–251. ISBN: 978-3-540-33088-2. DOI: `10.1007/3-540-33088-7_7` (cit. on p. 173).

Zaug, A. J. and T. R. Cech (**1986**). 'The intervening sequence RNA of tetrahymena is an enzyme'. *Science* 231.4737, pp. 470–475. DOI: `10.1126/science.3941911` (cit. on pp. 9, 41, 101, 140, 174).

Zhang, L., A. Peritz and E. Meggers (**2005**). 'A Simple Glycol Nucleic Acid'. *JAChS* 127.12, pp. 4174–4175. DOI: `10.1021/ja042564z` (cit. on p. 42).

Zhao, Z.-R. and X. Wang (**2021**). 'A plausible prebiotic selection of ribose for RNA - formation, dynamic isolation, and nucleotide synthesis based on metal-doped-clays'. *Chem* 7.12, pp. 3292–3308. DOI: `10.1016/j.chempr.2021.09.002` (cit. on p. 128).

Ziegler, M. (**2000**). 'New functions of a long-known molecule'. *Eur. J. Biochem.* 267.6, pp. 1550–1564. DOI: `10.1046/j.1432-1327.2000.01187.x` (cit. on p. 142).

Zweckmair, T., S. Böhmdorfer, A. Bogolitsyna, T. Rosenau, A. Potthast and S. Novalin (**2013**). 'Accurate Analysis of Formose Reaction Products by LC–UV: An Analytical Challenge'. *J. Chromatogr. Sci.* 52.2, pp. 169–175. DOI: `10.1093/chromsci/bmt004` (cit. on p. 116).